

---

# Landslide Susceptibility and Climate Change Scenarios in Flysch Areas of the Eastern Alps

Inaugural-Dissertation

zur Erlangung der Doktorwürde der

Philosophischen Fakultät I

der

Julius-Maximilians-Universität Würzburg

vorgelegt von

Bettina Neuhäuser

aus Wien

Würzburg 2014

---

Erstgutachterin: Professor Dr. Birgit Terhorst

Zweitgutachter: Professor Dr. Bodo Damm

Tag des Kolloquiums:

3. Dezember 2014

---

# Vorwort/Preface

## Danksagung

Großer Dank gilt der Österreichischen Akademie der Wissenschaften (ÖAW), welche die vorliegende Dissertation im Rahmen des DOC-ffORTE Stipendienprogrammes gefördert hat. Ohne diese Förderung wäre die Durchführung der Arbeit nicht möglich gewesen.

Besonderer Dank gilt meiner Dissertations-Betreuerin und Mentorin Prof. Dr. Birgit Terhorst, welche mir das Thema dieser Dissertation zur Verfügung gestellt hat. Ich möchte mich für die Unterstützung in meiner fachlichen Entwicklung in den letzten Jahren, für die angenehme und erfolgreiche Zusammenarbeit sowie die freundliche Aufnahme in Würzburg herzlich bedanken. Frau Prof. Terhorst verdanke ich außerdem einen neuen Blick auf die Landschaft und ihre Prozesse, der mir auch nach Beendigung der Dissertation erhalten bleiben wird.

Im Weiteren gilt besonderer Dank Herrn Prof. Dr. Bodo Damm, der durch seine zahlreichen fachlichen Inputs die vorliegende Arbeit entscheidend mitgestaltet hat. Ich möchte mich bei ihm für sein fachliches Engagement sowie für die konstruktive Kritik bei der Durchsicht meiner Manuskripte und der vorliegenden Arbeit bedanken.

Wesentliche Unterstützung im Hinblick auf die Bereitstellung von Daten erhielt ich durch die Geologische Bundesanstalt (GBA), den Geologischen Dienst der Baudirektion der Niederösterreichischen Landesregierung (LandNÖ) sowie den Forsttechnischen Dienst der Wildbach und Lawinenverbauung (dieWildbach). In diesem Zusammenhang möchte ich mich besonders bei den Herren Mag. Thomas Hofmann (GBA), Dr. Joachim Schweigl (LandNÖ) und Dipl.-Ing. Christian Amberger (dieWildbach) für Ihre Diskussionsbeiträge und die Bereitschaft mir Daten zur Verfügung zu stellen, bedanken.

Ich bedanke mich zudem bei den Arbeitsgruppenmitgliedern Daniel Jäger, Michael Lorenz, Michael Menke, Christine Sandmeier und anderen Kollegen für die nette Aufnahme in Würzburg.

Großer Dank gilt auch meiner Familie, ohne deren Unterstützung diese Dissertation unmöglich gewesen wäre. Ich möchte mich ganz besonders bei meinen Eltern bedanken, die durch die Betreuung meiner Kinder eine entscheidende Unterstützung waren. Meinem Mann danke ich für den Zuspruch in schwierigen Phasen der Arbeit und den technischen Hilfestellung bei hard- und softwaretechnischen Problemen.

## Acknowledgements

I would like to express my sincere gratitude to the Austrian Academy of Sciences (ÖAW), who supported my doctoral thesis in the framework of the DOC-ffORTE fellowship. The present work would not have been feasible without this support.

Special thanks go to my supervisor Prof. Dr. Birgit Terhorst, who provided the topic of this doctoral thesis. I would like to thank her for supporting my professional development within the last few years, for the pleasant and successful cooperation, as well as for the friendly reception in Würzburg. Prof. Terhorst helped me to gain a new insight to landscapes and related processes, which I will preserve in the future.

In addition, I would like to particularly thank Prof. Dr. Bodo Damm, who has had considerable influence on the present doctoral thesis due to his valuable scientific input and ideas. I would like to thank him for his professional dedication and his constructive criticism during the review process of my manuscripts and the present doctoral thesis.

---

---

Furthermore, I received major support by the Austrian Geological Survey (GBA), the Geological Survey of the Construction Board of the Provincial Government of Lower Austria (LandNÖ) and the Department of Torrent and Avalanche Controlling (dieWildbach) of the Federal Ministry of Agriculture, Forestry, Environment and Water Management in Austria. The mentioned institutions provided essential data for the present study. Above all, I would like to express my gratitude to Mr Thomas Hofmann (GBA), Dr. Joachim Schweigl (LandNÖ), as well as to Mr Christian Amberger (dieWildbach) for their willingness to make data available to me. This work could not have been carried out without their support.

In addition I would like to thank my colleagues Daniel Jäger, Michael Lorenz, Michael Menke, Christine Sandmeier and other colleagues of the team in Würzburg for the friendly welcome at the University.

I owe particular thanks to my family without whose support this doctoral thesis would have been impossible. Big thanks go to my parents who considerably relieved me by taking care of my kids. I would like to thank my husband for his encouragement in difficult phases of the work and his technical support concerning problems with hard- and software.

---

# Zusammenfassung/Summary

## Zusammenfassung

Das Thema der vorliegenden Arbeit umfasst die Beurteilung der Hangrutschungsgefährdung im nördlichen Wienerwald mit Hilfe von GIS-basierten, deterministischen und statistisch-probabilistischen Modellierungen. Für eine integrierte Beurteilung der Rutschanfälligkeit, welche nicht auf einen einzigen methodischen Ansatz und dessen inhärente Annahmen beschränkt ist, werden in dieser Arbeit zwei komplementäre Methoden durchgeführt.

Die statistisch-probabilistische Methode wird auf die gesamte Region des nördlichen Wienerwalds angewandt. Dieses regionale Modell untersucht die Grunddisposition zur Entstehung von Rutschungen unter Berücksichtigung von Steuerungsfaktoren, die über einen längeren Zeitraum hinweg als konstant angesehen werden können.

Die deterministische Methode wird in einem Detailgebiet im Hagenbachtal angewandt. Diese Detailmodellierungen zielen darauf ab, die variable Disposition für Rutschungen in Abhängigkeit von Substratfeuchte zu untersuchen, die wiederum von meteorologischen Bedingungen abhängig ist. Ein Hauptaspekt der Arbeit ist dabei die Entwicklung von Feuchteszenarien, die sowohl kurzfristige Witterungsphänomene, wie langanhaltenden Niederschlag oder Starkregen, berücksichtigen, die aber auch den Einfluss von mittelfristig bis langfristig veränderlichen meteorologischen und klimatischen Faktoren auf die Hangstabilität untersuchen.

Weiters ist die Abschätzung der Folgen der prognostizierten Klimaänderung auf die Rutschdisposition ein zentraler Aspekt der Arbeit. Dabei werden durchschnittliche monatliche Veränderungen der Lufttemperatur und des Niederschlages in den Modellierungen berücksichtigt, wie sie durch Regionale Klimamodelle

vorhergesagt werden. Hierbei soll geprüft werden, inwieweit Änderungen in der Substratfeuchte und der Hangstabilität als Folge von veränderten Klimabedingungen feststellbar und quantifizierbar sind.

Ein weiteres Ziel ist die Berücksichtigung von flachgründigen Rutschungen in quartären Sedimenten im Rahmen der Dispositionsmodellierung. Auf Grundlage geomorphologischer und sedimentologischer Studien kann davon ausgegangen werden, dass diese entscheidend die Hangentwicklung im Wienerwald beeinflussen. Bisher wurde allgemein davon ausgegangen, dass Rutschungen vor allem in den mergelreichen, verwitterten Sandsteinen des Flyschs entstehen. Geländebasierte Untersuchungen identifizieren allerdings häufig Rutschungen in den quartären Deckschichten, welche weite Bereiche des Anstehenden überlagern. In der vorliegenden Arbeit wird daher der Einfluss dieser Sedimente auf die Hangdynamik innerhalb der GIS-basierten Stabilitätsmodelle untersucht.

Die Ergebnisse der statistisch-probabilistischen Modellierung liefern Informationen über die Grunddisposition zur Rutschungsaktivität im nördlichen Wienerwald. Die resultierende Rutschanfälligkeitskarte zeigt, dass die Nordrandzone, eine tektonische Einheit im Norden des Untersuchungsgebietes, die ausgedehntesten Gebiete mit der höchsten Rutschanfälligkeit aufweist. In diesem Überschiebungsbereich zur Molassezone treten geologische Einheiten auf, die dem Modell zufolge als sehr rutschanfällig eingestuft werden. Die „Wolfpassing Formation“ und die „Kalkigen Klippen“ der Nordrandzone zeigen eine signifikant erhöhte Dichte an Rutschungen. Diese geologischen Einheiten beginnen im Norden in der Nähe von St. Andrä-Wörtern und verlaufen

---

weiter in Richtung Süd-Westen entlang der Bergrücken von Tulbinger Kogel, Klosterberg, Frauenberg und Eichberg.

Die statistische Gewichtung, die im Zuge der regionalen Bewertung der Rutschanfälligkeit durchgeführt wird, liefert Informationen über den räumlichen Zusammenhang zwischen Rutschungen und den Steuerungsfaktoren. Die Modellierung hebt die Bedeutung von tonschieferreichen Schichten als Dispositionsfaktor hervor. Die höchste Rutschanfälligkeit wird in den geologischen Einheiten berechnet, welche die tonschieferreichen Schichten des Gaultflysch enthalten. Darüber hinaus wird festgestellt, dass die Verbreitung von Rutschungen eng mit der räumlichen Verbreitung von Störungszonen und Deckengrenzen verbunden ist. Die tektonischen Bedingungen können daher als wesentlicher Steuerungsfaktor der Rutschungsaktivität im Untersuchungsgebiet angesehen werden. Eine erhöhte Häufigkeit von Massenbewegungen wird in unmittelbarer Nähe zum Gewässernetz festgestellt. In Verbindung mit starken Regenfällen kommt es im Untersuchungsgebiet zu wildbachähnlichen Abflüssen in den Gerinnen, wodurch in angrenzenden Hängen Instabilitäten auftreten können. Es wird ferner durch das Modell belegt, dass die Anfälligkeit für Rutschungen auf Nord-West exponierten Hängen erhöht ist. Der Vergleich mit meteorologischen Daten zeigt, dass die Nord-West-Hangexposition der dominierenden Windrichtung im Untersuchungsgebiet entspricht. Dadurch können entsprechend exponierte Hänge erhöhten advektiven Niederschlagsmengen ausgesetzt sein, welche die Bodenfeuchte und folglich die Rutschanfälligkeit erhöhen. Letztere Geofaktoren zeigen die Bedeutung der meteorologischen und hydrologischen Bedingungen für das Auftreten von Rutschungen im Untersuchungsgebiet.

Wie oben beschrieben basiert das regionale Bewertungsmodell auf Steuerungsfaktoren, die über längere Zeit hinweg gleichbleibend sind und daher als konstant angesehen werden können. Im Gegensatz dazu wird durch physikalisch-basierte, deterministische Modellierungen die Disposition für Rutschungen unter variablen Feuchtebedingungen im Substrat untersucht.

Zusammenfassend ist festzustellen, dass die Disposition zur Hanginstabilität im Untersuchungsgebiet stark in Abhängigkeit von der Substratfeuchte variiert. Ein Starkregen von 60mm/h kann eine Reduzierung der stabilen Bereiche um 23% im Vergleich zu durchschnittlichen monatlichen Feuchtebedingungen im Sommer (Juli) verursachen. Insgesamt zeigen die Feuchteszenarien, dass neben kurzfristigen Witterungserscheinungen, wie langanhaltendem Niederschlag oder Starkregen, auch langfristige Feuchtebedingungen im Substrat die Hangstabilität beeinflussen. So zeigen saisonal schwankende Feuchtebedingungen leichten aber messbaren Einfluss auf die Hangstabilität: Als Folge der erhöhten topographischen Feuchte im Wintermonat Februar ergibt sich eine Zunahme der instabilen Bereiche um 5% gegenüber dem Sommermonat Juli. Die Feuchteszenarien zeigen außerdem, dass die quartären Sedimente empfindlicher auf die wechselnden Feuchtebedingungen reagieren, als das Flyschgestein.

Die Ergebnisse der Modellierung, die auf prognostizierter Klimaänderung basiert, deuten darauf hin, dass eine moderate Änderung der Hangstabilität im Monatsdurchschnitt im Vergleich zu den Bedingungen in der Klimanormalperiode möglich ist. Eine angenommene durchschnittliche Erhöhung der Lufttemperatur um 2°C in Kombination mit einer um 30% erhöhten Niederschlagsmenge in den Wintermonaten führt im Modell zu einer Erhöhung des Grundwasserzuflusses um 7% gegenüber dem langjährigen Durchschnitt. Durch diesen erhöhten Zufluss zeigt sich im Modellvergleich eine leicht erhöhte topographische Feuchte im Winter. Diese Feuchtigkeitszunahme führt dazu, dass sich stabile Hangbereiche um rund 3% verringern und sich instabile Hangbereiche um den gleichen Betrag ausweiten. Diese leicht erhöhte Instabilität kann dazu führen, dass bereits geringere Niederschlagsmengen bzw. Intensitäten einzelner Regenereignisse eine Überschreitung der Grenzwerte im Stabilitätsgleichgewicht verursachen.

---

Im Sommer ist hingegen unter Berücksichtigung prognostizierter Klimaänderungen eine Verringerung instabiler zugunsten stabiler Hangbereiche festzustellen. Die berücksichtigte durchschnittliche Erhöhung der Lufttemperatur um 2,5°C hat in Kombination mit einem Rückgang der durchschnittlichen Niederschlagsmenge um 15% eine erhöhte Trockenheit im Substrat zur Folge. Folglich weiten sich stabile Bereiche um rund 11% der Fläche des Untersuchungsgebietes aus. Dieser Effekt ergibt sich im Modell durch eine geringere Niederschlagsmenge, aber auch durch erhöhte Evapotranspiration in Folge des Temperaturanstieges und des dadurch verringerten Zuflusses. Allerdings gilt künftig, trotz insgesamt verringerter monatlicher Niederschlagsmengen im Sommer, eine Zunahme der Niederschlagsintensitäten als wahrscheinlich. In diesem Zusammenhang lassen die Modellierungsergebnisse den Schluss zu, dass häufiger mit einer kurzfristig drastisch erhöhten Rutschanfälligkeit durch Starkregen im Sommer zu rechnen ist.

Die Ergebnisse der komplementären Methoden, werden anschließend zusammengeführt. Aus dieser Synthese kann folgendes Fazit gezogen werden: Die regionale Modellierung der Suszeptibilität ergibt, dass Hänge mit einer Neigung von 26° bis 31° hoch rutschanfällig sind. Die physikalisch-basierten Modellierungen deuten darauf hin, dass in diesem Hangneigungsbereich das Vorkommen quartärer Sedimente für Rutschungen von besonderer Bedeutung ist. Daher kann der Schluss gezogen werden, dass ein erheblicher Teil der im Flysch kartierten Rutschungen eigentlich in quartären Sedimenten aufgetreten sind.

## Summary

The topic of the present study focuses on landslide susceptibility assessment in the Northern Vienna Forest by GIS-based, statistic-probabilistic and deterministic modelling. The study is based on two complementary approaches for integrated landslide susceptibility assessment, which is not limited to one single methodology and its inherent assumptions.

A statistic-probabilistic method is applied to the whole region of the Northern Vienna Forest. This regional model investigates the basic disposition for landslides under consideration of controlling factors, which are persistent and more or less constant over time.

A deterministic method is applied on a larger scale in a sub-study site of the Hagenbach Valley. These detailed models aim to investigate the variable disposition as a function of substrate wetness, which is in turn dependent on meteorological conditions. A main aspect of the work is the development of various wetness scenarios, which consider short-term weather phenomena, like heavy or long-lasting rainfall, but which also investigate the influence of meteorological and climate conditions on slope stability, which may vary in mid-term and long-term.

Furthermore, the assessment of the effects of climate change on the disposition for landslides is a major aspect of the study. Hence, average changes in air temperature and precipitation as predicted by Regional Climate Models are incorporated into modelling. In this context, it is tested whether changes in substrate wetness and thus in slope stability can be identified and quantified as a consequence of changed climate conditions.

As further objective shallow slope movements are incorporated into disposition modelling. According to geomorphological and sedimentological studies, these quaternary sediments are essential for slope formation in the Vienna Forest. In general, it is assumed that landslides primarily occur in weathered flysch sandstones rich in marl. Field-based surveys, however, identified shallow landslide activity in the quaternary sediments covering the flysch bedrock in wide areas. Therefore, the influence of these sediments on slope dynamics is studied in the present work within GIS-based slope stability models.

The results of the statistic-probabilistic landslide susceptibility assessment provide information on the basic disposition of the Northern Vienna Forest for landslides. The resulting regional susceptibility map reveals that the Northern

---

Zone, a tectonic unit in the north of the study area, has extensive areas with the highest degree of landslide susceptibility. In this overthrust area in transition to the Molasse Zone there are geological units which are highly susceptible to landslides. The “Wolfpassing Formation” and the “Calcareous Klippen” of the Northern Zone show significant landslide densities. These geological zones start in the north near St. Andrä-Wördern and continue in south-western direction along the ridges of Tulbinger Kogel, Klosterberg, Frauenberg, and Eichberg.

Statistical weighting carried out in the course of regional landslide susceptibility assessment provides information on the spatial relation between landslide processes and specific controlling factors. The modelling highlights the relevance of zones rich in clay within the flysch formations as controlling geofactor. The highest landslide susceptibility is calculated for the geological units, which contain layers of Gaultflysch rich in clay and shale. Furthermore, a close correlation between the distribution of landslides on the one hand and the spatial distribution of the fault system and nappe boundaries on the other hand is ascertained. Hence, the tectonic conditions can be seen as crucial controlling geofactor for landslide activity in the study area. In the proximity of drainage lines an increased landslide frequency is revealed. In combination with heavy rainfall, torrential discharge can occur in creeks and may cause instabilities in adjacent hillslopes. In addition, the model documents an enhancement of landslide susceptibility on north-west facing slopes. In comparison to meteorological data it is obvious that the north-west exposition corresponds to the prevailing wind direction of the study area. Therefore, north-west facing slopes might be exposed to enhanced advective rainfall amounts, which can increase substrate wetness and thus landslide susceptibility. The latter geofactors indicate the significance of meteorological and hydrological conditions for the occurrence of landslides in the study area.

As described above, the regional assessment is based on controlling factors that are persistent over a long period of time and can therefore be

considered as constant. On the contrary, the large-scale, physically based deterministic modelling investigates the disposition for landslides under variable humidity conditions in the substrate. In conclusion it can be stated that the disposition for slope instability is strongly varying in dependence of the humidity conditions in the substrate. A heavy rainfall event causes a drastic reduction of stable areas by 23% compared to monthly average wetness conditions in summer (July). In summary the wetness scenarios demonstrate, that apart from short-term weather conditions, like long-lasting or heavy rainfall, the long-term-development of substrate moisture has impact on slope stability. The more persistent, seasonally fluctuating wetness conditions show measureable influence on slope stability: As a consequence of increased topographic wetness in the winter month February there is an increase of instable areas by 5% in comparison with the summer month July. The modelling further revealed that quaternary sediments are more moisture sensitive and the influence of changing wetness conditions is stronger in these layers than in the bedrock.

The results of modelling, which are based on climate change, indicate that a moderate change of slope stability on a monthly average is possible in comparison to the conditions of the climate normal period. An assumed average monthly temperature increase of 2°C in combination with a precipitation increase of 30% in the winter months lead to an augmentation of recharge of 7% in the model in comparison with the long-term average conditions. Due to this increased recharge, there is a slight increase of topographic wetness in the model. This wetness augmentation results in an extension of instable slope areas by 3% and a reduction of the stable slope areas proportional to this extension. This slightly increased instability reduces critical triggering thresholds for single rainfall events meaning that even lower precipitation amounts or intensities can cause instabilities.

In contrast to the winter months, the incorporation of forecasted climate change into the modelling reveals a reduction of instable slope areas in favour of stable areas in the

---

summer scenario. The forecasted average air temperature increase of 2.5°C in combination with a reduction of the average monthly precipitation amount of 15% drastically decreases substrate moisture. Consequently, instable slope areas are reduced by 11% of the study area. This effect on slope stability in the model mainly results from the reduced monthly rainfall amounts, but also from increased evapotranspiration as a consequence of the increased air temperature causing reduced recharge amounts. However, in spite of the monthly decrease of precipitation amounts, precipitation intensities are probable to rise according to climate studies. In this context the results of the modelling indicate, that a drastic, short-term increase of landslide disposition due

to heavy rainfall events has to be expected more frequently in summer.

The results of the complementary methods are then assembled. Based on this synthesis the following conclusion can be drawn: The regional landslide susceptibility assessment yields that hillslopes with an inclination of 26° to 31° are highly landslide prone. The physically based models indicate that in this slope gradient range the presence of quaternary sediments is of major importance for landslides. Therefore, it can be concluded that a considerable portion of known landslides mapped in flysch actually occurred in quaternary sediments.

---

# Table of Contents

<b>1</b>	<b>Introduction .....</b>	<b>3</b>
<b>2</b>	<b>State-of-the-art and challenges in landslide susceptibility assessment .....</b>	<b>8</b>
2.1	<i>Geomorphological and inventory analysis.....</i>	9
2.2	<i>Heuristic methods.....</i>	10
2.3	<i>Statistical methods.....</i>	11
2.4	<i>Probability/favourability methods.....</i>	14
2.5	<i>Distribution-free approaches .....</i>	16
2.6	<i>Geotechnical methods .....</i>	17
2.7	<i>Deficits in current methods and challenges .....</i>	18
<b>3</b>	<b>Study area .....</b>	<b>22</b>
3.1	<i>General overview.....</i>	22
3.2	<i>Geomorphological setting.....</i>	24
3.3	<i>Geological and sedimentological setting.....</i>	28
<b>4</b>	<b>Regional landslide susceptibility assessment .....</b>	<b>32</b>
4.1	<i>Methods and Data.....</i>	32
4.1.1	Archive studies for inventory compilation .....	32
4.1.2	Compilation of the controlling geofactors.....	34
4.1.3	Weights-of-Evidence modelling.....	38
4.1.3.1	Model assumptions and statistical parameters.....	38
4.1.3.2	Multi-class generalisation and weighting of the geofactors .....	40
4.1.3.3	Posterior probability and susceptibility index.....	41
4.2	<i>Results.....</i>	42
4.2.1	Results of the inventory compilation and analysis.....	42
4.2.2	Results of weighting of the geofactors.....	46
4.2.2.1	Cumulative analysis of the continuous datasets .....	46
4.2.2.2	Geology.....	48
4.2.2.3	Proximity to tectonic lines .....	52
4.2.2.4	Vegetation cover .....	54
4.2.2.5	Proximity to drainage lines (streams and creeks).....	56
4.2.2.6	Weighting of morphology .....	58
4.2.2.7	Weighting of the topographic position.....	61
4.2.3	Landslide susceptibility index and map.....	62
4.3	<i>Model assessment and validation .....</i>	64
4.3.1	Agterberg-Cheng test of conditional independence.....	64
4.3.2	Success rate and prediction rate.....	65
<b>5</b>	<b>Deterministic slope stability scenarios on large scale.....</b>	<b>66</b>
5.1	<i>Methods and data .....</i>	66
5.1.1	Stability Index Mapping (SINMAP).....	69
5.1.2	Process regions and their soil-mechanical parameters.....	76
5.1.3	Hydrological calculations for the determination of the wetness parameters .....	81
5.1.3.1	Transmissivity.....	81

---

5.1.3.2	“Short-term” recharge.....	82
5.1.3.3	Present-day, “mid-term” recharge.....	83
5.1.3.4	Future, “mid-term” recharge.....	87
5.1.4	Wetness scenarios.....	88
5.1.4.1	Flysch scenario (January).....	90
5.1.4.2	Scenario group - present-day “mid-term” disposition.....	90
5.1.4.3	Scenario group - future “mid-term” disposition.....	93
5.1.4.4	Scenario group- “short-term” disposition.....	96
5.1.5	Visual interpretation of ALS-based shaded relief images (large-scale) for landslide mapping.....	98
5.2	<b>Results.....</b>	<b>100</b>
5.2.1	Landslides in the Hagenbach gorge.....	100
5.2.2	Flysch scenario (January).....	102
5.2.3	Wetness scenario group “present-day, mid-term disposition”.....	107
5.2.3.1	Winter scenario (January).....	107
5.2.3.2	Winter scenario (February).....	112
5.2.3.3	Summer scenario (July).....	115
5.2.4	Wetness scenario group “future, mid-term disposition”.....	120
5.2.4.1	Future winter scenario (January).....	120
5.2.4.2	Future winter scenario (February).....	124
5.2.4.3	Future summer scenario (July).....	128
5.2.5	Wetness scenario group “short-term disposition”.....	132
5.2.5.1	Critical rainfall scenario.....	132
5.2.5.2	Heavy rainfall scenario.....	136
<b>6</b>	<b>Comparison.....</b>	<b>141</b>
6.1	<i>Flysch scenario (January) and winter scenario (January).....</i>	141
6.2	<i>Summer scenario (July) and winter scenario (February).....</i>	147
6.3	<i>Future summer scenario (July) and future winter scenario (February).....</i>	152
6.4	<i>Present-day summer scenario (July) and future summer scenario (July).....</i>	157
6.5	<i>Present-day winter scenario (January) and future winter scenario (January).....</i>	162
6.6	<i>Summer scenario (July) and critical rainfall scenario.....</i>	167
6.7	<i>Summer scenario (July) and heavy rainfall scenario.....</i>	172
<b>7</b>	<b>Discussion.....</b>	<b>177</b>
7.1	<i>Landslide inventory for the Northern Vienna Forest.....</i>	177
7.2	<i>Regional landslide susceptibility assessment.....</i>	178
7.3	<i>Local slope stability scenarios.....</i>	184
7.4	<i>Synthesis.....</i>	189
	<b>References.....</b>	<b>190</b>
	<b>Table of figures.....</b>	<b>206</b>

---

# 1 Introduction

In the alpine countries, such as Austria, geomorphological processes are responsible for a high risk in many regions (Rudolf-Miklau 2009, Rudolf-Miklau et al. 2011, Schweigl & Hervas 2009). Mass movements cause considerable economic loss and damage to properties, infrastructures, environment and human settlements. In Austria the Alps comprise 62% of the territory, and the foothills at the base of the Alps and Carpathians cover an additional 12%. Therefore, mass movements of different types are frequent and widespread in the country. Although large mass movements are rare in Austria, the resulting economic loss is huge because of the high number of small events which cause considerable damage to infrastructure and arable land (Schwenk et al. 1992).

According to Rudolf-Miklau et al. (2011) the vulnerability to landslide hazard is rising due to the spatial extension of endangered areas, which is a consequence of the rising settlement pressure and area consumption, the higher density of transportation routes in the Alps and their foreland as well as growth rates in tourism (Rudolf-Miklau 2009, Rudolf-Miklau et al. 2011, Schweigl & Hervas 2009).

The main natural triggering factors of landslides in Austria include long-lasting heavy rainfall and rapid snow melting (Schweigl & Hervas 2009). In this context also climate change studies gain more relevance in landslide hazard research. Several studies show that changing climate conditions can affect the frequency and magnitude of landslides due to increased precipitation rates, particularly in the winter months, and raised air temperature (Collison et al. 2000, Trauth et al. 2000, Soldati et al. 2004, Jakob & Lambert 2009).

Research related to mass movements mainly concentrates on the high alpine region in Austria, particularly on rock falls and debris flows. Nevertheless, numerous landslides occur in subdued mountains but there are only few landslide studies in the low mountain regions. Hence, the study area of the present doctoral thesis represents an undulating landscape in a low mountain region, located in flysch areas of the Vienna Forest region (Lower Austria and Vienna). In the Flysch Zone landslides are the dominating mass wasting processes (95%) (Schwenk et al. 1992, Wessely 2006). Compared to the other geological zones in Austria, the Flysch Zone is most frequently affected by landslides due to the geological situation (Schwenk et al. 1992). Although they constitute only 9% of Lower Austria (including the Klippen Zone), 61% of all landslides in Lower Austria are situated in flysch areas (Schwenk et al. 1992). Different types of mass movement occur in the Northern Vienna Forest region and create damage to infrastructure, buildings and building grounds (cp. Figure 1-1).

In the Northern Vienna Forest landslides frequently occur in weathered flysch bedrock. However, recent geomorphological studies showed that landslides also occur in quaternary sediments covering the bedrock in wide areas (Damm & Terhorst 2010). An example for a deep-seated landslide in weathered flysch bedrock happened in 2011 in the municipality of Purkersdorf in the immediate vicinity of a settlement area. The landslide was initiated after a period of abundant rainfall in spring 2011. The slide mass was deposited into a creek near a building ground and caused a high risk of flooding in the drainage line and the adjacent settlement areas (cp. Figure 3-4, page 27).

An example of a large landslide in the quaternary sediments happened in the Hagenbach gorge ("Hagenbachklamm"), a famous recreation and hiking area in the Vienna Forest in 1996. In general, the hillslopes of the Hagenbach valley in the municipality of St. Andrä-Wördern are affected by different types of mass movements. Besides events of rock fall and shallow to deep-seated landslides

in the bedrock, there are also landslides in the quaternary sediments. The landslide in 1996 occurred in loess surface formation on top of basal clays and marls after a period of long-lasting rainfall (cp. Figure 3-5, page 27). The landslide destroyed a wooden bridge and caused a log jam in the creek. In general, hiking paths and wooden bridges need to be maintained regularly in the Hagenbach gorge because of damage due to mass movements (cp. Figure 1-1). In spring 2014 the Hagenbach gorge was closed again due to extensive damage and the high risk for landslides.



Figure 1-1. Damage caused by mass movements in the Northern Vienna Forest: (A) destroyed bridge in the Hagenbach Valley, (B) damaged road in the study area, (C) announcement “No trespassing because of a destroyed bridge”, (D) No vehicles: “road closed because of landslide”. Photos: (A, C) B. Neuhäuser, (B, D) Department of Torrent and Avalanche Control.

In general, the awareness of landslides as a hazardous process has initiated mitigation and prevention efforts in Europe in the last twenty years (Rudolf-Miklau et al. 2011). The first stage in prevention represents the landslide susceptibility assessment which covers the hazardous processes and their spatial occurrence within an area of interest (Varnes 1978, Carrara et al. 1999, Fell et al. 2008). Hence, landslide susceptibility assessment is considered as a fundamental basis for landslide hazard assessment. It is usually determined on the basis of a set of controlling or preparatory geofactors and the distribution of previous, known landslides (Brabb 1984, Soeters & Van Westen 1996, Aleotti & Chowdhury 1999, Carrara et al. 1999, Chung & Fabbri 2003, Neuhäuser & Terhorst 2007, Kanungo et al. 2008). Landslide susceptibility maps can provide useful information and economic benefits for urban planning, development plans, engineering applications, land use planning and prevention (Carrara et al. 1999, Damm & Pflum 2004, Chung & Fabbri 2003, Schweigl & Hervas 2009). Nevertheless, there is no legal framework for the compilation of landslide

---

susceptibility maps in Austria. Although there is a legal framework for the assessment of floods, debris flow and avalanches, no regulations or laws concerning the compilation of landslide hazard or susceptibility maps exist at present (Bäk et al. 2011, Rudolf-Miklau et al. 2011). The legal framework in relation to floods, debris flow and avalanches includes the generation of the Hazard Zone Plan (“Gefahrenzonenplan”) by the Austrian Service for Torrent and Avalanche Control. This plan serves as a legal basis for land use planning of the municipalities concerned, as well as for the construction and security sectors. In this Hazard Zone Plan landslides are indicated only occasionally and in a generic way (as brown zones) with a merely indicative character. Therefore, landslide hazard is fragmentary and incompletely recorded in the Hazard Zone Plan (Pomaroli et al. 2011).

Due to the increasing importance of landslide susceptibility and hazard maps, the Geological Survey is developing a comprehensive hazard map for gravitated mass movements for the whole province of Lower Austria (Pomaroli et al. 2011). In this small-scale hazard map all geological zones of Lower Austria are integrated, but there is no specific assessment of flysch areas in relation to landslide evolution. In the Vienna Forest mass movements are registered by authorities dealing with mitigation measures, like the Austrian Service of Torrent and Avalanche Control or the Geological Survey of the Provincial Government of Lower Austria. Nevertheless, a regional landslide susceptibility map for the Northern Vienna Forest is not available.

A regional, geomorphological study of landslides, which concentrates on the area of the Vienna Forest, dates back to the works of Gustav Götzing in 1943 (Götzing 1943). Furthermore local geomorphological studies were carried out in the region (i.e. Damm et al. 2008, Terhorst et al. 2009, Damm & Terhorst 2010) with the aim to identify causes for landslides and to reconstruct the evolution and the sequences of sliding processes on a local scale. However, there is neither a regional approach for mapping and delineation of areas susceptible to landslides nor an assessment of spatial and temporal distribution of landslides related to specific disposition factors, which is focused on the region. Consequently the knowledge about landslide evolution and causes in the Vienna Forest Flysch Zone is limited.

According to the research status in the study area, as mentioned above, and the identified deficits in susceptibility modelling (cp. chapter 2.7 “Deficits in current methods and challenges), the following objectives are defined:

- (1) **Integrated approach to landslide susceptibility assessment:** An integrated assessment of landslide susceptibility is aspired, which is not limited to a single modelling approach. This objective is related to the fact that one of the shortcomings in landslide susceptibility applications is incompleteness due to the specific theoretical background of the selected modelling approach. Each model contains inherent assumptions and limited validity ranges of the used parameters, as a consequence the model is incomplete related to reality (Bailer-Jones 2002). Therefore, two dissimilar approaches applied from a small to a large scale are used. More precisely, a statistical-probabilistic method, first proposed by Bonham-Carter et al. (1989) and Bonham-Carter (2002) as well as a deterministic method based on the slope stability approach developed by Pack et al. (1998, 2005) are applied. By the application of two dissimilar modelling approaches the synthesis of the results shall provide a more complete assessment of the landside phenomenon in the study area.

- 
- (2) **Compilation of a landslide inventory for the Northern Vienna Forest:** A main objective of this study is the compilation of a comprehensive landslide inventory for the Northern Vienna Forest because the spatial occurrence of landslides is the fundamental basis for landslide susceptibility assessment. Landslide inventories represent the spatial distribution of landslides mapped on the basis of geomorphological field surveys, archive data on landslide occurrences or by means of remote sensing data (Wieczorek 1984, Soeters & Van Westen 1996, Aloetti & Chowdhury 1999, Van Westen 2004, Kanungo et al. 2008). A landslide inventory is the basis of subsequent modelling of landslide susceptibility.
- (3) **Regional landslide susceptibility assessment by a statistical/probabilistic modelling approach:** The aim is the delineation of landslide prone areas and the assessment of landslide susceptibility for the whole region of the Northern Vienna Forest. The landslide susceptibility shall be assessed after integration of various preparatory geofactors, which indirectly condition or control landslide activity in the study area. The statistical/probabilistic method, referred to as Weights-of-Evidence (WofE) (Agterberg et al. 1990, Bonham-Carter et al. 1989, Bonham-Carter 2002, Sawatzky et al. 2009) is applied in the GIS-environment in order to derive quantitative spatial information on the predisposition to landslides. This method is selected because it is able to handle aspects of uncertainty in susceptibility quantification. Apart from validation, the treatment of uncertainty is regarded as crucial quality criterion, which is often lacking (Chung & Fabbri 2003, Remondo et al. 2003, Van Westen et al. 2003, Fell et al. 2008). Specific objectives are defined for the regional approach, which are:
- **Assessment of the basic disposition to the occurrence of landslides:** The objective is to provide information - on a regional scale - on the basic disposition of the Northern Vienna Forest to develop landslides. The basic disposition describes the principal tendency of slopes to move, which is a result of the prevailing geofactors preparing mass movements. These geofactors can be regarded as static, i.e. as more or less constant over time.
  - **Creation of new knowledge on the preparatory geofactors:** The target is to gain new knowledge related to the landslide evolution in the Northern Vienna Forest by the assessment of spatial distribution of landslides with regard to specific preparatory geofactors, which steer or prepare mass movements.
  - **Provision of a regional landslide susceptibility map:** The aim is to delineate landslide prone areas in the study area and to provide a regional landslide susceptibility map.
- (4) **Development of local slope stability scenarios based on a physically based approach:** The objective is to further investigate the landslide phenomena by physically based slope stability scenarios in a selected valley in the Northern Vienna Forest. In contrast to the regional approach, the local modelling approach assesses the landslide susceptibility on the basis of geotechnical slope stability calculations. The applied slope stability assessment approach is based on Stability Index Mapping (SINMAP) according to Pack et al. (1998, 2005), but needs to be applied in an adapted manner. The specific aims of this approach are:

- 
- **Assessment of the variable disposition by means of wetness scenarios:** The development of various wetness scenarios for a comprehensive assessment of slope stability is a main aspect of this physically based approach. The objective is to investigate the variable landslide disposition as a function of different wetness conditions in sediments and unconsolidated rock. Variable disposition depends on conditions changing in the short and medium term, like substrate moisture, which varies according to meteorological conditions (Zimmermann et al. 1997, Heckmann & Becht 2006). Single precipitation events as well as monthly averages of precipitation are to be integrated for the assessment of substrate wetness. Thus, both short-term conditions due to singular weather events like abundant or heavy rainfall and mid-term conditions due to average monthly wetness conditions shall be considered in the scenarios.
  - **Incorporation of shallow landslides within the quaternary sediments:** A further objective is the integration of shallow slope movements occurring in the quaternary sediments of the Vienna Forest into disposition modelling. By virtue of the past research experience it is generally assumed in the science community that landslides primarily occur in the marl-rich weathered flysch sandstones (Götzinger 1943, Plöchinger & Prey 1993, Faupl 1996, Schwenk et al. 1992). The importance of these deep-seated movements is evident. Field surveys, however, identified shallow landslide activity in the quaternary sediments covering the flysch bedrock in wide areas (Damm et al. 2008, Terhorst et al. 2009, Damm & Terhorst 2010). The aim is to assess the relevance of quaternary sediments for slope dynamics in the Vienna Forest. In this context the target is the development of a site-specific process model which is able to incorporate movements into the quaternary deposits and the flysch bedrock, as well.
  - **Assessment of the impact of varying, long-term substrate wetness in the seasonal course:** The objective is to investigate if long-term substrate wetness has an influence on slope stability during the seasonal course. Long-term substrate moisture is still insufficiently integrated into slope stability and susceptibility assessment in current practice applications. Usually, single precipitation thresholds serve as the basis for the assessment of the hydrological conditions. Therefore, the development of a methodology to incorporate monthly averages of precipitation and air temperature into slope stability scenarios is pursued.
  - **Assessment of the impact of climate change on slope stability:** The objective of the present work is to investigate the influence of changing climate conditions on slope stability. In slope stability scenarios average changes in air temperature and precipitation, as predicted by Regional Climate Models (cp. Loibl et al. 2007, Reclip:more 2007, Formayer et al 2009), shall be considered. The target is to study whether changes in climate conditions affect substrate wetness and consequently slope stability and whether these changes can be quantified in slope stability models. Despite the growing relevance of changing climate conditions for landslide evolution, climate change is hardly included into landslide susceptibility studies at present.

---

## 2 State-of-the-art and challenges in landslide susceptibility assessment

Landslide susceptibility is defined as the degree to which a specific area is endangered by a hazardous process with regard to its spatial occurrence but without regarding the temporal likelihood (Brabb 1984, Hutchinson 1988, Soeters & Van Westen 1996, Cruden & Varnes 1996, Fell et al. 2008, Rudolf-Miklau et al. 2011). Susceptibility does not consider the temporal probability of failure, which belongs to the domain of landslide hazard. Consequently, landslide susceptibility does not include information on frequency (annual probability) of landslide occurrence (Brabb 1984, Cruden & Varnes 1996, Soeters & Van Westen 1996, Aleotti & Chowdhury 1999, Fell et al. 2008).

Landslide susceptibility assessment or zoning is focused on the classification, spatial extension (area) and spatial distribution of existing and potential landslides in the study area (Soeters & Van Westen 1996, Fell et al. 2008). Susceptibility zoning involves the rating of the terrain units according to their disposition to develop landslides with the aim to predict future events (Brabb 1984, Soeters & Van Westen 1996, Aleotti & Chowdhury 1999, Fell et al. 2008, Van Westen et al. 2008, Kanungo et al. 2009).

Landslide susceptibility can be assessed heuristically or statistically on the basis of a landslide inventory and the conditional or preparatory geofactors. In these approaches landslide susceptibility is usually expressed as probability of landslide occurrence or as relative degree of landslide proneness. Landslide susceptibility can also be investigated by physically based approaches focusing on slope stability. In these methods susceptibility is expressed as factor of safety or as probability of slope failure (Soeters & Van Westen 1996, Fell et al. 2008, Van Westen et al. 2008, Jemec & Komac 2011).

There is no clear consensus in the research field whether landslide susceptibility assessment may also include the magnitude of mass movements. However, recent approaches in landslide susceptibility assessment also contain a description of the travel distance, velocity and intensity of existing or potential landslides (Fell et al. 2008, Van Westen et al. 2008).

Landslide susceptibility assessment is focused on causal factors for slope movements. Triggers of landslides are not directly incorporated. However, it is crucial to distinguish between landslide triggers and their causes (Cruden & Varnes 1996). According to Dikau et al. (1996) the causes are defined as cumulative events which prepare a slope for the movement but do not necessarily trigger it. Therefore, they are also referred to as internal causes, conditional or preparatory factors, steering factors, causal or controlling factors. Contrary to this, triggers are processes which provoke instability, i.e. which actually activate the landslide (Dikau et al. 1996). The trigger is an episodic event, like a heavy rainfall event or intensive snowmelt, which induces the exceedance of parameter thresholds in slope stability.

In general, the methods used for landslide susceptibility assessment are based on spatial modelling by means of GIS. In the late seventies and early eighties GIS-based methodologies were applied for landslide hazard and susceptibility assessment for the first time (Carrara et al. 1982, Brabb et al. 1984). Important developments were achieved in the last twenty years, mainly driven by the progress in geoinformatics and remote sensing technologies. These techniques providing terrain and land information data in increasing quality and accuracy are applied among many others by

---

Nagarajan et al. (2000), Liu et al. (2004), Süzen (2002), Neuhäuser & Terhorst (2007), Van den Eeckhaut et al. (2007), and Neuhäuser et al. (2012).

Landslide susceptibility assessment approaches are usually divided into several major groups as qualitative and quantitative methods, experience-based and data-driven methods, or direct and indirect methods (Soeters & Van Westen 1996, Carrara et al. 1999, Aleotti & Chowdhury 1999, Fell et al. 2008, Kanungo et al. 2009).

Qualitative approaches assess susceptibility in qualitative classes, like “no, moderate, high susceptibility” without providing quantitative information on the degree of susceptibility. Methods of this qualitative group are inventory (or distribution) analysis and geomorphological analysis, which are experience-based because expert knowledge is used to assess susceptibility (Soeters & Van Westen 1996).

Quantitative methods deliver a quantitative value of landslide susceptibility and range from expert-based rating to complex statistical, mathematical, and logical systems. According to Van Westen et al. (2003) and other authors (e.g. Soeters & Van Westen 1996, Aleotti & Chowdhury 1999, Fell et al. 2008, Kanungo et al. 2009, Jemec & Komac 2011) some major groups of methods can be distinguished, which are summarised in the following paragraphs.

In the following a summary on existing methods, identified deficits and research challenges is provided. The summary is based on comparative studies in the research field, i.e. Varnes (1984), Soeters & Van Westen (1996), Aleotti & Chowdhury (1999), Guzzetti et al. (1999), Carrara et al. (1991), Dai et al. (2002), Chung & Fabbri (2003), Remondo et al. (2003), Van Westen et al. (2003), Suzen & Doyuran (2004), Van Westen (2004), Van Westen et al. (2006), Fell et al. (2008), Glade et al. (2005), Kanungo et al. (2008), and Jemec & Komac (2011).

## **2.1 Geomorphological and inventory analysis**

The traditional approach of landslide susceptibility assessment corresponds to a direct geomorphological analysis where an expert estimates the actual and potential slope failure in field surveys (Carrara et al. 1999, Guzzetti et al. 1999, Terhorst 2001).

The basis for geomorphological analysis was described in the seventies by Kienholz (1977), who elaborates a method for the development of a combined susceptibility map based on the mapping of silent witnesses (“stumme Zeugen”) (Aleotti & Chowdhury 1999, Fell et al. 2008, Kanungo et al. 2009). In the eighties and nineties geomorphological maps were produced by field mapping and/or the visual interpretation of stereoscopic aerial photographs (cf. Brunsden 1993, Turner & Schuster 1996). The increasing availability and accuracy of remote sensing data allow the exploitation of new technologies to detect and identify landslides over larger areas. An overview of recent and new techniques is given in Guzzetti et al. (2012). Such recent techniques include, the analysis of surface morphology by the use of high resolution digital elevation models (DEMs) (Van Den Eeckhaut et al. 2007, Hangeberg et al. 2009, Neuhäuser et al. 2010) on the one hand. On the other hand, satellite images, including panchromatic, multispectral and synthetic aperture radar (SAR) images, are interpreted and analysed (Marcelino et al. 2009, Gao & Maroa 2010, Fiorucci et al. 2011). Recent methodologies concentrate on three-dimensional visualisation of stereoscopic satellite images, techniques for semi-automatic detection of landslide features from the analysis of high-resolution DEMs (e.g. Passalacqua et al. 2010, Tarolli et al. 2010), object-oriented image classification methods (e.g. Martha et al. 2010, Lu et al. 2011, Stumpf & Kerle 2011), and multiple change detection techniques (e.g. Mondini et al. 2011) for the semi-automatic detection of landslides. Landslide

---

identification and mapping by geomorphological studies, either by direct expert judgment or remote-sensing supported approaches, are important and indispensable steps in landslide susceptibility assessment. They form the basis for inventories and quantitative methods for landslide susceptibility zoning (Aleotti & Chowdhury 1999, Fell et al. 2008, Kanungo et al. 2009). However, direct assignment of purely qualitative susceptibility zones remains a shortcoming, even if decision rules for the assessment of susceptibility are based on profound expert knowledge and site-specific conditions. Decision rules are often not visible for end users and are highly depending on the subjective judgement of an expert. Besides, updating of maps is difficult as new data become available (Kanungo et al. 2009). As the direct assessment is very time-consuming, this method is not suitable for large areas. Due to the emerging spectrum of quantitative assessment approaches, the direct geomorphological analysis is applied for studying specific sliding processes, but not as a susceptibility assessment method per se today.

The distribution or inventory analysis investigates the spatial distribution of existing landslides mapped from geomorphological field surveys or historical data of landslide occurrences (Wieczorek 1984, Neuhäuser et al. 2010). In general, landslide inventories provide the fundamental basis for subsequent landslide susceptibility assessment approaches. However, in some investigations the landslide inventory is used as landslide density map providing information on favourable locations for slope movement and therefore on landslide proneness (e.g. Wieczorek 1984, Cardinali et al. 2001, Trigila et al. 2010).

Landslide inventory maps do not provide quantitative information on the degree of landslide proneness. They offer information on landslide activity at a specific date in a specific area (Kanungo et al. 2009). However, they are an indispensable and crucial base for further modelling of landslide susceptibility. The creation of landslide inventory maps is strongly supported by new remote sensing technologies, as described in the following paragraphs.

## **2.2 Heuristic methods**

In some classification systems heuristic methods are referred to as “map combination approaches” or “index methods” (Aleotti & Chowdhury 1999, Kanungo et al. 2009). Heuristic methods do not directly evaluate the hazard, but indirectly by means of causal factors, which are weighted by an expert. They are experience-based because they require process knowledge gained by detailed studies and field observation (Carrara et al. 1999).

The preparatory, causal factors are identified and mapped. Based on personal experience the investigator assigns weights to the factors, which are proportionate to their relative importance for slope failure. Based on this weighting a susceptibility index is computed by an algebraic function. The most common form is the linear weighted addition (Soeters & Van Westen 1996, Aleotti & Chowdhury 1999, Van Westen 2004, Kanungo et al. 2009).

In general, weights are assigned by normalisation procedures, which transfer the values of classes to a consistent form in order to make all geofactor maps comparable with each other (Malczewski 1999, Ruff & Czurda 2007, Bathrellos et al. 2009). This is the precondition for a combination of layers to a final index map. There are many different methods for data normalisation. The simplest method is the assignment of new values ranging from 0 to 100, depending on the importance of a factor. Another common approach is the linear transformation, which is especially suitable for continuous data. The most frequently used method is the maximum score procedure where each value is divided by the maximum value of the data layer (Malczewski 1999). After normalisation the values of each

---

data layer range from 0 to 1. The advantage of this method is that values remain proportionally equal after normalisation (Malczewski 1999). Apart from the linear transformation other methods can be applied for normalisation, e.g. the value/utility equation, probabilities or fuzzy sets (Zadeh 1965).

Afterwards, a total assessment of the hazard is carried out by combination of normalised, weighted causal factors. The most popular approach is the simple additive weighting based on the weighted linear addition (Malczewski 1999, Ruff & Czurda 2007). Apart from the four fundamental algebraic operations addition, subtraction, multiplication, and division, any other arithmetic or statistic operation methods can also be used for combination (Castellanos Abella & Van Westen et al. 2008, Barredo et al. 2000, Perotto-Baldiviezo et al. 2004).

An early example of this methodology is reported by Stevenson (1977), who developed a heuristic formulation to assess geotechnical parameters. Examples for recent heuristic methods are the studies of Castellanos Abella & Van Westen (2007, 2008), and Bathrellos et al. (2009), who apply a multi-criteria decision matrix as weighting system. Ruff & Czurda (2007) use an index-based system and additive combination of data layers to assess the landside susceptibility. Other studies employing this experience-based approach are Barredo et al. (2000), Perotto-Baldiviezo et al. (2004), and Firdaini (2008).

The heuristic approach eliminates the shortcoming of “hidden rules” as given in the geomorphological approach (Aleotti & Chowdhury 1999). Due to weighting and algebraic combination a comprehensible assessment model exists (Aleotti & Chowdhury 1999, Kanungo et al. 2009). In principle, this technique can be used for any scale. However, the length of the operations inflates with the size and complexity of the study area. Furthermore, there can be subjective intervention, when weights are assigned to geofactor classes (Aleotti & Chowdhury 1999).

## **2.3 Statistical methods**

Equal to heuristic methods, statistical methods assess landslide susceptibility indirectly on the basis of causal factors that control and prepare a landslide. However, the weighting is not done on expert based assignment but on the basis of statistically measured relationship between each factor and the known landslide locations. Consequently, the knowledge of actual and past mass movements is required (Carrara 1983, Carrara et al. 1995, Van Westen et al. 2003). The relationships between causal factors and mapped landslides are quantified by means of statistical indices. The objective is to identify those factor combinations that caused landslides in the past and present. Degree as well as quality (significance) of spatial relationships between geofactors and landslides can be described and weights can be derived. The landslide susceptibility index is derived from a combination of all weighted causal factors. Thereby, it is possible to gain quantitative assessment on landslide proneness in areas where no landslides have occurred, or at least none are known, but similar causal factors are present (Aleotti & Chowdhury 1999, Fell et al. 2008, Kanungo et al. 2009).

The major challenge in this method group is to systematically identify and assess preparatory factors related to landslides (Carrara 1983, Carrara et al. 1991). These cause-effect relationships are often complex and interrelated (Aleotti & Chowdhury 1999). Various statistical approaches adopted to analyse the spatial relationship between factors and landslide sites are available. In principle, they can be divided into (i) bivariate methods and (ii) multivariate methods (e.g. Soeters & Van Westen 1996, Fell et al 2008, Aleotti & Chowdhury 1999, Kanungo et al. 2009).

As this assessment is also data-driven, subjectivity can be more or less excluded and a high transparency in the assessment is given. Susceptibility is rated more objectively compared with

---

heuristic methods because factors and their interrelationships are evaluated on a statistical basis (Aleotti & Chowdhury 1999, Fell et al. 2008). A problem which arises during the application of multivariate methods like logistic regression as well as discriminant analysis is the fact that the investigated statistical groups differ strongly from each other. As landslides are rather rare events, the group including landslides is much smaller than the group without landslides (Soeters & Van Westen 1996, Aleotti & Chowdhury 1999, Fell et al. 2008, Kanungo et al. 2009). However, multivariate methods are suitable for an investigation of groups that are rather similar in size. As a consequence, the probabilities are often underestimated by these methods (Begueria & Lorente 1999). In bivariate statistical methods a high density of landslides within a rather small geofactor variable leads to an inflation of the probabilities, resulting in an overestimation in absolute terms (Neuhäuser & Terhorst 2007, Neuhäuser et al. 2010).

Bivariate statistical methods analyse the relation of one independent (preparatory factors for landslides) and one dependent variable (landslides). Once a statistically significant relationship between the variables is identified, a causal connection between two variables can be assumed. In case of landslide susceptibility assessment the relation between steering factors and landslides is investigated and quantified (Soeters & Van Westen 1996, Aleotti & Chowdhury 1999, Van Westen et al. 2003, Fell et al. 2008, Kanungo et al. 2009). Bivariate statistical approaches analyse each factor separately by combining them one by one with the landslide sites. Statistical parameters quantify the spatial relation of landslide distribution and single geofactors and in such way that weighting can be derived. In most of the applications, weighting is based on frequency or density of landslides within geofactor classes. The combination of weighted factors results in the hazard or susceptibility index (Aleotti & Chowdhury 1999).

One of the early methods in bivariate statistical modelling, mainly used in the nineties, is the Frequency Analysis Approach (e.g. Pachauri & Pant 1992, Mehrotra et al. 1996). There the normalised frequency distribution of landslides is determined per unit area for all classes of geofactors. By overlaying the landslide inventory with each of the geofactors separately, the frequency values are derived per geofactor class. The frequency values represent a rating of the geofactor classes. These ratings and weights for the factors and their categories are combined to create a landslide susceptibility map (Soeters & Van Westen 1996, Aleotti & Chowdhury 1999, Kanungo et al. 2009).

A further commonly used method is to utilise landslide density in each variable class as basis for the weighting of geofactors. In many studies this approach is referred to as Information Value Approach (infoVal) and is applied, among others, by Yin & Yan (1988), Van Westen et al. (1997), Lin & Tung (2003) and Saha et al. (2005). In these particular cases, the area density is calculated by dividing the number of pixels in the causal factor that contains a landslide through the total number of pixels within each variable class. In order to assess the influence of each variable class, the density per class is related to the total landslide density in the study area. This relation is transferred to a logarithmic scale (Van Westen et al. 1997). By the application of the density relation the resulting value can be considered as the probability of landslide occurrence within each class of a geofactor. It represents the weighting of geofactors with respect to their importance for landslide occurrence. Finally, weights are combined to compose a final susceptibility index (Soeters & Van Westen 1996, Aleotti & Chowdhury 1999, Kanungo et al. 2009).

Another similar approach is known as Landslide Nominal Susceptibility Factor (LNSF) used by Gupta & Joshi (1990) and more recently by Saha et al. (2005). The statistical relationships between geofactors

---

and landslides are assessed by the ratio of a landslide number in a particular geofactor class and an average landslide number in various categories of that factor.

In contrast to bivariate methods, multivariate statistics investigate the combined influence of causal factors on landslide evolution. There are many different methodical approaches within multivariate statistics. The most commonly used methods in geosciences are multiple logistic regression analysis and discriminant analysis (Soeters & Van Westen 1996, Aleotti & Chowdhury 1999, Van Westen et al. 2003, Fell et al. 2008, Kanungo et al. 2009). Further multivariate methods are factor analysis and cluster analysis. One of the important criteria to select the appropriate method is the measurement scale and statistical distribution of variables.

The multiple logistic regression is a well-tested and commonly used method for landslide susceptibility assessment. The method does not require normal distribution of the variables as other statistical methods. This fact is a major advantage because most of the topographic geofactors are not normally distributed. Therefore, logistic regression is widely applied among others by Atkinson & Massari (1998), Guzzetti et al. (1999), Gorsevski et al. (2000), Lee & Min (2001), Dai et al. (2001), Dai & Lee (2002), Thein (2000), Ohlmacher & Davis (2003), and Ayalew & Yamagishi (2005). The aim of these studies is to statistically “explain” landslide occurrences, which represent the target variables. At the same time the impact of the causal factors, which represent the explaining variable, on the evolution of landslides is statistically investigated. Usually, regression analysis delivers a target value with Boolean character, with values of either zero or one. As a quantitative description of the relationship between geofactors is aspired in susceptibility studies, the probability of the target variable is used instead of the target variable itself. When probabilities are applied, the target variable can have any positive value. Probability is usually expressed in probability ratios (odds). For logistic regression the natural logarithm of probability ratios, the logits are applied. A linear relationship between logits and independent variables is assumed. By gradually adding or deleting variables to this regression equation, the quality of the model is tested by the variation of the chi-square value, which serves as a measure for the quality of the prediction. Consequently, factors with optimal values can be selected and integrated into the final model. As soon as the regression equation is determined, it is used to calculate probabilities for future landslides for the whole study area.

Discriminant analysis is similar to regression analysis except that the dependent variable is categorical rather than continuous. First introduced by Fisher (1936), discriminant analysis classifies samples into alternative groups on the basis of a set of measurements. In general, the objective is to investigate whether and how complete different groups can be divided and classified. In case of landslide susceptibility applications an optimal separation of pixels or terrain units into those containing and not containing landslides is targeted.

For landslide susceptibility assessment the mentioned method was utilised among others by Reger (1979), Carrara et al. (1982, 1991), Begueria & Lorente (1999), Guzzetti et al. (1999, 2005, 2006a), Nagarajan et al. (2000), Baeza & Corominas (2001), Cardinali et al. (2002b), Santacana et al. 2003, Baeza & Corominas (2001), Santacana et al. (2003), and Van den Eeckhaut (2009).

In a first step the whole study area is to be classified into two groups, which are defined either as (i) areas free of landslides (stable terrain), or (ii) areas containing landslides (unstable terrain). The basic assumption in discriminant analysis states that the two groups are distinct and that a mapping unit belongs to one group only (e.g. Baeza & Corominas 2001, Santacana et al. 2003, Van den Eeckhaut 2009). The scope of the analysis is to determine the group membership of a mapping unit by identifying a linear combination of the geofactors (independent), which maximises the differences

---

between stable and unstable units (Van den Eeckhaut 2009). In this process the discriminate function is estimated by optimally dividing the two groups. The geofactors are the basis for the formulation of this function (Gorsevski et al. 2000). The resulting model is adjusted in order to divide mapping units into appropriate groups with minimal error. The standardised discriminant function coefficients can be used to evaluate the relative contribution of each geofactor to the discriminating function and consequently to the occurrence of landslides (Aleotti & Chowdhury 1999). The classification system is most commonly used with probabilities and is subsequently applied to all terrain units in the area. The final susceptibility map shows the expected spatial probability of landslide occurrence (Guzzetti et al. 2006a).

## 2.4 Probability/favourability methods

Favourability functions are often used in combination with statistical approaches. Therefore, a strict separation of the two groups is not always applicable (Soeters & Van Westen 1996, Aleotti & Chowdhury 1999). Nevertheless, they are often treated as separate groups of methods. The term favourability function was introduced by Chung & Fabbri (1993, 2003) as overall term for those mathematical basics, which are applied for spatial prediction modelling. Similar to statistical methods the relationship between landslides and geofactor classes forms the basis for landslide susceptibility assessment (Kanungo et al. 2009). According to the applied favourability function it is possible to derive an index which represents the degree of probability, reliability, belief or plausibility that the specific unit or pixel is part of a landslide in future (Ghinoi 2003, Kanungo et al. 2009). The favourability function can be estimated in different ways, depending on the availability of data and the basic assumptions of the modelling process. Examples of such models are developed by Shortliffe & Buchanan (1975), Bonham-Carter (1994), and Chung (2006). These approaches are outlined in the following paragraphs.

Favourability modelling comprises quantitative methods where expert knowledge can be incorporated, particularly when data are not sufficient or reliable. In this modelling approach thematic data can be transformed into continuous data by considering the degree of relationship between landslides and categories of each thematic data layer. Each continuous or non-continuous category can be transformed into a value, called favourability value, representing the degree of susceptibility. The major restriction results from the inherent assumptions of the specific methodology (Kanungo et al. 2009).

The Certainty Factor Approach (CF) is a simple and effective approach which uses a favourability function embedded in the conditional probability framework. The method was originally proposed by Shortliffe & Buchanan (1975) and later modified by Heckerman (1986). In general, probabilities are estimated based on knowledge of the occurrence of events in the past under similar conditions. This probability is called prior probability. In landslide susceptibility assessment it is estimated on the basis of the total number of landslides occurring in the study area. The prior probability can be modified by the occurrence of specific controlling geofactors, which influence the evolution of landslides and consequently the probability of landslide occurrence (Malczewski 1999). If these additional geofactors are integrated into the assessment of probability, it is addressed as conditional probability or posterior probability. The conditional probability describes the probability of occurrence of an event under the prerequisite that specific factors are present. The Certainty Factor describes the conditional probability for landslides within the geofactor classes in relation to the prior probability. The method is applied, among others, in Chung & Fabbri (1993), Lan et al. (2004), Damm et al. (2010), and Sujatha et al. (2012). A major advantage of this method is that the Certainty

---

Factor enables a coherent interpretation of the importance of factors: Whereas a negative Certainty Factor corresponds to a decreasing certainty of landslide occurrence in the specific geofactor variable, a positive Certainty Factor corresponds to an increasing certainty that landslides will occur in the specific variable. The derived probabilities of geofactor classes are finally integrated into the probability function to derive a combined susceptibility index.

The Weights-of-Evidence (WofE) method is based on Bayesian probability framework and was first introduced by Bonham-Carter (1989), Agterberg et al. (1990), Aspinall (1992), and Bonham-Carter (2002) in Geoscience. Generally, WofE uses the concept of prior and conditional/posterior probability. By means of the Bayes-theorem it is possible to draw conclusions from the effect of an event on its causal factors on the assumption of prior probability (Malczewski 1999). In the WofE model, prior probability is the total number of events divided by the total study area. Prior probability is modified by specific factors, so-called items of evidence, causing either an increase or a decrease in prior probability (Bonham-Carter et al. 1989, Agterberg et al. 1990, Bonham-Carter 2002, Sawatzky et al. 2009).

Weights-of-Evidence is widely applied for landslide susceptibility applications among others by Lee & Choi (2004), Van Westen et al. (2003), Suzen & Doyuran (2004), Neuhäuser & Terhorst (2007), Magliulo et al. (2008), Neuhäuser & Terhorst (2009), and Neuhäuser et al. (2012a). In these susceptibility studies evidence is represented by controlling geofactors for sliding processes. The prior probability represents the total number of landslides in the study area. The modified probability is addressed as conditional or posterior probability, which is defined as the probability of a landslide, in the presence of a geofactor (Neuhäuser et al. 2012a). The statistical association between the single class of a factor and the landslide distribution is determined by overlaying landslides with each of the geofactors (evidence). By means of these statistical measures, a weighting of evidence can be done with respect to their importance for the occurrence of landslides (Neuhäuser et al. 2012a). A pair of weights, the positive and the negative weight, is calculated for each item of evidence. A positive weight expresses the likelihood for the occurrence of a landslide in case of the evidence being present. It conveys a positive association of landslides and a specific geofactor. Analogously, a negative weight describes the likelihood for a landslide in case of absence of the evidence (Agterberg et al. 1990, Bonham-Carter 2002). It is a measure of negative association of both variables. Apart from the weights other statistical measures are derived, which quantify significance of the weights and uncertainty in the probability estimations (Bonham-Carter et al. 1989, Agterberg et al. 1990, Bonham-Carter 2002). Finally, the weighted factors are combined using Bayesian rule in a multimap overlay operation to produce a single posterior probability map of landslide occurrence (Aspinall 1992, Van Westen et al. 2003, Sawatzky et al. 2009).

The application of a probabilistic prediction model based on Likelihood Ratio Function and Likelihood-Frequency for landslide susceptibility mapping was discussed by Chung (2006). Likelihood ratios are used to assess the conditional probability for landslide occurrence. This approach is applied, among others, by Lee & Min (2001), Lee (2004), Chung (2006), Lee et al. (2007), and Akgun (2012).

In general, likelihood functions are applied for statistical inference. Especially, they are used to estimate a parameter from a set of statistics in order to describe a fixed outcome. According to Chung (2006) a set of geofactors correlated with the landslide locations is selected. In the study of Chung (2006) these geofactors are integrated into a data matrix for quantitative analysis. The matrix is further connected with the study area, which is subdivided into proper terrain units. Thus, each unit contains a set of values, one for each geofactor. Moreover, the terrain units contain binary

---

information on landslide occurrence. In detail this means that the study area is classified as “stable or not affected by landslides” or “unstable or affected by landslides” by using the landslide sites. According to Chung (2006) a function can be established for each terrain unit, which describes the relative susceptibility for landslides. The likelihood ratio approach is based on the assumption that the character of the geofactor in stable areas is distinctly different from that in unstable areas. In order to describe the characteristic of geofactors, empirical frequency distribution functions are used, which are subsequently compared by likelihood ratios for all categories (Chung 2006, Kanungo et al. 2009). In general, the landslide susceptibility map is compiled by the application of likelihood ratio values as ratings of categories.

## 2.5 Distribution-free approaches

This group of methods has in common that they are not limited to the assumptions of specific statistical distributions of variables, i.e. geofactors and landslides. Recently, the Fuzzy Set Theory, the Artificial Neural Networks (ANN), the Dempster-Shafer Theory (DS), and the Combined Neural and Fuzzy Approaches have been used to generate landslide susceptibility maps (Kanungo et al. 2009).

An advantage of these distribution-free approaches is the ability to analyse complex data with different measurement scales such as continuous, categorical and binary data (Jemec & Komac 2011). They are not based on distributional assumptions or bias of data. Furthermore, the weights are computed in an objective manner. In Chi et al. (2002) a detailed discussion of the effectiveness of Fuzzy Set theory in landslide susceptibility applications is provided.

The influence of many preparatory geofactors on landslide evolution gradually increases or decreases, for example in the case of slope gradient or the distance to fault zones. In such cases it is hardly possible to determine a distinct threshold for contribution or relevance of a factor as a cause for landslides. This gradual influence can be modelled by means of the Fuzzy Set Theory according to Zadeh (1965). In classical set theory, there are only two possibilities of membership. An element can either belong to a set or not. In contrast to this, Fuzzy Sets use the degree of membership to a set instead of factual values. Fuzzy inference networks apply a variety of different fuzzy operators, especially a combination of fuzzy OR and fuzzy gamma operator, which are used for data integration to prepare a landslide susceptibility map (e.g. Ercanoglu & Gokceoglu 2004). Tangestani (2004, 2009) also performed a landslide susceptibility assessment using the Land Hazard Evaluation Factor (LHEF) rating scheme of Anbalagan (1992) for the determination of fuzzy membership values and fuzzy gamma operator for geofactor integration. Gorsevski et al. (2005) demonstrated that landslide susceptibility mapping can be achieved by an integration of GIS, fuzzy k-means and Bayesian modelling approaches (Kanungo et al. 2009).

One of the most recent methods related to landslide susceptibility assessment are Artificial Neural Network (ANN) tools. For tasks like regression and classification Artificial Neural Networks are suitable tools because complex data can be analysed (Jemec & Komac 2011). The basic concept of ANN is learning from data with known characteristics in order to derive a set of weighting parameters, which are subsequently used to recognise the so-called “unseen” data (Horton 1945). Arora et al. (2004), Gomez & Kavzoglu (2005), Wang et al. (2005), and Pradhan & Lee (2010) use an ANN black box approach for landslide susceptibility mapping. This approach determines weights in an iterative process but weights remain hidden in this case. In this process, a so-called multilayer perceptron with back propagation learning algorithm is used.

---

Landslide susceptibility assessment can also be performed on the basis of hypotheses. The Dempster-Shafer-Theory (DS) offers a systematic decision process (Shafer 1976). The method is applied, among others, by Gorsevski et al. (2005), Tangestani (2009), and Park (2011). On principle, the method allows to model “knowledge” and “ignorance” or uncertainties. It is based on a basic set of hypotheses, the so-called frame of discernment. In landslide susceptibility modelling the process is started with at least two hypotheses: First, the hypothesis that a specific area is stable and second that a specific area is instable. Geofactors either support the first or the second hypothesis. A so-called mass function is filled with probabilities for each factor of the set of hypotheses. This process is called basic probability assignment and determines the degree or the power of the factor to support a hypothesis. This assignment is done on the basis of fuzzy values. Several of these functions are finally normalised to one single function by means of Dempster’s rule of combination (Shafer 1976).

## 2.6 Geotechnical methods

In contrast to heuristic, statistical, probabilistic and distribution-free approaches, the deterministic group of methods is not based on the analysis of the relation between a set of geofactors and landslide distribution. Deterministic approaches assess landslide susceptibility based on physical, i.e. geotechnical analysis of specific slopes. The physical properties, like soil and rock mechanical characteristics, are quantified and applied to a specific mathematical model (Aleotti & Chowdhury 1999). Such approaches require knowledge of slope geometry, soil or rock mechanical properties and, in some cases, hydrological conditions. In general, slope stability models result in an assessment of safety factors or the probability for slope failure. Slope stability models are widely applied in civil engineering and engineering geology as well as for landslide susceptibility mapping especially since the introduction of GIS (Aleotti & Chowdhury 1999). A review of deterministic models used in landslide susceptibility models is given in Van Westen (2004) and Van Westen et al. (2006). In many cases the safety factor or probability of slope failure of each terrain unit is finally assigned to a susceptibility class.

Deterministic models provide quantitative information in form of a safety factor or probabilities of failure. Therefore, the results can be directly used in the design of engineering works or in the quantification of risk (Soeters & Van Westen 1996, Kanungo et al. 2009). Nevertheless, a main problem with these methods is simplification of highly complex phenomena.

A further restriction of deterministic approaches results from the detailed knowledge of processes and the level of detail of input parameters. A large amount of detailed input data derived from laboratory tests and field measurements are required, therefore these methods can only be applied to small areas on large scales (Van Westen 2004). The heterogeneity of natural conditions on a regional scale and large variability in geotechnical properties conflicts with homogeneity required by deterministic models (Soeters & Van Westen 1996). Costs and time consumption connected with geotechnical parameters are often obstacles in the application of deterministic approaches for large areas (Soeters & Van Westen 1996).

An effective approach in deterministic modelling is based on the assessment of soil wetness and critical pore pressure threshold (Van Westen 2004). Such approaches are suitable to analyse shallow rainfall-induced landslides. Authors like Terlien et al. (1995), Gritzner et al. (2001), and Chen & Lee (2003) developed models coupling a dynamic hydrological model, which simulate pore pressure over time, with a slope stability model that quantifies susceptibility in form of the critical pore pressure threshold. Schmidt & Dikau (2004) applied a model on groundwater variation in combination with a

---

stability model to assess climate variations in slope stability. Van Beek & Van Asch (2003) developed a model that couples a distributed hydrological model with a probabilistic assessment of slope stability. The model was used to predict the impact of land use changes on changes in slope stability (cf. Van Asch et al. 1999, Van Beek & Van Asch 2003).

Furthermore, there are geotechnical approaches which combine the Infinite Plane Slope Stability Model with a steady-state hydrological model. For example Dietrich et al. (1992) developed a physically based model which combines the infinite slope equation and a hydrological component which is based on steady-state shallow subsurface flow. This model is called Shallow Landsliding Stability Model (SHALSTAB) and is designed to assess shallow landside potential (Montgomery & Dietrich 1994). It predicts the steady state rainfall necessary for slope failure. The output represents a logarithmic hydrological ratio, which corresponds to the amount of water infiltration into the soil versus the water flow within the soil (Meisina & Scarabelli 2007). Susceptibility studies based on this approach are carried out by several authors, like Morrissey et al. (2004), Meisina & Scarabelli (2007), Ramos et al. (2007), and Weppner et al. (2008).

Another deterministic method is Stability Index Mapping (SINMAP), which is also based on the infinite slope equation (Pack et al. 1998). Similar to SHALSTAB, this method combines a hydrologic model to generate a steady-state pore water pressure with infinite slope stability analysis according to Hammond et al. (1992). This stability model was integrated into the slope stability programme 'Level I Stability Analysis' of the US Forest Service. The SINMAP model expresses the ratio of slope stabilising and slope destabilising factors as a factor of safety according to hydrogeological parameters of soil moisture and slope gradient (Meisina & Scarabelli 2007). The output is a stability index, which corresponds to the probability of slope failure considering the factor of safety and the uncertainty, or bandwidth, of the soil-mechanical and hydrological variables. SINMAP has been applied, among others, by Calcaterra et al. (2004), Meisina & Scarabelli (2007), Thiebes (2007), Terhorst & Kreja (2009), and Bai et al. (2010).

There are deterministic approaches designed for earthquake-induced landslide hazard analysis. Most of them are based on the simplified Newmark Slope Stability Model, which was integrated into GIS computational environments. Examples for such susceptibility studies are Miles & Ho (1999), Khazai & Sitar (2000), Jibson et al. (2000), and Refice & Capolongo (2002).

## **2.7 Deficits in current methods and challenges**

Despite of the achievements in landslide susceptibility assessment in the last few decades, research history reveals several deficits, which are addressed in the following (Carrara et al. 1999, Chung & Fabbri 2003, Remondo et al. 2003, Van Westen et al. 2003).

Although models are useful and valid representations of real processes, they cannot fully represent the complexity of a system (Bailer-Jones 2002). A model is focused on a limited space and a defined phenomenon and thus, they are incomplete in comparison to reality (Bailer-Jones 2002). Furthermore, incompleteness results from the inherent assumptions of a chosen modelling approach. Besides, each model is based on a special parameter constellation, which has a clear range of validity. Chung & Fabbri (2003) stated that one of the major deficits in landslide susceptibility assessment results from the lack of information on the model assumptions. All quantitative prediction models are based on certain basic assumptions of the model. In order to allow a correct interpretation of the susceptibility map, information on the model choice including the decisive criteria and model assumptions should be listed.

---

Besides, data availability is a common reason for incomplete assessments. Hence, a model is dependent on available data and reflects the specific state of information at a certain moment. Particularly in statistical, probabilistic as well as in distribution-free approaches, landslide susceptibility assessment is usually based on an inventory of landslides, related to conditional or preparatory causal geofactors (Soeters & Van Westen 1996, Fell et al. 2008, Van Westen et al. 2008, Jemec & Komac 2011). Therefore, the identification of these geofactors is essential for the resulting map. Ideally, the selection of geofactors is due to detailed process knowledge. In many cases this selection is also driven by the availability of area-wide data and by limitations in time and financial resources. The absence of area-wide data on relevant geofactors often results in their exclusion from the assessment procedure. Therefore, information on the neglected data should be provided. This enables the inclusion of missing data and hence an update of the susceptibility map at a later point of time.

Imprecision and uncertainty are further general constraints in modelling. Imprecision in landslide susceptibility assessment is provoked by the necessary simplification of input data. Continuous data, like slope gradient, are often reclassified into few classes. This categorisation causes a loss of the original characteristics of the data by subjective intervention. Nevertheless simplification is often indispensable due to the inability of the chosen methodology to handle a mixture of discrete and continuous data because of their different measurement scales. Uncertainty in models results from insufficient quality of the input data due to errors in mapping or incomplete landslide inventories as well as poor resolution of data sets (Carrara et al. 1999, Chung & Fabbri 2003, Remondo et al. 2003, Van Westen et al. 2003). The quality of susceptibility models can be improved by offering information on uncertainties of the derived indices, which quantify landslide susceptibility, due to data capturing methods and processing methods of the input data.

Purely qualitative landslide susceptibility classification is a major drawback in particular for qualitative assessment approaches like geomorphological analysis and heuristic methods. A shortcoming of qualitative classification is a zonation of the study area with discrete boundaries and Boolean character. Some methods classify the area, for example, into “endangered” and “not endangered”. However, such a strict separation is hardly applicable to natural phenomena (Chung & Fabbri 2003). Qualitative classification, like “high”, “moderate” and “low” hazard, without further quantification, leads to the fact that a map cannot be interpreted equally by experts and laymen. Without quantitative estimation, like probability or likelihood of landslides, decision makers for regional planning can only make a vague economic cost-benefit analysis (Chung & Fabbri 2003). Therefore, the main effort in the research field is focused on quantitative, data-driven methods. However, also in many quantitative approaches the final continuous susceptibility index is subsequently transferred into classes with subjectively selected class borders. The classes are frequently termed with qualitative descriptions like “high, moderate, low and no susceptibility”. In such cases it is important to ensure that the original quantitative meaning of the susceptibility index is visible for end users and a valid classification scheme of the susceptibility indices is chosen.

According to Chung & Fabbri (2003), Remondo et al. (2003) and others the independent assessment of hazard maps is indispensable for landslide susceptibility studies. Nevertheless, in most studies measures for reliability, efficiency and predictive power are missing. Hence, the model remains an untested hypothesis. The validation of results or at least the quantification of uncertainties is essential. The crucial question is how reliable prediction results are (Remondo et al. 2003).

A further problem in many landslide susceptibility models, particularly in non-physically based models, is the assessment of the relevance of geofactors in relation to the landslide process. The

---

relationships between the geofactors and the landslides are often assessed statistically rather than physically. Statistical, probabilistic and distribution-free methods offer specific measures or weights which enable conclusions on the relevance of geofactors. However, it has to be recognised that they cannot prove a clear cause-effect relationship between a geofactor and landslide occurrence because the geomorphological processes themselves are not investigated, but statistical relations only. The effective internal causes for landslides may be indirectly linked to the investigated geofactors. Therefore, a spatial relation between geofactors and landslides does not evidence a direct physical relationship between the selected geofactors and landslides.

Most of the landslide susceptibility studies which take into account hydrological conditions of substrate use precipitation data. Also hydrological studies of mass movements deal with the determination of rainfall-related thresholds (Klose et al. 2012). In many cases the objective is to identify critical rainfall levels, which can initiate slope failures when exceeded (cf. Guzzetti et al. 2006a). Most common thresholds consider the intensity and duration of rainfall events, which are able to trigger landslides (cf. Cain 1980, Guzzetti et al. 2008), or the cumulative precipitation prior to landslide occurrence. Antecedent rainfall thresholds take account of wet periods prior to the triggering precipitation event (cf. Chleborad 2003, Jakob & Weatherly 2003, Ibsen & Casagli 2004, Zêzere et al. 2005, Cardinali et al. 2006, Jakob et al. 2006). The remaining question is whether soil moisture conditions, which are indeed partly regulated by precipitation, can be explained properly by any kind of rainfall data (cf. Brocca et al. 2008, Klose et al. 2012).

Climate change is hardly included in landslide susceptibility studies. The majority of susceptibility studies comprise past and current landslides, and their causes are investigated in order to assess future landslide proneness. They are based on the accepted principle “the past and the present are keys to the future” (Varnes, 1984, Carrara et al. 1991). This includes the assumption that landslides will develop under equal or similar preparatory geofactors as in the past and the present. However, this assumption is not applicable when climate change is taken into account because the preparatory geofactors that prevailed in the past may be significantly altered by climate change, which mainly consists in increasing temperatures and changed precipitation patterns (Collison et al. 2000, Trauth et al. 2000, Soldati et al. 2004, Crozier & Glade 2006, Jakob & Lambert 2009, Klose et al. 2012). Any change of these critical factors has an impact on the hydrological and soil-mechanical conditions and affects the frequency and magnitude of mass movements (Collison et al. 2000, Trauth et al. 2000, Soldati et al. 2004, Jakob & Lambert 2009, Rudlof-Miklau et al. 2011).

According to the mentioned deficits in susceptibility assessment, specific challenges are accepted for the present modelling. The overall challenge is to avoid incompleteness of the assessment. Therefore an integrated assessment of landslide susceptibility is aspired in the actual work, which is not limited to the methodology of one single assessment approach. By the selection of two dissimilar modelling approaches, the syntheses of the results provide a more complete assessment of the landslide phenomenon in the study area. The statistic-probabilistic landslide susceptibility zonation, as carried out in this work, provides information on the basic disposition of the Northern Vienna Forest. It takes into account landslide causes which are persistent and more or less constant over time. The landslide phenomenon is further investigated by physically based scenarios in the Hagenbach Valley in the Vienna Forest. The objective is to investigate the variable disposition to develop landslides in a comprehensive way and on a larger scale. Variable disposition is a result of temporally variable geofactors depending on conditions changing in the short or medium-term, like meteorological or climate conditions varying during the day or during a whole season (Zimmermann et al. 1997, Heckmann & Becht 2006).

---

A major challenge is the integration of varying substrate wetness into the assessment of present-day slope stability. Therefore, slope stability is investigated as a function of substrate wetness, which is in turn dependent on meteorological conditions. The development of various wetness scenarios in order to assess possible changes in slope stability is a main aspect of the work. Several studies prove that there is a clear interrelation between meteorological conditions (e.g. precipitation and air temperature), substrate wetness and the soil and rock mechanical parameters (e.g. pore water pressure, cohesion) in slopes (Govi et al. 1985, Van Asch et al. 1999, Klose et al. 2012). The challenge is to develop an approach which is able to incorporate substrate wetness into slope stability modelling on the basis of meteorological data. A major difficulty is that the assessment of substrate wetness is highly variable in space, but also in time.

A further crucial challenge is the adaption of landslide susceptibility assessment to climate change. Therefore, changed air temperature and precipitation amounts are considered in detail in the modelling of future slope stability. Scenarios are developed, which investigate the slope stability under forecasted conditions until 2050 (Reclip:more 2007), in order to study the impact of changes in climate conditions. For that purpose, monthly rates of change related to air temperature and precipitation are applied. In this context the adaption of the used slope stability index mapping method was necessary.

The selection of data-driven assessment approaches and the modelling of susceptibility in form of probabilities are regarded as important in order to derive quantitative measures. The handling of imprecision and uncertainty is seen as a crucial criterion for the choice of the modelling approaches. Therefore, in case of the physically based model, the applied methods allow handling of uncertainty ranges. In case of the statistical approach, a measure of uncertainty can be calculated to assess the reliability of the susceptibility index.

Furthermore, the validation of susceptibility maps is considered as indispensable. Hence, the regional, statistical model will be validated by statistical methods by using known landslides not integrated into the modelling. The local, physically based model is checked by geomorphological field surveys.

---

## 3 Study area

### 3.1 General overview

The study area comprises 573 km<sup>2</sup> and is located in the northern parts of the Vienna Forest (Figure 3-1). The Vienna Forest region is a forested area, which is composed of 75% of broad-leaved forest and 25% of conifer forest (Rieder 2002), is situated in Lower Austria and comprises the outskirts of the city of Vienna. For the detailed physically based modelling the Hagenbach Valley in the Vienna Forest near St. Andrä-Wördern is selected as sub-study area because detailed sedimentological, pedological and geomorphological investigations have been carried out there providing detailed process knowledge for the modelling (Damm et al. 2008, Terhorst et al. 2009, Damm & Terhorst 2010). The catchment of the Hagenbach creek is located approximately 15 km north-west of Vienna. The location of the study area is shown in Figure 3-1.

The Northern Vienna Forest is part of the north-east margin of the Eastern Alps and belongs to the Rhenodanubian Flysch Zone, orientated in a west-east direction (Faupl 1996, Wessely 2006). The Flysch Zone is a narrow zone at the northern front of the Northern Calcareous Alps. It covers two alpine paleogeographic zones, the Helveticum and the Penninicum, mainly sequences from the Lower Cretaceous to the Paleogene (Oberhauser 1980). The Flysch Zone subsides in the east below the Vienna Basin, a tertiary basin in the periphery of the city of Vienna. In the north the Vienna Forest is limited by the Molasse Zone, which is subdivided into tertiary basins, like the Tullner Basin, and the quaternary gravel of the Danube River (Thenius 1974, Oberhauser 1980, Wessely 2006).

The Klippen Zones appearing within the areas of the Rhenodanubian Flysch must be regarded as tectonically independent units (Plöchinger & Prey 1993). Nevertheless, they are included into the study area because of their geographical position within the Flysch Zone and their relevance as landslide prone area (Schwenk et al. 1992). In principle, the Klippen are allochthonous fragments of different origin than the flysch sediments. Older substrata from the Upper Triassic to the early Lower Cretaceous are present in the Klippen Zones (Oberhauser 1980, Plöchinger & Prey 1993, Faupl 1996, Wessely 2006).

The southern part of the Vienna Forest belongs to East Alpine unit, more precisely the Northern Calcareous Alps (Figure 3-1). Landslides occur more rarely in this part and have different causal factors than those in the Flysch Zone (Schwenk et al. 1992). Therefore, the study area is limited to Flysch areas.

The Vienna Forest is situated in a transition region of the subatlantic and the pannonian-continental climate system. The average annual air temperature of the Northern Vienna Forest for the 1971–2000 period was 9.2°C, the average annual precipitation 742 mm (ZAMG 2002).

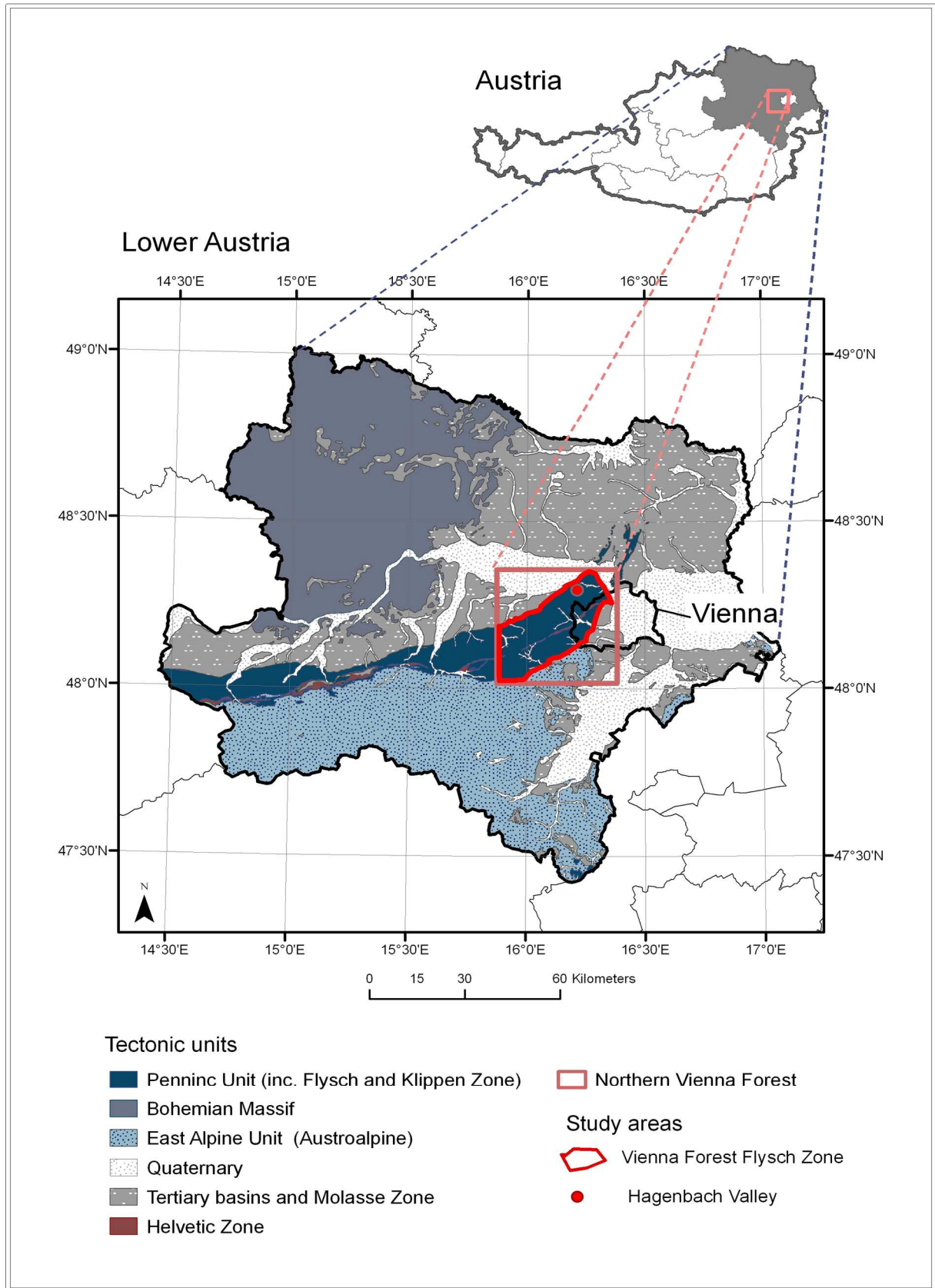


Figure 3-1 . Study areas of the “Northern Vienna Forest” for the regional investigation and location of the “Hagenbach Valley” for the large-scale study. The areas are located in the Flysch Zone. Tectonically these zones belong to the Penninic unit. The study area is limited by the Molasse Zone towards the north and the East Alpine unit towards the south. The map is based on Schnabel (2002).

---

## 3.2 Geomorphological setting

From the geomorphological point of view the Northern Vienna Forest represents an undulating landscape of the central European low mountain regions. Altitudes range between 300 and 400 m a.s.l. with single mountains reaching up to 900 m a.s.l. The gentle, rounded ridges of the region are deeply incised by valleys mainly running in west-eastern direction and partly forming gorges with oversteepend slopes, like the Hagenbach Valley (Wiche 1952, Plöchinger & Prey 1993, Wessely 2006).

In the Northern Vienna Forest wide hillslope areas are affected by mass movements of different types. Steeper slopes are mainly affected by translational and rotational slides as well as rock falls (Poisel & Eppensteiner 1986). The flatter landforms show soil or rock creep processes (Götzinger 1943). In particular the slopes of the Hagenbach Valley are nearly completely affected by mass movements of different types. The major part of eastern and western slopes are characterised by slide processes of translational and rotational type. Rock fall occurs in relation to these slide areas, close to the Hagenbach creek. Zones with rock fall processes are mainly present in steep slopes where compact rock bodies of the flysch sandstone are exposed.

Typically for the landscape of the Northern Vienna Forest is a high density of streams, small creeks and temporarily water-bearing gullies. The Hagenbach creek originates 400 m a.s.l. in several springs, crosses the village of Unterkirchbach and flows through a gorge with oversteepend slopes (Figure 3-2). In the area of St. Andrä-Wördern the Hagenbach creek leaves the flysch area and flows through the quaternary gravel of the Tullner Basin into the Danube River. The differences in elevation between the valley floor and the flat mountain tops vary between 70 and 120 m. The upper slopes largely show gentle gradients between 7° and 12°, whereas the lower parts of the slopes are inclined between 30° and 50° (Damm & Terhorst 2010).

In general, the drainage lines are characterised by torrential dynamics related to heavy rainfall (Neubauer & Höck 2000). Water-impermeable layers of flysch bedrock rich in clay and marl influence the surface runoff behaviour. Heavy or long-lasting rainfall causes rapid surface runoff leading to flooding and the hydrological regime is mainly driven by rainfall (pluvial flow regime) (Brix 1972, Plöchinger & Prey 1993). This specific runoff behaviour affects the geomorphological processes in the study area. Therefore, the main causes for mass movements in the Northern Vienna Forest are related to precipitation events and the specific runoff behaviour. The Austrian Geological Survey has registered mass movements in Austria since 1978 and states that about 90% of the registered landslides are linked to extreme weather events, like heavy or long-lasting rainfall or snow melt. Further landslides are caused by flooding in the drainage lines, leading to fluvial erosion of hillslopes (Kociu et al. 2007).



(A)

(B)

Figure 3-2. Hagenbach Valley: (A) the Hagenbach creek and the valley bottom with its oversteepend slopes, (B) Ridges of flysch bedrock. Photo: B. Neuhäuser.

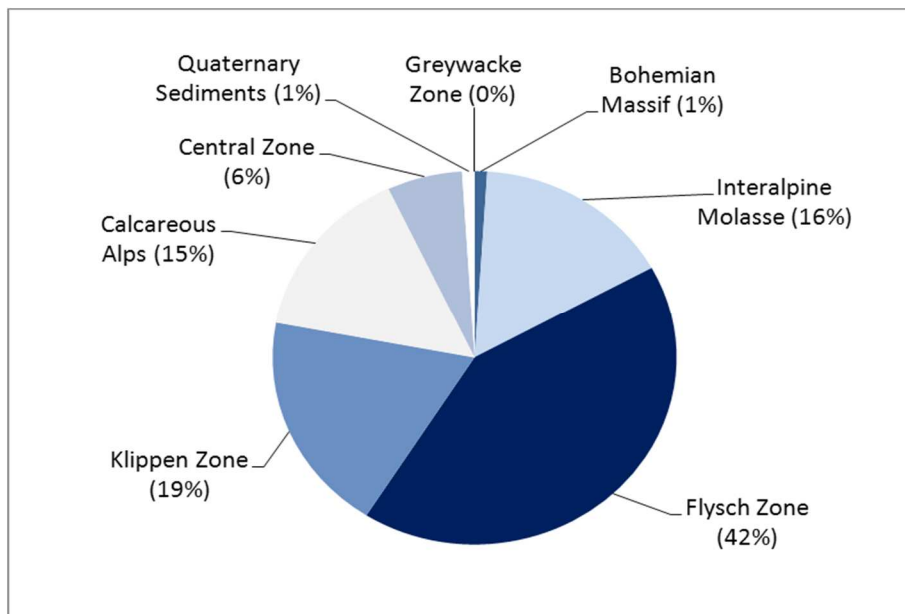


Figure 3-3. Proportion of landslides related to the main geological units in Lower Austria. The landslides were mapped between 1953 and 1990 by the Austrian Geological Survey (Schwenk at al. 1992, modified).

---

The high landslide activity in the Northern Vienna Forest is caused by the properties of the clay and marl rich flysch bedrock, which has an outstandingly high susceptibility to mass movements. This fact is also shown in a comprehensive study on mass movements in Lower Austria conducted by the Austrian Geological Survey (Schwenk et al. 1992). In this study 1,138 mass movements were registered in Lower Austria in the period from 1953 to 1990 (Schwenk et al. 1992, Kociu et al. 2007). When the registered landslides are related to the relevant geological zone, it becomes obvious that the Flysch and the Klippen Zone are most frequently affected by landslides (Schwenk et al. 1992) (Figure 3-5). Although the Flysch Zone constitutes only 9% of Lower Austria, 61% of all landslides are situated in flysch areas including the Klippen Zone.

In general, the high susceptibility to landslides is caused by the specific stratification of the flysch. Flysch is a turbidite sequence composed of various layers of (calcareous) sandstones, marly shales, calcareous marls and clay shists. Due to alternation of such permeable and impermeable layers in the bedrock, flysch is prone to landslides activity (Götzinger 1943, Wessely 2006). The differences in permeability in the lithological layers are the main causes for landslides, in general (Varnes 1987). Besides, the flysch formations in the Vienna Forest are largely formed by variable solid and strongly deformed bedrock. In many cases the formations are composed of interbedded marly sandstones, lime marls, sandstones, and calcareous sandstones. In particular the "Mürbsandstein", a brittle sandstone, is highly susceptible to moisture penetration (Wessely 2006).

Apart from the petrography of the flysch bedrock the soil-mechanical properties of the quaternary sediments affect the actual slope dynamics as indicated in new sedimentological and geomorphological studies (Damm et al. 2008, Terhorst et al. 2009, Damm & Terhorst 2010). It has turned out that loess layers, periglacial cover beds and sandstones, partly decomposed, form the slope surface and are partly responsible for the development of landslides. It is assumed that the discrepancy between the permeability of the loess-influenced layers and the underlying basal periglacial cover bed, mainly consisting of marly and clayey material, is a fundamental controlling factor for the initiation and spatial distribution of mass movements (Damm et al. 2008, Terhorst et al. 2009).

On the basis of geomorphological, pedological studies as well as soil-mechanical analyses of selected landslides in the study area, a reconstruction of the evolution and sequences of typical sliding processes in flysch areas is feasible (Damm & Terhorst 2010). On the one hand, mass movements can occur directly in the Flysch bedrock. Figure 3-4 shows an example of a deep-seated landslide in weathered flysch sandstone of the Kahlenberg Formation in the municipality of Purkersdorf. After first small slope movements between 1995 and 1997, the latest landslide event took place after abundant rainfall in April 2009.

On the other hand, quaternary slope deposits are frequently affected by landslide processes. Figure 3-5 represents the scar of a landslide that occurred in the municipality of St. Andrä-Wördern in the Hagenbach Valley in 1996. The mass movement developed in loess surface formation on top of basal clays and marls.



*Figure 3-4. Deep-seated landslide in the municipality of Purkersdorf: the mass movement occurred in weathered flysch sandstone of the Kahlenberg Formation in 2009. Photo: B. Neuhäuser (2010).*



*Figure 3-5. Landslide in the municipality of St. Andrä-Wördern. The Figure shows the scar caused by a landslide in 1996. The mass movement occurred in loess surface formation on top of basal clays and marls. Photo: Terhorst et al. (2009).*

---

### 3.3 Geological and sedimentological setting

Due to tectonic processes, the Rhenodanubian Flysch is highly deformed and includes several thrust faulting and folding, as well as thrust nappes (Schnabel 1992). Four main tectonic units appear in the study area (Figure 3-6): the Greifenstein Nappe in the north, the Laab Nappe in the south, and the Kahlenberg Nappe to the south-east. A separate narrow imbricated zone, the Northern Zone, occurs at the northern edge of the Flysch Zone (Plöchinger & Prey 1993).

In the Vienna Forest area the Flysch Zone is bordered by the Northern Zone in the north, which mainly consists of Lower Cretaceous flysch sediments of the Wolfpassing Formation. These beds are composed of Neocomian Flysch and Gaultflysch. Gaultflysch is composed of coloured clay shales in alteration with quartzite sandstones (Götzinger 1952, Faupl 1996). The Northern Zone includes Klippen cores consisting of limestone and calcareous sandstones. This solid rock is covered by softer sequences of Gaultflysch and clay shales of the Middle Cretaceous (Plöchinger & Prey 1993, Wessely 2006).

The Greifenstein Nappe appears in the south of the Northern Zone. It is composed of thick layers of the Altlenzbach beds of the Upper and Lower Cretaceous period, which is interbedded with Greifenstein sandstones, representing the Eocene facies (Götzinger 1952, 1954). The Altlenzbach beds are the prevalent layer in the Greifenstein Nappe. They represent thick turbidite sequences of grey sandstones, marly shales to lime marls and green-grey clay shales. The brittle sandstones ("Mürbsandstein") are mainly coarse-grained and easily disintegrate to clay, loam, loamy debris and sand by decalcification. Zementmergel beds (cement marls), a marl-dominated formation with a high content of calcium carbonate (Wessely 2006), occur more rarely and in thin layers.

The Kahlenberg Nappe is adjoined by the Greifenstein Nappe in the south. This nappe can be divided into the Kahlenberg ridges, extending in the north-east to the Bisamberg area and in the south-east to the Satzberg ridge (Oberhauser 1980, Plöchinger & Prey 1993). Green quartzitic sandstones and black, grey-green and coloured clay shales as well as Gaultflysch (Plöchinger & Prey 1993) are characteristic for the Upper Cretaceous. The Kahlenberg Nappe is further composed of the Kahlenberg Formation, which overlays a basis of Middle Cretaceous. The layers are mainly thin and are found at the Vienna hills, i.e. Kahlenberg, Leopoldsberg and Bisamberg (Plöchinger & Prey 1993). The nappe shows an anticline structure within its main strata, the Kahlenberg Formation. In the south it is thrust upon the Sievering Formation, which is composed of Upper Cretaceous rock rich in sandstone (Plöchinger & Prey 1993). The Sievering Formation is composed similarly to the Altlenzbach Formation and runs south alongside the Kahlenberg ridge. It accompanies the main Klippen Zone, which takes its course in south-east direction and continues south-west into the Greifenstein Nappe (Schwenk et al. 1992, Wessely 2006).

The area between the main Klippen Zone and the thrust zone of the Calcareous Alps is referred to as Laab Nappe (Götzinger 1954). The prevailing stratum is designated Laab Formation, which is divided into Hois and Aggsbach sub-formations (Schwenk et al. 1992). In comparison to the other flysch layers the Laab Formation is tectonically less disrupted. The Hois layers are composed of siliciclastic flysch, showing calcareous intercalations and varying thickness. The Aggsbach beds represent thick layers with sequences of grey, brown and dark-grey clay marls and clay shales interbedded with thin layers of calcareous-siliceous sandstones (Prey 1965, Faupl 1996). Furthermore, the Laab Nappe is composed of the Kaumberg Formation, which builds the northern margin of the Laab Nappe. This stratum is characterised by violet-purple and red clay stones and clay shales, alternating with grey and green-grey clay stones and marls interbedded with thin layers of calcareous sandstone (Wessely 2006).

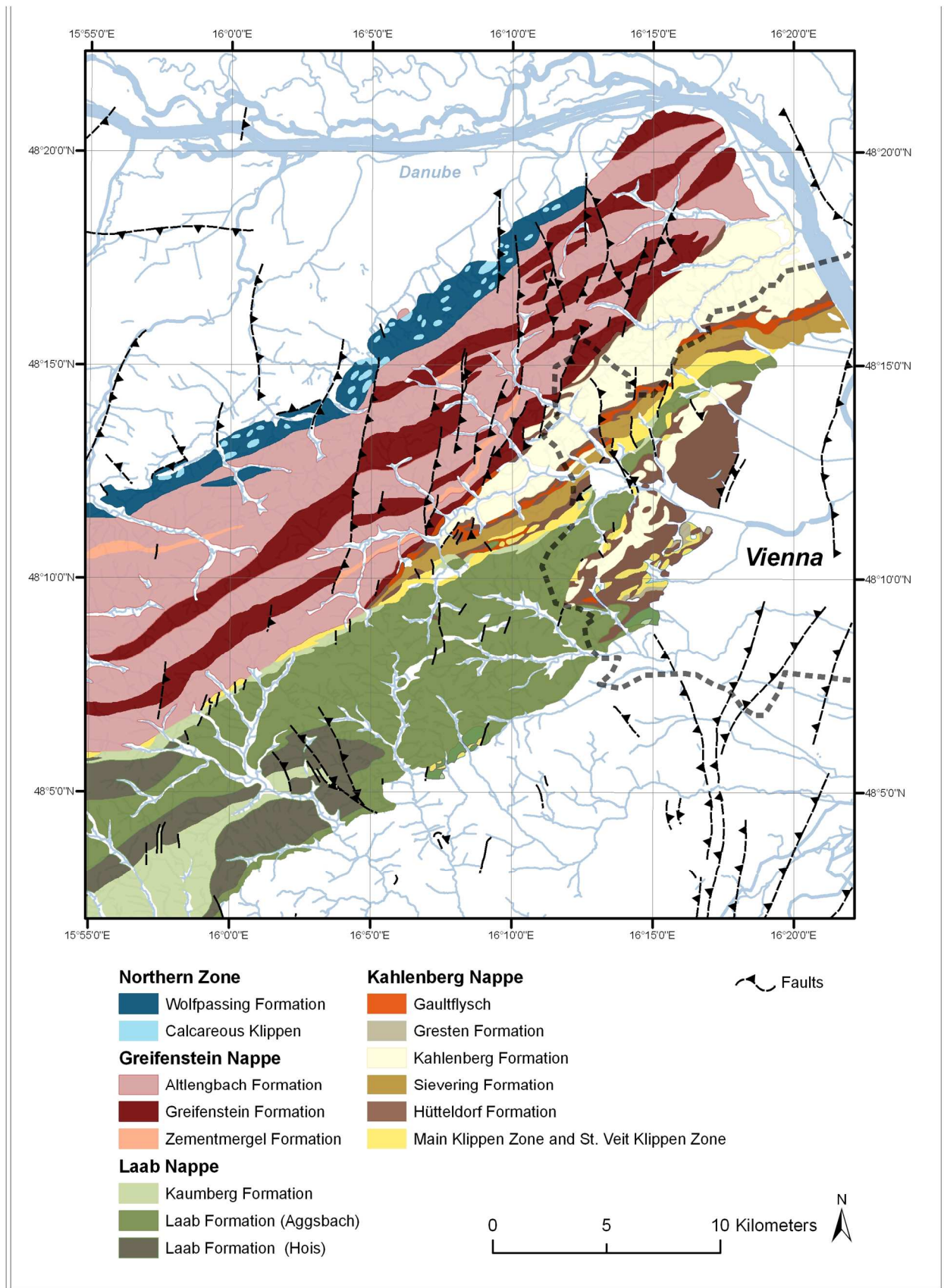


Figure 3-6. Geological and tectonic setting of the Northern Vienna Forest. The northern edge of the Flysch Zone is tectonically divided into the Northern Zone, which is a narrow imbricated zone, and the Greifenstein Nappe. The Kahlenberg Nappe is situated in the south-east and the Laab Nappe in the south (derived from the digital geological map 1:200,000 based on Schnabel (2002), simplified).

The formations inside the Hagenbach Valley belong to the Altlenzbach and the Greifenstein beds, mainly calcareous quartzitic sandstones, marls and clays, which are blanketed by quaternary periglacial cover beds and loess (Damm & Terhorst 2010). The valley is crossed by a wrench fault striking south-east (Brix 1969) (Figure 3-7).

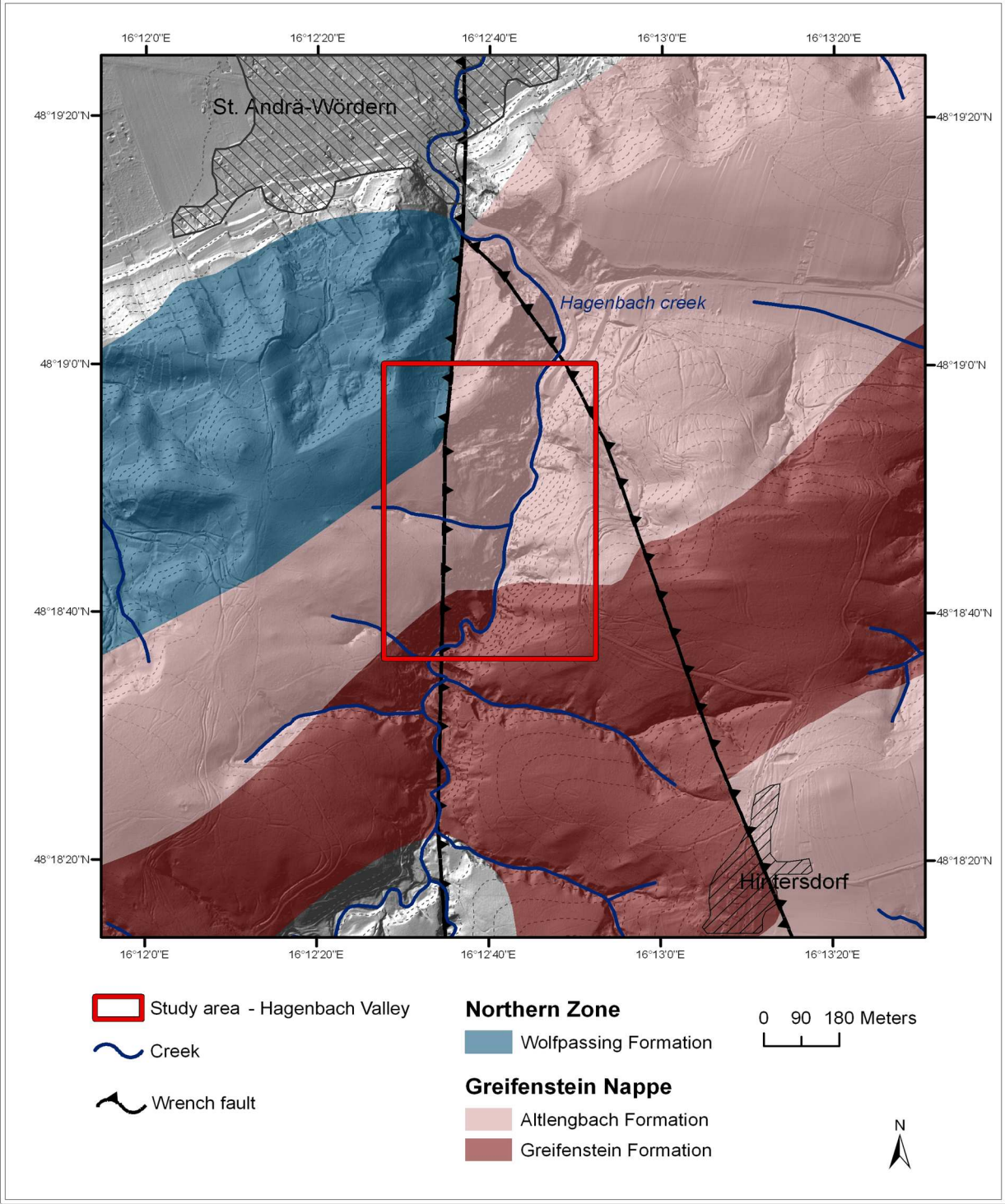


Figure 3-7. Location of the Hagenbach Valley, the sub-study area for detailed physically based modelling. The map is derived from the geological map 1:200,000 based on Schnabel (2002). The location of the sub-study area within the Vienna Forest is shown in Figure 3-1, page 23.

---

There are no current area-wide maps describing quaternary sediments or unconsolidated rock for the Vienne Forest at present. However, pedological and sedimentological studies in the Hagenbach Valley yield detailed information on the structure and composition of the slopes (Damm et al. 2008, Mayerhofer et al. 2008, Terhorst et al. 2009)

The bedrock consists of calcareous and marly sandstones, marly shales, calcareous marls and clay schist. On the upper slopes, it has been blanketed by loess and periglacial cover beds. On the lower slopes, sandstones and marls crop out at the slope surfaces, as recent processes caused the erosion of the mature soils that had developed there. Numerous landslide scarps in unconsolidated quaternary sediments, partly obscured by erosion, exposed slip planes, as well as relics of slide masses are indicative of the importance of landslides for erosive processes in the lower slope positions (Damm & Terhorst 2010).

In contrast, the upper parts of the slopes have been largely covered by Pleistocene loess and the upper periglacial cover bed, which mainly consists of loess as well. The Pleistocene sediments completely cover landslide scarps and sliding blocks. The typical soil developed in the periglacial sediments is a Luvisol consisting of a thin A-horizon, an E-horizon underlain by a transitional EBt-horizon, a Bt-horizon and, as the parent material, loess or the loess-bearing middle periglacial cover bed that forms the C-horizon. The basal part of the loess is frequently characterised by the occurrence of redoximorphic features such as thin brownish and greyish iron bands resulting from the stagnant properties of the underlying cover bed (Mayerhofer et al. 2008, Damm & Terhorst 2010).

Underneath the aeolian deposits there is a further periglacial cover bed, which consists of clays, marls, and debris. It is densely bedded, has intensively undulating upper and lower boundaries and exclusively consists of fragments of flysch bedrock. The latter meets the diagnostic prerequisites for the classification as the basal periglacial cover bed (Terhorst 2007, Semmel & Terhorst 2010, Damm & Terhorst 2010). The basal periglacial cover bed is impermeable to water and therefore locally responsible for the occurrence of "Nassgallen", which are permanently wet areas and pocket springs. In the middle and lower slope recent morphodynamic processes caused soil erosion (Damm & Terhorst 2010).

In the middle and mainly in the lower slope sections of the Hagenbach Valley, the upper soil and sediment strata of the periglacial cover beds are affected by morphodynamic processes such as erosion and landslides. The bedrock has frequently been uncovered there. In positions where the flysch sandstone has been exposed at the surface, decomposition of the bedrock prevails (Damm & Terhorst 2010).

---

## 4 Regional landslide susceptibility assessment

### 4.1 Methods and Data

Landslide susceptibility is expressed as possibility that a landslide occurs in a certain area. It is defined on the basis of the relationship between controlling geofactors that create landslide predisposition and the spatial distribution of landslides that occurred in the past (Brabb 1984). Mapping of spatial occurrence of landslides in a landslide inventory is an indispensable basis for landslide susceptibility assessment. Therefore, the compilation of a landslide inventory by means of archive studies is the initial step for subsequent susceptibility modelling.

There are a number of different methods to create landslide susceptibility maps, including inventory-based, heuristic, statistical, and deterministic approaches (cf. Soeters & Van Westen 1996, Kanungo et al. 2009) as elaborated in chapter 2 “State-of-the-art and challenges in landslide susceptibility assessment”. In the present work, a statistical/probabilistic method, referred to as Weights-of-Evidence (WofE) (Agterberg et al. 1990, Bonham-Carter et al. 1989, Bonham-Carter 2002, Sawatzky et al. 2009) is applied in the GIS-environment in order to derive quantitative spatial information on landslide predisposition. Due to the scale of the study area (573 km<sup>2</sup>) and the data availability, the WofE method is considered as the appropriate approach. There are no region-wide, detailed geological maps (below a scale of 1:50,000), pedological maps, data on quaternary deposits or on soil-mechanical properties so that physically-based models cannot be applied on a regional scale. The major advantage of the WofE method is the ability to deal with generalised and manifold information. Furthermore, it represents a robust and well tested method for studying natural hazards and supporting spatial planning (Kanungo et al. 2009).

#### 4.1.1 Archive studies for inventory compilation

The insight into spatial distribution and temporal frequency of landslides is of great importance for studying landslide phenomena (Van Westen et al. 2008). Temporal occurrence is definitely required for hazard estimations but it is no obligatory information in landslide susceptibility assessment because susceptibility does not consider the temporal probability of failure (Brabb 1984, Cruden & Varnes 1996, Soeters & Van Westen 1996, Aleotti & Chowdhury 1999, Fell et al. 2008).

An inventory provides information on the spatial distribution of existing landslides mapped from geomorphological field surveys or historical data of landslide occurrences (Wieczorek 1984, Neuhäuser et al. 2010). It can be prepared by different methods, depending on the extent of the study area, the scales of base maps, and the availability of remote sensing data (Guzzetti et al. 1999, Van Westen et al. 2008).

The traditional approach for mapping landslides is a geomorphological field survey, which is suitable for medium to large scales (Carrara et al. 1991, Guzzetti et al. 1999, Terhorst 2001). For the compilation of landslide inventories on a regional scale this approach is complex and time-consuming. At present, it is not applied as stand-alone method on a regional scale but rather as method to check the plausibility of landslide data known from literature and archives (Wieczorek 1984). Archive studies are suitable for compiling a landslide inventory on a regional scale (Radbruch-Hall et al. 1982, Van Westen et al. 2008). In this case data from public organisations, private consultants, chronicles, journals, and scientific reports are collected. Archive studies are applied in order to establish a landslide inventory for the whole region of the Northern Vienna Forest Flysch

Zone. The data are derived from a landslide map (Götzinger 1943) as well as from databases owned by authorities and agencies concerned with natural hazards in Austria. The latter are the Construction Group of the Geological Survey of the Provincial Government of Lower Austria, the Austrian Geological Survey, and the Department of Torrent and Avalanche Controlling of the Federal Ministry of Agriculture, Forestry, Environment and Water Management (Table 4-1).

*Table.4-1. Sources used for the landslide inventory: maps, databases and documents of different authorities and agencies concerned with natural hazards in Austria. In total the available data cover a time span of approximately 90 years. (Neuhäuser et al. 2012b, modified).*

Source	Document type	Years of compilation	Percentage
Geographical Society of Vienna (Götzinger 1943)	Landslide map 1:50,000	~ 1920-1943	90%
Construction Group of the Geological Survey (Provincial Government of Lower Austria 2010)	Building Ground Register	1926-2010	5%
Austrian Geological Survey (GBA 2010)	Mass movement in Austria, web database	1955-1977	2%
Austrian Service for Torrent and Avalanche Control (WLV 2010)	Technical reports of the Forest-Technical Unit, Austrian hazard zone maps	1987-2010	2%
Damm et al. (2008), Terhorst et al. (2009), Damm & Terhorst (2010)	Field investigations, profile mappings	2006-2010	1%

The documented landslides are represented as geo-referenced points. This approach is chosen because a considerable part of the available landslide documentations use point representation. Secondly, the applied landslide susceptibility assessment requires point datasets as input. In the regional statistical susceptibility assessment landslides are not considered with respect to their size but as dichotomous parameter, thus in terms of their presence or absence (Neuhäuser et al. 2012a).

The mass movements shown in the original map of Götzinger (1943) are represented as areal objects. In order to create a homogeneous database, landslides were digitised as points, with point position near the scar of the landslide. The accurate positioning of landslides in the GIS-based inventory is of utmost importance for all further modelling approaches. The precision of data capturing is decisive, in particular because analogue data sources, like the 1:50,000 historical map of Götzinger (1943), are incorporated. The maximum achievable precision is pursued for digitising, geo-referencing and rectification of the historical map. Geo-referencing uses topographic information of the Digital Landscape Model (DLM) of the Federal Office of Meteorology and Surveying, which represents the most accurate (3 m accuracy) map in Austria. Difficulties in this processing step result from divergences in topography of historical and present-day maps. Only locations which could be identified distinctively and accurately in both, the historical and the present-day maps, were used, like railway lines, historical buildings and mountain peaks (Neuhäuser et al. 2012a).

The databases from the authorities are checked in order to ensure that only landslides are covered, disregarding other types of mass movements, like rock fall and soil depression. In addition, landslides

related to building and road construction activities as well as mining and dumping sites are excluded because of anthropogenic trigger mechanisms. Furthermore, landslides triggered by floods are not integrated into the inventory. Due to statistical assumptions a further 3.7% of the total landslides must be sorted out. The assessment model requires an occurrence of only one landslide per unit area or cell, which is the basic unit for all calculations in the model (Neuhäuser et al. 2012a).

In contrast to the subsequent GIS-based modelling, which is a spatial analysis, a first distribution analysis is performed by statistical means. In particular, the relative frequency of landslide occurrence related to slope gradient and geological formations is investigated (Neuhäuser et al. 2012b). Besides, the chronological distribution of the landslides is analysed, however, this investigation is limited to the subset of the inventory comprising 170 landslides for which the date of event is exactly known. On the basis of this subset it was attempted to detect sliding phases on the chronological scale in order to get information on the overall development and frequency as well as on climatically induced landslide formation (Neuhäuser et al. 2012b).

#### 4.1.2 Compilation of the controlling geofactors

The controlling geofactors need to be determined before modelling. They are defined as those factors which create the predisposition to slope failure. Data capturing of the relevant geofactors is limited by the availability of comprehensive data.

The data for this study include topographical conditions in form of an ASTER Global Digital Elevation Model (Aster 2010). Information on geology and tectonic structure is available as digital map with a scale of 1:200,000 (Schnabel 2002) and 1:75,000 (Götzinger 1952). Drainage lines (streams and creeks) could be extracted from the Digital Landscape Model (DLM) (BEV 2010) and remotely sensed land cover data of the CORINE Land Cover dataset. These data sources are the initial base for the derivation of geofactors and subsequent modelling (Table 4-2).

Table 4-2. Available data sources for the study area, their source and owner, resolution/ scale (Neuhäuser et al. 2012a, 2012b, modified).

Category	Description/Source	Owner	Resolution /Scale
Terrain	ASTER Global Digital Elevation Model (ASTER 2010)	Earth Remote Sensing Data Analysis Center (ERSDAC)	30m
Geology	Digital Geological Map of the Republic of Austria based on Schnabel (2002) showing the main geological and tectonic units	Austrian Geological Survey	1:200,000
	Analogue Geological Map of the Surroundings of Vienna (Götzinger et al. 1952)		1:75,000
Drainage network	Digital Landscape Model (DLM) (BEV 2010)	Federal Office of Metrology and Surveying	Scale-free
Land cover	CORINE (Coordination of Information on the Environment) land cover 1990 data set (CLC 1990)	European Environment Agency (EEA)	100m

---

Most of the geofactors in this study are gained by further processing (i.e. geomorphometric, topographic, and distance analysis) the original data. Land cover data and geology units are applied as original data in the model. The following section describes the geofactors used and the processing steps.

- (1) **Geology:** The available geological maps with scales of 1:200,000 (Schnabel 2002) and 1:75,000 (Götzinger 1952), describe the main stratigraphic units on the basis of geological formations. In the present study the different flysch formations were used as geological classes in the model. The Penninic Klippen (i.e. Klippen in the Northern Zone, the Grestener-, Ybbsitzer-, Sulz and St. Veit Klippen) are grouped together because they represent a lithological homogenous unit, differing from the flysch formations. The sedimentary cover of the Klippen (i.e. Buntmergelserie – multi-coloured marl series), which tectonically also belongs to the Klippen Zones, are treated separately (Neuhäuser et al. 2012b). The different flysch strata are not directly regarded as controlling geofactors for landslides. They are considered as units which carry special lithological properties directly or indirectly linked to the soil-mechanical characteristics of slopes. Corresponding geological properties are degree of consolidation, clay content, coherence, permeability of unconsolidated rock and other soil and rock mechanical parameters (Neuhäuser et al. 2012a).
- (2) **Proximity to tectonic structures (nappe boundaries and thrust faults):** The study area is characterised by an intensive tectonic disruption (Oberhauser 1980, Schnabel 1992). The geological maps with the scale of 1:200,000 (Schnabel 2002) and 1:75,000 (Götzinger 1952) record the tectonic structures (nappe boundaries and thrust faults) as lines. The horizontal Euclidean distance to the tectonic lines is calculated in order to investigate the relationship between tectonic settings and landslide distribution. The resulting dataset represents a continuous grid where each grid cell represents the shortest distance to the closest tectonic structure (Neuhäuser et al. 2012b).
- (3) **Proximity to drainage lines (streams and creeks):** The drainage lines are provided by the detailed Digital Landscape Model (DLM) from the Federal Office of Metrology and Surveying (BEV 2010). The proximity to the drainage network is calculated by horizontal Euclidean distance analysis. The result is a continuous raster dataset, which provides the distance to the closest drainage line at each grid cell (Neuhäuser et al. 2012b).
- (4) **Vegetation cover:** The vegetation cover of the study area was captured by the CORINE land cover data (CLC 1990). As the CORINE classification distinguished between forested areas and several types of treeless areas, the classification of the land cover could be directly used in the model (Neuhäuser et al. 2012b).
- (5) **Morphometric parameters:** Geomorphometry, which determines steepness and shape of hillslopes and hence the impact of gravity on the slope, defining shear strength and shear stress accordingly, is of major importance for landslide susceptibility. The slope gradient was extracted from ASTER GDEM (Aster 2010) by calculation of the maximum rate of change in the elevation value in relation to its surroundings. Besides, slope shape can probably affect the susceptibility to landslides in several ways. Therefore, plan and profile curvature were extracted from the DEM by using a fourth-order polynomial (Neuhäuser et al. 2012b).

---

(6) **Slope aspect:** The aspect of a slope can influence landslide predisposition. To investigate the relative relationship between landslide frequency and slope aspect, ASTER GDEM (ASTER 2010) was used to calculate the aspect of a slope. The aspect identifies the downslope direction of the pixels with the maximum rate of change in the elevation value from each cell to its neighbours. The resulting aspect dataset is then reclassified into main cardinal directions, north, north-east, east, south-east, south, south-west, west, north-west and flat surfaces (Neuhäuser et al. 2012b).

(7) **Landform category:** Apart from geomorphometric parameters (slope gradient, plan curvature, profile curvature), morphological settings of a site can control mass wasting processes. Geomorphological features, like individual hills, valleys, plains and many others are important for many physical processes on the landscape (Blaszczynski 1997) and can therefore influence landslide susceptibility in different manners. In this study a landscape position model (Fels 1994, Fels & Zobel 1995, Weiss 2001) is applied, which classifies the landscape not only based on morphology but also integrating the position of the land surface in relation to its surroundings. In this process landform classes, like gullies with deeply incised streams, local ridges and upper flat slopes, etc. could be derived (Figure 4-1) (Neuhäuser et al. 2012b).

The Topographic Position Index (*TPI*) (Weiss 2001, Jenness 2006) forms the basis of the classification system and represents a measure for the relative height position of a unit in comparison with the adjacent terrain. It is computed as the difference between a cell elevation value and the average elevation of the neighbourhood around that cell. Positive *TPI* values indicate that the cell is higher than the adjacent terrain, while negative *TPI* values mean that the cell position is lower than its surroundings (Neuhäuser et al. 2012b).

The landform is determined by classification of the terrain using two *TPI* grids created with small and large sized cell neighbourhoods. The first *TPI* grid is calculated on the basis of a small cell neighbourhood (5x5 cell square), taking into account a small terrain around the cell, and the second is generated by a larger cell neighbourhood (12x12 cell square), which considers larger surroundings of the cell. Various landform types are distinguished by the combination of the *TPI* values from different scales (Neuhäuser et al. 2012b).

A high *TPI* value situated in a small neighbourhood combined with a low *TPI* value in a large neighbourhood is classified as a local ridge or hill in a larger valley whereas a small neighbourhood *TPI* combined with a high large neighbourhood *TPI* is classified as an upland drainage or depression. Figure 4-1 shows a detail of the study area with the landform categories and the corresponding classification regime with 10 landform classes according to Weiss (2001).

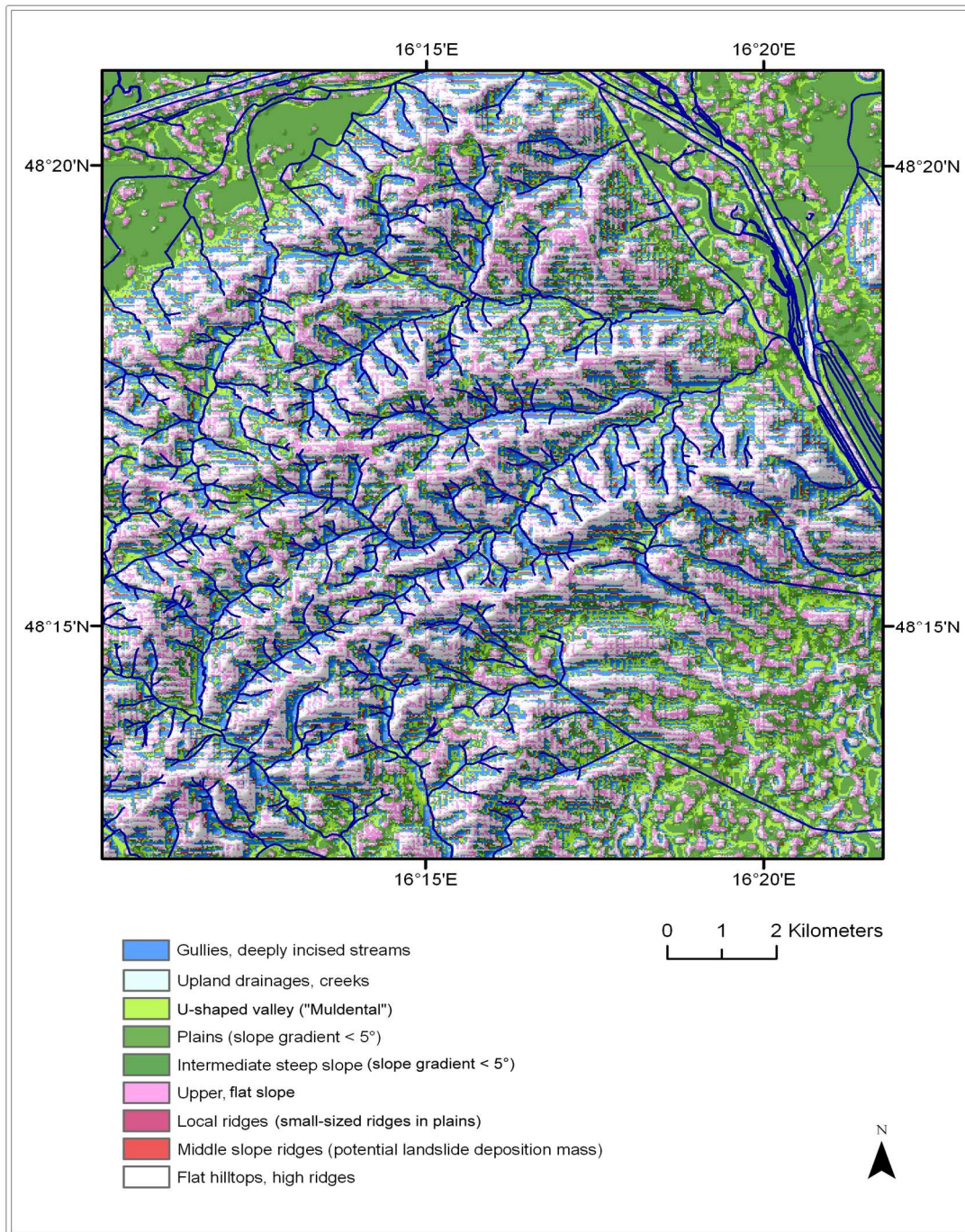


Figure 4-1. Landform classification by the two Topographic Position Indexes (Weiss 2001). The landform is defined by comparison of the two TPI values and the slope gradient.  $TPI_s$  = TPI calculated from a small (5x5 cell square) area;  $TPI_L$  = TPI calculated from a large (12x12 cell square) area (Neuhäuser et al. 2012a).

All the described geofactors have to be converted into a grid dataset of similar pixel resolution to be able to process them in the WofE model. In order to keep the level of detail of the elevation data, a pixel size of 30m is used in the model. The probabilities are calculated on the basis of so-called unit areas, measured in square kilometres, which is a constant parameter set at the beginning of the modelling. The estimated size of the landslides as well as the level of detail and resolution of the available geofactors corresponds to the determination of the basic unit area with a size of 0.008 km<sup>2</sup> (Neuhäuser et al. 2012a).

---

### 4.1.3 Weights-of-Evidence modelling

For the calculation of landslide susceptibility, the landslide inventory is combined with the relevant geofactors in the Weights-of-Evidence (WofE) model. It is a bivariate approach using the log-linear form of Bayes' theorem in order to predict the probability of occurrence of a response variable (Bonham-Carter et al. 1989, Agterberg et al. 1990, Bonham-Carter 2002, Sawatzky et al. 2009). In this study the WofE approach is used to produce a predictive model of landslide occurrences. Most of the applications of WofE are used for mapping mineral potential. Bonham-Carter (1989) and others applied the method in explorative mineralogy. In the last decade the method was also implemented in the range of natural hazards, like avalanches and forest fires. In recent years Bayesian inference has been applied for landslide susceptibility mapping (e.g. Van Westen et al. 2003, Lee & Choi 2004, Suzen & Doyuran 2004, Neuhäuser & Terhorst 2007, Magliulo et al. 2008, Neuhäuser & Terhorst 2009, Neuhäuser et al. 2012a). The mainly expected advantages of the method are: (I) the method is suitable for large study areas with varying ground conditions; (II) the model is able to incorporate discrete and continuous data types independently from the measurement scales, therefore the categorisation of continuous data and the connected simplification and loss of data quality can be avoided; (III) subjective influence on the model input and consequently on the generated conclusions is avoided by stochastic analysis for the weighting of controlling geofactors; (IV) the approach allows to weight the statistical associations between geofactors and distribution of landslides; (V) measures of uncertainty, in particular estimates of error and relative error in the probability values, are calculated. Consequently, this information can be offered to the end users of the susceptibility map, who are able to estimate the reliability of the map then (Van Westen et al. 2003, Neuhäuser et al. 2012a).

The WofE method comprises the following main processing steps: (I) separation of the landslide inventory into a modelling and validation set, (II) derivation of the controlling geofactors from source data by GIS-based analysis, (III) calculation of weights for each controlling geofactor by using the modelling set of the landslides, (IV) multi-class generalisation of continuous evidence based on cumulative weighting, (V) calculation of the posterior probability map (i.e. combination of the controlling geofactors to predict potential landslide occurrences), and (VI) model validation by using the validation set of the inventory (Neuhäuser et al. 2012a).

A detailed description of the mathematical formulation is available in Bonham-Carter (2002) and Bonham-Carter et al. (1989). Generally, WofE uses the concept of prior and conditional/posterior probability. Prior probability is the probability that an event ( $L$ ), for example a landslide, occurs without considering any additional information. It can be determined empirically with data on past landslide occurrence and their preparatory geofactors. In the WofE model the prior probability is the total number of landslide points divided by the total study area. The prior probability ( $P(L)$ ) is modified in the presence of certain factors, so-called evidences ( $B$ ), causing either an increase or a decrease. In the present study evidences are represented by controlling geofactors for sliding processes. The modified probability is addressed as conditional or posterior probability, which is defined as the probability of an event ( $L$ ) (landslide) in the presence of a geofactor  $B$ , e.g. a specific slope gradient or a geological layer (Neuhäuser et al. 2012a).

#### 4.1.3.1 Model assumptions and statistical parameters

It is of great relevance for the interpretation of the results to consider the fundamental assumptions of the method. Similar to other statistical methods, it is assumed that future landslides occur under conditions and factors equal or similar to those for comparable landslides in the past. It is further

supposed that controlling factors for the mapped landslides remain almost constant over time. This can only be assumed for one single landslide type since causes vary from type to type. Thus, the method must be separately applied to each landslide type. The most important assumption specific for WofE derives from the application of Bayes' probability theory in the model. It is presumed that factors are conditionally independent from each other with regard to the occurrence of landslides. Dependent factors need to be excluded from subsequent analyses. Thus, this basic presumption of conditional independence is considered a limitation of the method. When this assumption is violated, posterior probability estimates are likely to be biased upwards.

By overlaying landslide locations in pairs with each of the geofactors (evidences), the statistical association between single classes of a factor and landslides is determined. Evidences can be weighted with respect to their importance for the occurrence of landslides by means of these statistical measures. A pair of weights, ( $W^+$ ) and ( $W^-$ ) is calculated for each of the evidences. The values of the weights are dependent on the spatial relation between the landslides and the evidence (Bonham-Carter et al 1989, Bonham-Carter 2002). This calculation is done by application of likelihood ratios, which describe the probability of landslide occurrence both in the case of presence and of absence of evidence: a positive weight ( $W^+$ ) expresses the likelihood of landslide occurrence in case the evidence is present. It expresses a positive association of the landslide with a specific geofactor.

The logarithmic likelihood ratio is used to express the positive relationship between the training data and the evidence (out of a set  $i$  of evidences, i.e. evidence is present) and is therefore also addressed as positive weight ( $W^+$ ) (Bonham-Carter et al 1989, Bonham-Carter 2002):

$$(4-1) \quad W_j^+ = \ln \frac{P\{B_i|D\}}{P\{\bar{B}_i|D\}}$$

Analogously, a negative weight ( $W^-$ ) describes the likelihood of a landslide in case of absence of the evidence. It is a measure for the negative association of both variables (Neuhäuser et al. 2012a, 2012b). The logarithmic likelihood ratio is used to express the negative relationship between the training data and the evidence (out of a set  $i$  of evidences, i.e. evidence is not present) and is therefore also addressed as negative weight ( $W^-$ ) (Bonham-Carter et al 1989, Bonham-Carter 2002):

$$(4-2) \quad W_j^- = \ln \frac{P\{\bar{B}_i|D\}}{P\{B_i|D\}}$$

As spatial data are treated in GIS, the areas or pixels are used for the calculation. Therefore equations 4-1 and 4-2 can be described as follows (Bonham-Carter et al 1989, Bonham-Carter 2002):

$$(4-3) \quad W_j^+ = \ln \frac{\frac{N_1}{N_1 + N_2}}{\frac{N_3}{N_3 + N_4}} \quad \text{and} \quad (4-4) \quad W_j^- = \ln \frac{\frac{N_2}{N_1 + N_2}}{\frac{N_4}{N_3 + N_4}}$$

For each evidence class, for which the positive and the negative weight is calculated, each can be larger or smaller than zero (Bonham-Carter et al 1989).

If the positive weight is  $W^+ > 0$  and the corresponding negative weight is  $W^- < 0$ , there is a positive relationship between the training data and the evidence, i.e. the evidence did not occur incidentally but there is a positive correlation. The larger the positive weight, the better is the qualification of the evidence class as a predictor (Bonham-Carter et al 1989, Bonham-Carter 2002).

If the positive weight is  $W^+ < 0$  and the corresponding negative weight is  $W^- > 0$ , there is a negative correlation between the training data and the evidence. The evidence class is an indicator that *no*

landslide will occur (Bonham-Carter et al 1989, Bonham-Carter 2002). This negative correlation ( $W^+ < 0$  and  $W^- > 0$ ) is not interchangeable with any spatial relation. If the evidence is uncorrelated with the training data, there is no dependence between them, so  $W^+ = W^- = 0$ .

In WofE an additional measure is applied to quantify the correlation – the contrast ( $C_w$ ), which results from the difference of positive and negative weights. Therefore the contrast is defined as:

$$(4-5) \quad C_w = W^+ - W^-$$

In order to assess the degree of uncertainty in the calculation, the variances  $S^2$  are calculated for the positive and negative weights (Bonham-Carter et al 1989, Bonham-Carter 2002). The variance for the contrast results from the sum of variances of the weights (cp. equations 4-6, 4-7).

$$(4-6) \quad s^2(W^+) = \frac{1}{N\{B \cap D\}} + \frac{1}{N\{B \cap \bar{D}\}}$$

$$(4-7) \quad s^2(W^-) = \frac{1}{N\{\bar{B} \cap D\}} + \frac{1}{N\{\bar{B} \cap \bar{D}\}}$$

Apart from the weights, the contrast ( $C_w$ ) as well as the difference between ( $W^+$ ) and ( $W^-$ ), represents a measure of spatial relationship. For a positive spatial association, ( $C_w$ ) is positive; ( $C_w$ ) is negative for a negative association. The studentised contrast ( $C_s$ ) is calculated as the ratio of ( $C_w$ ) with its standard deviation. ( $C_s$ ) serves as a measure of significance of the contrast (Bonham-Carter et al 1989, Bonham-Carter 2002).

#### 4.1.3.2 Multi-class generalisation and weighting of the geofactors

All geofactors are overlaid with landslide distribution data of the inventory in order to calculate the weights. In case of categorical data, like geology, vegetation cover, landform, plan, profile curvature (classified in “convex”, “flat”, “concave”), and slope aspect, the weights are calculated separately for each class of the geofactor.

In case of continuous datasets, like slope gradient, proximity to drainage lines, and proximity to tectonic lines, the weights are calculated cumulatively. The results from weighting are used for the interpretation of the importance of geofactor classes on landslide proneness. In particular, a cut-off value can be identified where the evidence has no influence on the occurrence of landslides, for example a specific distance to streams or a certain slope gradient. In this cumulative weighting the measures ( $C_w$ ) and ( $C_s$ ) are employed to identify break-points in the spatial association. In general, the maximum value of the contrast ( $C_w$ ) constitutes the cut off at which the predictive accuracy of the resulting class is maximised (Bonham-Carter et al. 2002). Based on this rule, the contrast ( $C_w$ ) is utilised to select the cut off for classifying continuous datasets into fewer classes. However, in case of classes with small areas and a small number of occurrence points, the uncertainty of the weight could be large and consequently ( $C_w$ ) can be meaningless. In this case, the studentised contrast ( $C_s$ ) is a useful measure to define the cut off for subsequent classification (Bonham-Carter et al. 1989, Neuhäuser & Terhorst 2007).

For the final calculation of the posterior probability, continuous datasets are generalised according to the identified break-points and cut-off values. This is an iterative process where class borders are dropped or added according to the identified break-points, until the original spatial character is well represented. Finally, the classification reflects the original spatial association of geofactors and landslides as shown in the cumulative weighting. The purpose of this process is to maximise the statistical relationship between landslide locations and geofactor classes (Sawatzky et al. 2009). This reduction of classes leads to an enhancement of the statistical robustness of the weights (Bonham-Carter et al. 2002, Neuhäuser & Terhorst 2007).

#### 4.1.3.3 Posterior probability and susceptibility index

Finally, the weighted factors are combined for the calculation of posterior probability and confidence using Bayesian rule in a multi-map overlay operation. The prior probability of an occurrence is modified by the addition of predictor variables and their weights to produce a single posterior probability map of occurrence. That means that the weight for each evidence class is subsequently used for the prediction of landslides after integration of all evidences (Bonham-Carter et al. 1989). In this calculation the probabilities are expressed in an odds ratio ( $O$ ), which is related to the probability  $P$  as  $O=P/(1-P)$ . In addition, the natural logarithm of the odds is used. Based on the significant spatial associations in geofactor classes, the final result is a predictive map (Bonham-Carter et al. 1989).

In particular, after the weights for the evidence classes have been calculated, they are used in the next step to make a final prediction for the whole study area by integrating all evidences and by applying the posterior probability in form of odds. The posterior odds expressing the occurrence of a landslide  $D$  in case of present evidence  $B$  are calculated as follows:

$$(4-8) \quad O\{D|B\} = O\{D\} \cdot \frac{P\{B|D\}}{P\{\bar{B}|D\}}$$

Equally, the posterior odds expressing the occurrence of a landslide  $D$  in case of absent evidence  $\bar{B}$  are calculated as follows:

$$(4-9) \quad O\{D|\bar{B}\} = O\{D\} \cdot \frac{P\{\bar{B}|D\}}{P\{B|D\}}$$

As mentioned above, the natural logarithm is utilised in WofE with the likelihood ratios so that the posterior logits can be derived from the posterior odds. The natural logarithm is applied to both sides of equations 4-8 and 4-9 (Bonham-Carter 2002). This results in the following expressions in simplified notation (replacement by  $W^+$  and  $W^-$ ).

The posterior logits of a landslide  $D$  for present evidence  $B$  are calculated as follows:

$$(4-10) \quad \ln O\{D|B\} = \ln O\{D\} + W^+$$

The posterior logits of a landslide  $D$  for absent evidence  $\bar{B}$  are correspondingly calculated with:

$$(4-11) \quad \ln O\{D|\bar{B}\} = \ln O\{D\} + W^-$$

If there are more evidences  $B_n$  that have to be integrated into the model, they are combined as given in equations 4-12 and 4-13.

$$(4-12) \quad \ln O\{D|B_1 \cap B_2 \cap B_3 \cap \dots \cap B_n\} = \ln O\{D\} + \sum_{i=1}^n W^+$$

$$(4-13) \quad \ln O\{D|\bar{B}_1 \cap \bar{B}_2 \cap \bar{B}_3 \cap \dots \cap \bar{B}_n\} = \ln O\{D\} + \sum_{i=1}^n W^-$$

The posterior probability map estimates the potential distribution of future landslides, based on the mapped landslide occurrences, and predicts the distribution of yet unidentified occurrences (Aspinall 1992, Van Westen 2003). Due to the application of Bayes' probability theory, conditional independence between the factors ( $D$ ) related to the occurrence of landslides is assumed. The assumption can be described for the factors ( $B_1$ ) and ( $B_2$ ) as  $P(B_1 \cap B_2 | D)$  equals  $P(B_1 | D) \cdot P(B_2 | D)$ .

---

## 4.2 Results

### 4.2.1 Results of the inventory compilation and analysis

The landslide inventory compiled by the archive studies provides information on the spatial distribution of existing landslides in the Northern Vienna Forest. The main purpose of the inventory is the exact spatial mapping of sliding processes; a temporal assignment was not possible in all cases. The inventory covers 471 datasets on landslides which occurred during a time span of approximately 90 years (cp. Figure 4-2).

In order to enable validation of the final susceptibility map, landslides which are independent from the model are required. Therefore, the inventory is split into a modelling and a validation set. 15% of the landslides are selected for validation and excluded from the modelling by random selection. This relatively low percentage is chosen in order to keep statistical robustness in the model because the reduction of the modelling landslides leads to a decrease of probability values and lowering of the confidence of the weights. In order to avoid that some classes of the controlling geofactors do not meet the confidence criteria in the model, the landslides are not further reduced. As the landslides in the validation set are not used in the model, they can be considered as new or undiscovered landslides.

A first inventory analysis was done on the basis of the mapped landslides in Figure 4-2. Parts of the landslides have a size of approximately  $0.07 \text{ km}^2$  (= 7 ha), however, the major part comprises smaller slide masses with an average extension of  $0.008 \text{ km}^2$  (= 0.8 ha). A considerable part of the landslides is about  $0.0001 \text{ km}^2$  (=  $100 \text{ m}^2$ ) and smaller (Neuhäuser et al. 2012b).

The landslide inventory shows a visible relationship between the geology and the spatial pattern of the mass movements (Table 4-3). Landslides have been most frequent in the area of the Altengbach Formation, mainly consisting of interbedded, intensely folded, and deformed calcareous sandstones, calcareous marls, marly shales, and clay shists. Mass movements in this stratum have been most frequent in the so-called "Mürbsandstein", a brittle marly sandstone, parts of which tend to easily disintegrate under conditions of waterlogging. In contrast, the Kahlenberg and Laab Formations show a clearly reduced rate of sliding processes (Table 4-3) (Neuhäuser et al. 2012b).

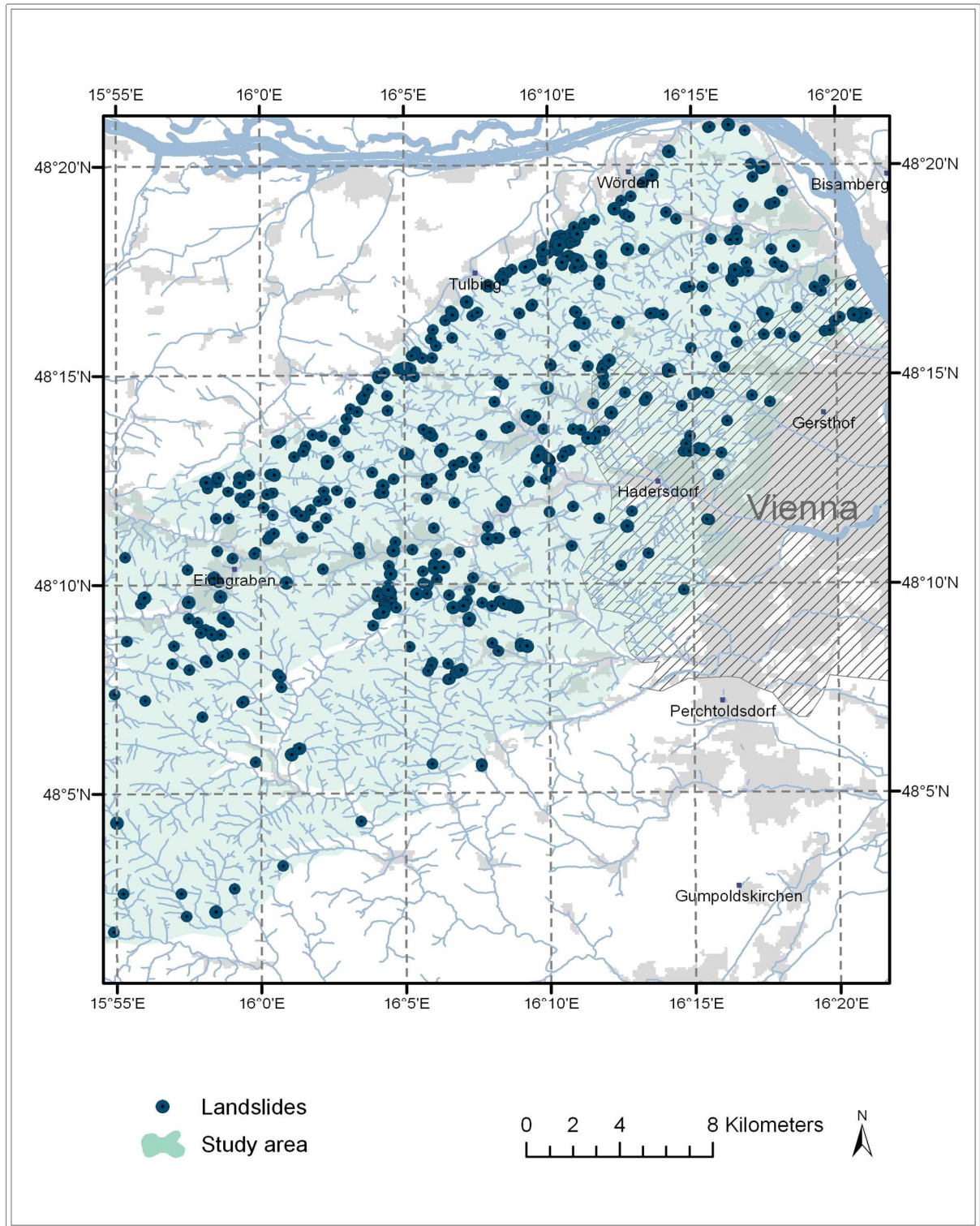


Figure 4-2. Landslide inventory of the Vienna Forest Flysch Zone covering 471 events. The sources for the compilation of the inventory are listed in Table 4-1. The actual map is based on the digital geological map (Schnabel 2002) and the topographic map, i.e. the digital landscape model (BEV 2010).

Table 4-3. Mass movement in the Vienna Forest and their proportion in flysch rock formations, quaternary sediments and Klippen Zone (Neuhäuser et al. 2012b, modified)

Geological period	Rock formation	Rock components	Geotechnical Characteristics	Sliding Processes [%]
<b>Rhenodanubian Flysch</b>				
Upper Cretaceous	Altlingbach	Calcareous sandstone, marly sandstone, clay shist, lime marl, interbedded	Solid rock, friable, variable solid, "Mürbsandstein", strongly folded, strongly deformed	32%
Lower Cretaceous	Wolfpassing	Sandstone, clay shist, marl	Solid rock, variable solid, strongly folded, strongly deformed	15%
Palaeogene	Greifenstein	Sandstone, shale, partly coarse-grained, interbedded	Solid rock, variable solid, strongly folded, strongly deformed	11%
Upper Cretaceous	Kahlenberg	Sandy limestone, calcareous sandstone, clay shist, interbedded	Solid rock, variable solid, strongly folded, strongly deformed	9%
Lower Tertiary	Laab	Clay shists, marls	Solid rock, variable solid	7%
Upper Cretaceous	Hütteldorf	Sandstone, clay shist, marl	Solid rock, variable solid	5%
Lower Cretaceous	Gaultflysch	clay-shales, sandstones and quartzites	Solid rock, variable solid, strongly folded, strongly deformed	4%
Quaternary	Quaternary sediments	Terraces, pebbles, alluvial fills	Loose rock, variable solid	8%
--	other	Sandstone, clay, marls, etc.	---	4%
<b>Klippen Zones (Main Klippen Zone and Klippen of St. Veit, Ybbsitz and Sulz)</b>				
Middle Jurassic – Lower Cretaceous	Klippen	Calcareous sandstone	Solid rock, variably solid	4%

Figure 4-3 illustrates the landslide frequency, the cumulative number of landslides as well as the landslide density in the slope gradient classes. The cumulative number of landslides shows that there is an increase in landslide frequency below 19° inclination. The maximum number of landslides occurs at 7° slope gradient. However, the highest landslide density is observed at a gradient of 27° and above (Neuhäuser et al. 2012a, 2012b).

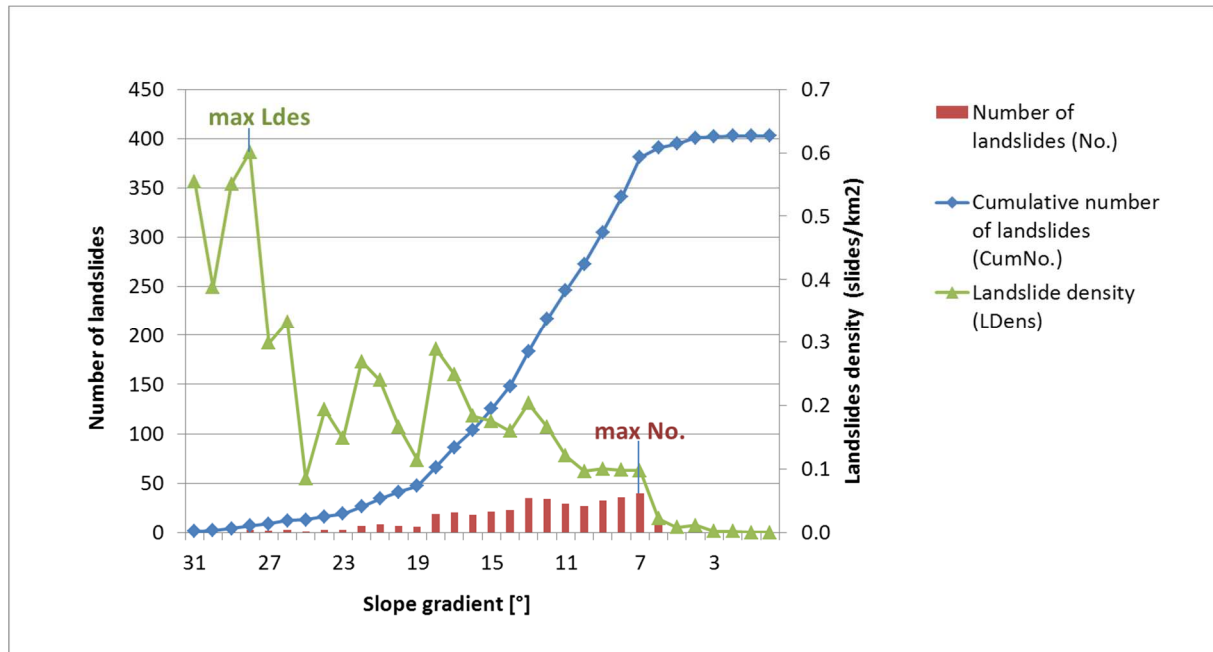


Figure 4-3. Landslide frequency versus slope gradient (Neuhäuser et al. 2012b, modified). The diagram shows the distribution of landslides over the slope gradient range in the study area. In particular, the number of landslides, the cumulative number of landslides and landslide density versus slope gradient is given. The diagram is produced by statistical analysis (frequency analysis) of the landslide inventory.

The first analysis of the temporal distribution of a subset of the landslide inventory proved that there is no evidence of an overall increasing frequency of landslides in the Vienna Forest. However, the distribution shows single years with intensified landslide activity. The comparison with meteorological data indicates a possible relation of increased landslide activity with years of intensified rainfall and rapid snow melting, like in 2009. That year was characterised by severe thunderstorms, intensive precipitation events and extreme temperature variations leading to massive snow melting. Both, rapid snow melting and long-lasting and heavy rainfall are considered to be the major triggers for landslides (Govi et al. 1985, Kraut 1999, Schweigl & Hervas 2009).

---

## 4.2.2 Results of weighting of the geofactors

Prior to the final weighting of all geofactors, the continuous datasets are weighted and analysed without previous generalisation in order to study the spatial relationship between landslide locations and geofactors (cp. chapter 4.1.3.2 “Multi-class generalisation and weighting of the geofactors”). Subsequently all geofactors are weighted categorical.

### 4.2.2.1 Cumulative analysis of the continuous datasets

Figure 4-4 illustrates results from the cumulative weighting of the slope gradient. The weights are calculated starting at the highest slope gradient (in descending order) because it is assumed that the influence of slope gradient is reduced with decreasing gradient. It is shown that in total the statistical significant range of slope gradient can be found between 7° and 30°. The maximum ( $C_s$ ) is reached at 7° indicating that there is no significant influence of slope gradient below this value. It is further demonstrated that the maximal ( $W^+$ ) are located between 26° and 30°. Only 3% of the landslides are located in the range of 7° to 30° but in relation to the relatively small area of this range, landslide density is high. The slope gradients ranging from 18° to 26° comprise 13% of the landslides. As the positive weights ( $W^+$ ) are still positive and the corresponding negative weights ( $W^-$ ) are small, a positive spatial association can be assumed. Below 18° there is a considerable increase of ( $C_s$ ), which is caused by the increase of landslide occurrences in this range. 79% of the landslides are situated in the slope gradient range from 7° to 18°. According to the results from the cumulative weighting, a multi-class generalisation is performed with the classes 0° to 7°, 7° to 18°, 18° to 26° and 26° to 31° (Neuhäuser et al. 2012a, 2012b).

A similar analysis of cumulated statistical parameters is processed with the distance to streams and tectonic lines. The strongest positive relation between landslides and tectonic lines can be found in the range of 0m to 75m (Figure 4-5). Above 75m distance the positive weights decrease with increasing distance from the drainage lines. At a distance of 277m to the next tectonic line the maximum ( $C_s$ ) is reached representing the cut-off value for this geofactor. Thus, influence of tectonic lines on the occurrence of landslides can be assumed from 0m to 277m. A multi-class generalisation is done, using the local maxima of ( $C_s$ ) found at 75m, 135m and the cut-off value for the spatial association of 277m (Neuhäuser et al. 2012a).

As regards the proximity to the drainage lines, influence on the occurrence of landslides is evident up to a distance of 185m. At a distance of 185m the maximum ( $C_s$ ) is reached and the influence of drainage lines decreases with increasing distance (Figure 4-6). The strongest positive association is identified in the first 70m. In this range 22% of the landslides are situated. These two values are taken as the first two class borders for the generalisation of the evidence (Neuhäuser et al. 2012a).

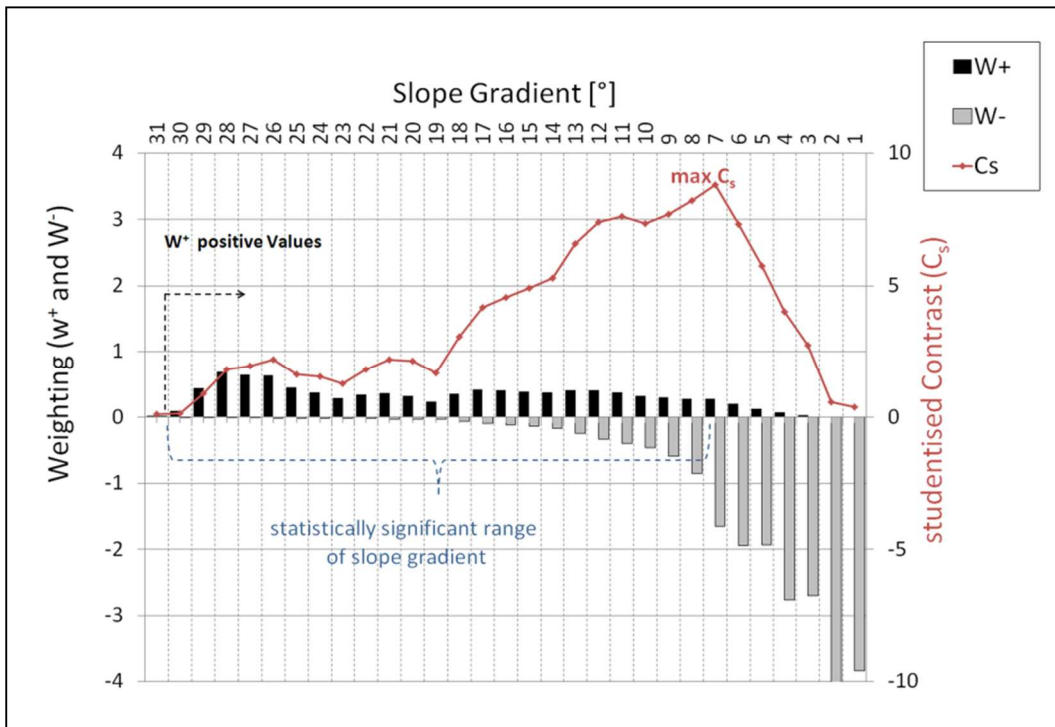


Figure 4-4. Cumulative descending weighting of the slope gradient. The analysis of the cumulatively calculated weights ( $W^+$  and  $W^-$ ), and studentised contrast ( $C_s$ ) allows to define proper break-points for a subsequent multi-class generalisation of the evidence (Neuhäuser et al. 2012a, 2012b).

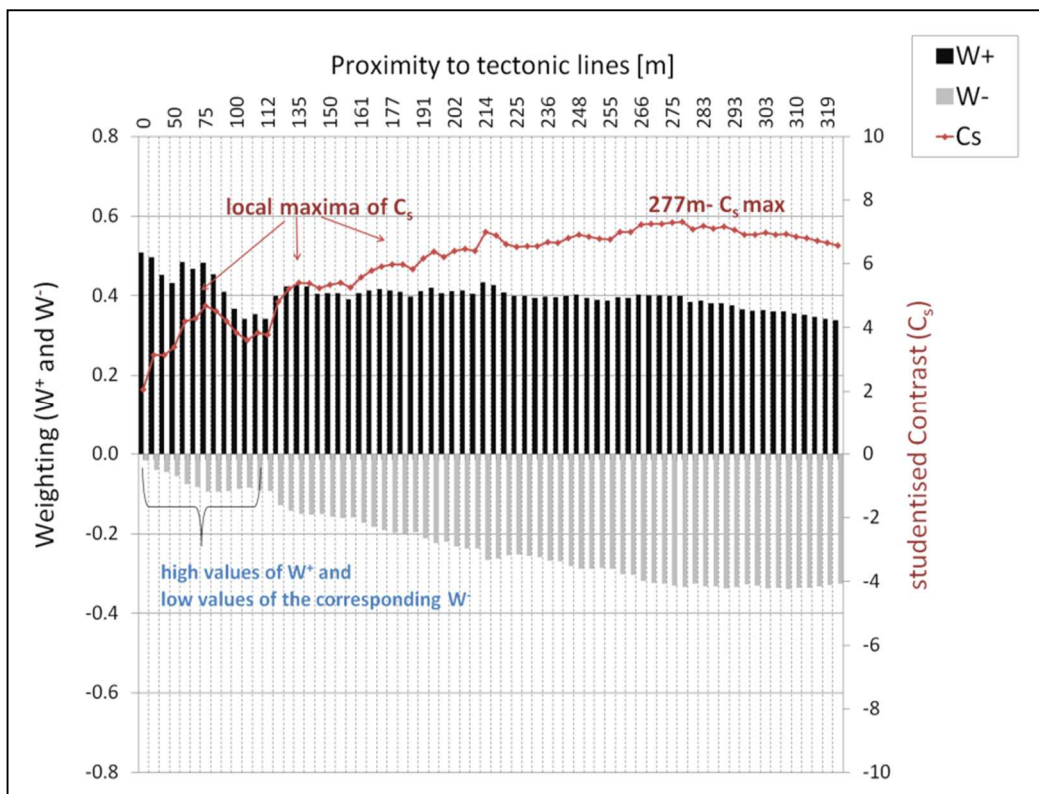


Figure 4-5. Cumulative ascending weighting of the tectonic lines. The analysis of the cumulatively calculated weights ( $W^+$  and  $W^-$ ), and studentised contrast ( $C_s$ ) allows to define proper break-points for a subsequent multi-class generalisation of the evidence (Neuhäuser et al. 2012a).

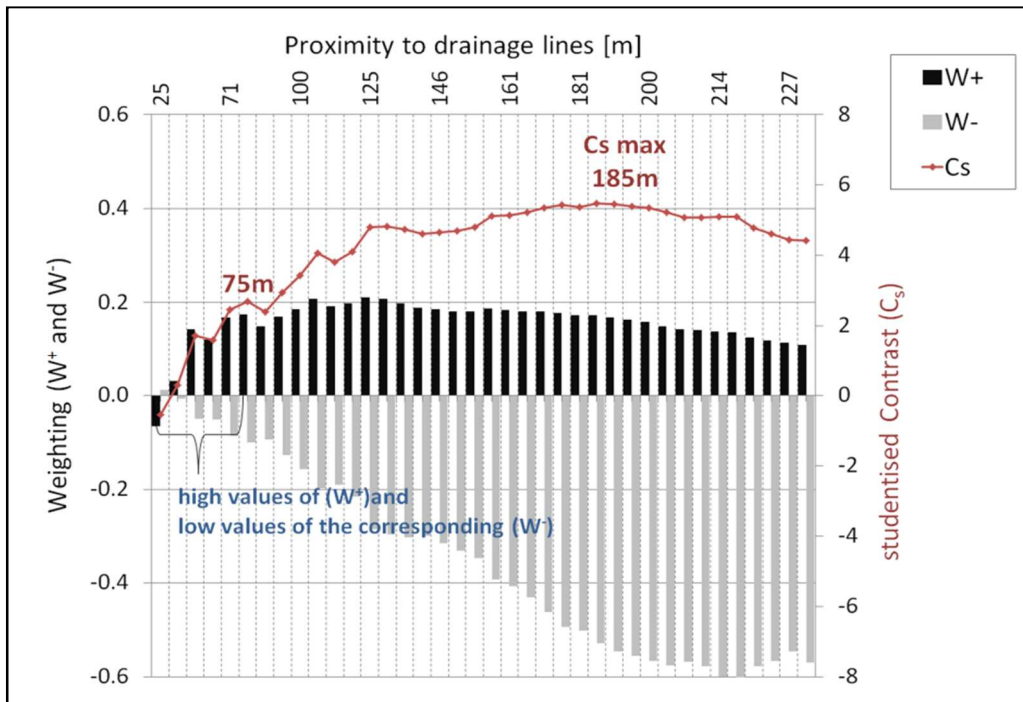


Figure 4-6. Cumulative ascending weighting of drainage lines. The analysis of the cumulatively calculated weights ( $W^+$  and  $W^-$ ), and studentised contrast ( $C_s$ ) allows to define proper break-points for a subsequent multi-class generalisation of the evidence (Neuhäuser et al. 2012a).

#### 4.2.2.2 Geology

Table 4-4 shows the flysch formations related to the tectonic units and their weighting. The formations are given in descending order with respect to the studentised contrast ( $C_s$ ), which is, together with the positive weight ( $W^+$ ), a measure for the relevance of the class as predisposing factor. Corresponding to Table 4-4, Figure 4-7 illustrates the results of the weighting of the geological unit. The weighting of geological classes shows that the Northern Zone (cp. Figure 3-6, page 29) is the tectonic unit with the highest susceptible geological classes. Table 4-4 indicates that the Wolfpassing formation ( $W^+=1.26$ ) and the calcareous Klippen ( $W^+=1.12$ ), both located within the Northern Zone, are highly susceptible to landslides. Moreover, some geological classes of the Kahlenberg Nappe (cp. Figure 3-6, page 29) are highly landslide prone (Table 4-4). The boundary of the city of Vienna touches the Kahlenberg Nappe. In some small areas it predominantly consists of the Gaultflysch series, which denotes a strong predictive value ( $W^+=1.62$ ) linked with the highest significance ( $C_s = 5.72$ ) in the model (Neuhäuser et al. 2012a, 2012b).

Furthermore, the areas in the Kahlenberg Nappe classified as debris have a strong predictive value ( $W^+=1.63$ ), however, with a relatively low significance ( $C_s = 2.27$ ). This is due to the small number of landslides (2 events) situated in this unit. The highly positive value of the weight is caused by the small size of this geological class ( $0.6\text{km}^2$ ), which results in a high landslide density of the debris unit. The Kahlenberg as well as the Hütteldorf Formation, which also occur in the Kahlenberg Nappe, reveal a moderate predictive value.

Table 4-4. Weighting of geological classes based on geological maps (Schnabel 2002, Götzingler et al 1952). The table shows positive weight ( $W^+$ ), negative weight ( $W^-$ ), contrast ( $C$ ) and studentised contrast ( $C_s$ ). The table is sorted according to the studentised contrast as a measure of significance of the weighted class. Rows marked with italic characters have a positive association with the occurrence of landslides (Neuhäuser et al. 2012b).

<b>Geological class</b>	<b>Tectonic unit</b>	<b><math>W^+</math></b>	<b><math>W^-</math></b>	<b><math>C</math></b>	<b><math>C_s</math></b>	<b>Area [%]</b>	<b>Landslides [%]</b>
<i>Wolfpassing Formation</i>	<i>Northern Zone</i>	1.26	-0.11	1.37	9.24	4%	15%
<i>Gaultflysch</i>	<i>Kahlenberg Nappe</i>	1.49	-0.03	1.52	5.72	1%	4%
<i>Calcareous Klippen</i>	<i>Penninic Klippen</i>	1.12	-0.03	1.15	4.18	1%	4%
<i>Debris ("Hangschutt")</i>	<i>Kahlenberg Nappe</i>	1.63	0.00	1.63	2.27	0%	0.5%
<i>Altlenzbach Formation</i>	<i>Greifenstein Nappe</i>	0.16	-0.07	0.23	2.09	28%	32%
<i>Kahlenberg Formation</i>	<i>Kahlenberg Nappe</i>	0.15	-0.01	0.16	0.89	8%	9%
Sulz Formation	Klippen Zone of Sulz and Mauer	0.44	0.00	0.44	0.62	0%	0.5%
Alluvial sediments of the younger valley bottom (gravel, haugh)	-	0.10	-0.01	0.11	0.60	8%	8%
Hütteldorf Formation	Kahlenberg Nappe	0.06	0.00	0.07	0.28	5%	5%
Alluvial sediments of the older valley bottom (gravel, sand)	-	0.00	0.00	0.00	0.00	0%	0%
Buntmergel (multi-coloured marl) series and equivalents (Klippen cover)	Main Klippen Zone	0.00	0.00	0.00	0.00	1%	0%
Gresten Formation	Kahlenberg Nappe	0.00	0.00	0.00	0.00	0%	0%
Zementmergel Formation	Greifenstein Nappe	-0.15	0.00	-0.15	-0.22	1%	1%
Greifenstein Formation	Greifenstein Nappe	-0.04	0.01	-0.05	-0.30	12%	11%
Sievering Formation	Kahlenberg Nappe	-0.69	0.01	-0.70	-1.38	2%	1%
Kaumberg Formation	Kahlenberg Nappe	-0.99	0.03	-1.02	-2.47	4%	2%
Laab Formation (Hois sub-Formation)	Laab Nappe	-3.09	0.06	-3.15	-3.15	6%	0%
Laab Formation (Aggsbach sub-Formation)	Laab Nappe	-0.98	0.13	-1.11	-5.45	19%	7%

---

The further geological classes of the Kahlenberg Nappe do not reflect a positive statistical association with landslide occurrences (Neuhäuser et al. 2012a, 2012b).

The calcareous Klippen are weighted as strong predictive geofactor ( $W^+=1.12$ ) that exhibits a high statistical significance ( $C_s=4.17$ ). The majority of the landslides (32%) are observed in the Altlenzbach Formation, which appears in the Greifenstein Nappe. However, this formation covers a huge area ( $156\text{km}^2$ ) and, as a consequence, it shows only moderate positive association with landslide occurrence ( $W^+=0.16$ ). In the remaining geological units of the Greifenstein Nappe (Greifenstein as well as Zementmergel Formation) no positive relation to the mass movements is ascertained (Neuhäuser et al. 2012a, 2012b).

The formations of the Laab Nappe reveal negative values for ( $W^+$ ), which denotes a negative relationship to the landslides. Consequently, the Hois and Aggsbach sub-formations can be considered as geofactors, which indicate slope stability.

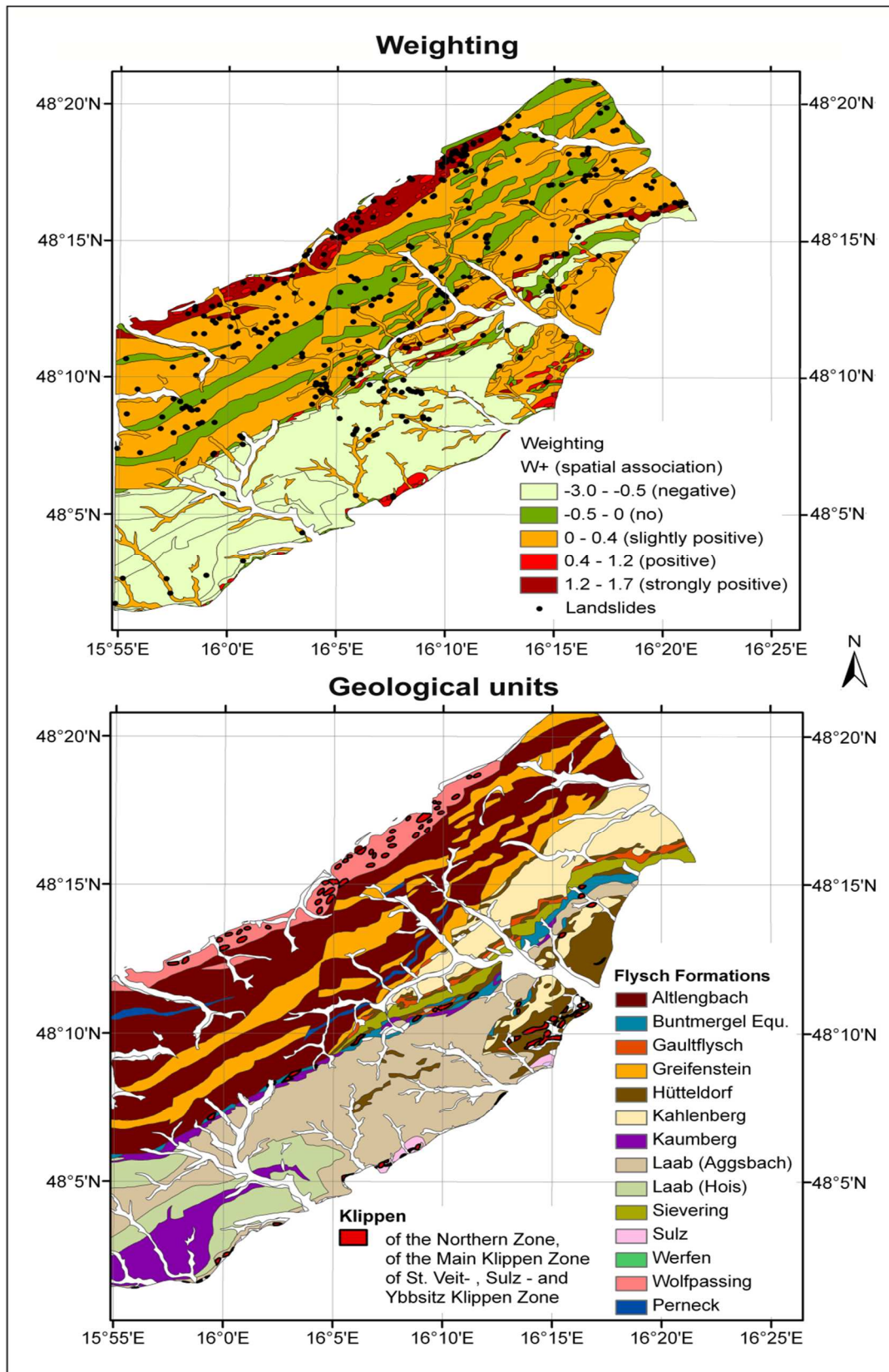


Figure 4-7. Results of the weighting of the geology geofactor. Top: geological formations revealing positive spatial association with the landslide occurrences. Below: the associated positive weights ( $W+$ ) in the geological classes. The higher the weight, the stronger is the spatial association between the geological class and the distribution of landslides. The map is derived from the geological map 1:200,000 based on Schnabel (2002) (Neuhäuser et al. 2012a).

#### 4.2.2.3 Proximity to tectonic lines

With respect to the distribution of landslides, the influence of thrust faults and nappe boundaries on the occurrence of landslides is of interest. Table 4-5 shows the results of categorical weighting.

*Table 4-5. Weighting of the proximity to tectonic lines, i.e. thrust faults and nappe boundaries based on geological map by Schnabel (2002). The table shows positive weight ( $W^+$ ), negative weight ( $W^-$ ), contrast ( $C$ ) and studentised contrast ( $C_s$ ). The classes from 0-277m have a positive association with the occurrence of landslides and thus enhance the susceptibility in the final calculation. The strongest positive association is present in the range of 0 to 75m. Rows marked with italic characters have a positive association with the occurrence of landslides (Neuhäuser et al. 2012b).*

Distance to tectonic lines [m]	$W^+$	$W^-$	$C$	$C_s$	Area [%]	Landslides [%]
<i>0-75</i>	<i>0.46</i>	<i>-0.09</i>	<i>0.55</i>	<i>4.22</i>	<i>13%</i>	<i>20%</i>
75-135	0.24	-0.02	0.27	1.56	8%	10%
135-215	0.47	-0.06	0.54	3.68	10%	15%
<i>215-277</i>	<i>0.24</i>	<i>-0.02</i>	<i>0.26</i>	<i>1.37</i>	<i>7%</i>	<i>8%</i>
277-350	0.01	0.00	0.01	0.05	7%	7%
350-450	-0.09	0.01	-0.10	-0.52	8%	7%
450-550	-0.48	0.03	-0.50	-2.03	7%	5%
550-650	0.03	0.00	0.03	0.14	6%	7%
650-750	-0.81	0.03	-0.85	-2.50	5%	2%
750-850	-0.88	0.03	-0.91	-2.39	4%	2%
850-950	-0.45	0.01	-0.46	-1.36	4%	2%
950-1050	-0.46	0.01	-0.47	-1.32	3%	2%
1050-1150	-0.31	0.01	-0.32	-0.88	3%	2%
1150-1250	-0.86	0.01	-0.87	-1.73	3%	1%
1250-1350	-0.31	0.01	-0.31	-0.76	2%	2%
1350-1450	0.00	0.00	0.00	0.00	2%	0%
1450-1550	0.03	0.00	0.03	0.07	2%	2%
1550-1650	-0.50	0.01	-0.50	-0.86	1%	1%
1650-1750	-1.26	0.01	-1.26	-1.26	1%	0%
1750-3367	0.10	0.00	0.10	0.40	4%	5%

The spatial association between landslide distribution and tectonic lines is apparent (Figure 4-8). Mass movements are closely connected to the thrust faults and nappe boundaries. Similar to cumulative weighting, categorical analysis displays the strongest positive relation between landslides and tectonic lines between 0 and 75m. A considerable amount of landslides (20%) are within a

distance between 0 and 75m to the nearest tectonic line (Figure 4-8), such as nappe boundaries and thrust faults. This distance class reveals strong predictive value ( $W^+=0.46$ ) in combination with highest significance ( $C_s = 4.22$ ). The distance classes 75 to 135m, 135 to 277m and 277 to 350m have a positive association with the landslide occurrence as well. The remaining classes are negatively associated with landslides; hence there is no evident statistical influence of the tectonic lines on the landslides anymore.

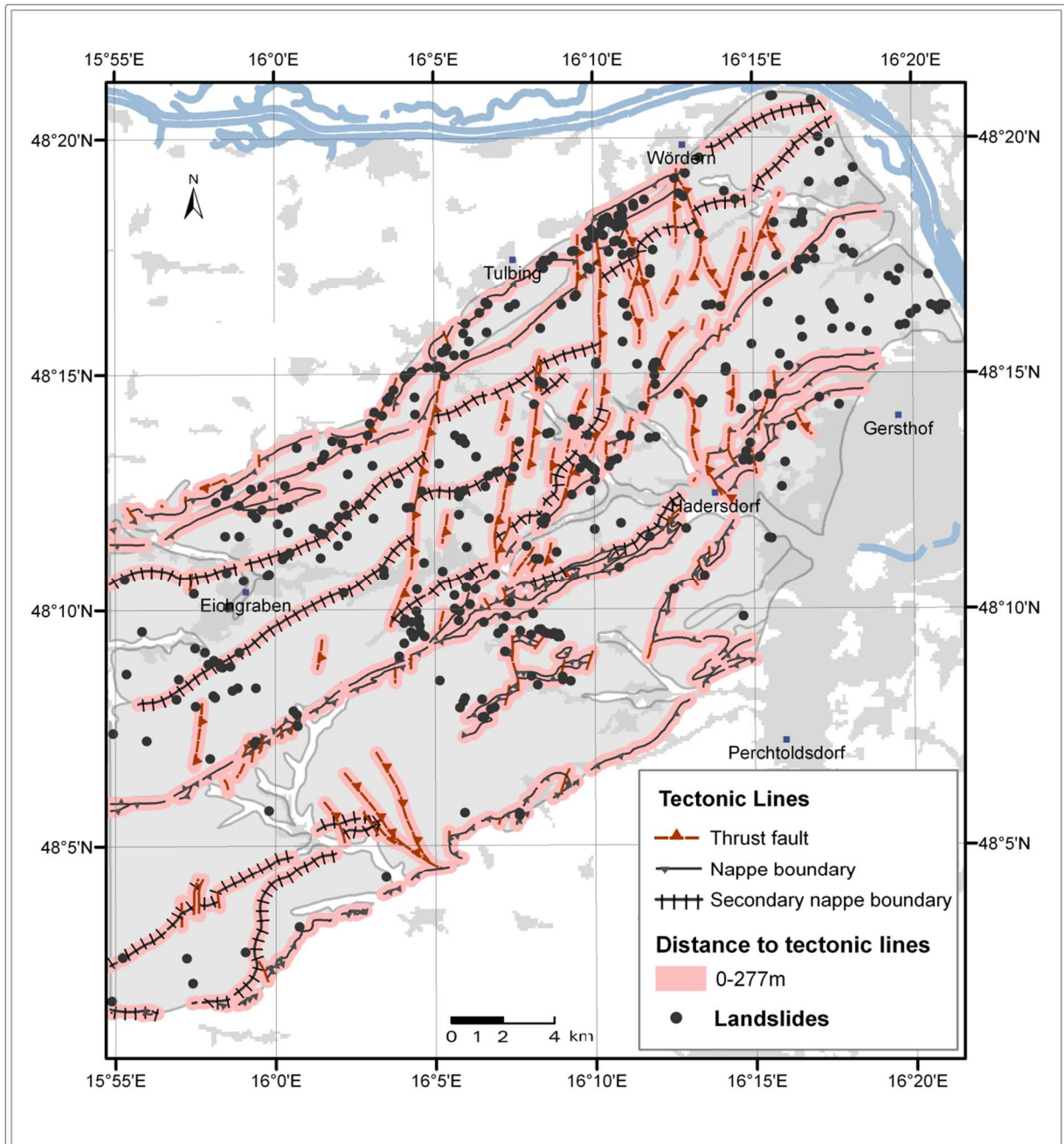


Figure 4-8. Results of the weighting of the proximity to tectonic lines. The weighting shows that the distribution of landslides closely follows tectonic structures. Influence of tectonic lines on the occurrence of landslides is identified up to 277m. 54% of the landslides are located within this distance (i.e. nappe boundary or fault) (derived from the geological map 1:200,000 based on Schnabel (2002) and the Digital Landscape Model of the Federal Office of Metrology and Surveying) (Neuhäuser et al. 2012a, 2012b).

#### 4.2.2.4 Vegetation cover

Most of the area is covered by broad-leaved forest typical for the Vienna Forest. 52% of the registered landslides are situated in broad-leaved forest (Figure 4-9). However, no positive relation to the forest areas is shown in weighting due to the low density of landslide occurrences in this class. However, a predictive value is revealed in the treeless areas, like meadows, which are classified as “heterogeneous agricultural land” according to CORINE nomenclature. This land cover type is further divided into classes of “agricultural land with significant areas of natural vegetation” (e.g. meadows) and “areas with complex cultivation patterns” (Table 4-6). This denotes a strong association of these treeless classes with the landslide sites, connected with a high significance ( $C_s > 4$ ). Besides, moderate positive association is given in the classes “Vineyards” and “Continuous urban fabric” (Neuhäuser et al. 2012b).

Table 4-6. Weighting of vegetation cover classes based on CORINE land cover data (CLC 1990). The table shows positive weight ( $W^+$ ), negative weight ( $W^-$ ), contrast ( $C$ ) and studentised contrast ( $C_s$ ). The classes marked with italic characters have a positive association with the occurrence of landslides (Neuhäuser et al. 2012b).

Vegetation cover (CORINE Nomenclature)	$W^+$	$W^-$	$C$	$C_s$	Area [%]	Landslides [%]
<i>Agricultural areas (Agricultural areas with complex cultivation pattern)</i>	0.69	-0.06	0.75	4.45	5.4%	10.8%
<i>Meadows (Land principally occupied by agriculture, with significant areas of natural vegetation)</i>	0.88	-0.04	0.92	4.32	2.7%	6.5%
<i>Settlement areas (Discontinuous urban fabric)</i>	0.29	-0.04	0.33	2.19	10.1%	13.5%
<i>Vineyards</i>	0.79	0.00	0.79	1.36	0.4%	0.8%
<i>Pastures</i>	0.14	-0.01	0.15	0.85	8.2%	9.4%
Industrial, commercial and transport units	0.00	0.00	0.00	0.00	0.0%	0.0%
Road and rail networks and associated land	0.00	0.00	0.00	0.00	0.0%	0.0%
Green urban areas	0.00	0.00	0.00	0.00	0.3%	0.0%
Sports and leisure facilities	0.00	0.00	0.00	0.00	0.1%	0.0%
Non-irrigated arable land	0.00	0.00	0.00	0.00	0.4%	0.0%
Coniferous forest	0.00	0.00	0.00	0.00	0.1%	0.0%
Water bodies	0.00	0.00	0.00	0.00	0.0%	0.0%
Mixed forest	-0.57	0.06	-0.63	-3.02	11.9%	6.7%
Broad-leaved forest	-0.15	0.19	-0.33	-3.19	60.4%	52.3%

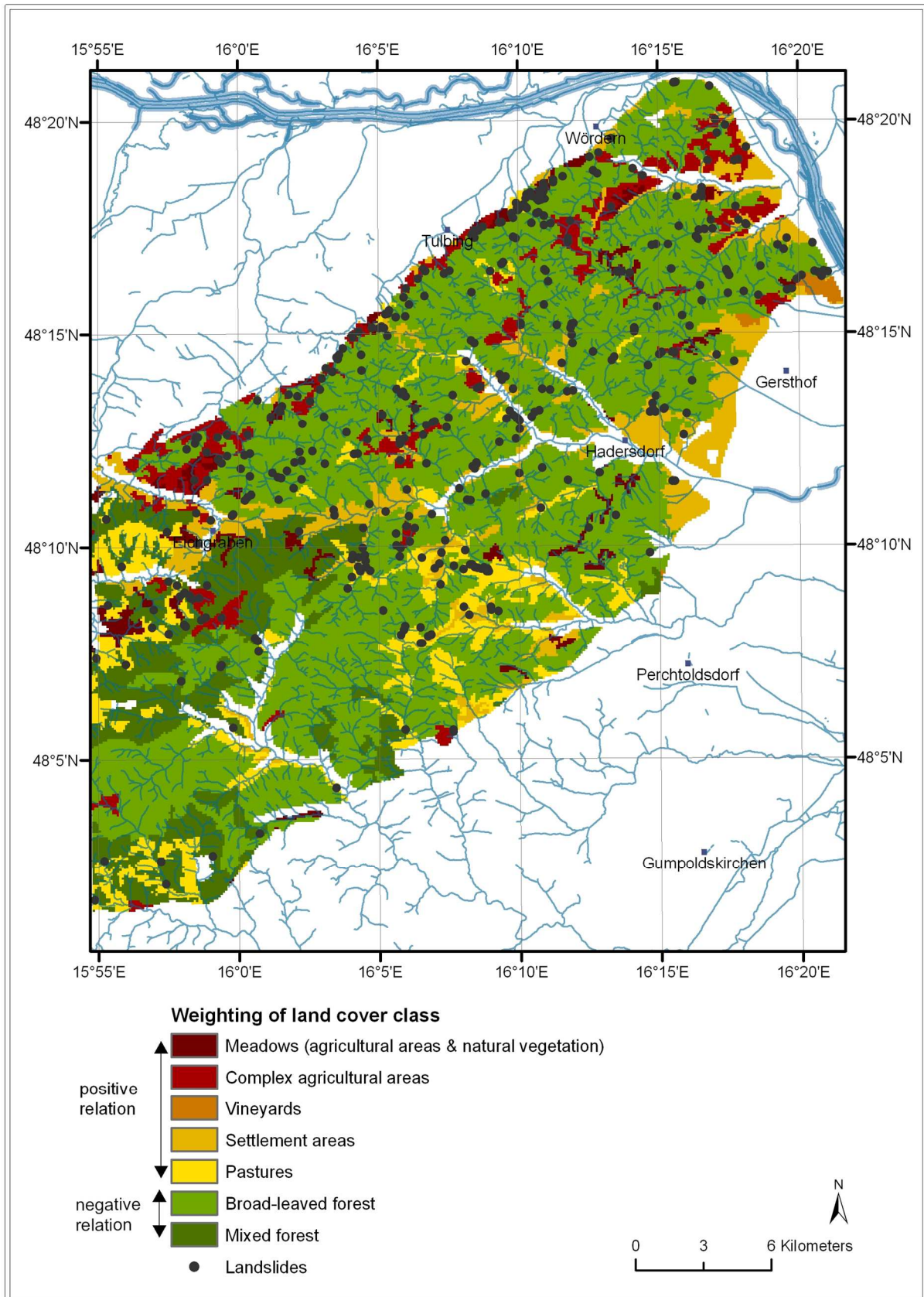


Figure 4-9. Results of the weighting of land cover on the basis of CORINE land cover data (CLC 1990). Although 52% of the landslides occur in the forest, the highest density of mass movements is identified in the treeless areas which are used for agriculture.

#### 4.2.2.5 Proximity to drainage lines (streams and creeks)

The study area is characterised by a high density of small creeks and temporally water-bearing gullies. Weighting shows that landslides are clearly located in the proximity of the drainage system (Figure 4-10). The occurrence of landslides is significant at a distance between 0 and 195m to drainage lines. The strongest positive association is evident at distances up to 70m (Table 4-7). This latter range covers 38% of all landslide events used for modelling, 45% can be found at a distance of 70-185m (Neuhäuser et al. 2012a, 2012b).

Table 4-7. Weighting of the proximity to drainage lines based on the Digital Landscape Model, which has a spatial accuracy of 3m (Table 4-1). The Table shows positive weight ( $W^+$ ), negative weight ( $W^-$ ), contrast ( $C$ ) and studentised contrast ( $C_s$ ). The classes 0-70 m and 70-195 m have a positive spatial association with the occurrence of landslides. The highest density of slides is evident at a distance of 0-70m to the drainage lines (Neuhäuser et al. 2012b).

Distance to drainage lines [m]	$W^+$	$W^-$	$C$	$C_s$	Area [%]	Landslides [%]
0-70	0.22	-0.11	0.33	3.08	31%	38%
70-195	0.13	-0.09	0.22	2.10	40%	45%
195-300	-0.67	0.10	-0.77	-4.25	18%	9%
300-400	-0.40	0.02	-0.43	-1.71	7%	5%
400-500	-0.64	0.01	-0.65	-1.29	2%	1%
500-600	0.02	0.00	0.02	0.04	1%	1%
600-700	0.18	0.00	0.18	0.25	1%	1%

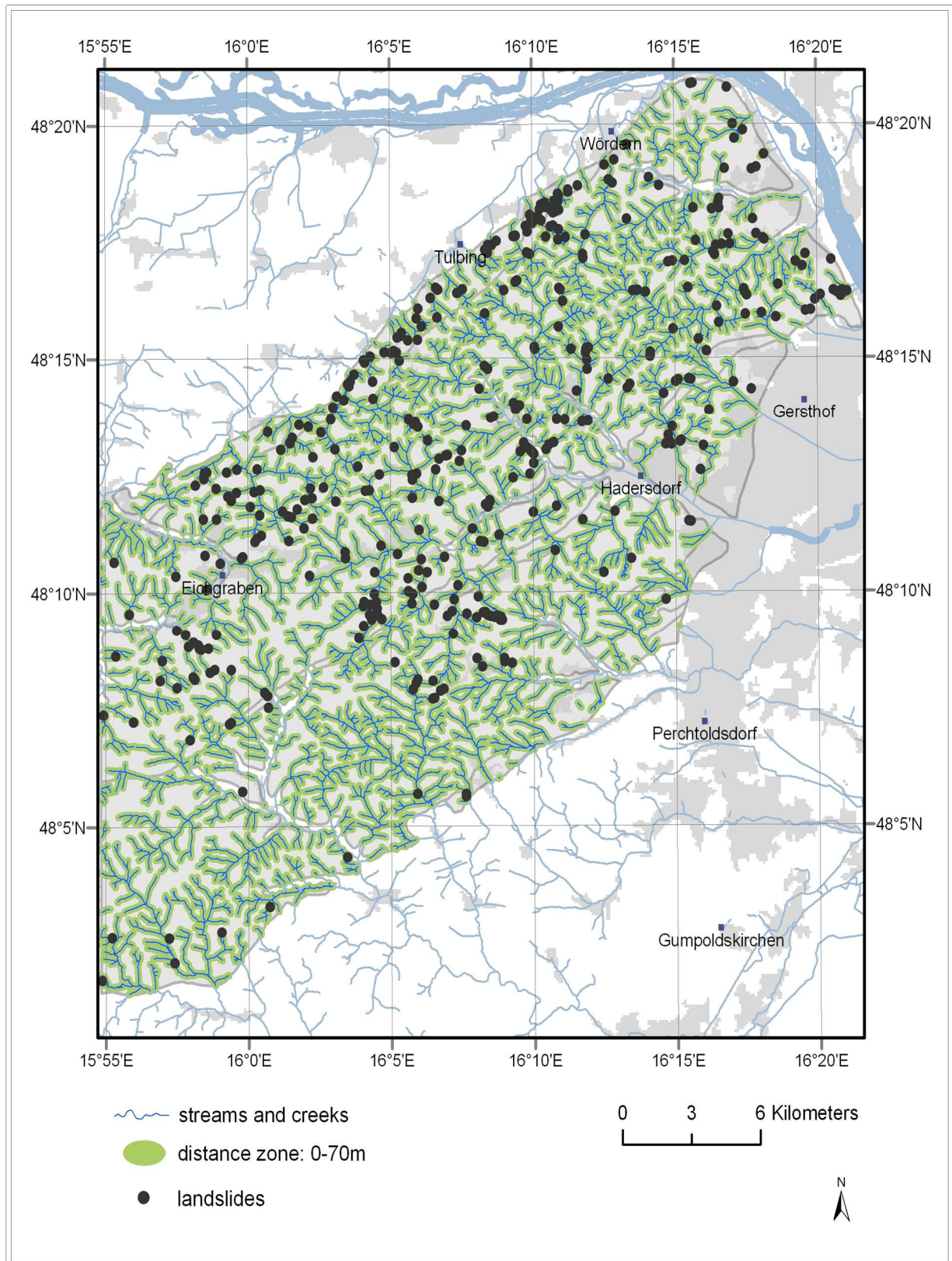


Figure 4-10. Results of the weighting of the proximity of drainage lines based on flow lines of the Digital Landscape Model (source in Table 4-2). The occurrence of landslides is significantly enhanced at a distance of 0-70m to the drainage lines.

#### 4.2.2.6 Weighting of morphology

In general, morphometrics determines steepness and shape of hillslopes and is therefore important for the assessment of landslide susceptibility. Weighting of slope aspect, slope gradient, and curvature (profile and plan) is summarised in Table 4-8.

Weighting of the slope aspect indicates that slopes facing north, west and north-west are highly landslide prone. The spatial distribution of the slope directions is displayed in Figure 4-11. In case of statistically significant positive weights the slope aspect has an evident positive association with landslide distribution (Neuhäuser et al. 2012a, 2012b). Furthermore, Figure 4-11 illustrates the prevailing wind direction (north-west and west) in the Vienna Forest, which shows conformity with the high susceptible slope aspect classes. Data about the distribution of wind direction are derived from the meteorological station in Mariabrunn in the study area (Zamg 2010c).

As far as the slope gradient is concerned, weighting indicates that landslide occurrence is statistically connected to slope gradients between 7° and 31°. The highest landslide density and strongest association with landslide distribution is located between 26° and 31°. This class denotes the highest predictive value ( $W+ = 0.93$ ) and is highly landslide prone (Neuhäuser et al. 2012a, 2012b).

In contrast to slope gradient, slope shape (profile and plan curvature) has a relatively weak predictive value. According to the weighting of the slope shape (profile and plan curvature), this geofactor has a relatively slight predictive value (maximum  $W+ = 0.13$ ). The profile curvature shows marginal positive association with convex curvatures only (Table 4-10). The weighting of the plan curvature results in a positive association with concave slopes (Neuhäuser et al. 2012a, 2012b).

Table 4-8. Weighting of slope aspect, slope gradient and curvature (profile and plan) based on ASTER DEM data (Aster 2010). The table shows positive weight ( $W+$ ), negative weight ( $W-$ ), contrast ( $C$ ) and studentised contrast ( $C_s$ ). The classes shown in italic characters have a positive association with the occurrence of landslides.

Morphological parameter		W+	W-	C	Cs	Area [%]	Landslides [%]
Aspect	<i>North (337.5°-360°)</i>	0.47	-0.05	0.52	3.13	7%	11%
	<i>West (247.5°-292.5°)</i>	0.30	-0.04	0.34	2.15	9%	12%
	<i>North-west (292.5°-337.5°)</i>	0.26	-0.04	0.30	2.01	11%	14%
	Flat	0.32	0.00	0.33	0.79	1%	2%
	North (0°-22.5°)	-0.07	0.01	-0.07	-0.39	9%	8%
	South-west (202.5°-247.5°)	-0.13	0.01	-0.14	-0.79	10%	9%
	North-east (22.5°-67.5°)	-0.12	0.02	-0.13	-0.84	14%	12%
	South (157.5°-202.5°)	-0.13	0.02	-0.15	-1.02	15%	13%
	East (67.5°-112.5°)	-0.27	0.03	-0.30	-1.71	12%	10%
	South-east (112.5°-157.5°)	-0.29	0.03	-0.32	-1.77	12%	9%

Slope gradient	0°-7°	-0.86	0.28	-1.14	-7.88	35.8%	15%
	7°-18°	0.28	-0.49	0.77	6.66	54.9%	72%
	18°-26°	0.20	-0.02	0.22	1.28	8.1%	10%
	26°-31°	0.93	-0.01	0.95	2.79	1.0%	3%
	31°-56°	0.00	0.00	0.00	0.00	0.2%	0.0%
Profile curvature	convex	-0.079	0.025	-0.104	-0.842	25%	23%
	elongated	-0.003	0.003	-0.005	-0.049	50%	50%
	<i>concave</i>	0.076	-0.027	0.103	0.887	25%	27%
Plan curvature	<i>convex</i>	0.126	-0.067	0.193	1.789	32%	37%
	elongated	-0.032	0.029	-0.061	-0.584	48%	46%
	concave	-0.153	0.035	-0.188	-1.365	20%	17%

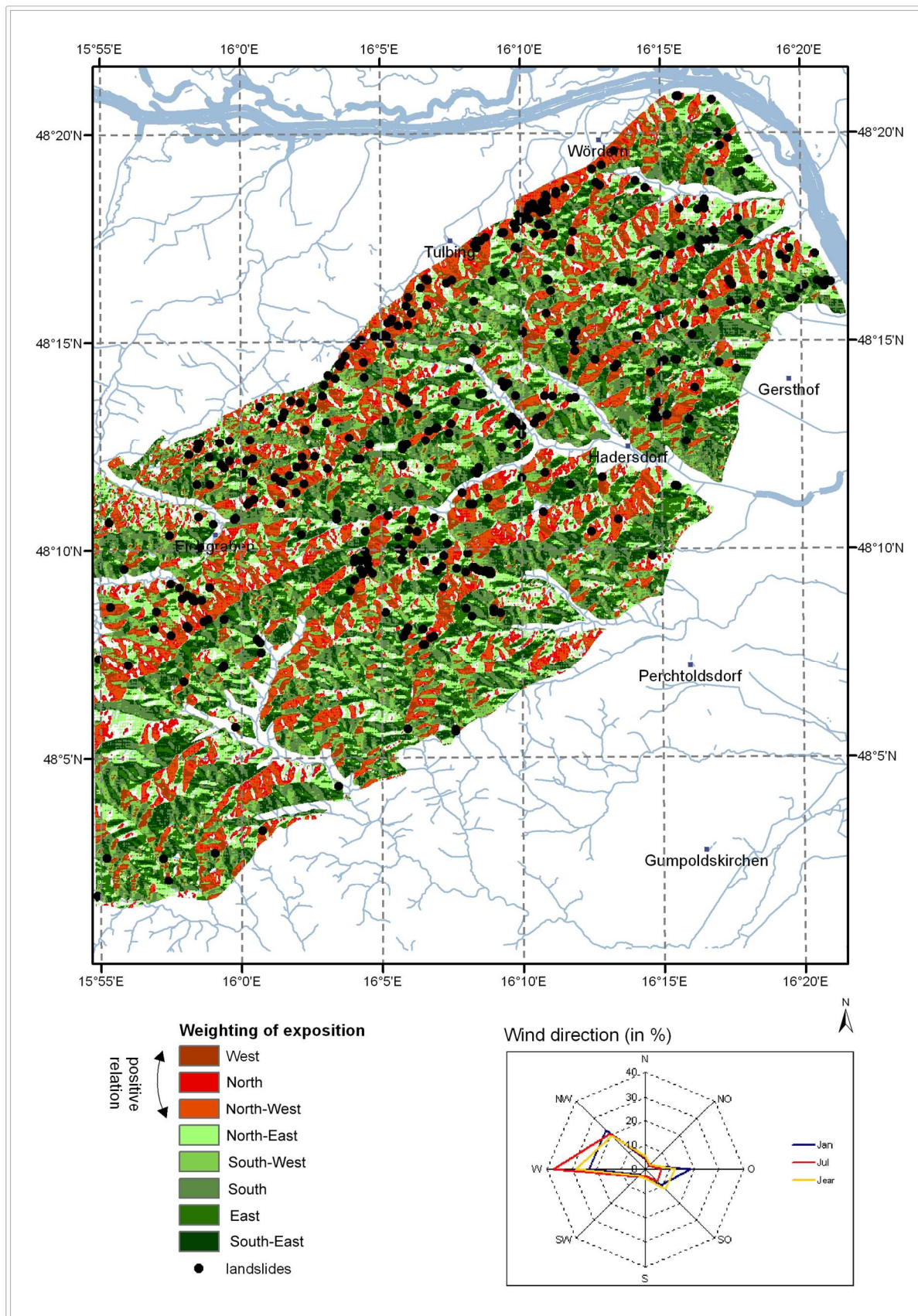


Figure 4-11. Results of the weighting of the slope aspect based on ASTER GDEM (Aster 2010). Slopes facing north, west and north-west are highly susceptible to landslides. The legend illustrates the prevailing wind direction (north-west and west) in the Vienna Forest which shows conformity with the high susceptible slope aspect classes. The data are derived from the meteorological station in Mariabrunn (Zamg 2010c).

#### 4.2.2.7 Weighting of the topographic position

In the present model specific landforms and slope positions (in relation to the surroundings) are investigated. The landslide distribution has a positive association with slopes near valleys and incised streams (Table 4-9). The majority of the landslides (36%) occur in gullies with deeply incised streams or creeks. Moreover, intermediate, steep slopes with a slope gradient above 5° are susceptible to landslides (Neuhäuser et al. 2012a, 2012b).

Plains, upper flat slopes and flat hilltops show a negative spatial relation to landslide distribution and can therefore be regarded as stable areas.

Table 4-9. Weighting of landform categories based on ASTER GDEM data. The Table shows positive weight ( $W^+$ ), negative weight ( $W^-$ ), contrast ( $C$ ) and studentised contrast ( $C_s$ ). The classes shown in italic characters have a positive association with the occurrence of landslides (Neuhäuser et al. 2012b).

Landform category	W+	W-	C	C <sub>s</sub>	Area [%]	Landslides [%]
<i>Gullies, deeply incised streams</i>	0.34	-0.15	0.50	4.60	26%	36%
<i>Intermediate, steep slopes (slope gradient &gt; 5°)</i>	0.27	-0.03	0.29	1.69	8%	10%
<i>U-shaped valleys ("Muldentäl")</i>	0.15	-0.03	0.18	1.30	15%	17%
<i>Middle slope ridges (potential landslide deposition mass)</i>	0.24	-0.01	0.24	0.83	3%	3%
Local ridges (small-sized ridges in plains)	-0.06	0.00	-0.06	-0.14	2%	1%
Upland drainage, creeks	-0.22	0.00	-0.22	-0.50	3%	4%
Plains (slope gradient < 5°)	-1.31	0.02	-1.33	-2.30	3%	1%
Upper, flat slopes	-0.37	0.05	-0.42	-2.41	14%	10%
Flat hilltops, high ridges	-0.38	0.11	-0.49	-3.62	26%	18%

---

### 4.2.3 Landslide susceptibility index and map

The derived weights of geofactor classes are finally combined in order to assess the overall landslide susceptibility. The statistical parameters are integrated into the posterior probability calculation based on Bayes' theory (Bonham-Carter et al. 1989, Agterberg et al. 1990, Bonham-Carter 2002, Sawatzky et al. 2009). In other words, the weight for each geofactor class is subsequently used for the prediction of landslides by integrating all the classes.

The derived probability map represents the landslide susceptibility degree of the terrain. Posterior probability values are calculated between 0 and 0.18. For a more coherent interpretation, class borders for the susceptibility index are based on the prior probability of 0.0008. This value provides a measure for landslide probability without considering any geofactors. On the contrary, posterior probability is calculated by integration of all geofactor classes. Therefore, it records where the prior probability is increased or decreased due to presence or absence of specific geofactors (Neuhäuser et al. 2012a).

Related to the different flysch nappes (Figure 3-6, page 29) there is a varying degree of susceptibility in the Vienna Forest. The Northern Zone has extensive areas characterised by the highest degree of landslide susceptibility (Figure 4-12). Geological units which are highly susceptible to landslides are present in this overthrust area to the Molasse Zone. The Wolfpassing Formation and the Klippen of the Northern Zone show significant landslide densities. These geological zones start in the north near St. Andrä-Wördern and continue in south-west direction along the ridges of the Tulbinger Kogel, Klosterberg, Frauenberg, and Eichberg (Neuhäuser et al. 2012c).

The Greifenstein Nappe, which occurs in the south of the Northern Zone, reveals moderate susceptibility in total, nevertheless there are locally higher dispositions dependent on specific topographical parameters, i.e. slope gradient and aspect. In addition, slopes near the valley bottom in the vicinity of streams and creeks are highly susceptible. Furthermore, the high density of tectonic faults is a main steering factor for landslides within the Greifenstein Nappe (Neuhäuser et al. 2012a).

In general, the Kahlenberg Nappe is characterised by moderate to locally high susceptibility, similar to the Greifenstein Nappe. The main steering factor in this nappe is the series of the Gaultflysch rich in clay, which drastically enhances susceptibility. This stratum occurs at the north-eastern edge of Vienna and in Purkersdorf in Lower Austria. The Gaultflysch beds run along the south of the Vienna Hills, Cobenzl and Kahlenberg, as a narrow zone, continue in the district of Penzing at the ridge of the Hochbruckenbergr and finally end in the town of Purkersdorf in Lower Austria in the area of the Glaskogel ridge (Neuhäuser et al. 2012a).

In the south of the study area, the Laab Nappe hillslopes are classified with the lowest landslide susceptibility. No significant relation between the present geological formations and the occurrence of landslides could be identified within this nappe. Moreover, this is the nappe with the lowest tectonic exposure in the Northern Vienna Forest. In comparison to the Greifenstein Nappe and the Northern Zone there are only few thrust faults (Neuhäuser et al. 2012a).



---

### 4.3 Model assessment and validation

Model assessment is carried out in order to quantify the uncertainties in the model and to test effectiveness of the prediction made by the hazard map. This is an important procedure, in particular when susceptibility or hazard maps are designated for application in regional and spatial planning. Therefore, in the following chapters the test of conditional independence, which directly influences the probability values, the success rate, and the prediction rate, is described.

#### 4.3.1 Agterberg-Cheng test of conditional independence

A one-tailed test for checking conditional independence was carried out according to Agterberg & Cheng (2002). Conditional independence of the geofactors implies that  $(T)$ , the sum of the weighted posterior probabilities, is equal to  $(n)$ , being the total number of landslides used for the model. A full conditional independence of geofactors, however, can hardly be accomplished, because it principally goes against the natural relationships. Thus, in practical applications  $(T)$  generally exceeds  $(n)$  indicating a possible lack of conditional independence (Agterberg & Cheng 2002, Bonham-Carter 2002).

The present model reveals a value of 0.65 for the relation of  $(n)$  to  $(T)$ . A value of 1 and above means full conditional independence, which can be hardly achieved in practice. Values of 0.5 and below indicate conditional dependence in the model. According to Bonham-Carter (2002) the sum of posterior probabilities  $(T)$  should not exceed the number of training points  $(n)$  by more than 15 %. Hence, the resulting value of 0.65 in the present model shows some conditional dependence in the model. A one-tailed test was applied to check whether or not  $(T-n)$  is significantly greater than zero (Agterberg & Cheng 2002), which indicates that the hypothesis of conditional independence in the model does not have to be rejected, but some conditional dependence is given. To some extent the basic assumption has been violated, which consequently results in a bias and an inflation of the probability values in absolute terms. However, regarding the probabilities as relative susceptibility values, the validity of the model is not reduced. Besides, the weights of the geofactor classes are not affected by the violation of the assumption. The final susceptibility map should therefore not only provide the probability values but should illustrate that the values are relative estimates by using a classification of low to high susceptibility. The purpose of the application of this method in landslide susceptibility analysis is to delineate areas susceptible to landslides and not to determine occurrence probability. The different flysch strata are not regarded as controlling geofactors for landslides in a direct manner. They are considered as units which carry special lithological properties directly or indirectly linked to the soil-mechanical characteristics of slopes. Corresponding geological properties are degree of consolidation, clay content, coherence, permeability of unconsolidated rock, and other soil and rock mechanical parameters (Neuhäuser et al. 2012a, 2012b). Therefore, the problem that  $(T)$  may exceed  $(n)$  in WofE is unrelated to the delineation of susceptible areas. If the purpose of the model was the determination of exact occurrence probability, other influences apart from conditional independence would have to be regarded in modelling. If there are undiscovered landslides in the study area, the prior probability is likely to be underestimated (Agterberg & Cheng 2002), which leads to a bias in the calculations. The final probability values are dependent on the number of landslides used for modelling. The number is decisive for the prior probability which influences the absolute range and stability of the weights of the factors.

### 4.3.2 Success rate and prediction rate

Prior to the modelling process the landslide inventory was separated into a modelling (85%) and a validation group (15%). The modelling set allows the assessment of the model performance. However, for the validation of the susceptibility map an independent group of landslides is required, which is represented by the validation set of landslides. By random selection 15% of the landslides were selected as validation group. This group is not incorporated into the model and can therefore be treated as unknown or future events (Neuhäuser et al. 2012a, 2012b).

A relatively low percentage of the validation group keeps statistical robustness, as the reduction of the modelling group leads to a decrease of probability values as well as lowering of confidence of the weights. In order to avoid that some classes of the controlling geofactors do not meet the confidence criteria, the landslides are not further reduced (Neuhäuser et al. 2012a, 2012b).

With the modelling group the success rate (Chung & Fabbri 2003) is calculated to evaluate the model performance. It indicates that for example 30% of the susceptibility map captures 70% of the landslides, which are used in the model (Figure 4-13) (Neuhäuser et al. 2012a, 2012b).

Furthermore, the prediction rate (Figure 4-13) calculates the percentage of the validation group, which could be “predicted” with the highest level of susceptibility, similar to the success rate. 15% of the susceptibility map, classified as highly susceptible, contains already 40% of the validation group. 50% of the map’s cumulated area also classified as highly susceptible to landslides contains 80% of the independent landslides and can therefore be considered as “predicted” (Neuhäuser et al. 2012a, 2012b).

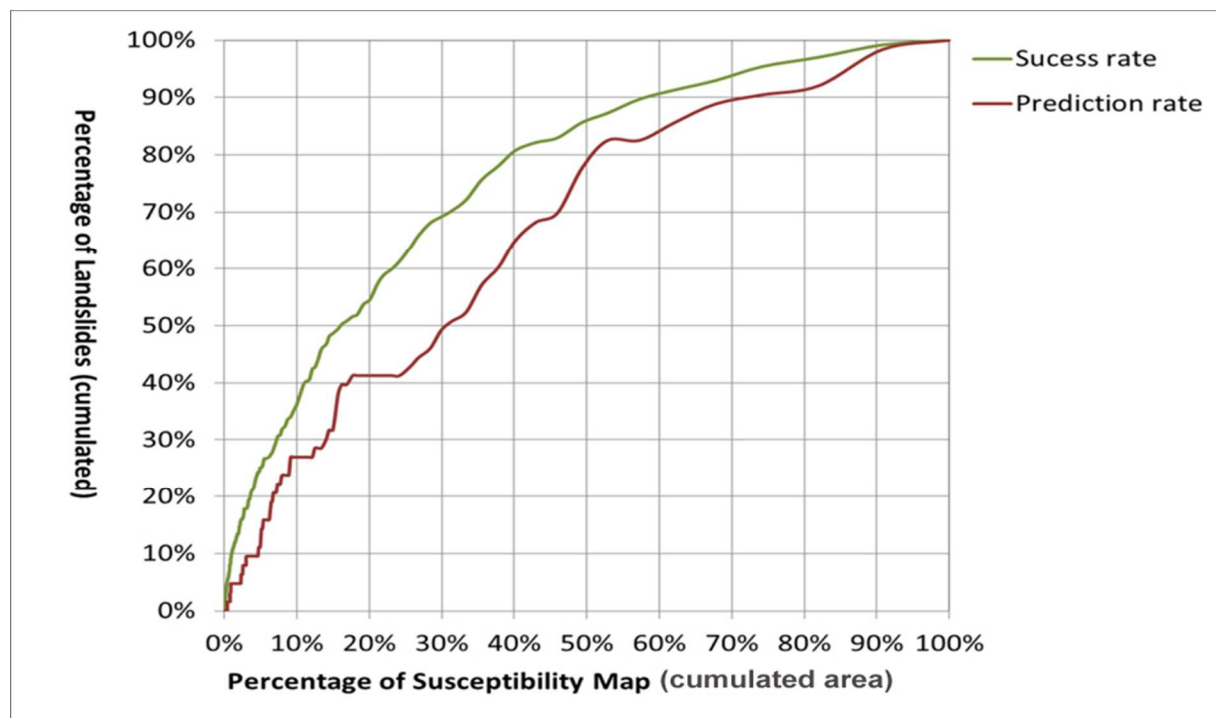


Figure 4-13. Prediction rate and success rate curve. The prediction rate curve shows the cumulated number of landslides captured by the susceptibility map (cumulated area) starting with the most susceptible areas (red) (Neuhäuser et al. 2012a).

---

## 5 Deterministic slope stability scenarios on large scale

The landslide phenomenon is further investigated by physically-based scenarios in the Hagenbach Valley in the Vienna Forest. The location of the study area is shown in Figure 3-1 (page 23) and a more detailed view on the Hagenbach gorge is provided in Figure 3-7 (page 30).

### 5.1 Methods and data

The developed method must be suitable to facilitate an investigation of the variable disposition to landslides in a comprehensive way and on a larger scale (scale 1:4,000). Variable disposition depends on alterable conditions like substrate wetness (Zimmermann et al. 1997, Heckmann & Becht 2006).

In order to integrate data about soil-mechanical properties as well as wetness conditions in sediments and unconsolidated rock, a physically-based approach, i.e. slope stability calculations are selected for the Hagenbach gorge (“Hagenbachklamm”) and are applied in various wetness scenarios. Meteorological and climate conditions, which change in the short and medium term and consequently affect slope stability, are taken into account in the development of the wetness scenarios.

The Stability Index Mapping (SINMAP) approach according to Pack et al. (1998, 2005) based on the infinite slope stability model combined with a steady-state hydrological model (Hammond et al. 1992, Montgomery & Dietrich 1994) is applied. This way stability classification maps which are determined by the specific catchment area, the slope gradient and soil-mechanical parameters are drawn up. However, SINMAP is applied in a modified approach, which is characterised by the following adaptations:

- (1) **Stability Index Mapping (SINMAP) without re-calibration of soil-mechanical parameters:** Usually, slope stability assessments using SINMAP are based on pedological (cf. Wawer & Nowocien 2003, Meisina & Scarabelli 2007) or geological mapping units (cf. Lan et al. 2004, Terhorst & Kreja 2009, Bai et al. 2010, Klimes & Blahut 2012) assuming that the geotechnical properties are related to these units. By applying several mapping units, so-called calibration regions, the physical input parameters can vary within the study area. In many cases these soil-mechanical input values are applied for the development of an initial slope stability classification map, which is subsequently calibrated by means of a landslide inventory (cf. Pack et al. 1998, Meisina & Scarabelli 2007, Bai et al. 2010). That means that the initial soil-mechanical parameters are adapted. They are modified interactively until the known landslides are ideally “predicted” by the slope stability index map. This conventional SINMAP approach is schematically illustrated in Figure 5-1. Due to this re-calibration the original input values may be significantly altered.

In the present paper the soil-mechanical parameters are captured by field and laboratory investigations (Damm et al. 2008, Mayerhofer et al. 2008, Terhorst et al. 2009, Damm & Terhorst 2010) and are not subsequently modified.

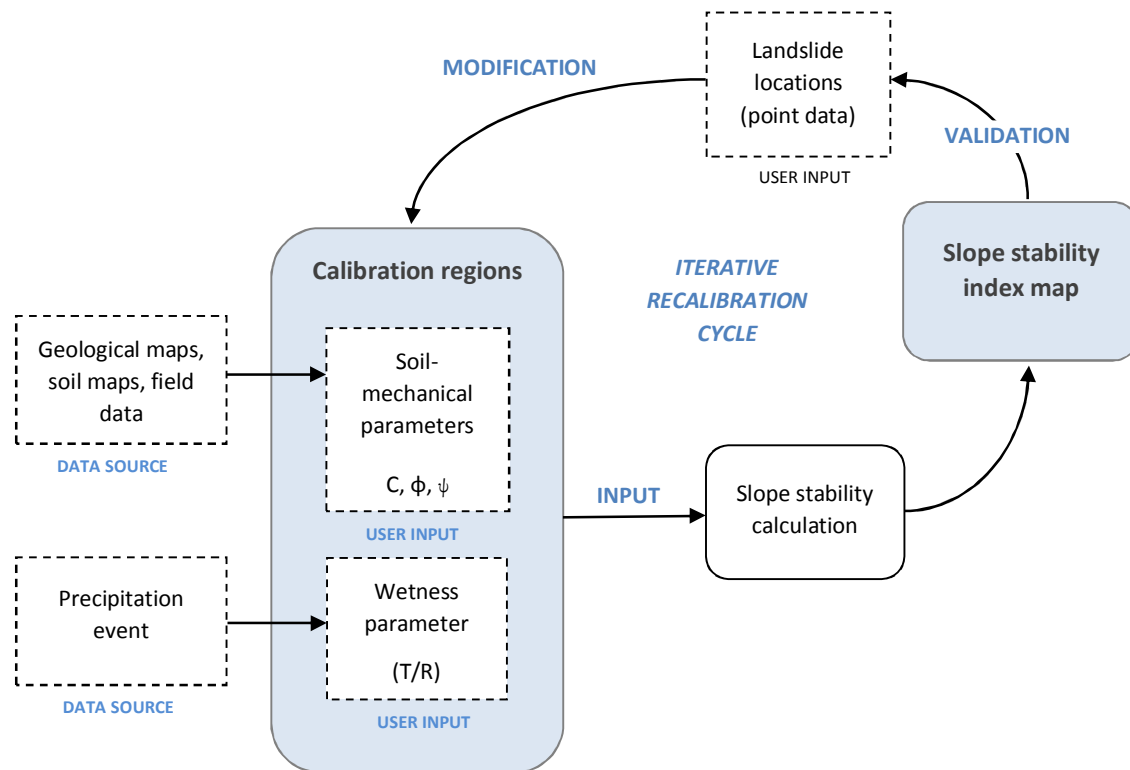


Figure 5-1. Conventional workflow in SINMAP application as described by Pack et al. (1998). During the modelling the input parameters are modified in an iterative recalibration cycle until the landslides, which are mapped as points, are ideally predicted by the slope stability index map. Therefore, the finally applied soil-mechanical parameters may differ from the initial values. The wetness conditions are based on a single precipitation event. Therefore the final slope stability index map shows a condition limited in time.

- (2) **Integration of process regions:** A further adaption of the SINMAP approach is related to the mapping units. They are used to implement a concept of process regions as a new mapping unit. The basis for the calculation of the stability index is constituted by process regions, which consider different potential sliding surfaces. The regions are based on a geomorphological model on slope formation according to Terhorst & Damm (2009) and Damm & Terhorst (2010). This enables the assessment of landslides in the flysch bedrock but additionally slope movements in the quaternary sediments covering the bedrock in wide areas. In this context it must be stated that the method of SINMAP is designed for shallow translational landsliding phenomena controlled by shallow groundwater flow convergence (Pack et al. 1998, 2005). Consequently, it applies to movements in the quaternary sediments, whose stability is mainly controlled by the influence of water (Damm & Terhorst 2010). The application of the approach for the deep-seated movements in the flysch bedrock, which occur on slope positions where the sediments are already eroded, might be subject to some restrictions due to the theoretical background. Therefore, an adequate and critical interpretation of the results is crucial, taking into account the concerns in regard to applicability of the method for this particular case.
- (3) **Hydrological calculations of the wetness parameter:** There is a further difference to other SINMAP approaches concerning the treatment of the wetness parameter  $(T/R)$ , which is, apart from cohesion and friction angle, an input parameter for the slope stability calculation. This hydrological value shows soil transmissivity  $(T)$  in relation to steady-state recharge  $(R)$ . In

this context the parameter (R) is not only understood as the portion of rainfall which infiltrates the substrate during a short-term weather event as proposed by Pack et al. (1998, 2005). This study also considers the parameter (R) as an average monthly recharge, which is deduced by water-balance calculations, taking into account soil water storage, surface runoff, evapotranspiration and snow melting or storage. Calculations are based on monthly averages of air temperature and precipitation. Transmissivity (T) is deduced from field investigations (Damm et al. 2008, Mayrhofer et al. 2008, Terhorst et al. 2009, Damm & Terhorst 2010). The modified approach is schematically shown in Figure 5-2.

- (4) **Wetness scenarios:** In comparable SINMAP applications a single precipitation event serves as input for the estimation of topographic wetness and consequently of slope stability only (Pack et al. 1998, Meisina & Scarabelli 2007, Terhorst & Kreja 2009, Bai et al. 2010, Klimes & Blahut 2012). The present study considers heavy and long-lasting rainfall events but also antecedent substrate wetness is taken into account. Hence, slope stability is investigated as a function of substrate wetness, which in turn depends on meteorological conditions. The development of various wetness scenarios with the aim to assess possible changes in slope stability is a main aspect of the work.

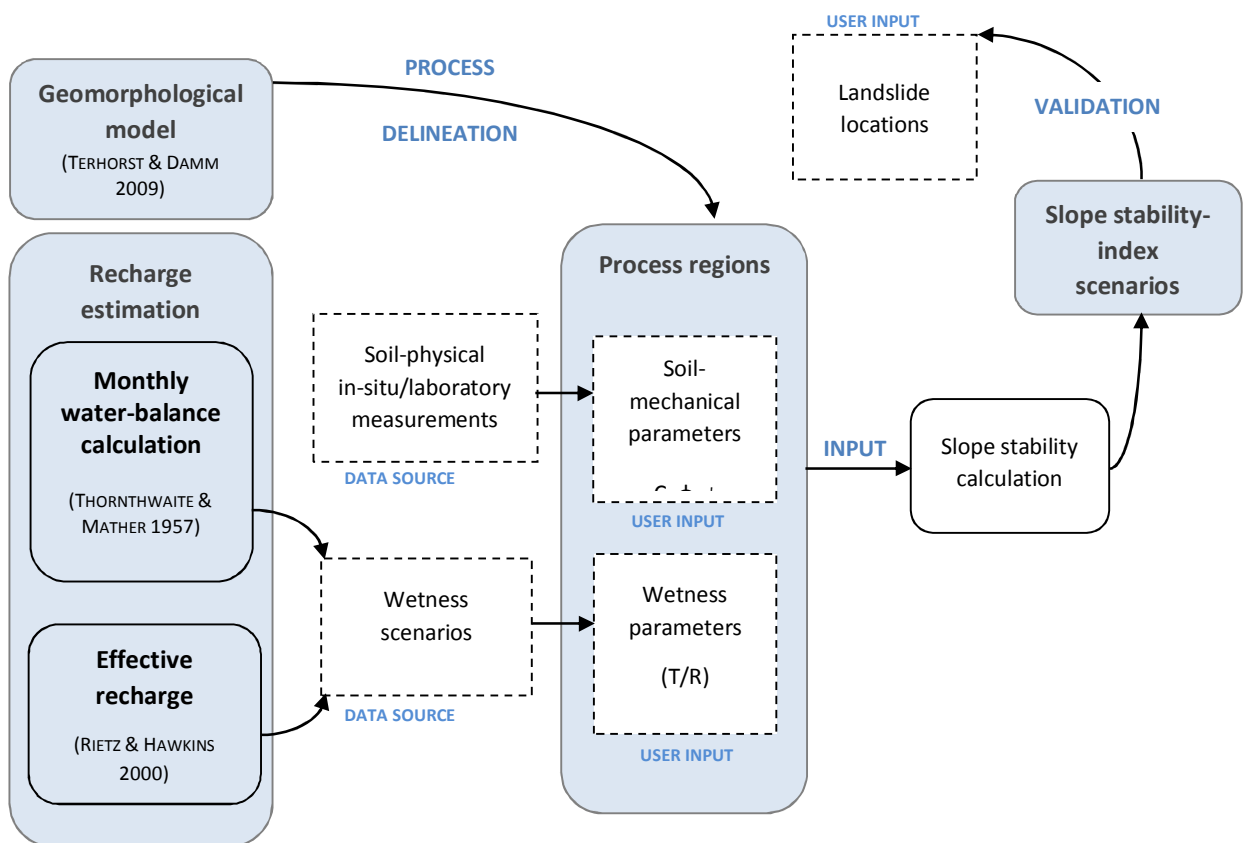


Figure 5-2. Adapted slope stability assessment. The basis for the calculation is constituted by process regions which consider different potential sliding surfaces. The regions are based on a geomorphological model on slope formation according to Terhorst & Damm (2009) and Damm & Terhorst (2010). The wetness parameter is defined by monthly water-balance calculations to elaborate seasonally varying wetness conditions and by effective recharge estimation to investigate effects of heavy rainfall. This recharge estimation results in different wetness scenarios, which enable a holistic assessment of variable disposition.

- 
- (5) **Landslide mapping by visual interpretation of shaded relief images:** Usually a landslide inventory comprising point data on landslide sites is used for the recalibration of the soil-mechanical and hydrological parameters. Instead of recalibration, structural information on landslides is used for the interpretation of stability index mapping in relation to future slope dynamics. Landslides are not mapped as points but as areal objects containing structural information. Visual interpretation of landslide phenomena on shaded relief images, produced on high-resolution DEMs, is applied to map landslides. The landslides are not used for recalibration during slope stability modelling but for interpretation and evaluation of the results (Figure 5-2).

### 5.1.1 Stability Index Mapping (SINMAP)

The SINMAP (Stability Index Mapping) methodology is based on the infinite slope stability model (e.g. Hammond et al. 1992, Montgomery & Dietrich 1994) that balances the destabilising components of gravity and the restoring components of friction and cohesion on a failure plane parallel to the ground surface (edge effects are neglected). The method combines steady-state hydrology assumptions with the infinite slope stability model to quantify slope stability (Pack et al. 2005).

Important inherent assumptions include that the subsurface hydrologic boundary is parallel to the surface and that soil thickness and hydraulic conductivity are uniform. Soil thickness is measured perpendicularly to the slope. Other hypotheses are a steady state shallow subsurface flow and the absence of deep-drainage and flow in the substratum (Meisina & Scarabelli 2007, Pack et al. 2005)

SINMAP derives its terrain stability classification from topographic parameters as well as from parameters which quantify the material properties of the substrate and a hydrological wetness parameter (Pack et al. 2005). On the one hand the wetness parameter depends on steady-state recharge and, on the other hand, on transmissivity of the substrate, hence the ability to drain lateral discharge (Pack et al. 2005). Transmissivity can be determined by hydraulic conductivity and substrate depth. The quantity of recharge depends on the applied estimation method and meteorological conditions that are investigated. The topographic parameters, in particular slope gradient and drainage area, are derived from a digital elevation model (DEM). The geotechnical parameters, i.e. friction angle and cohesion, which characterise the material properties of the involved layers, are user inputs.

The stability index does not quantify terrain stability by an absolute factor of safety but in terms of the probability that the factor of safety is  $> 1$ , in consideration of the defined parameter ranges. Therefore, inherent uncertainties or natural variability in the parameters can be integrated in the calculations (Pack et al. 2005). In particular, the parameters are specified in terms of upper and lower bounds, which define their parameter ranges. The stability index (SI) is defined as the probability that a location is stable assuming uniform distributions of the parameters over these uncertainty ranges. This value ranges between 0 (most unstable) and 1 (least unstable). A “best-case” and a “worst-case” scenario applying the optimistic and the pessimistic parameter range in relation to shear strength is computed to calculate a factor of safety (Pack et al. 2005).

The class definition of the stability index is used as proposed by Pack et al. (2005). The breakpoints for class borders and the appropriate characterisation of the classes of slope stability are shown in Table 5-1. In general, a stability index is computed in a worst-case scenario using the most conservative combination of parameters, i.e. the most unfavourable combination of parameters in relation to shear strength. If the model results in stability despite this pessimistic parameter set, the

---

stability index is defined as the factor of safety at this location. This yields a value  $> 1$  and the areas are classified as unconditionally stable. The stability classes “stable”, “moderately stable” and “quasi-stable” are defined by a stability index  $> 1$ . Slopes which are classified  $> 1$  are stable with the most conservative parameters in the specified parameter ranges. In these cases the stability index equals the factor of safety, which gives a measure of the magnitude of destabilising factors required to produce instability. External causes, like for example deforestation, road construction or local loading are necessary to destabilise the slopes (Pack et al. 2005).

The classes “lower threshold” and “upper threshold” define areas with a probability for instability according to the uncertainty ranges of the specified parameters. Instability arises in the model due to the combination of parameter values within the specified bounds. Therefore, external factors are not additionally required to influence slope stability. In the “lower threshold” class the stability index is between 0.5 and 1, indicating that the probability for instability is less than 50%. The class “upper threshold” is defined by a stability index between 0 and 0.5, expressing a probability for instability greater than 50% (Pack et al. 2005).

A best-case scenario is calculated using the most optimistic combination of parameters, i.e. the most favourable combination of parameters in relation to shear strength. If the model results in instability despite this optimistic parameter set, the factor of safety is  $< 1$ . The stability index, i.e. the probability that the location is stable, is set to 0. Locations where a stability index is smaller than 0 are unconditionally unstable and are classified as “defended”. In this stability class the slopes are unstable for the whole parameter’s ranges (Pack et al. 2005).

Where such “defended” slopes are present in the field, stabilising forces, for example bedrock outcrops, are responsible for stability (Pack et al. 2005). Field investigations in the study area showed solid bedrock ridges which often build the flanks of ancient landslides. The areas between these solid ridges are affected by mass movements in many cases (Kötttritsch 2008). A similar phenomenon is also described by Tufescu (1970) in the flysch-Carpathians where resistant layers of the vertically bedded bedrock build the flanks of landslides, which occur in the less resistant layers (Figure 5-3). While the brittle sandstone “Mürbsandstein” of the Altenglengbach formation is highly landslide prone due to its sensitivity to moisture penetration, sequences of more resistant “Wördener” sandstones can be responsible for solid bedrock outcrops (Kötttritsch 2008).

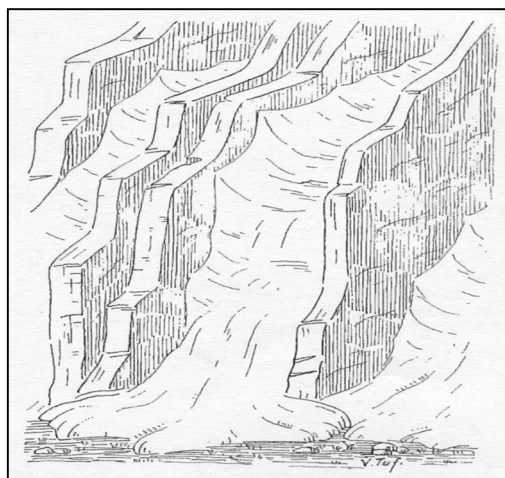


*Figure 5-3. Landslides between solid bedrock outcrops of vertically bedded layers (Tufescu 1970, modified).*

Table 5-1. Stability class definition according to Pack et al. (2005), modified.

Class	Condition	Predicted state	Parameter range	External and internal influences on stability
1	SI > 1.5	Stable	Range cannot model instability (unconditionally stable)  Slope stability index equals factor of safety	Stable even under pessimistic parameters of the model; significant external, destabilising factors are required for instability; stable even under pessimistic parameter range in relation to shear strength
2	1.5 > SI > 1.25	Moderately stable		Still stable under pessimistic parameters of the model; moderate external, destabilising factors are required for instability
3	1.25 > SI > 1.0	Quasi-stable		Narrowly stable under pessimistic parameters of the model; minor external, destabilising factors could lead to instability
4	1.0 > SI > 0.5	Lower threshold	Probability for instability > 50%; pessimistic half of range is required for instability	Stable under optimistic parameters; external destabilising factors are not required for instability; pessimistic parameters can cause instability
5	0.5 > SI > 0.0	Upper threshold	Probability for instability < 50%; optimistic half of range is required for stability	External destabilising factors are not required for instability; stabilising factors may be responsible for stability
6	0.0 > SI	Defended	Range cannot model stability (unconditionally unstable)	Instable for all parameters ranges of the model; stabilising factors are required for stability, like solid bedrock outcrops

The factor of safety calculation (FS) is based on the infinite slope form of the Mohr–Coulomb failure law as expressed by the ratio of stabilising forces (shear strength) to destabilising forces (shear stress) on a failure plane parallel to the ground surface according to Hammond et al. (1992).

$$(5-1) \quad FS = \frac{C_r + C_s + \cos^2 \theta [\rho_s g (D - D_w) + (\rho_s g - \rho_w g) D_w] \tan \phi}{D \rho_s g \sin \theta \cos \theta}$$

Wherein  $C_r$  is root cohesion [ $N/m^2$ ],  $C_s$  is soil cohesion [ $N/m^2$ ] and  $\theta$  represents slope angle (arc tangent of slope). Variable  $\rho_s$  stands for wet soil density [ $kg/m^3$ ],  $\rho_w$  denotes the density of water [ $kg/m^3$ ] and  $g$  is the gravitational acceleration ( $9.81m/s^2$ ). The variables  $D$  and  $D_w$  denote the vertical soil depth [m] and the vertical height of the water table within the soil layer [m], respectively. The internal friction angle of the soil [ $^\circ$ ] is represented by  $\phi$ .

SINMAP is based on a dimensionless form of the infinite slope stability mode, which is reached by some modifications. In particular, soil thickness is interpreted perpendicularly to the slope, rather than soil depth measured vertically. Therefore, soil thickness  $h$  [m], and depth are related as formulated in equation (5-2). The ratio of ( $h_w$ ) to  $h$  is interpreted as relative wetness (equation 5-3). The density of water ( $\rho_w$ ) to soil ( $\rho_s$ ) is referred to as ( $r$ ) (equation 5-5). Cohesion is combined into a dimensionless cohesion factor with soil density and thickness (equation 5-4). It can be regarded as the ratio of cohesive strength in relation to the weight of the soil (Pack et al. 2005).

$$(5-2) \quad h = D \cos \theta$$

$$(5-3) \quad w = \frac{D_w}{D} = \frac{h_w}{h}$$

$$(5-4) \quad \frac{(C_r + C_s)}{h \rho_s g}$$

$$(5-5) \quad r = \frac{\rho_w}{\rho_s}$$

With the modifications, mentioned above, the factor of safety (FS) is reduced to

$$(5-6) \quad FS = \frac{C + \cos \theta [1 - wr] \tan \phi}{\sin \theta}$$

The infinite slope stability model is combined with a topographic wetness index, which integrates the concept of the “specific catchment area” ( $a$ ). The respective hydrological model according to Beven & Kirkby (1979) is integrated into the slope stability calculation and comprises the following assumptions according to Pack et al. (2005):

- Shallow lateral subsurface flow follows topographic gradients. This implies that the contributing area is given by the specific catchment area ( $a$ ) defined from surface topography
- Lateral discharge ( $q$ ) at each point is in equilibrium with a steady state recharge  $R$  [m/h]
- The capacity for lateral flux at each point is  $T \sin \theta$  where  $T$  is the soil transmissivity [ $m^2/h$ ], i.e. hydraulic conductivity [m/h] multiplied by soil thickness,  $h$  [m]. It is assumed that conductivity of a soil mantle is uniform.

Combining the assumption on the specific catchment area and on steady state recharge, lateral discharge (depth integrated per unit contour length) can be defined by:

$$(5-7) \quad q = Ra \text{ [m}^2\text{/h]}$$

When lateral flux is assumed as  $T \sin \theta$ , the relative wetness is:

$$(5-8) \quad w = \min\left(\frac{Ra}{T \sin \theta}, 1\right)$$

The relative wetness, which defines the relative depth of the perched water table within the soil layer, has an upper bound of 1 with any excess assumed to form overland flow. The ratio  $R/T$  in equation (5-8) quantifies the relative wetness in terms of assumed steady state recharge relative to the soil's capacity for lateral drainage of water. The ratio  $R/T$ , which SINMAP treats as a single parameter, therefore combines both climate and hydrogeological factors. The quantity  $(T/R) \sin \theta$  [m] may be thought of as the length of the hillslope (planar, not convergent) required to develop saturation in the critical wet period being considered (Pack et al. 2005).

In this study topographic wetness is analysed in detail related to possible changes. Therefore, the classification of the topographic wetness index is described below. The wetness index quantifies specific conditions in regard to saturation where relative wetness ( $w$ ) equals 1 in equation 5-8.

The wetness parameter ( $R/T$ ) can be denoted as ( $x$ ) and is defined by a minimum ( $x_1$ ) and a maximum ( $x_2$ ) value representing its variability. The range can be described as  $x \sim U(x_1, x_2)$  (Pack et al. 2005) by means of the parameter range with the upper and lower bounds. There are three possible cases in equation 5-8 which represent the classification regime of the topographic wetness index. The possibilities and the classes are shown in Table 5-2.

Table 5-2. Definition of topographic wetness classes based on three cases of the wetness parameter ( $x$ ) according to Pack et al. (2005).

Case	Relative wetness	Condition	Class	Predicted condition
1	$w=1$ for the full range ( $x_1, x_2$ )	$x_1 \frac{a}{\sin \theta} > 1$	Saturated	The areas are saturated for the whole range of the wetness parameter
2	$w=1$ for part of the range ( $x_1, x_2$ )	$x_2 \frac{a}{\sin \theta} > 1$ and $x_1 \frac{a}{\sin \theta} < 1$	Threshold saturation	There is a probability for saturation because saturation is reached under the maximum wetness ( $x_2$ ) and not reached under the minimum wetness ( $x_1$ ) condition
3	$w \neq 1$	$1 > x_2 \frac{a}{\sin \theta} > 0$ and $x_2 \frac{a}{\sin \theta} > 0.1$	Partially wet	The area is never saturated over the whole range of wetness; a level of wetness greater than 0.1 is given; the wetness level is encoded as degree of wetness between 0 and 1 assuming maximum wetness ( $x_2$ )
4	$w \neq 1$ for the full range ( $x_1, x_2$ )	$1 > x_2 \frac{a}{\sin \theta} > 0$ and $x_2 \frac{a}{\sin \theta} < 0.1$	Low moisture	The area is never saturated over the whole range of wetness; a level of wetness less than 0.1 is given; the wetness level is encoded as degree of wetness between 0 and 1 assuming maximum wetness ( $x_2$ )

To define the stability index, the wetness index from equation (5-8) is incorporated into the dimensionless factor of safety, equation (5-6), which becomes

$$(5-9) \quad FS = \frac{C + \cos \theta \left[ 1 - \min \left( \frac{R}{T} \frac{a}{\sin \theta}, 1 \right) r \right] \tan \phi}{\sin \theta}$$

The specific catchment area ( $a$ ) and the slope angle ( $\theta$ ) are derived from the DEM, whereas the values of cohesion ( $C$ ), the friction angle ( $\tan\phi$ ), the water to soil density ratio ( $r$ ), and the wetness parameter ( $R/T$ ) are user input. The density ratio ( $r$ ) is treated as constant with a value of 0.5. In the remaining variables uncertainty through the specification of lower and upper bounds is incorporated. These bounds are defined by uniform probability distributions within which these quantities are assumed to vary at random (Pack et al. 2005).

$R/T=x$ ,  $\tan\phi=t$  and the uniform distributions with lower and upper bounds are denoted as  $C\sim U(C_1, C_2)$ ,  $x\sim U(x_1, x_2)$  and  $t\sim U(t_1, t_2)$  (Pack et al. 2005). The smallest value for the cohesion ( $C=C_1$ ) and the friction angle ( $t=t_1$ ) together with the largest value for the wetness parameter ( $x=x_2$ ) define the worst-case scenario with the most pessimistic parameters (equation 5-10) under their assumed uncertainty or variability (Pack et al. 2005).

$$(5-10) \quad FS_{min} = \frac{C_1 + \cos \theta \left[ 1 - \min \left( x_2 \frac{a}{\sin \theta}, 1 \right) r \right] t_1}{\sin \theta}$$

Areas where the factor of safety is  $> 1$  in the worst-case scenario ( $FS_{min}$ ) are unconditionally stable in terms of this model. For areas where the minimum factor of safety ( $FS_{min}$ ) is  $< 1$  there is a possibility of failure, expressed as the spatial probability that the location is stable (Pack et al. 2005). These cases are formulated in Table 5-3 as cases 1 and 2.

Contrary to the worst-case scenario, the best-case scenario takes into account the optimistic half of the parameter ranges, in particular the largest cohesion ( $C=C_2$ ) and friction angle ( $t=t_2$ ) in combination with the smallest wetness parameter ( $x=x_1$ ) (equation 5-11) (Pack et al. 2005).

$$(5-11) \quad FS_{max} = \frac{C_2 + \cos \theta \left[ 1 - \min \left( x_1 \frac{a}{\sin \theta}, 1 \right) r \right] t_2}{\sin \theta}$$

In areas where the factor of safety in the best-case scenario ( $FS_{max}$ ) is  $< 1$  the probability that the location is stable is set to 0. Hence, the stability index equals 0 (Pack et al. 2005). These cases are formulated in Table 5-3 as case 3.

Table 5-3. Definition of factor of safety and stability index according to Pack et al. (2005).

Case	Stability scenario	Factor of safety	Stability index	Predicted condition
1	Worst-case scenario	$FS_{min} > 1$	$SI = FS_{min}$ , $SI > 1$	Unconditionally stable
2	Worst-case scenario	$FS_{min} < 1$	$SI = \text{Prob}(FS > 1)$	Probability of instability
3	Best-case scenario	$FS_{max} < 1$	$SI = \text{Prob}(FS > 1) = 0$	Unconditionally unstable

The cases of Table 5-3 describe functions, which are illustrated in Figure 5-4. They are applied to delineate the stability classes dependent on the relative wetness, in particular the degree of saturation. The diagram shows the slope angle ( $\Theta$ ) on the x-axis and the specific catchment area ( $a$ ) on the y-axis. The curves in the diagram which define the stability classification are derived from probability functions (cf. Pack et al 2005). The probability functions are dependent on the relative wetness (equation 5-8).

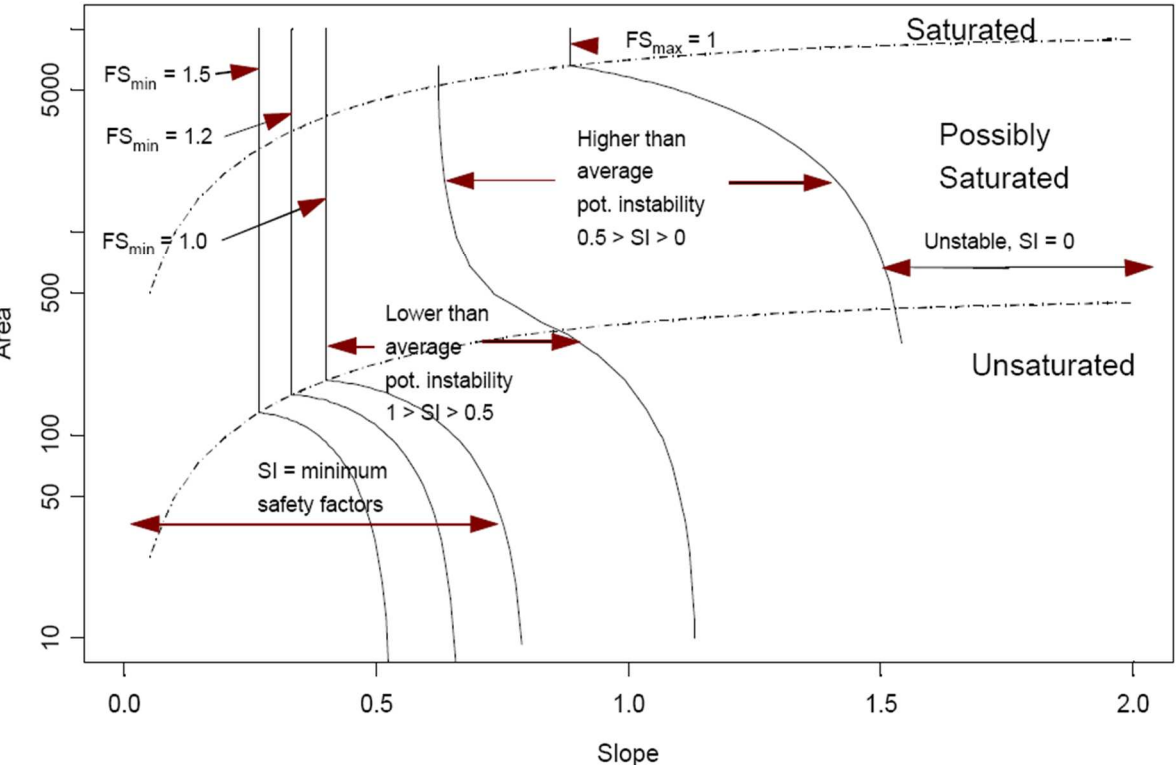


Figure 5-4. Stability Index defined in area-slope space (Pack et al. (2005). The vertical lines in the diagram are defined by stability scenarios shown in Table 5-3 and by a cumulative distribution function (cp. equation 5-14).

As the expression “min” in equation 5-8 indicates, limits on the occurrence of saturation are considered. Therefore, saturation is reached when  $w = 1$  in equation 5-8, which can be modified to the relation

$$(5-12) \quad \text{---} = \text{---}$$

This equation (5-12) evaluated for the minimum wetness parameter  $R/T$  (i.e.  $x=x_1$ ) defines the upper dashed line in Figure 5-4. It represents conditions where saturation is reached ( $w=1$ ) even under the minimum wetness in the catchment area. It delineates the range between saturated and possibly saturated (Pack et al. 2005).

Similarly, the equation (5-12) evaluated for the maximum wetness conditions  $R/T$  (i.e.  $x=x_2$ ) defines the lower dashed line. It represents conditions where saturation is reached ( $w=1$ ) under the maximum wetness. Therefore, it delineates the ranges unsaturated and possibly saturated (Pack et al. 2005).

The straight vertical lines in Figure 5-4 are the slopes that provide a particular factor of safety under saturated conditions. In the case of saturation (i.e.  $w=1$ ) the factor of safety is independent of the specific catchment area ( $a$ ) and is obtained by solving the factor of the safety equation (5-9) for the prevailing slope gradient (Pack et al. 2005).

The functions are derived by computing equation 5-9 for the slope gradient. This results in a function (equation 5-13), which is subsequently used for evaluation for user inputs ( $t$ ), ( $C$ ), ( $w$ ) and appropriate fixed arguments for ( $FS$ ), namely  $FS_{min} = 1.5$ ,  $FS_{min} = 1.0$  and  $FS_{max} = 1.0$  (Pack et al. 2005).

$$(5-13) \quad csw(t, C, w, FS) = \cos^{-1} \left( \frac{-c(1-rw)t + \sqrt{FS^2(FS^2 + (1-wr)^2t^2 - C^2)}}{FS^2 + (1-wr)^2t^2} \right)$$

The curves defining the factor of safety under unsaturated conditions are obtained by solving equation 5-9 for the variable ( $a$ ) and for the case that saturation is not reached  $w < 1$ . This calculation is converted into function (5-14), which defines the lines in Figure 5-3 corresponding to the fixed factor of safety ( $FS$ ) in unsaturated condition (Pack et al. 2005).

$$(5-14) \quad af(\theta, C, T, x, FS) = \frac{\sin \theta}{x r} \left( 1 - \frac{FS \sin \theta - C}{t \cos \theta} \right)$$

Equations (5-13) and (5-14) are sufficient to compute a stability index for unconditionally stable and unstable regions (cp. Table 5-3). However, the region shown in Figure 5-3, which is located between unconditionally stable and unstable regions, is derived probabilistically. For that probabilistic determination of the stability index, distributions are derived from the factor of safety ( $FS$ ) given by equation 5-6. A cumulative distribution function is drawn up and results in the line shown in Figure 5-3. A detailed derivation of the cumulative distribution functions can be found in Pack et al. (2005). In general, cohesion and friction angle are considered as uniformly distributed random variables. The probability functions depend on the degree of saturation.

### 5.1.2 Process regions and their soil-mechanical parameters

A major objective is to consider landslides which occur in the flysch bedrock and additionally slope movements in quaternary sediments, which are crucial for slope formation in the Vienna Forest (Terhorst et al. 2009, Damm & Terhorst 2010). Therefore, a process model is applied in the Stability Index Mapping procedure. Process regions represent areas where different sliding surfaces are relevant. These regions are delineated by means of a geomorphological model on slope development in the study area (Terhorst & Damm 2009, Damm & Terhorst 2010). The process regions contain the soil-mechanical parameters measured in the field investigations (Damm et al. 2008, Mayrhofer et al. 2008, Terhorst et al. 2009, Damm & Terhorst 2010).

The geomorphological model has been developed on the basis of geomorphological field surveys, geotechnical as well as laboratory investigations (Damm et al. 2008, Mayrhofer et al. 2008, Terhorst et al. 2009, Damm & Terhorst 2010). Based on these investigations, it was possible to describe the evolution and the development of the morphodynamic processes and slope stability for the Hagenbach Valley (Terhorst & Damm 2009, Damm & Terhorst 2010). Different stages of slope formation which cause a distinct spatial distribution of quaternary sediments and decomposed flysch bedrock at the present land surface are defined. In the present study this model of slope formation is used for the spatial delineation of process regions in the study area. The geomorphological model according to Damm & Terhorst (2010) and the mapping of the process regions in GIS are described below.

---

The flysch rock formations of the studied area, especially the Altlenbach Formation, are largely formed by variable solid and strongly deformed bedrock. The geological formations are composed of interbedded marly sandstones, lime marls, sandstones, and calcareous sandstones, which are highly susceptible to moisture penetration. The flysch bedrock is superimposed by periglacial cover beds and loess layers in wide areas. The quaternary sediments are affected by erosive processes in the middle and mainly in the lower slope sections of the Hagenbach Valley. Due to erosive processes the bedrock is locally uncovered. As soon as the flysch sandstone is exposed, decomposition by carbonate leaching starts (Terhorst & Damm 2009, Damm & Terhorst 2010).

Taking into account the relation between the sedimentological structure and the soil/rock mechanical properties, it was possible to derive a temporal sequence of morphodynamic processes and slope stability for the Hagenbach Valley (Terhorst & Damm 2009, Damm & Terhorst 2010). The study of the spatial distribution of slope surfaces and sediments there, with respect to recent and present landslides, comprises five phases of slope development, which can be summarised as follows (Damm & Terhorst 2010):

Primarily, the (I) 'first initial phase' is constituted by a completely developed slope sequence (Figure 6-6). Periglacial cover beds and loess sediments are present on top of the bedrock. During the (II) 'second phase' of slope formation a first sliding process occurs, which causes sliding of the permeable loess deposits on top of the impermeable basal periglacial cover beds. Subsequently, a transition to the (III) 'third phase' is initiated, which corresponds to an erosional phase in the sequence. Erosion of the basal periglacial cover beds uncovers solid bedrock. The (IV) 'fourth phase' corresponds to the decomposition phase. During this process the flysch sandstones, notably the calcareous sandstones ('Mürbsandstein'), are affected by profound weathering proceeding fast under the influence of humidity. The (V) 'fifth phase' represents a second sliding phase. The decomposed sandstone is affected by further, shallow, translational slides after exceeding a critical mass. This process results in the uncovering of unweathered flysch sandstones. Afterwards, the phases four and five can reoccur in an alternating pattern and/or rockfall starts in sandstone slopes (Damm & Terhorst 2010).

On the basis of the geomorphological model according to Damm & Terhorst (2010), as described above, the following process regions are defined for slope stability assessment:

- (1) **Process region (1)** – flysch bedrock of the Altlenbach Formation: Landslides occur directly in the flysch bedrock with an estimated depth of 8m to 20m. There are no measurements on the depth of the bedrock but it is assumed on the basis of the depth of ancient landslides in the Hagenbach Valley. The actual slope dynamics frequently uncovers solid bedrock, which is in turn exposed to fast decomposition. Therefore, consolidated sandstones up to complex decomposition products like sand-silt layers are present (Damm & Terhorst 2010). In the slope stability calculation specific parameter ranges can be used for such variations, offering an upper and lower parameter limit.
- (2) **Process region (2)** – quaternary sediments: Shallow landslides with an observed depth of 4m take place directly in the quaternary deposits overlaying the flysch bedrock. An impermeable basal periglacial cover bed, mainly consisting of clay and marls, has been identified as sliding surface (Terhorst et al. 2009, Damm & Terhorst 2010). It is superimposed by loess layers and loess-influenced middle and upper periglacial cover beds, which represent the critical slide mass. After exceeding critical parameter values in the equilibrium parts of the sequence of the quaternary sediments slide down along the basal layer.

---

Field investigations are considered for the delineation of the process regions (Damm et al. 2008, Mayrhofer et al. 2008, Terhorst et al. 2009, Damm & Terhorst 2010). According to these investigations, evidence for the presence of quaternary sediments is given in the upper slope shoulder, above the oversteepend decline of the gorge. The impermeable basal periglacial cover bed is responsible for shallow movements and crops out at a level of 280m a.s.l., accordingly (Köttritsch 2008).

Below this level the basal layer is hardly relevant for mass movements because geomorphological processes have already eroded them, uncovering the Flysch bedrock. Therefore, in the lower slope positions mass movements occur directly in the Flysch bedrock, which is affected by profound decomposition (Damm & Terhorst 2010). Hence, Process region (1) is assigned to slope positions where the quaternary cover beds are eroded (below 280m a.s.l.). This is a simplification because on principle deep-seated movements in the bedrock are probable at the whole cross section. However, shallow movements are most probable at the upper slope positions where the cover beds are in place (above 280m a.s.l.).

The delineation of the process regions is processed on the basis of contour lines, providing information on the crop out level of the basal layer of the periglacial cover bed. The basis for the digital data is the high-resolution DGM (Provincial Government of Lower Austria 2006) providing detailed information on surface morphology. Figure 5-5 shows the borderline of the process regions, where the lower slope positions (below 280m a.s.l.) are assigned to process region (1) and the upper slope shoulder (above 280m a.s.l.) is assigned to process region (2). The figure shows further the topographic character of the gorge in a slope gradient map together with structural information on former landslides, which are mapped on shaded relief images. The slope gradient map illustrates the oversteepend slopes near the Hagenbach creek with slopes with an inclination from 36° to 78°.

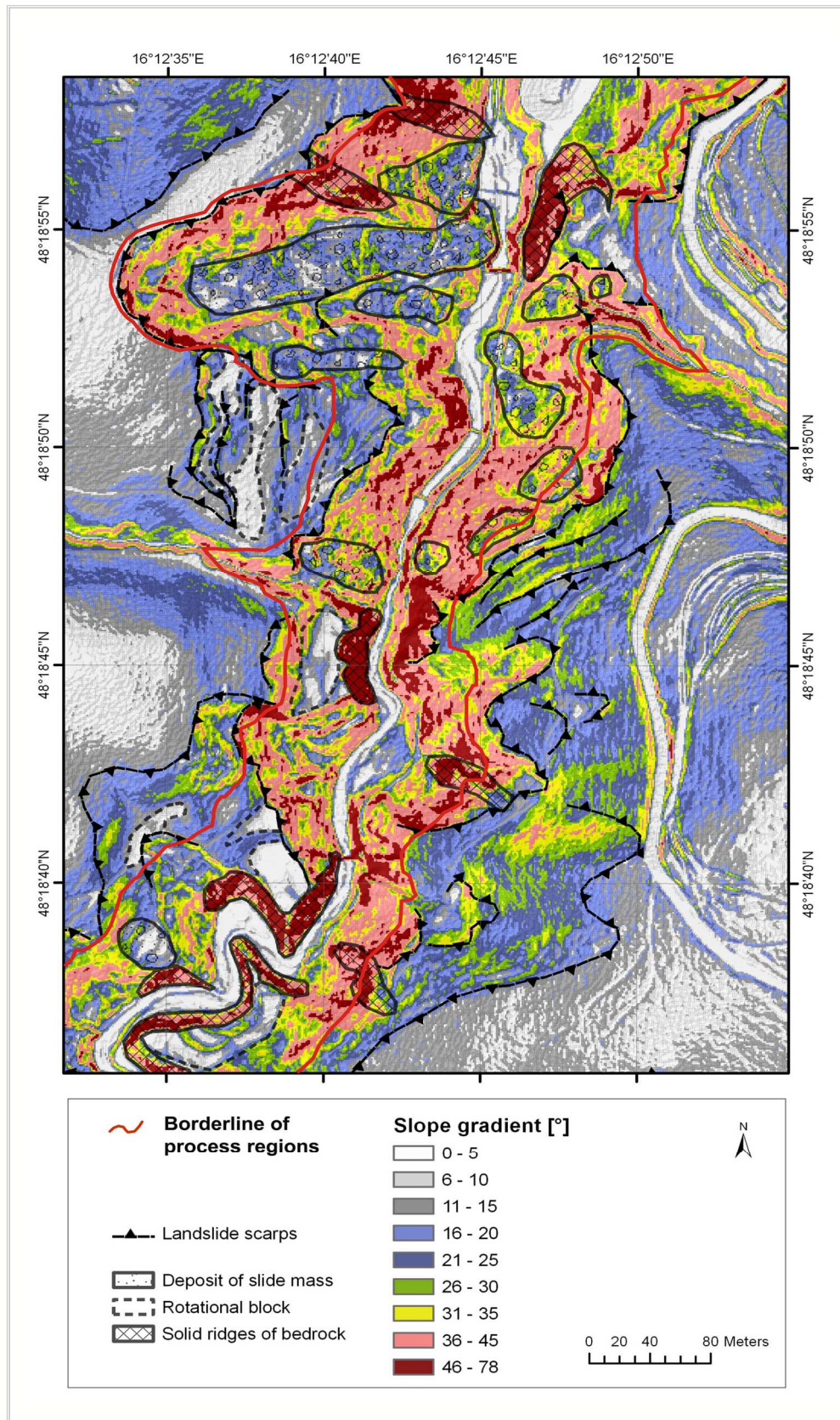


Figure 5-5. Borderline of process region (1), the flysch bedrock located at the steep decline near the valley bottom), and process region (2), the quaternary sediment (located at the upper slope positions and the flatter slope shoulder). The map shows the slope gradient and structural information on former landslides. The map is based on a high-resolution digital elevation model produced by LiDAR technique and is provided by the Provincial Government of Lower Austria (2006)

The process regions, as described above, are characterised by properties of the substrate, which are required for the slope stability calculation. In particular, soil-mechanical parameters, like cohesion, friction angle and specific weight must be defined as user input. The parameters applied are derived from measurements in the study area (Damm et al. 2008, Mayrhofer et al. 2008, Terhorst et al. 2009, Damm & Terhorst 2010). In particular, these studies comprise sedimentological and pedological investigations. Several drillings and exposures were analysed to study the distribution and composition of bedrock and quaternary sediments. Laboratory analyses include the determination of grain size, the soil-mechanical properties such as friction angle, cohesion and deformability (Damm et al. 2008, Mayrhofer et al. 2008, Terhorst et al. 2009, Damm & Terhorst 2010).

The soil-mechanical parameters have a natural variability in the process regions. The SINMAP method considers ranges by the definition of upper and lower bounds for the parameters. Therefore, maximum and minimum values of cohesion and friction angle are defined.

For process region (1), the flysch bedrock, a friction angle of 32.5° to 35° was measured in the decomposed sandstones, depending on the density of bedding (Damm & Terhorst 2010). These values represent the lower ( $\phi$ -min) and upper ( $\phi$ -max) bounds for the parameter range of “friction angle” for this process region. This sand-silt mixture of the decomposed sandstones is not cohesive (Damm & Terhorst 2010). Therefore, the decomposed sandstones have a cohesion of 0 kN/m<sup>2</sup>, which represents the lower bound for cohesion (c-min) in this process region. Landslides in flysch have a depth of 8-20m and affect not only the shallow weathered zone of the bedrock but also solid bedrock, which is in many cases brittle, marl and sandstone rich in clay (Damm & Terhorst 2010). Therefore, an upper bound 40kN/m<sup>2</sup> is defined for cohesion, which is a characteristic value (DIN 1055). The friction angle of 35°, measured in the decomposed sandstones, is also valid for solid bedrock rich in marl (DIN 1055), therefore no adaption of (c -max) was necessary in this case. Table 6-7 summarises the used values.

For process region (2), the quaternary sediments, the soil mechanical properties of the periglacial cover beds and loess layers are used. For the loess sediments a friction angle of 27.5° and cohesion of 5 kN/m<sup>2</sup> is measured (Damm & Terhorst 2010). The stability of the clays and marls of the periglacial cover beds is comparable to that of the loess sediments. A friction angle of 22.5° and cohesion of 10 kN/m<sup>2</sup> are measured (Damm & Terhorst 2010). The values obtained represent the lower and upper bounds for cohesion and friction angle in the model (Table 6-7).

As the SINMAP calculations require dimensionless cohesion, a transformation of the original values is done according to equation 5-4 (Pack et al. 1998) incorporating soil weights and substrate depth. The soil-mechanical parameters, as input to the models, are described in Table 5.4.

Table 5-4. Soil-mechanical parameters, cohesion (C) and friction angle ( $\phi$ ) of the process regions, based on field measurements (Damm & Terhorst 2010). Dimensionless cohesion (c') is derived from equation 5-4.

No.	Process region	Bounds	Cohesion [C]	Dimensionless cohesion [C']	Friction angle [ $\phi$ ]	Depth [m]	Specific weight [kN/m <sup>3</sup> ]
(1)	flysch bedrock of the Aitlengbach Formation	min	0	0	32.5	8	20
		max	40	0.25	35.0	20	
(2)	quaternary sediments	min	5	0.06	27.5	2	20.5
		max	10	0.12	22.5	4	

### 5.1.3 Hydrological calculations for the determination of the wetness parameters

Apart from the soil-mechanical parameters described above, a wetness parameter (R/T) is required for each of the process regions. As the wetness conditions on slopes are highly variable in space but also in time, a set of wetness scenarios are developed which take into account different climate and meteorological conditions. The wetness scenarios are described in the following chapter 5.1.4 “Wetness scenarios”. In the actual chapter the hydrological calculations are described together with the utilised climate and meteorological data. These calculations form the basis for determination of the wetness parameters, applied in the slope stability calculations.

In general, the wetness parameter is composed of transmissivity (T) and the amount of recharge (R), which is the subsurface lateral flow contributing to the perched water table according to Pack et al. (2005). The ratio (R/T) in (equation 5-8) quantifies the relative wetness in terms of assumed steady state recharge relative to the soil's capacity for lateral drainage of water. Although the wetness index (R/T) contains two variables (R) and (T), it is treated as a single user input parameter in SINMAP. As this value cannot be measured directly in the field, the adequate estimation of the parameter is crucial for the modelling process.

#### 5.1.3.1 Transmissivity

Transmissivity is proportional to the hydraulic conductivity of the substrate, which can be measured in the field. Transmissivity (T) is the rate of the horizontal flow of subsurface water through the substrate layer with a depth (h). It is directly proportional to the hydraulic conductivity ( $k_f$ ) (Höiting et al. 2009) and can be formulated as

$$(5-15) \quad T = \sum_{i=1}^n (k_f \cdot h)_i$$

Hydraulic conductivity was determined in the Geoecological Laboratory (Institute for Spatial Analysis and Planning in Areas of Intensive Agriculture, University of Vechta) on the basis of undisturbed soil cores obtained in the field by double-ring infiltrometers. Observations in field are used for the depth of the layer (h). Flysch bedrock is characterised by high to very high permeability. The permeability of the quaternary sediments varies over the whole sequence. The basal layer shows low to moderate permeability and the loess layer high permeability. Table 5-5 indicates the values for average hydraulic conductivity, considered depth of layer and resulting transmissivity as applied in the modelling.

Table 5-5. Average hydraulic conductivity and sediment thickness as measured in the field and the Geoecological Laboratory (Institute for Spatial Analysis and Planning in Areas of Intensive Agriculture, University of Vechta). On the basis of these values transmissivity is deduced (equation 5-15).

No.	Process region	Considered depth	Average hydraulic conductivity [m/s]		Transmissivity [m <sup>2</sup> /s]	
			min	max	min	max
(1)	flysch bedrock of the Altlengbach Formation	8-20	6.43*10 <sup>-06</sup>	2.45*10 <sup>-05</sup>	1.29*10 <sup>-04</sup>	4.91*10 <sup>-04</sup>
(2)	quaternary sediments	2-4	1.97*10 <sup>-06</sup>	8.22*10 <sup>-05</sup>	7.88*10 <sup>-06</sup>	1.65*10 <sup>-04</sup>

Apart from transmissivity (T), the amount of recharge (R) is contained in the parameter (R/T). Recharge (R) is highly dependent on the specific meteorological conditions and can hardly be measured on site. As there are no measured recharge volumes, it is estimated by hydrological water-balance calculations and empirical functions, as described in the following chapters.

### 5.1.3.2 “Short-term” recharge

In the present paper recharge volumes, which are produced by meteorological conditions limited in time, like single rainfall events or a certain period of rainfall, are referred to as “short-term” recharge. For such cases recharge (R) is calculated by an empirical function which determines effective precipitation. It represents the amount of rainfall which reaches the surface and partly infiltrates into the ground causing an increase in soil moisture and recharge in the strata. Effective precipitation is estimated by the Runoff Curve Number (RCN) method (Hjelmfelt 1980, Chen 1982, Rietz & Hawkins 2000). This empirical method estimates the direct runoff or infiltration from rainfall. According to this concept, total runoff must exceed an initial abstraction before runoff or recharge is generated (Hjelmfelt 1980, Rietz & Hawkins 2000).

This method is suited for the study area because it is able to consider the effects of interception in forested areas. Besides, it takes different sediment types into account like soils rich in clay, which are present in the study area. The effective precipitation ( $P_{eff}$ ) estimation is done according to equation (5-16) (Rietz & Hawkins 2000) in consideration of the sediment/soil type and land use, or land cover, respectively.

$$(5-16) \quad P_{eff} = \frac{(P - I_a)^2}{P - I_a + S}$$

(P) represents the precipitation quantity and (S) is the potential maximum soil moisture retention, which occurs after runoff. This parameter represents a constant, which is determined from empirical curves, describing the relation between precipitation quantity and runoff, depending on soil type and land use. The empirical constant is 77 for stratum rich in clay and forest. ( $I_a$ ) represents the initial abstraction, such as rainfall interception by vegetation. It is generally assumed that ( $I_a$ ) is proportional to (S) by  $I_a = 0.2S$ .

The function (5-16) is applied to two specific rainfall amounts. An extreme rainfall intensity of 60mm/h with a return period of 50 years is selected. This value represents the design depth of precipitation calculated by the Hydrographical Service for the study area (eHYD 2011, Weilguni 2009). The design depth of precipitation is the maximum probable daily precipitation in a specific catchment area and is provided for hydrological calculations. A point grid of 6 per 6 km is offered for the design depth of precipitations with durations from 5min to 6 days and return periods from 1 to 100 years. The grid point number 2655 near the Hagenbach Valley is used.

Additionally, the calculation is applied to a long-lasting rainfall event with a measured intensity of 90mm/day in June 2009 (ZAMG 2010a). The Federal Meteorological Service (ZAMG 2010a, 2010b) and the Hydrographical Yearbook of Austria for 2009 (Hydrographischer Dienst 2009) report above-average rainfall in 2009. The average monthly precipitation normal for the Vienna Forest region was exceeded by 275% related to the climate normals for the period of 1961-1990 (Figure 5-6). The meteorological stations St. Pölten and Vienna measured amounts of 70 to 90 mm per day after a period of rainfall (ZAMG 2010a, Hydrographischer Dienst 2009). It is recorded that at the end of June a long-lasting rainfall event delivered an amount of 90 mm within 24 hours and caused flooding in the streams in Lower Austria as well as landslides (ZAMG 2010a). The mid-term records of the

climate normals for the period of 1961 - 1990 captured at the meteorological station of Mariabrunn showed that the average maxima in June, July and August are above 90 mm per day.

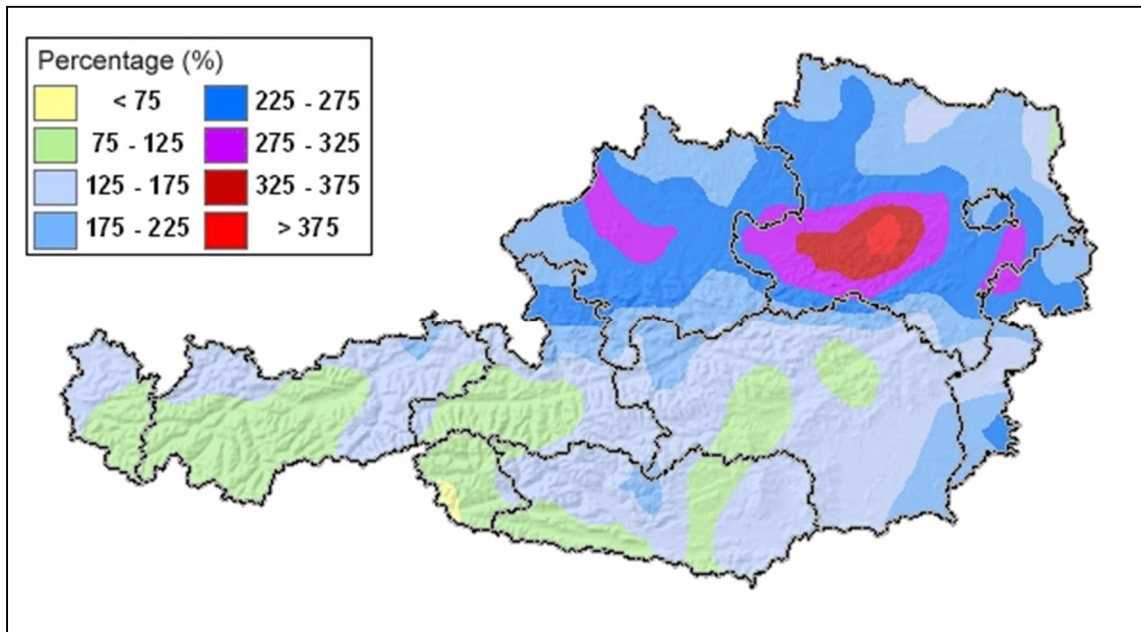


Figure 5-6. Difference (in %) to precipitation normals in June 2009 related to the climate normals for the period of 1961-1990 (ZAMG 2010a, modified).

### 5.1.3.3 Present-day, “mid-term” recharge

Wetness conditions in the substrate, which are generated by persistent climate conditions, like monthly precipitation and air temperature, are referred to as “mid-term” conditions. To assess antecedent substrate wetness, an average “mid-term” recharge is calculated on the basis of monthly climatological data. The estimations rely on the water-balance conception according to Thornthwaite & Mather (1957). This conception describes and quantifies the components of the hydrological cycle and enables an estimation of recharge (R) (Figure 5-7). According to Steenhuis & Van der Molen (1986) recharge (R) is defined by precipitation (P) and soil-moisture storage (ST) minus direct surface runoff (DRO) and potential evapotranspiration (PET) by

$$(5-17) \quad R = P + ST - DRO - PET$$

In order to calculate the components (ST), (DRO) and (PET) a monthly water-balance calculation is processed according to McCabe & Markstrom (2007) as well as Hamon (1961). This method allows determination of the various components of the hydrological system (like potential and actual evapotranspiration, soil-moisture storage, direct runoff and snow storage) according to the Thornthwaite & Mather (1957) theory on the basis of monthly data on precipitation and air temperature. The water-balance model analyses the portion of various components in the hydrologic system using a monthly accounting procedure (Thornthwaite 1948, Mather 1979, McCabe & Wolock 1999). The method does not regard each month individually and separately from each other but takes surplus created in previous months into account. This surplus can be produced by the excess-water from soil-storage as well as by snow melting depending on temperature.

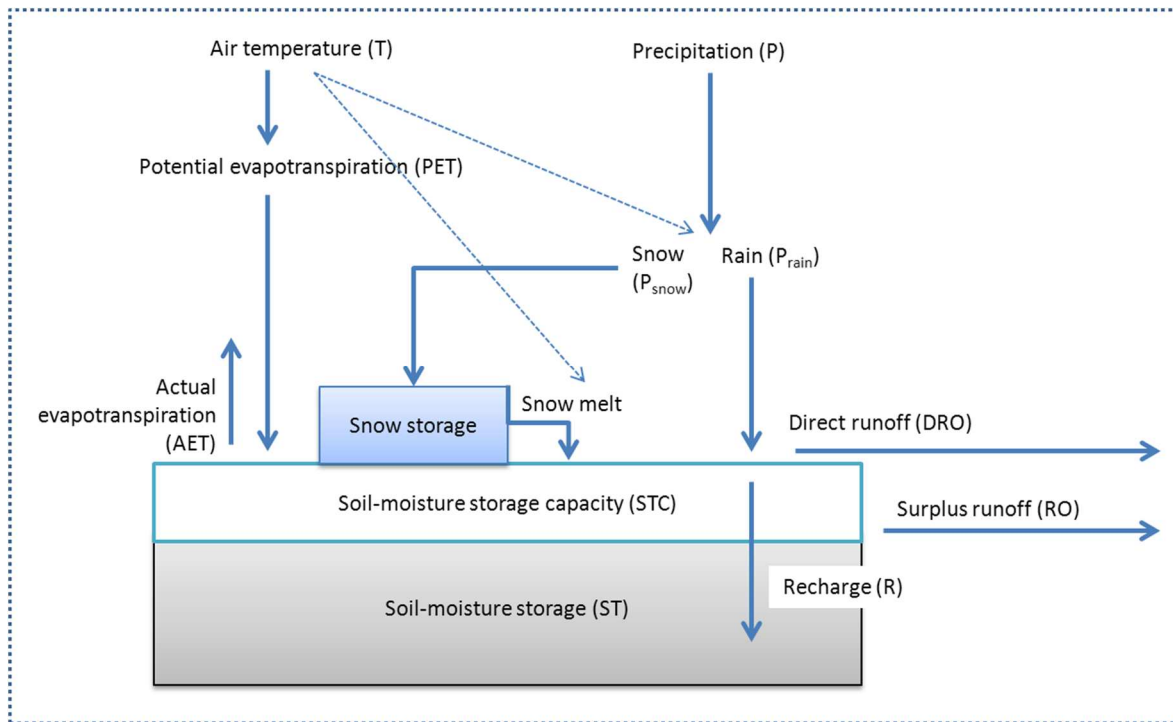


Figure 5-7. Scheme of the hydrological cycle according to the water balance model of Thornthwaite & Mather (1957) (McCabe & Markstrom 2007, modified).

The estimation of soil-moisture storage (ST) is carried out in several steps. The first hydrological component, which is calculated in the water-balance model, is the portion of monthly precipitation occurring as rain ( $P_{rain}$ ) or as snow ( $P_{snow}$ ), depending on specified rain and snow thresholds of air temperature ( $T_{snow}$ ,  $T_{rain}$ ) (equation 5-18 and 5-19). The precipitation which occurs as snow is quantified as snow storage (SST) (McCabe & Markstrom 2007).

(5-18) \_\_\_\_\_

(5-19)

The hydrological component referred to as direct runoff (DRO) represents the surface runoff or runoff resulting from infiltration-excess overflow (McCabe & Markstrom 2007). According to Wolock & McCabe (1999) a fraction of 5% of rain ( $P_{rain}$ ) is determined to produce direct runoff (DRO) (equation 5-20).

(5-20)

Direct runoff (DRO) is subtracted from the rain fraction ( $P_{rain}$ ) to compute the infiltrating precipitation ( $P_{infiltr}$ ), which is relevant for soil-moisture storage and recharge (equation 5-21) (McCabe & Markstrom 2007)

(5-21)

The amount of snow storage that melts in a month is computed from the mean monthly temperature and a maximum melt rate of 5% (McCabe & Wolock 1999). The snow melt fraction is (SMF) computed in equation 5-22 (McCabe & Markstrom 2007). If the computed SMF is greater than the maximum melt rate of 5%, the snow melt fraction (SMF) is set to this maximum melt rate. The amount of snow melting in a month (SM) is proportional to the snow storage (SST) depending on the snow melt fraction (equation 5-23) (McCabe & Markstrom 2007).

$$(5-22) \quad SMF = \frac{T - T_{snow}}{T_{rain} - T_{snow}} \cdot 0.5$$

$$(5-23) \quad SM = SST \cdot SMF$$

Finally the amount of snow melting (SM) is added to the infiltrating precipitation ( $P_{infiltr}$ ) (equation 5-24). This way the total liquid water input ( $P_{total}$ ) to the soil is estimated (McCabe & Markstrom 2007).

$$(5-24) \quad P_{total} = SM + P_{infiltr}$$

Apart from the total liquid water input ( $P_{total}$ ) potential and actual evapotranspiration must be determined to finally estimate soil-moisture storage. An accounting procedure is applied for this purpose (equation 5-27) (McCabe & Markstrom 2007). In the first step evapotranspiration is computed. The latitude of the location is used for the computation of the length of day, which is needed for the calculation of potential evapotranspiration (PET). In particular potential evapotranspiration is estimated by (Hamon 1961) equation (5-25).

$$(5-25) \quad PET = 13.97 \cdot d \cdot D^2 \cdot W_t$$

Variable (d) represents the number of days of a month and (D) the average monthly sunshine hours. Variable ( $W_t$ ) is the saturated water vapour density term, which is calculated according to McCabe & Markstrom (2007) by

$$(5-26) \quad W_t = (4.95 \cdot e^{0.062 \cdot T}) / 100$$

In the accounting procedure several cases are distinguished which compare the results from potential evapotranspiration (PET) to the total liquid water input ( $P_{total}$ ): In case that the total liquid water input for a month ( $P_{total}$ ) is less than the potential evapotranspiration (PET), actual evapotranspiration (AET) is equal to the total precipitation plus the amount of soil-moisture that can be withdrawn from water storage in the soil. Soil-moisture storage withdrawal (STW) linearly subsides with decreasing soil-moisture (ST) as the soil becomes drier, water becomes more difficult to remove from the soil and less is available for evapotranspiration (AET). It is calculated according to McCabe & Markstrom (2007) by

$$(5-27) \quad STW = ST_{i-1} \cdot \left[ |P_{total} - PET| \cdot \left( \frac{ST_{i-1}}{STC} \right) \right]$$

( $ST_{i-1}$ ) represents the soil-moisture storage of the previous month and (STC) is the soil-moisture storage capacity, which is estimated by an empirical value of 150mm (Wolock & McCabe 1999). If the sum of liquid water input ( $P_{total}$ ) and soil-moisture storage withdrawal (STW) is less than potential evapotranspiration (PET), a water deficit is calculated as (PET–AET). If liquid water input for a month ( $P_{total}$ ) exceeds potential evapotranspiration (PET), actual evapotranspiration (AET) is equal to potential evapotranspiration (PET). The water exceeding potential evapotranspiration (PET) replenishes soil-moisture storage (ST). When soil-moisture storage (ST) is greater than the soil-moisture storage capacity, the excess water becomes a surplus (S) and is eventually available for runoff (McCabe & Markstrom 2007). With this soil-moisture storage calculation, all components of the hydrological cycle are calculated which are required to compute recharge (equation 5-17).

In order to assess characteristic present-day conditions, data from the climate normal period are used. Climate or climatological normals represent arithmetic averages of air temperature or precipitation over a 30-year period (World Meteorological Organization 1989). This time span is determined because the duration allows filtering out any inter-annual variations or anomalies. Despite this filtering it is possible to keep the actual climatic trend in the averaged data. Therefore, climate normals are ideal reference values to compare current climatological trends to those of the past (World Meteorological Organization 2007). These data are suitable for the present study because the “normal” slope stability condition is investigated and compared to the future situation as proposed by regional climate forecasts (Reclip:more 2007).

The period from 1961 to 1990 is the official normal period defined by the World Meteorological Organisation (WMO), which provides a standard reference and a baseline period for many impact studies (World Meteorological Organization 1989). The Meteorological Survey of Austria publishes climatological standard normals from several meteorological stations for the period of 1961 to 1990 (Auer et al. 2001, ZAMG 2010c). The station Mariabrunn situated 226 m a.s.l. and located at the western outskirts of Vienna, is selected for the Vienna Forest (Table 5-6).

Table 5-6. Climate data of Austria (ZAMG 2010c): climate normals for air temperature and precipitation for the period of 1961 to 1990 (meteorological station Mariabrunn).

Period	Air temperature [°C]				Precipitation [mm]		
	monthly average	monthly		absolute		monthly sum	max sum in 24 h
		max	min	max	min		
1961-1990							
January	-1.5	10.0	-14.2	14.4	-25.6	45	43
February	0.7	11.8	-12.0	18.9	-25.3	48	42
March	4.7	19.4	-8.4	25.3	-23.1	49	53
April	9.3	23.6	-3.2	27.8	-6.5	62	53
May	13.8	27.2	0.9	31.2	-2.5	71	42
June	17.1	30.4	5.3	33.9	0.5	77	96
July	18.9	32.1	7.2	36.2	4.0	83	104
August	18.4	31.9	6.3	36.8	3.6	75	94
September	14.9	28.2	2.3	32.5	-3.6	54	45
October	9.5	21.9	-2.8	25.3	-7.1	50	66
November	4.0	15.9	-6.7	22.0	-14.8	61	43
December	0.3	11.3	-13.3	16.8	-23.7	50	31

---

#### 5.1.3.4 Future, “mid-term” recharge

In order to integrate climate change, monthly rates of change related to air temperature and precipitation are considered, as forecast by Regional Climate Models (RCM) until 2050 for Austria (Reclip:more 2007). Table 5-7 shows the changes in air temperature and precipitation amount according to Reclip:more (2007) as applied in the actual work. The standard normals of the period 1961 to 1990 (Table 5-6) are modified according to these values. The modified values are input into the recharge calculation based on the water balance calculations (Steenhuis & Van der Molen 1986 and McCabe & Markstrom 2007) as described before, for the present-day, “mid-term” recharge (chapter 5.1.3.3). That means, that the calculations are repeated with the adapted values, which consider forecast climate change.

In general, Regional Climate Models (RCMs) use downscaling-methods in order to consistently combine global climate models with regional climate data (Matulla et al. 2002). Although the different RCMs, which are produced for the Alpine region, differ in the quantity of the expected change, they accordantly show a temperature rise and a change of precipitation pattern. According to results of the project Reclip:more (2007) a temperature rise of +1.3 to 2 °C is forecast for the winter months December, January and February. A warming of +1.8 to 2.5 °C is forecast for spring. The summer months June, July and August will show a warming of +2 to +2.5 °C. The strongest temperature augmentation for Austria is predicted for autumn with a plus of +2.5 to +3 °C. In autumn and summer the temperature rise is mainly due to the precipitation decrease in these periods (Formayer et al. 2009).

The calculated precipitation pattern for Austria up to the middle of the 21<sup>st</sup> century shows seasonally and regionally different tendencies. Actually, the majority of the RCMs for Lower Austria show no significant changes in yearly precipitation amounts but a shift of precipitation from the summer to the winter period. Additionally, an increase in precipitation intensity is forecast for the summer months despite the decreasing monthly precipitation rates (Loibl et al. 2007, Formayer et al. 2009).

In the east of Austria overall precipitation amounts will decline. The highest precipitation decrease is denoted in the summer and autumn periods. It must be stated that precipitation forecasts are not in full accordance for all RCMs. In eastern Austria a precipitation drop of -15% or a precipitation growth of +15% to +30% in the summer period is probable. In winter and autumn a regionally varying augmentation is forecast. In the east of Austria a precipitation increase of +15 to +30% is denoted accordingly (Loibl et al. 2007, Reclip:more 2007, Formayer et al. 2009). Table 5-7 shows the changes in air temperatures and precipitation amounts as applied in the present study, based on the results of Reclip:more (2007).

Table 5-7. Changes in air temperatures and precipitation amounts as integrated in the water balance calculations. The values are averages derived from the forecast ranges of air temperature and precipitation changes (Loibl et al. 2007, Reclip.more 2007, Formayer et al. 2009).

Month	Air temperature change [°]	Precipitation change [%]
Jan	+2	+30%
Feb	+2	+30%
Mar	+2.5	+15%
Apr	+2.5	+15%
May	+2.5	+15%
Jun	+2.5	-15%
Jul	+2.5	-15%
Aug	+2.5	-15%
Sep	+3	-15%
Oct	+3	-15%
Nov	+3	-15%
Dec	+2	+30%

#### 5.1.4 Wetness scenarios

A set of wetness scenarios based on the slope stability index mapping method (SINMAP), the concept of process regions and the soil-mechanical and hydrological calculations, as described in the previous chapters, is developed.

The purpose of the wetness scenarios is to investigate slope stability in dependence of varying substrate wetness, which in turn relies on meteorological conditions. Wetness conditions vary according to daytime or season (Zimmermann et al. 1997, Heckmann & Becht 2006). Therefore, the scenarios are targeted to take account of the short-term condition and mid-term-development of substrate moisture content as crucial parameter in landslide activity (Klose et al. 2012). This is due to the fact that a critical amount of rainfall can trigger landslides but the persistent wetness conditions in the soils and unconsolidated rock create the disposition for slope movements (Govi et al. 1985, Kraut 1999).

A further distinction of variable disposition into “short-term” and “mid-term” disposition is required for ensuring a clear denomination of the scenarios. “Short-term” disposition refers to landslide proneness under a single meteorological situation like heavy or long-lasting rainfall. In contrast to this, “mid-term” disposition is related to average conditions changing in a time span of a month.

All the scenarios are based on the process regions, as described above (chapter 5.1.2 “Process regions and their soil-mechanical parameters”), and integrate flysch bedrock as well as quaternary sediments as potential sliding layers. The exception is the so-called “flysch scenario (January)”, which only incorporates the flysch bedrock as process region. This scenario serves as a basis for comparison with the other scenarios, which also consider slope activity in the quaternary sediments.

Apart from the “flysch scenario (January)”, eight other wetness scenarios are developed. The scenarios take varying recharge volumes into account, which are calculated from climate and meteorological data as described in chapter 5.1.3 “Hydrological calculation for the determination of

the wetness parameters". Table 5-8 provides an overview of the scenarios, their group assignment, the considered wetness conditions (expressed in the wetness parameter (T/R)) and the utilised climate or meteorological data base.

*Table 5-8. Wetness scenarios and their data base. One "flysch scenario (January)" is based on process region (1) (flysch bedrock only) and eight wetness scenarios are based on process regions (1) and (2) (flysch bedrock and quaternary sediments). The wetness scenarios are assigned to three groups which investigate present-day and future "mid-term" disposition to landslides as well as "short-term" disposition. The scenarios are based on varying recharge amounts as calculated from climatic and meteorological data as described in chapter 5.1.3.*

Scenario group	Scenario	Wetness condition (recharge)	Data source	Process regions
	Flysch scenario (January)	present-day, "mid-term" recharge in January	Climate normals of the period 1961-1990, meteorological station Mariabrunn in Lower Austria (Auer et al. 2001) (ZAMG 2010c)	(1) (flysch bedrock)
Present-day, "mid-term" disposition	Summer scenario (July)	present-day, "mid-term" recharge in July	Climate normals of the period 1961-1990, meteorological station Mariabrunn in Lower Austria (Auer et al. 2001) (ZAMG 2010c)	(1) (flysch bedrock) and (2) (quaternary sediments)
	Winter scenario (January)	present-day, "mid-term" recharge in January		
	Winter scenario (February)	present-day, "mid-term" recharge in February		
Future, "mid-term" disposition	Future summer scenario (July)	future "mid-term" recharge in July	Rate of changes of monthly air temperatures and precipitation amounts based on Regional Climate Model "Reclip:more" (Loibl et al. 2007) (Reclip:more 2007)	(1) (flysch bedrock) and (2) (quaternary sediments)
	Future winter scenario (January)	future "mid-term" recharge in January		
	Future winter scenario" (February)	future "mid-term" recharge in February		
"short-term" disposition	Critical rainfall scenario	Severe weather event in June 2009 with 90mm/day precipitation	Monthly review of the meteorological stations of St. Pölten and Vienna (ZAMG 2010a).	(1) (flysch bedrock) and (2) (quaternary sediments)
	Heavy rainfall Scenario	Extreme rainfall of 60mm/h with a 50-year return period	Design depth of precipitation of the Austrian Hydrographic Service (eHYD 2011) (Weilguni 2009)	

#### 5.1.4.1 Flysch scenario (January)

This scenario investigates slope stability as determined by the flysch bedrock of the Altenglengbach Formation. In contrast to the other wetness scenarios, quaternary sediments are not regarded as steering layer in slope dynamics. In terms of slope stability modelling that means that only process region (1), the flysch bedrock, is applied in the model.

This model is compared with the subsequent wetness scenarios which incorporate slope activity in the quaternary sediments in addition to movements in the bedrock strata. The objective is to identify changes in the slope stability index when the quaternary sediments are integrated. The comparison of the “flysch scenario (January)” with the wetness scenario which is calculated on the basis of equal wetness conditions but by integrating quaternary sediments enables the investigation of the relevance of quaternary sediments for the slope stability in the Vienna Forest.

This is of interest because it is generally assumed that landslides primarily occur in the weathered flysch sandstones rich in marl (Götzinger 1943, Plöchinger & Prey 1993, Faupl 1996, Schwenk et al. 1992). Field surveys, however, identified shallow landslide activity in quaternary sediments covering the flysch bedrock in wide areas (Damm et al. 2008, Terhorst et al. 2009, Damm & Terhorst 2010). By means of comparison of the two scenarios the changes in slope stability are investigated, which enables conclusions on the causes and steering factors for the actual slope dynamic.

In the “flysch scenario (January)” slope stability is estimated by using air temperature and precipitation normals for January (for the period 1961 to 1990) as measured in the study area (Auer et al. 2001, ZAMG 2010c). Table 5-9 lists the recharge volume (R) and the derived wetness index (T/R), which are input for the “flysch scenario (January)”.

*Table 5-9. Recharge (R) and wetness index (T/R) for the “flysch scenario (January)”. Recharge (R) is estimated by water-balance calculations (McCabe & Markstrom 2007 and Steenhuis & Van der Molen 1986). Transmissivity (T) is computed by hydraulic conductivity and depth of the substrate layer (Hölting et al. 2009). The maximum and minimum values for (T/R) are obtained by using the upper and lower bounds of (T) (Table 5-5).*

Scenario [name]	Process region [No.]	Recharge [mm/M]	Recharge [m/h]	Wetness index [T/R]	
				min	max
Flysch scenario (January)	flysch bedrock (1)	175	$2.4 \cdot 10^{-04}$	1968	7515

#### 5.1.4.2 Scenario group - present-day “mid-term” disposition

In contrast to the “flysch scenario (January)”, as described above, scenarios of this and the following groups also consider landslides in the quaternary sediments in addition to movements in the flysch bedrock. In terms of slope stability modelling this means that process regions (1) and (2) are incorporated into the model. The applied soil-mechanical parameters and transmissivity of the process regions are given in Tables 5-4 and 5-5.

This scenario group investigates the landslide disposition under average monthly wetness conditions. The scenarios are based on present-day, “mid-term” recharge calculations based on water balance calculations (chapter 5.1.3.3). Table 5-10 indicates the input values for the water-balance calculation, i.e. monthly air temperature and precipitation according to the 30-year averages in Mariabrunn

(ZAMG 2010a). Furthermore, it shows the results of the water-balance calculations, i.e. potential evapotranspiration, soil-moisture storage, actual evapotranspiration, snow-melt rate, surplus runoff and direct runoff and finally the estimated monthly recharge.

Table 5-10. Estimation of potential evapotranspiration, direct runoff and soil-moisture storage based on average monthly precipitation and air temperature of the climate normals for the meteorological station of Mariabrunn (ZAMG 2010a). On the basis of potential evapotranspiration, direct runoff and soil-moisture storage the monthly recharge (R) is estimated in mm/h (Steenhuis & Van der Molen 1986).

Month	Input		Output of water-balance calculations (hydrological parameters)						Recharge	
	Temp [°C]	Precipitation [mm/M]	Pot. evapotrans. [mm/M]	Soil-moisture storage [mm/M]	Act. evapotrans. [mm/M]	Snow storage [mm/M]	Surplus runoff [mm/M]	Direct runoff [mm/M]	Recharge [mm/M]	Recharge [mm/h]
Jan	-1.5	45	10	142	8	45	13	2	175	0.24
Feb	0.7	48	14	197	14	23	9	2	228	0.33
Mar	4.7	49	27	200	27	11	19	2	220	0.30
Apr	9.3	62	46	200	46	6	21	3	213	0.30
May	13.8	71	79	195	79	0	12	4	184	0.25
Jun	17.1	77	103	165	103	0	8	4	134	0.19
Jul	18.9	83	114	136	108	0	6	4	101	0.14
Aug	18.4	75	92	122	85	0	5	4	102	0.14
Sep	14.9	54	55	120	53	0	3	3	117	0.16
Oct	9.5	50	30	138	30	0	3	2	156	0.21
Nov	4.0	61	15	181	15	0	3	3	224	0.31
Dec	0.3	50	10	200	10	0	12	3	237	0.31

The results show the seasonally varying wetness conditions in regard to potential evapotranspiration, soil moisture storage, and finally recharge. On the basis of these results, the following “summer scenario” and two “winter scenarios” are selected.

- (1) **Winter scenario (January):** The month January is selected because it reveals the most dramatic changes of recharge in relation to climate change according to the water balance calculations. In particular, the comparison of the present-day, “mid-term” recharge obtained under normal climate conditions (Table 5-10) with the future, “mid-term” recharge considering forecast climate changes indicates that the month January shows the highest recharge augmentation (cp. Figure 5-8). Therefore, this month is used to calculate an additional “winter scenario”. Table 5-11 shows the estimated recharge in mm/h and the wetness index (T/R) for the “winter scenario (January)”.

Table 5-11. Recharge (R) and wetness index (T/R) for the “winter scenario (January)”. Recharge (R) is estimated by water-balance calculations (McCabe & Markstrom 2007 and Steenhuis & Van der Molen 1986). Transmissivity (T) is computed by hydraulic conductivity and depth of the substrate layer (Hölting et al. 2009). The maximum and minimum values for (T/R) are obtained by using the upper and lower bounds of (T) (Table 5-5).

Scenario [name]	Process region [No.]	Recharge [mm/M]	Recharge [m/h]	Wetness index [T/R]	
				min	max
Winter scenario (January)	flysch bedrock (1)	175	$2.4 \cdot 10^{-04}$	1968	7515
	quaternary sediments (2)			121	2517

- (2) **Winter scenario (February):** The water balance calculations indicate that the highest amount of recharge occurs in November, December and February, despite the low precipitation amounts between 48 to 61 mm/M (Table 5-10). These high recharge volumes are produced because evapotranspiration is low in the winter months due to low air temperatures. Besides, there is an additional fraction of water infiltration into the soil, namely the portion of snow storage that melts. Measured in mm/h the highest amount of recharge is revealed in February with 0.33mm/h. Therefore, these monthly data are used in the “winter scenario“ enabling the assessment of slope stability under maximal wetness in the course of a year. Table 5-12 shows the estimated recharge in mm/h and the derived wetness parameter (T/R). The values for transmissivity (T), which are utilised in (T/R), are provided in Table 5-5.

Table 5-12. Recharge (R) and wetness index (T/R) for the “winter scenario (February)”. Recharge (R) is estimated by water-balance calculations (McCabe & Markstrom 2007 and Steenhuis & Van der Molen 1986). Transmissivity (T) is computed by hydraulic conductivity and depth of the substrate layer (Hölting et al. 2009). The maximum and minimum values for (T/R) are obtained by using the upper and lower bounds of (T) (Table 5-5).

Scenario [name]	Process region [No.]	Recharge [mm/M]	Recharge [m/h]	Wetness index [T/R]	
				min	max
Winter scenario (February)	flysch bedrock (1)	228	$3.3 \cdot 10^{-04}$	1412	5392
	quaternary sediments (2)			87	1806

- (3) **Summer scenario (July):** According to the 30-year averages, the largest precipitation amounts between 77 to 83 mm/M arise in the summer months of June and July (Table 5-10). In spite of this high precipitation amount the water balance calculation reveals low recharge in the seasonal course due to the high evapotranspiration in the summer months. In July the lowest recharge (R) of 101mm/M and 0.14 mm/h was calculated (Table 5-10). Therefore, the “summer scenario” is based on this recharge value, considering maximal dry conditions in the seasonal course. Table 5-13 shows the estimated recharge for July in mm/h and the wetness index (T/R), which results from the division of transmissivity (T) (Table 5-5) and the July recharge (R). The maximum and minimum values for (T/R) are obtained by using the upper and lower bounds of (T).

Table 5-13. Recharge (R) and wetness index (T/R) for the “summer scenario (July)”. Recharge (R) is estimated by water-balance calculations (McCabe & Markstrom 2007 and Steenhuis & Van der Molen 1986). Transmissivity (T) is computed by hydraulic conductivity and depth of the substrate layer (Hölting et al. 2009). The maximum and minimum values for (T/R) are obtained by using the upper and lower bounds of (T) (Table 5-5).

Scenario [name]	Process region [No.]	Recharge [mm/M]	Recharge [m/h]	Wetness index [T/R]	
				min	max
Summer scenario (July)	flysch bedrock (1)	101	$1.4 \cdot 10^{-04}$	3410	13024
	quaternary sediments (2)			209	4362

#### 5.1.4.3 Scenario group - future “mid-term” disposition

Similar to the wetness scenarios which are dedicated to the present-day, “mid-term” disposition, the scenarios of this group consider slope movements in the flysch bedrock as well as landslides in the quaternary sediments. This scenario group investigates the disposition to landslides under forecast climate conditions until 2050. Climate change is incorporated in the scenarios in order to study its impact on slope instability. Monthly rates of change, related to air temperature and precipitation, are forecast by Regional Climate Models (RCM) until 2050 for Austria (Reclip:more 2007) as described in chapter 5.1.3 “Hydrological calculations for the determination of the wetness parameters”. In summary, the considered regional Climate Models (Reclip:more 2007) forecast a temperature rise of 2°C and an increased precipitation amount of 30% for the winter months. In spring a warming of 2.5°C and a plus of 15% for precipitation is taken into account in the wetness scenarios. In contrast to winter and spring, a reduction of precipitation of 15% is considered for the summer and autumn periods. For this period an increase in air temperature of 2.5° for the summer and 3°C for the autumn months is applied. The climate data of the climate normals are adapted according to this forecast (cp. Table 5-7) and a future, “mid-term” recharge is computed on a monthly basis, which is used in this scenario group.

The water balance calculations applied to derive recharge volumes indicate clear changes in wetness as a consequence of changed air temperature and precipitation as forecast (Loibl et al. 2007, Reclip:more 2007, Formayer et al. 2009). Figure 5-8 shows the change of recharge, soil moisture storage and potential evapotranspiration due to climate change in percentage and on a monthly basis. The comparison is based on data of the climate normals (ZAMG 2010c).

The calculations show drastic reduction of the wetness conditions in the summer and autumn periods and a distinct surge in January. In the summer period recharge (R) dropped by 42% (June) to 75% (August). In autumn a decrease in recharge (R) between 65% (September) and 42% (November) is revealed. Also the winter month December is drier, the recharge is reduced by approximately 17%. In contrast to this wetness decline in summer and autumn, recharge (R) and soil-moisture storage (ST) grows in January and February. Concerning the potential evapotranspiration, a relative constant enhancement of 15% to 24% is estimated over the year.

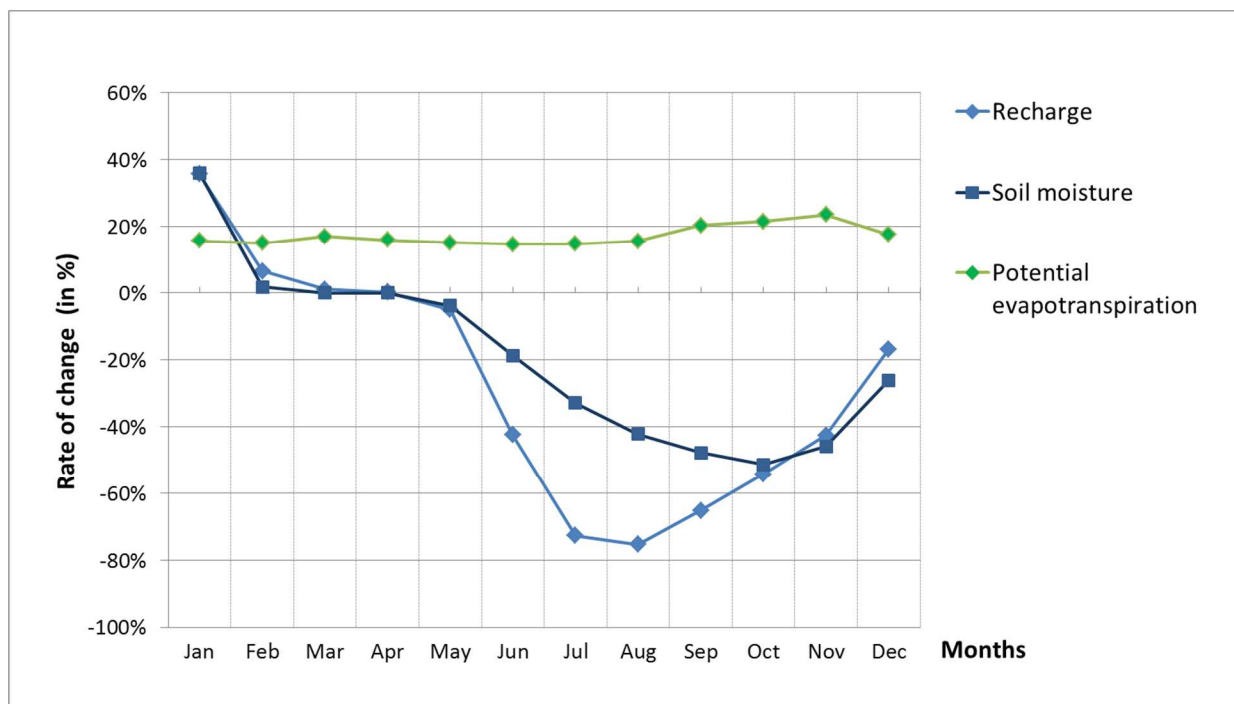


Figure 5-8. Change of recharge (R), soil moisture storage (ST), and potential evapotranspiration (PET) in percentage based on the forecast temperature and precipitation development according to the Regional Climate Models (LOIBL et al. 2007) compared with the climate normals from the period of 1961-1990 (AUER et al. 2001).

Corresponding to the scenarios based on data of the climate normal period, a “summer scenario (July)” and two “winter scenarios” (January and February) are computed on the basis of the altered recharge values.

- (1) **Future “winter scenario (January)”**: The “future winter scenario (January)” is developed because it was affected by the most drastic change in comparison to the climate normal period (Figure 5-8). It shows a recharge (R) of 238 mm per month, which means an increase of 36%. Consequently, it is the month with the largest wetness augmentation. Table 5-14 shows the estimated recharge in mm/h and the wetness index (T/R), which results from the division of the upper and lower bounds of the transmissivity (T) calculated for the process regions (Table 5-5) and the future “mid-term” recharge (R) in January.

Table 5-14. Recharge (R) and wetness index (T/R) for the scenarios “future winter scenario (January)”, which is dedicated to climate conditions as forecast in climate scenarios (Loibl et al. 2007, Reclip:more 2007, Formayer et al. 2009). The maximum and minimum values for (T/R) are obtained by using the upper and lower bounds of (T) (Table 5-5).

Scenario [name]	Process region [No.]	Recharge [mm/M]	Recharge [m/h]	Wetness index [T/R]	
				min	max
Future winter (January)	flysch bedrock (1)	238	$3.2 \cdot 10^{-04}$	1324	5058
	quaternary sediments (2)			81	1694

- (2) **Future “winter scenario (February)”**: In February recharge (R) is raised by 7%. February, just like January, is the month with the highest rate of recharge (R) and soil-moisture storage (ST) (Figure 6-9). Table 5-15 shows the estimated recharge in mm/h and the wetness index (T/R), which is calculated from the ratio of transmissivity (T) and future “mid-term” recharge (R) in February.

Table 5-15. Recharge (R) and wetness index (T/R) for the scenarios “future winter scenario (February)”, which is dedicated to climate conditions as forecast in climate scenarios (Loibl et al. 2007, Reclip:more 2007, Formayer et al. 2009). The maximum and minimum values for (T/R) are obtained by using the upper and lower bounds of (T) (Table 5-5).

Scenario [name]	Process region [No.]	Recharge [mm/M]	Recharge [m/h]	Wetness index [T/R]	
				min	max
Future winter (February)	flysch bedrock (1)	243	$3.5 \cdot 10^{-04}$	1412	5392
	quaternary sediments (2)			87	1806

- (3) **Future “summer scenario (July)”**: The “future summer scenario” is based on the July recharge (R) of 28 mm per month, which shows the most dramatic decrease of recharge (R) in comparison to the climate normal period (Figure 5-8). Table 5-16 shows the estimated recharge in mm/h and the wetness index (T/R), which results from the division of the upper and lower bounds of the transmissivity (T) calculated for the process regions (Table 5.5) and the future “mid-term” recharge (R) in July.

Table 5-16. Recharge (R) and wetness index (T/R) for the scenarios “future summer scenario (July)”, which is dedicated to climate conditions as forecast in climate scenarios (Loibl et al. 2007, Reclip:more 2007, Formayer et al. 2009). The maximum and minimum values for (T/R) are obtained by using the upper and lower bounds of (T) (Table 5-5).

Scenario [name]	Process region [No.]	Recharge [mm/M]	Recharge [m/h]	Wetness index [T/R]	
				min	max
Future summer (July)	flysch bedrock (1)	28	$3.7 \cdot 10^{-05}$	12441	47518
	quaternary sediments (2)			763	15912

#### 5.1.4.4 Scenario group- “short-term” disposition

This scenario group investigates the variable disposition under a single meteorological situation like heavy and long-lasting rainfall, which is limited in time. Therefore, these scenarios describe a short-term condition in regard to substrate moisture and slope stability. The investigation is dedicated to precipitation events with different intensities as described in chapter 5.1.3 “Hydrological calculations for the determination of the wetness parameters”.

- (1) **Critical rainfall scenario:** A long-lasting rainfall event, which happened in June 2009, delivered 90 mm rain in 24 hours in the study area and caused flooding as well as landslides in Lower Austria (ZAMG 2010a). In general, long-lasting rainfall events are relevant because they create soil water contents, which are able to cause a critical level in shear strength in the hillslope sediments (Klose et al. 2012). This critical rainfall event, which caused landslides in the past, is integrated into this scenario. Table 5-17 shows the estimated recharge in mm/h and the wetness index (T/R), which is computed from the division of the upper and lower bounds of the transmissivity (T) calculated for the process regions and the “short-term” recharge (R) for this rainfall event.

Table 5-17. Recharge (R) and wetness index (T/R) based on the “critical rainfall scenario”. (R) is estimated by effective precipitation calculation based on the Runoff-Curve-Number method (Hjelmfelt 1980, Rietz & Hawkins 2000). The maximum and minimum values for (T/R) are obtained by using the upper and lower bounds of (T) (Table 5-5).

Scenario [name]	Process region [No.]	Recharge [m/h]	Wetness index [T/R]	
			min	max
Critical rainfall scenario (90mm/d)	flysch bedrock (1)	$1.6 \cdot 10^{-03}$	186	1092
	quaternary sediments (2)		18	366

- (2) **Heavy rainfall scenario:** Heavy rainfall of 60 mm/h is applied in the modelling (Weilguni 2009, eHYD 2011). For the initiation of slope movements heavy rainfall events can be decisive (Dahal et al. 2008b, Guzetti et al. 2008, Deb & El-Kadi 2009). Strong moisture penetration, as caused by heavy or long-lasting rainfall, predisposes instability as it constantly lowers shear strength and thus reduces critical triggering thresholds of both causative factors (cf. Guzetti et al. 2008, Klose et al. 2012).

By the incorporation of this rainfall event, the present-day disposition, related to an extreme event, can be studied. Besides, it is relevant to study future landslide proneness considering the effect of climate change because Regional Climate Models indicate an increase in precipitation intensities (Frei et al. 2006, Formayer & Kromp-Kolb 2006). Although the future development of extreme precipitation in Austria is not clearly determined by Regional Climate Models (Formayer et al. 2009, Formayer & Kromp-Kolb 2006), a general monthly decrease in precipitation amounts and a growth of precipitation intensities are forecast (Frei et al. 2006, Formayer & Kromp-Kolb 2006). Furthermore, the investigations of extreme precipitation in the project PRISK-CHANGE of the Federal Meteorological Service (ZAMG) show that the intensities of a precipitation event with a 30-year return value will increase by about 15% to 25% (Hofstätter et al. 2010). The analysis is based on the Global Climate

Models (GCM) and daily precipitation sums from 50 meteorological stations for a period from 1963 to 2006.

Table 5-18 shows the estimated recharge in mm/h and the wetness index (T/R), which results from the division of the upper and lower bounds of the transmissivity (T) calculated for the process regions and the “short-term” recharge (R) for the rainfall event.

*Table 5-18. Recharge (R) and wetness index (T/R) based on “heavy rainfall scenario”. (R) is estimated by effective precipitation calculation based on the Runoff-Curve-Number method (Hjelmfelt 1980, Rietz & Hawkins 2000). The maximum and minimum values for (T/R) are obtained by using the upper and lower bounds of (T) (Table 5-5).*

Scenario [name]	Process region [No.]	Recharge [m/h]	Wetness index [T/R]	
			min	max
Heavy rainfall scenario (60mm/h)	flysch bedrock (1)	$5.7 \cdot 10^{-02}$	8	31
	quaternary sediments (2)		1	10

---

### 5.1.5 Visual interpretation of ALS-based shaded relief images (large-scale) for landslide mapping

For the interpretation and evaluation of the slope stability index calculation detailed information on landslides is required like structural information, which is captured in a large-scale landslide inventory. For medium and large-scale inventories the visual or automated interpretation of high-resolution remote sensing data can be used. Optical images with resolutions larger than 3m are considered as useful for visual interpretation of large landslides (Van Westen et al. 2008). Very high-resolution imagery is applicable even on medium and large scales. Another approach is the visual interpretation of landslide phenomena on shaded relief images produced on high-resolution DEMs from which the objects on the earth surface have been removed, so-called earth-DEMs (Haugerud et al. 2003, Van den Eeckhaut et al. 2007, Van Westen et al. 2008). This method is particularly suited for heavily forested areas, like the present study area (Haneberg 2004, Van Westen et al. 2008).

A high-resolution digital elevation model (DEM), captured by airborne laser-scanning (ALS), with a resolution of 1m is available for the Hagenbach valley. The ALS-data were provided by the Provincial Government of Lower Austria (2006). This highly precise DEM allowed the accurate mapping of landslides on the basis of shaded relief images produced by the ALS-data.

Air-borne laser-scanning (ALS) is a method which is often addressed as “light detection and ranging (LiDAR)” technique in literature (Haugerud et al. 2003, Van den Eeckhaut et al. 2007, Van Westen et al. 2008). It collects highly accurate and dense points of height measurements of the terrain. In principle, the height of the terrain is determined by the measured distance between the terrain and the aircraft. A pulse laser emits a discrete laser beam, which is reflected from the terrain below (Haneberg 2004, Van Westen 2004, Haneberg 2009). Distance between the aircraft and the ground is calculated from the laser travel time. The distance data are combined with a high-accuracy internal and external reference system, recording the position of the aircraft as well as its role, the pitch and heading (orientation), yielding highly accurate, 3D coordinates from the terrain (Haneberg 2004, 2009).

The DEM, produced by LiDAR technique and provided by the Government of Lower Austria (2006), was used to generate a slope gradient map and shaded relief images with varying illumination angles. Figure 5-9 shows the study area illuminated from different angles. In terms of GIS-modelling the hillshades are defined as hypothetical illumination of a surface according to a specified azimuth and altitude for the source of light. Hillshading creates a three-dimensional effect by means of a shaded relief, normally used for cartographic purposes. In the present paper the relative measure of incident light, provided by the hillshades, is used for the identification of landslides. Shaded reliefs are produced from different azimuth-angles, i.e. 360° (north), 315° (north-west), 270° (west), 225° (south-west), 180° (south), 135° (south-east), 90° (east) and 45° (north-east).

The identification of landslides on the hillshade and the slope gradient map is based on the recognition of landslide characteristics, as main scarps, reverse slopes indicating ancient rotational slide blocks and convex landslide toes representing deposits of former landslide masses. The GIS-based mapping is subsequently checked in appropriate geomorphological field surveys where additional information on the type of process was gathered.

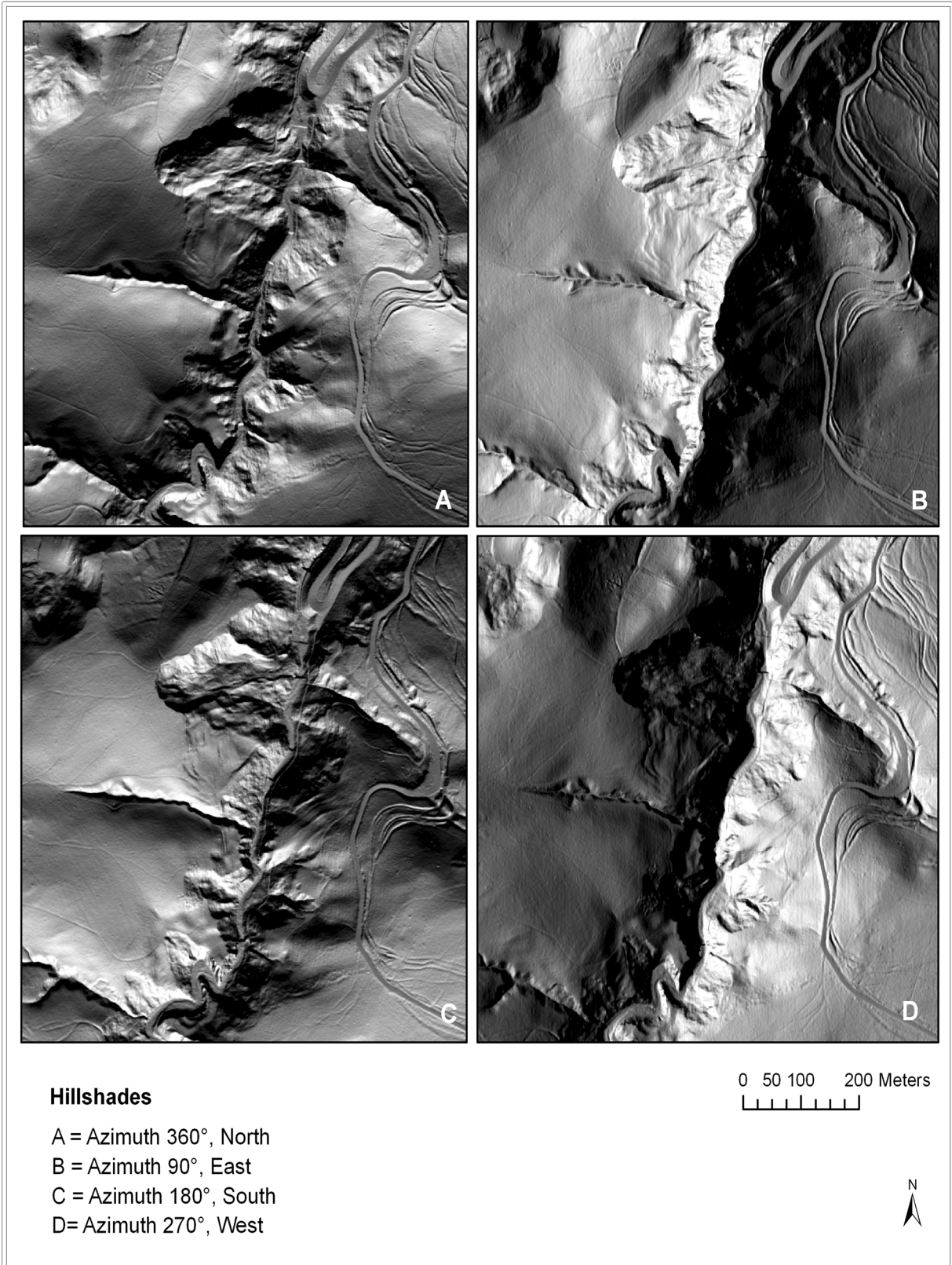


Figure 5-9. Shaded relief images for the study area. The hillshades are produced by different azimuth angles; these derivatives of the high-resolution digital elevation model (DEM) are used for landslide identification and mapping. The DEM is produced by LiDAR technique and is provided by the Provincial Government of Lower Austria (2006). The location of the study area within the Vienna Forest is shown in Figure 3-1.

---

## 5.2 Results

The results of scenario-modelling comprise the slope stability index as well as the topographic wetness index. Both are used to evaluate the specific situation in the single wetness scenarios in terms of slope dynamics. The used classification system of the stability index is described in detail in Table 5.1 (page 71) and that of topographic wetness is given in Table 5.2 (page 73). Both are utilised to describe the results in a quantitative sense and are also relevant for appropriate understanding of the results.

In the qualitative description of the results of scenario-modelling the actual slope composition and structure is taken into account. Therefore, the results of landslide mapping, which is carried out by visual interpretation of shaded relief images (cp. Figure 5-10, page 101) are described prior to the scenario results.

### 5.2.1 Landslides in the Hagenbach gorge

The results of landslide identification and mapping are illustrated in Figure 5-10. The focus of this mapping is on the structural components of landslides, like scarps, rotational blocks and deposition areas of landslide masses. Furthermore, solid ridges of bedrock outcrops are mapped because such areas are excluded from landslide activity and are rather exposed to events of rock fall.

The structures of landslides are crucial for the description and interpretation of the results of slope stability calculations.

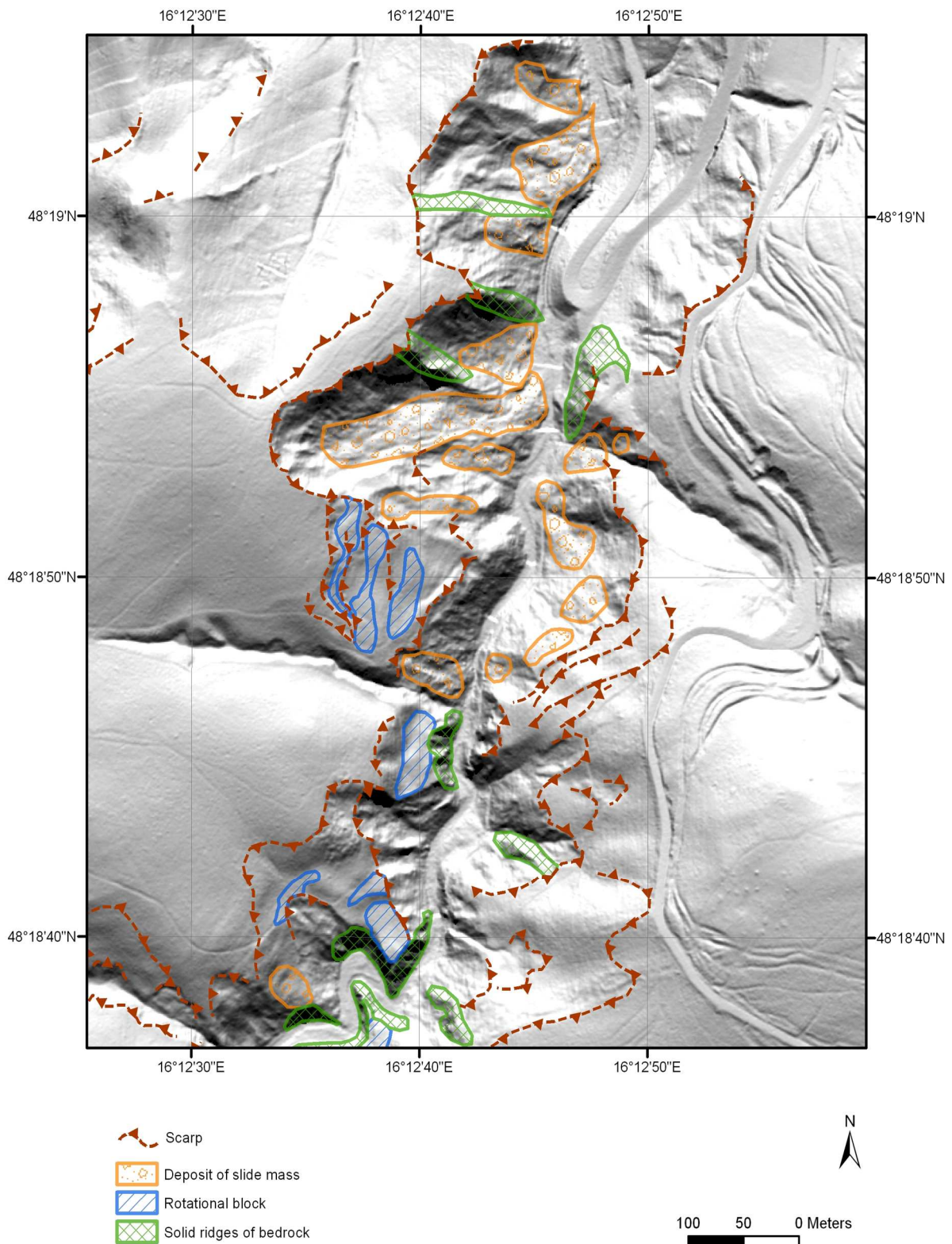


Figure 5-10. Large-scale landslide inventory. The inventory is produced by visual interpretation of shaded relief images. These images are based on airborne laser-scanning data (ALS) with a resolution of 1m, produced and offered by the Provincial Government of Lower Austria (2006).

---

## 5.2.2 Flysch scenario (January)

This scenario investigates slope stability as determined by the flysch bedrock of the Altengbach Formation. In contrast to other wetness scenarios, quaternary sediments are not regarded as steering layer in slope dynamics.

In the first step of slope stability index mapping, topographic wetness is derived on the basis of the assumed wetness in the scenario. The resulting topographic wetness map is illustrated in Figure 5-11, which illustrates the derived classification of the wetness conditions in the substrate. Besides, the legend provides the proportion of the classes in percentage of the study area. Considering an average “mid-term” recharge of 175mm/M, the scenario shows low substrate moisture because areas classified with “low moisture” are dominant with a proportion of 78% of the study area. A further 19% of the study area is classified as “partially wet”. According to the theoretical background of the topographic wetness index that means that both classes are never saturated over the whole range of assumed wetness.

Areas with saturation tendency (“threshold saturation”) and already saturated zones (“saturation”) cover an area of 4%. Slopes with “saturation tendency” have, by definition, a probability for saturation. In particular, saturation is reached under the upper bounds of the assumed wetness in the model. Slopes classified with “saturation” for the whole parameter range feature water-saturation. According to the present model such areas are found in hollow forms and depressions (cp. Figure 5-11). Saturation concentrates at accumulation lines, which mainly develop at deposits of ancient slide masses.

A slope stability index is derived based on topographic wetness. The results of slope stability index mapping are illustrated in Figure 5-12. The map indicates that the most instable areas occur near the valley bottom at the oversteepened slopes near the Hagenbach creek. The information on inclination is illustrated in the slope gradient map shown in Figure 5-5 (page 79). Small-sized instable areas are further found at some scarps of previous landslides where slope gradient is locally increased. Areas at the upper slope positions with a moderate inclination are classified as “stable” to “quasi-stable”.

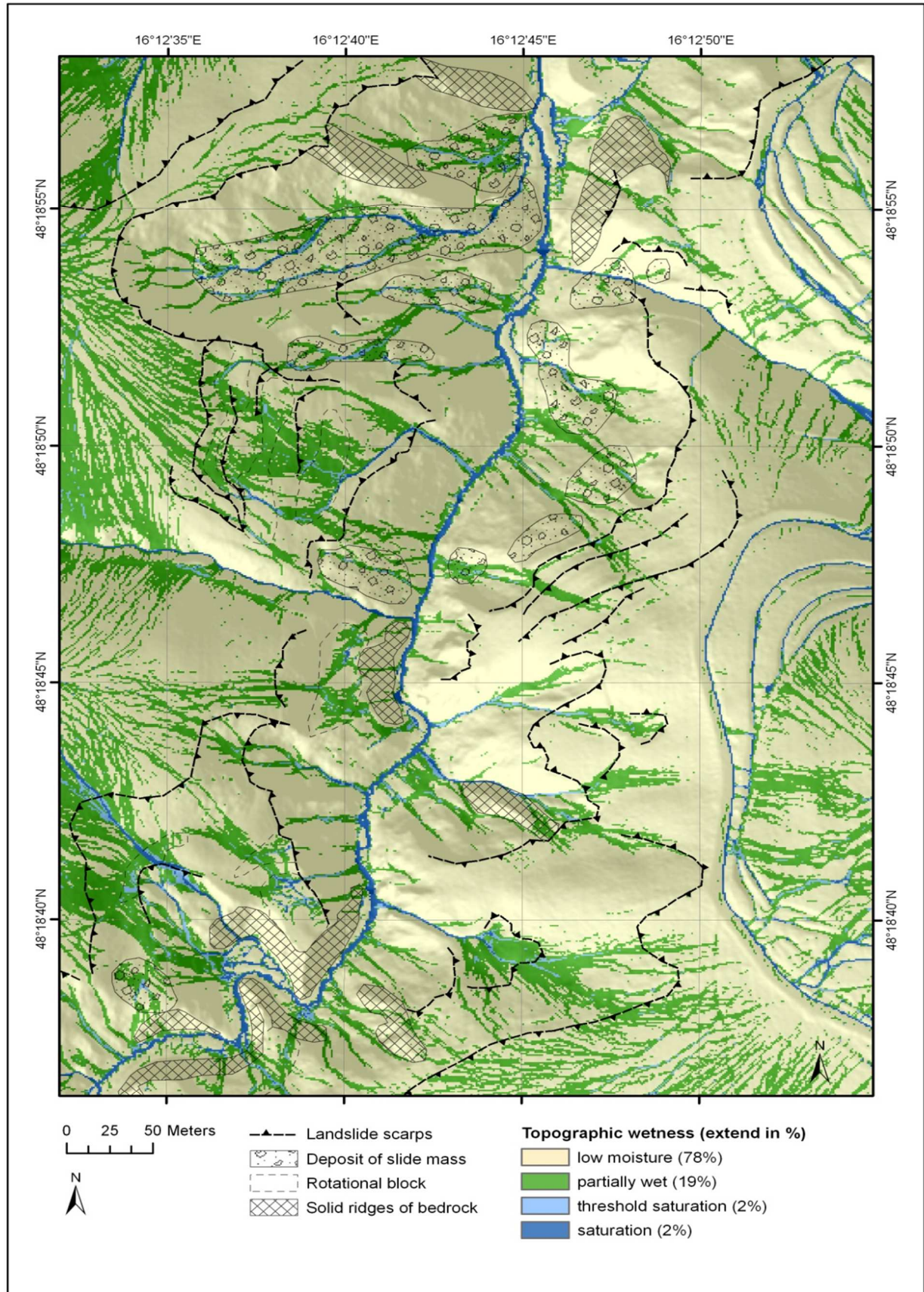


Figure 5-11. Topographic wetness map for “flysch scenario (January)” based on transmissivity of substrate in process region (1), the flysch bedrock, and average monthly recharge for January.



---

For a more detailed view on the extension of instable and stable areas, the proportion of the slope stability class in relation to the study area is given in Figure 5-13. The diagram shows that 54% of the study area is classified as “stable”, an additional 10% as “moderately stable” and 10% as “quasi-stable”. The latter three stability classes have a factor of safety greater than 1, consequently in total 75% of the study area is assessed as unconditionally stable in relation to these average January wetness conditions. External causes are required to cause instability in these zones. However, the class “quasi-stable” can be considered as narrowly stable and can be compared to a condition near the limit equilibrium in terms of slope stability. Even marginal external influences can cause instability in such slopes.

Analysis of slope inclination within the stability classes demonstrates that these stable areas (classified as “quasi-stable”, “moderately stable”, and “stable”) have an average slope gradient of 13° to 28°. This is indicated in Figure 5-14 illustrating the minimum, maximum as well as mean slope gradient per stability class. The slope stability index map (Figure 5-12) shows that such areas are mainly located at the upper slope positions.

For 23% of the study area there is a probability for instability under the defined variability of the specified parameters. They are classified as “lower threshold” and “upper threshold” (cp. Figure 5-13). For such areas no external causes are necessary to create instability because the inherent conditions can already create slope failure. These conditionally instable slopes have a mean slope gradient between 35° (“lower threshold”) and 43° (“upper threshold”). According to the slope stability index map (Figure 5-12) such areas are predominantly situated at the decline to the Hagenbach creek and at scarps of older landslides. An area of 2% is classified as “defended”, representing the unconditionally unstable zones. That means that these areas are instable for the whole parameter ranges of the model. As these slopes are still intact there are stabilising forces, which are not incorporated into the model, like solid bedrock outcrops. The existence of ridges of solid sandstones altering with the brittle material affected by movements is mentioned before (cp. Figure 5-3, page 70).

The analysis of slope gradient within this class demonstrates that oversteepened slopes with a mean slope gradient of 52° (Figure 5-14) prevail. This fact underlines the presence of bedrock outcrops in these zones, which can be consequently excluded from the landslide phenomenon. Such areas are rather susceptible to events of rock fall. The slope stability index map (Figure 5-12) further shows that the “defended” areas concentrate at the mapped ridges of solid bedrock.

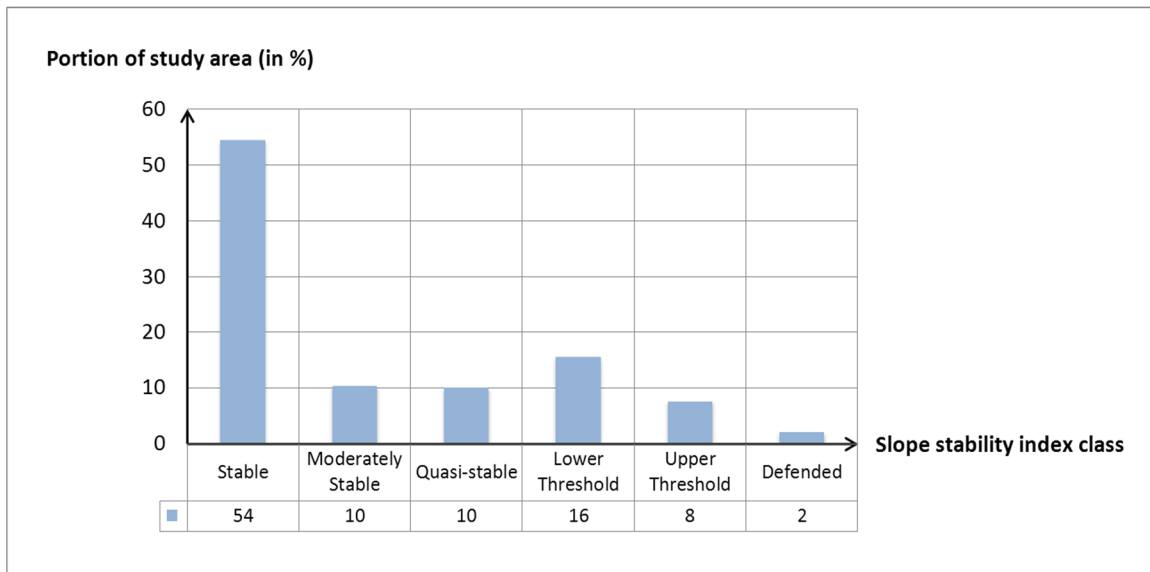


Figure 5-13. Slope stability index classification for “flyph scenario (January)”. The bars show the proportion of the stability classes in relation to the study area in percentage.

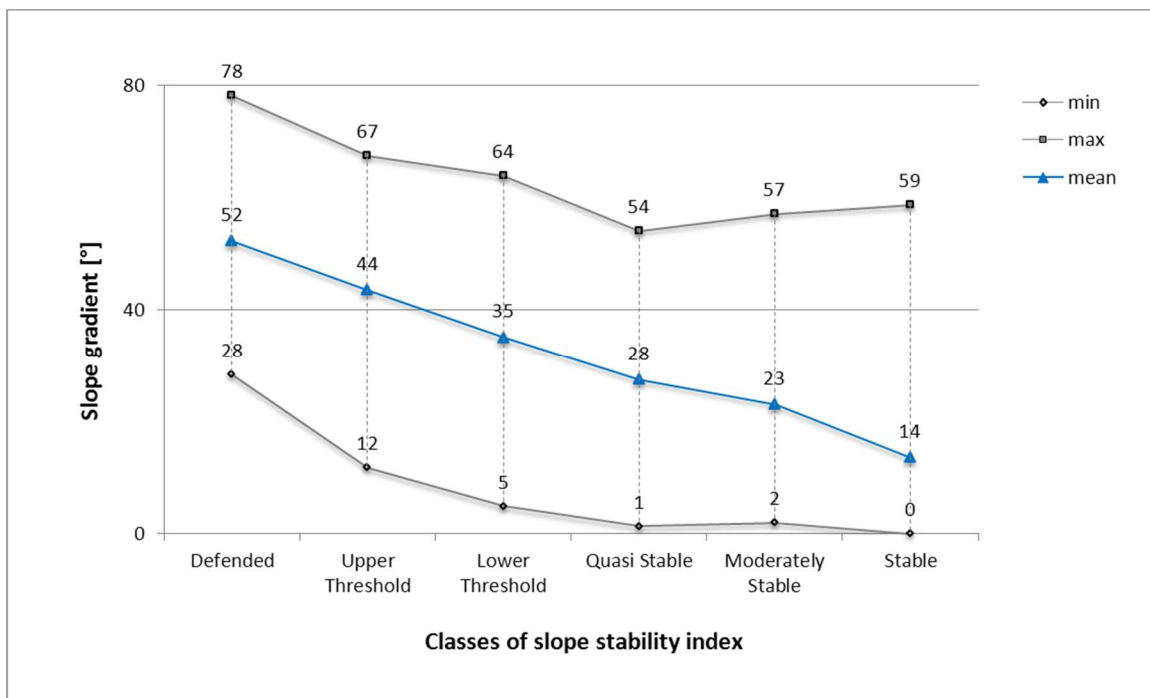


Figure 5-14. Slope gradient analysis within slope stability classes for “flyph scenario (January)”. The diagram shows the mean (blue line), minimum (lower line) and maximum (upper line) slope gradient per stability class.

---

## 5.2.3 Wetness scenario group “present-day, mid-term disposition”

### 5.2.3.1 Winter scenario (January)

Before stability index mapping is described in detail, topographic wetness is elaborated because it has a direct influence on the stability index classification. The scenario takes an average “mid-term” recharge of 175mm/M in January into account, similar to the “flysch scenario (January)”, but in contrast to this, quaternary sediments are integrated as process region. Quaternary sediments are characterised by varying permeability. In general, the transmissivity is considerably lower than that of the flysch bedrock (cp. Table 5-5). Consequently, the incorporation of quaternary sediments into the model changes the results of the topographic wetness index.

In this scenario “low moisture” to “partially wet” conditions are dominant with a proportion of 74% on the study area, as illustrated in Figure 5-15. There the borderline which divides the process regions is shown. It indicates that the model derives low moisture from the flysch bedrock in contrast to the quaternary sediments. According to the classification system of topographic wetness, these areas never reach saturation under the assumed wetness conditions. However, there is a degree of wetness under pessimistic conditions, i.e. the maximum recharge. The topographic wetness maps (Figure 5-15) shows that flow is mainly accumulated in the deposition zones of ancient landslides and that saturation is reached at linear flow lines.

It is further pointed out that a considerable proportion of the topographic wetness map, i.e. 23% of the study area, develops a saturation tendency (“threshold saturation”). These areas, which mainly occur in the quaternary sediments in the upper slope positions, develop saturation under maximum assumed wetness. Therefore, topographic wetness is essential for slope stability in these zones.

Full saturation over the whole range of assumed wetness is derived for 3% of the study area. These areas concentrate at the drainage lines in the study area (Figure 5-15).

Slope stability is derived from the resulting topographic wetness in this scenario. The resulting slope stability index map is given in Figure 5-16. In general, this map shows extensive zones of highest instability at the crown and the scarp of ancient landslides where the quaternary sediments crop out. Consequently, the actual slope dynamic is dominated by backward denudation, which leads to an extension of existing landslides by movements in the quaternary sediments. In this scenario the moderately inclined areas at the upper slope positions are also classified as instable (cp. Figure 5-16). The slope gradient map in Figure 5-5 (page 79) provides the information on the inclination.

The deposited slide masses of former landslides are mainly classified as stable (Figure 5-16). These disposal areas are characterised by a locally varying curvature and slope gradient, bringing about mounds and depressions. Instabilities concentrate in small-sized areas where saturation in the substrate is derived. In this context the topographic wetness map (Figure 5-15) demonstrates that flow accumulation is given in this deposition zones. Apart from deposits of slide masses, rotational blocks of ancient deep-seated movements are classified as “stable”, which can be attributed to the slight inclination. As the slope gradient map displays, the blocks have an inclination of 0° to 5°.

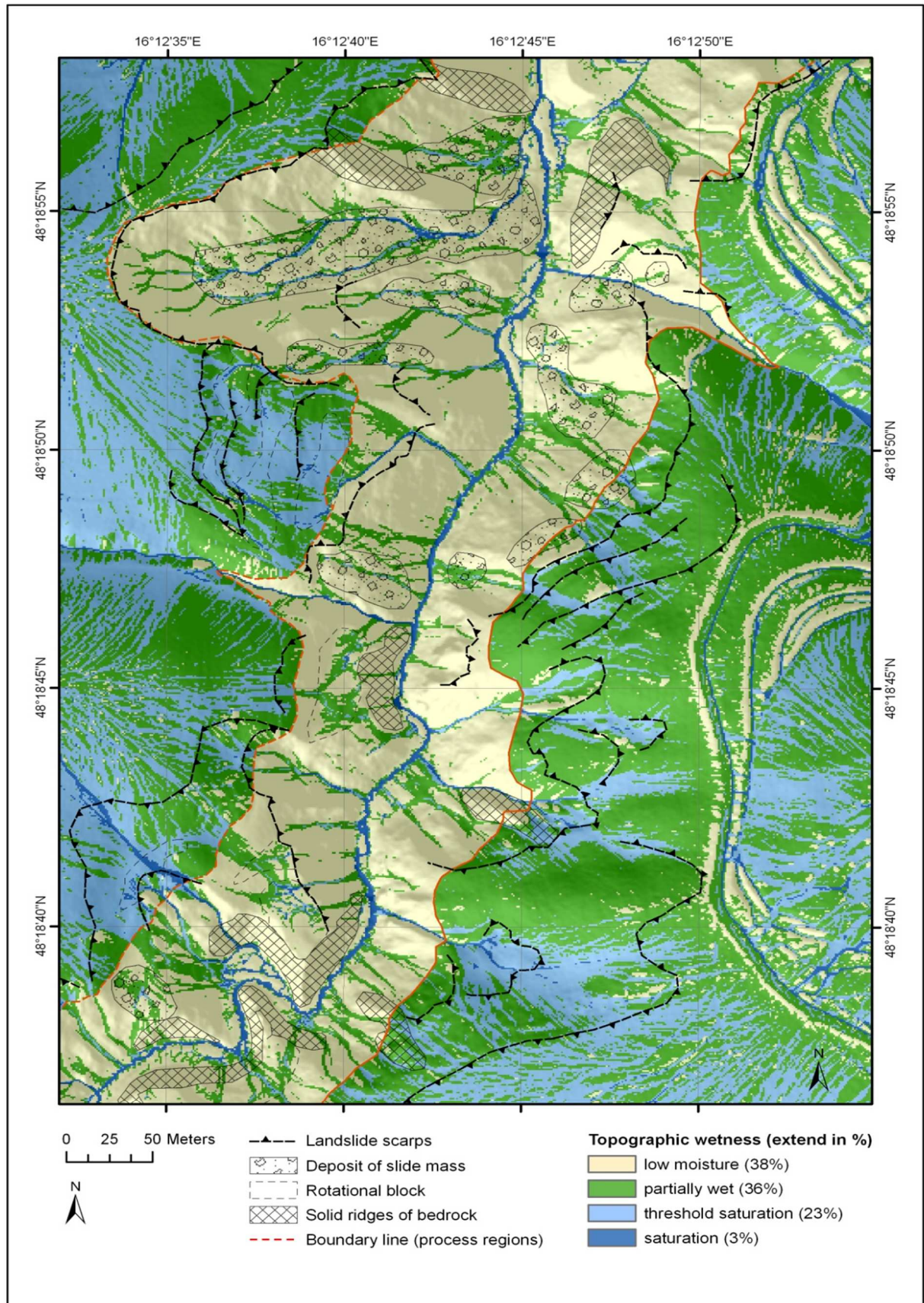


Figure 5-15. Topographic wetness map based on average monthly recharge in January. This scenario regards the transmissivity of the flysch bedrock and the impermeable quaternary sediments in relation to the estimated recharge in January.

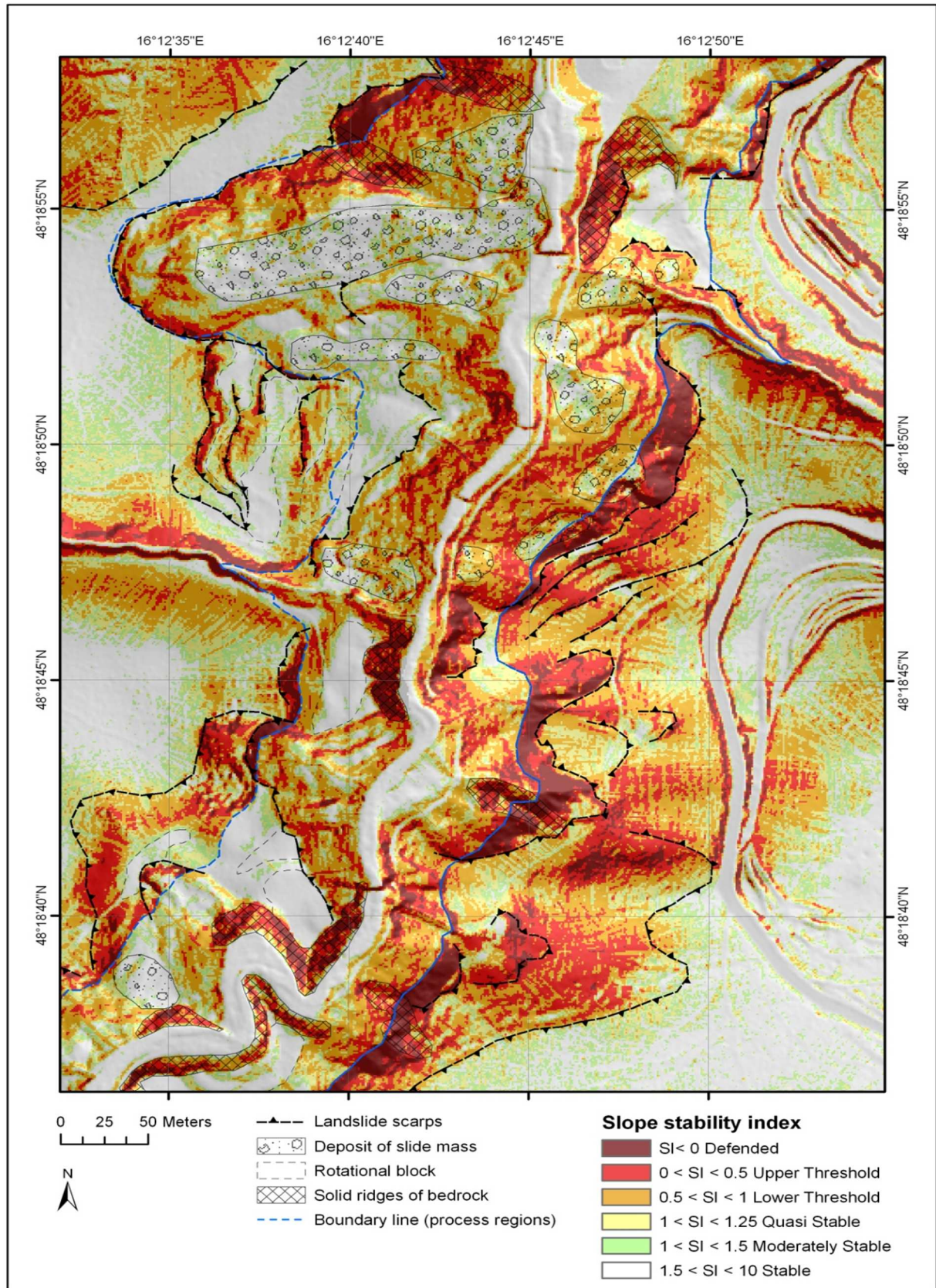


Figure 5-16. Stability index map for the "winter scenario (January)". The scenario is based on mid-term average recharge for January and the soil-mechanical parameters for flysch bedrock (process region (1)) and quaternary sediments (process region (2)). The boundary line (blue line) divides both process regions. Quaternary sediments occur at the upper slope positions while flysch bedrock is uncovered below the decline to the valley floor.

---

The proportion of the slope stability classes in relation to the study area is given in Figure 6-16. The diagram reveals that an area of 29% of the study area is classified as “stable”, 11% as “moderately stable” and a further 16% as “quasi-stable”. According to the classification system that means that 55% of the study area is unconditionally stable. Consequently, the inherent material properties cannot cause instability under the assumed average monthly wetness in January in this range. Nevertheless for 16% (“quasi-stable”) even minor external causes can lead to slope failure because the factor of safety is very small, i.e. between 1 and 1.25. Values below 1 have a probability for instability.

The diagram (Figure 5-17) further demonstrates that in total 39% (summing up the classes “lower threshold” and “upper threshold”) of the study area has a probability for slope failure. The possibility of slope instability results from the substrate properties, slope gradient and the assumed wetness conditions. Hence, no external causes are needed to create instability at these slopes. The analysis of slope gradient within the stability classes in Figure 5-18 shows that these instable areas have a mean slope gradient between 29° (“lower threshold”) and 36° (“upper threshold”). The slope gradient map in Figure 5-5 (page 79) indicates that such an inclination dominates in the upper slope positions. At this topographic position the quaternary sediments cover the flysch bedrock. Consequently, a major part of landslide disposition can be attributed to quaternary sediments. As the slope gradient is moderate, the soil-mechanical properties of the sediments and the resulting topographic wetness are responsible for slope activity. The topographic wetness map (Figure 5-15) reveals that there is a probability for saturation in the quaternary sediments under the upper bound of assumed wetness in the model (“threshold saturation”).

Apart from the quaternary sediments, the flysch bedrock is classified as instable (“upper threshold” and “lower threshold”) over large areas. The diagram (Figure 5.17) shows that even a higher proportion of the flysch layers is classified as instable in comparison to the quaternary sediments. This scenario does not represent substrate wetness to a critical degree, i.e. saturation or saturation tendency in the flysch layers under the assumed average recharge. As the topographic wetness map (Figure 5-15) illustrates, low moisture conditions predominate. Consequently, the instability can be mainly attributed to the rock-mechanical properties and the considerable slope gradient. As the slope gradient map in Figure 5-5 (page 79) illustrates, hillslopes with an inclination of 36° and higher are prone to instability. Such strongly inclined areas are present at the steep declivity to the valley bottom, i.e. the flanks of the gorge, as well as near the scarps of earlier landslides.

Finally an area of 6% is classified as “defended”, that means that these zones are instable over the whole parameter range, even under the most favourable combination of parameters in regard to shear strength. The existence of solid bedrock ridges is already discussed in the “flysch scenario (January)” and appropriate areas are mapped. The “defended” slopes concentrate on these ridges, which are not predisposed to landslide activity but rather to rock fall. Nevertheless, considerable areas are classified as unconditionally unstable (“defended”) at scarps and crowns of ancient landslides, as shown in the slope stability index map (Figure 5-16). In these areas quaternary sediments are present. According to the modelling results they are regarded as permanently instable due to shallow movements in the quaternary cover beds.

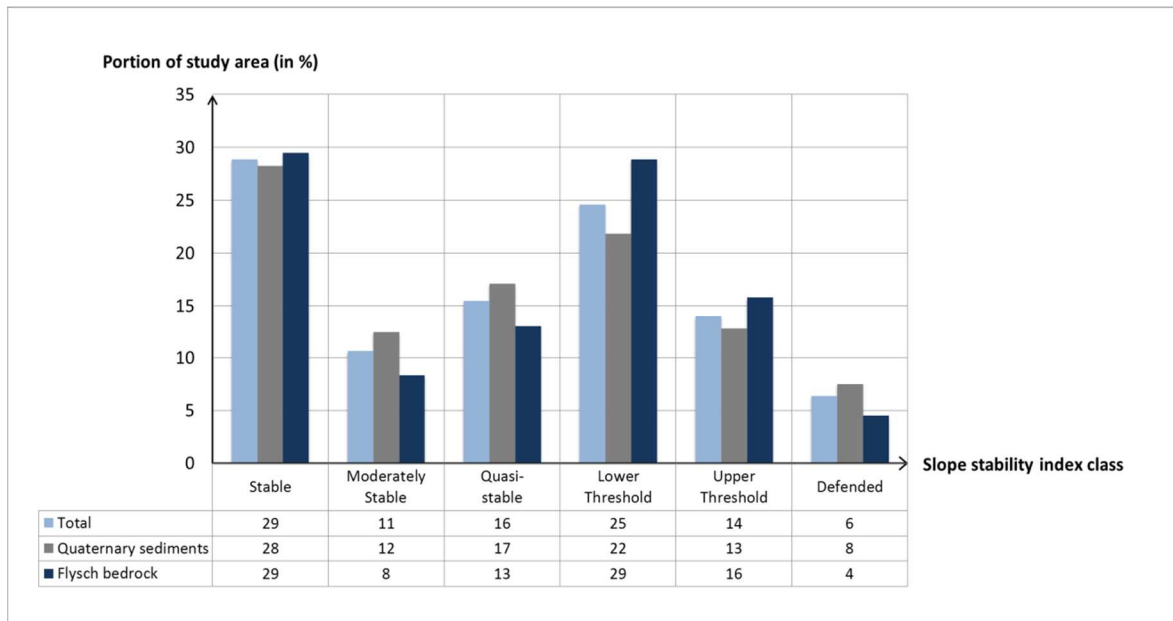


Figure 5-17. Slope stability classification for “winter scenario (January)”. The bars show the extension of the stability classes in relation to the study area and the process regions in percentage. The proportion of the classes within the study area is given in total (blue bar). The proportion of the classes within the process regions, the flysch bedrock (dark blue bar) and process region (2), the quaternary sediments (grey bar) are given, respectively.

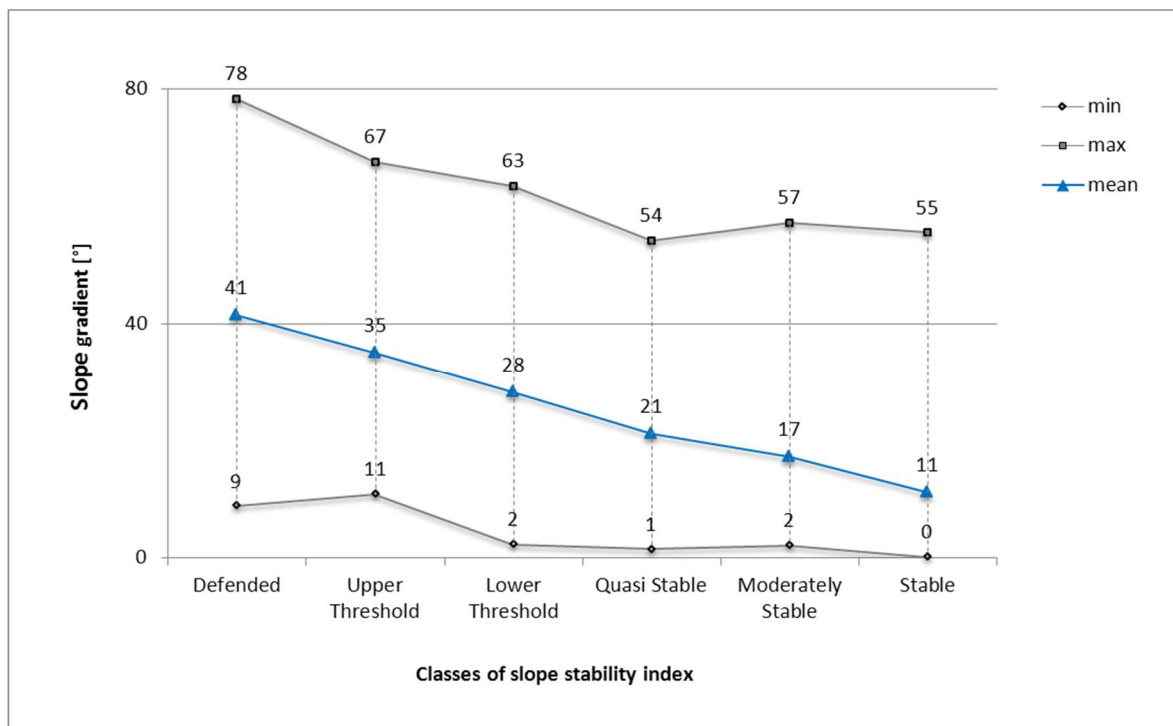


Figure 5-18. Slope gradient analysis within slope stability classes for “winter scenario (January)”. The diagram shows the mean (blue line), minimum (lower line) and maximum (upper line) slope gradient per stability class.

---

### 5.2.3.2 Winter scenario (February)

The “winter scenario (February)” is based on the wettest conditions (measured on an average monthly basis) in the seasonal course, measured in the recharge volume (mm/h). An average recharge of 228mm/M is assumed in February.

33% of the study area is classified as “partially wet” (Figure 5-19). A further 29% of the area reveals a saturation tendency (“threshold saturation”) and is saturated under the upper bound of assumed wetness. Such areas mainly occur in process region (2) where the quaternary sediments are regarded. There are wide areas of “low moisture” covering 35% of the study area. These areas are predominantly found in process region (1) where the flysch bedrock is considered (Figure 5-19).

Permanent saturation over the whole range of assumed wetness is derived for 3% of the study area. These areas concentrate at the drainage lines in the study area (Figure 5-19).

The results of slope stability index mapping are shown in Figure 5-21. In regard to slope dynamic there is no essential change in comparison to the “winter scenario (January)”, which is based on the average January recharge. In summary it can be stated that the most extensive areas of instable zones concentrate at the scarps and crowns of ancient landslides where the quaternary sediments are evident. Therefore, the probability for new shallow movements is given. The slide masses and rotational blocks of previous landslides are classified as stable.

The relative extension of the stability classes in relation to the study area is illustrated in Figure 5-21. It indicates that 27% of the study area is classified as “stable”, 10% as “moderately stable”, and an additional 15% as “quasi-stable” (Figure 5-21). These classes have a factor of safety greater than 1, consequently they are considered to be stable over the whole parameter ranges. However, external impacts can create instability. Only minor destabilising factors are able to cause slope failure regarding the “quasi-stable” areas.

The diagram (Figure 5-21) further indicates that for 26% (“upper threshold”) and an additional 16% (“lower threshold”) a probability for slope failure is caused by internal factors as material properties, slope gradient and wetness conditions. These conditionally instable areas are predominantly located in the upper slope positions where quaternary sediments cover the bedrock (Figure 5-20). A moderate slope gradient prevails at these topographic positions as shown in the slope gradient map in Figure 5-5 (page 79), however, topographic wetness is increased in comparison to process region (1) where flysch bedrock is considered (Figure 5-21). In the quaternary sediments “partially wet” conditions and “threshold saturation” are dominant. For the latter class saturation is reached under the upper bound of assumed wetness conditions.

Similar to the “winter scenario” 6% of the area is classified as “defended”, that means that these zones are instable over the whole parameter range even under the most favourable combination of parameters in regard to shear strength. The existence of solid bedrock ridges is already discussed in the “flysch scenario (January)”. The ridges are classified as “defended” slopes (Figure 5-20), indicating correctly the existence of solid bedrock outcrops. These areas are not predisposed to landslide activity but rather to events of rock fall. Furthermore additional areas are classified as unconditionally unstable (“defended”) at scarps and crowns of ancient landslides (Figure 5-20). In the present scenario they are regarded as permanently instable due to shallow movements in the quaternary cover beds.

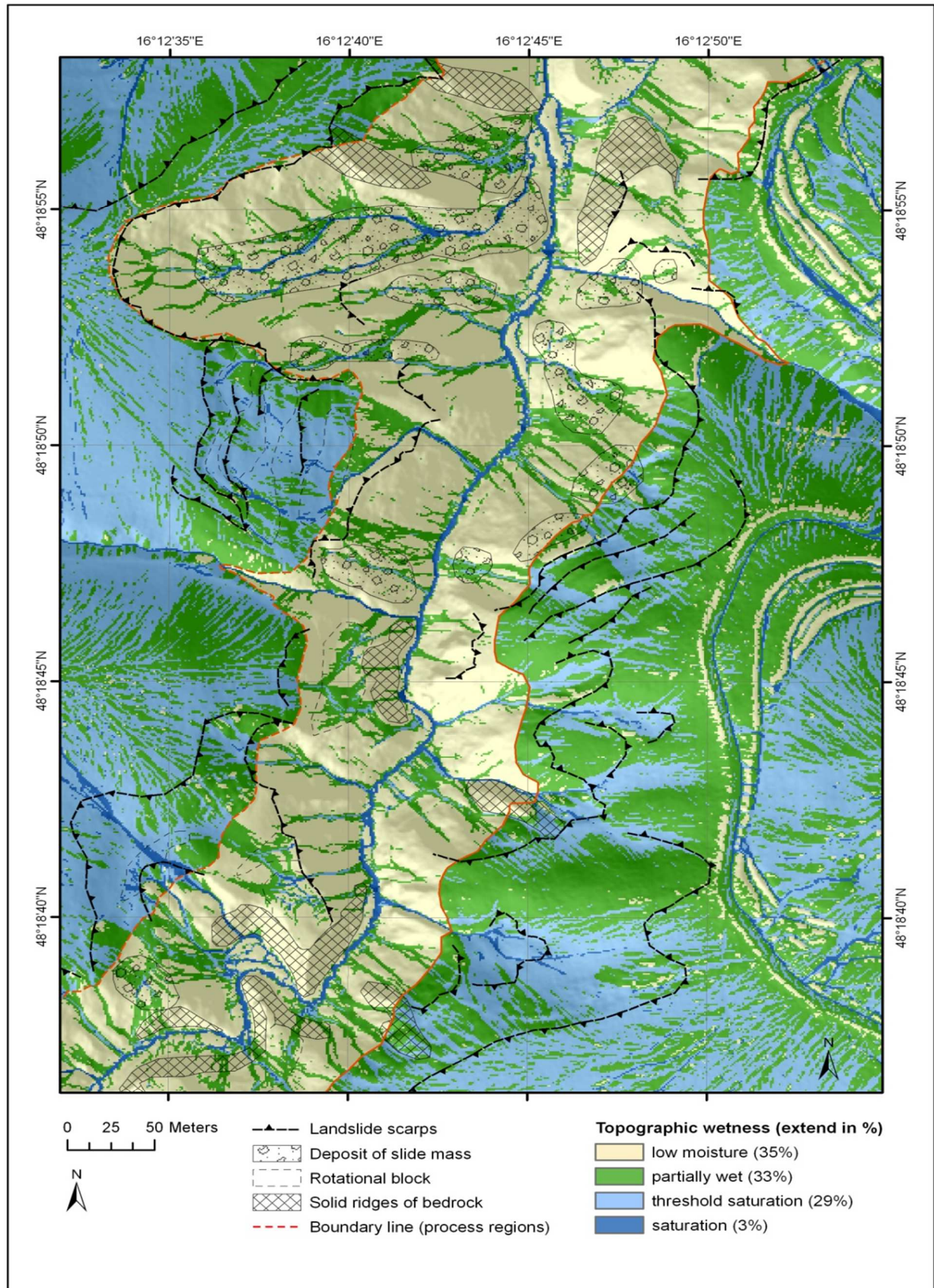


Figure 5-19. Topographic wetness map based on average monthly recharge in February. This scenario regards the transmissivity of the flysch bedrock and the impermeable quaternary sediments in relation to the estimated recharge in February.

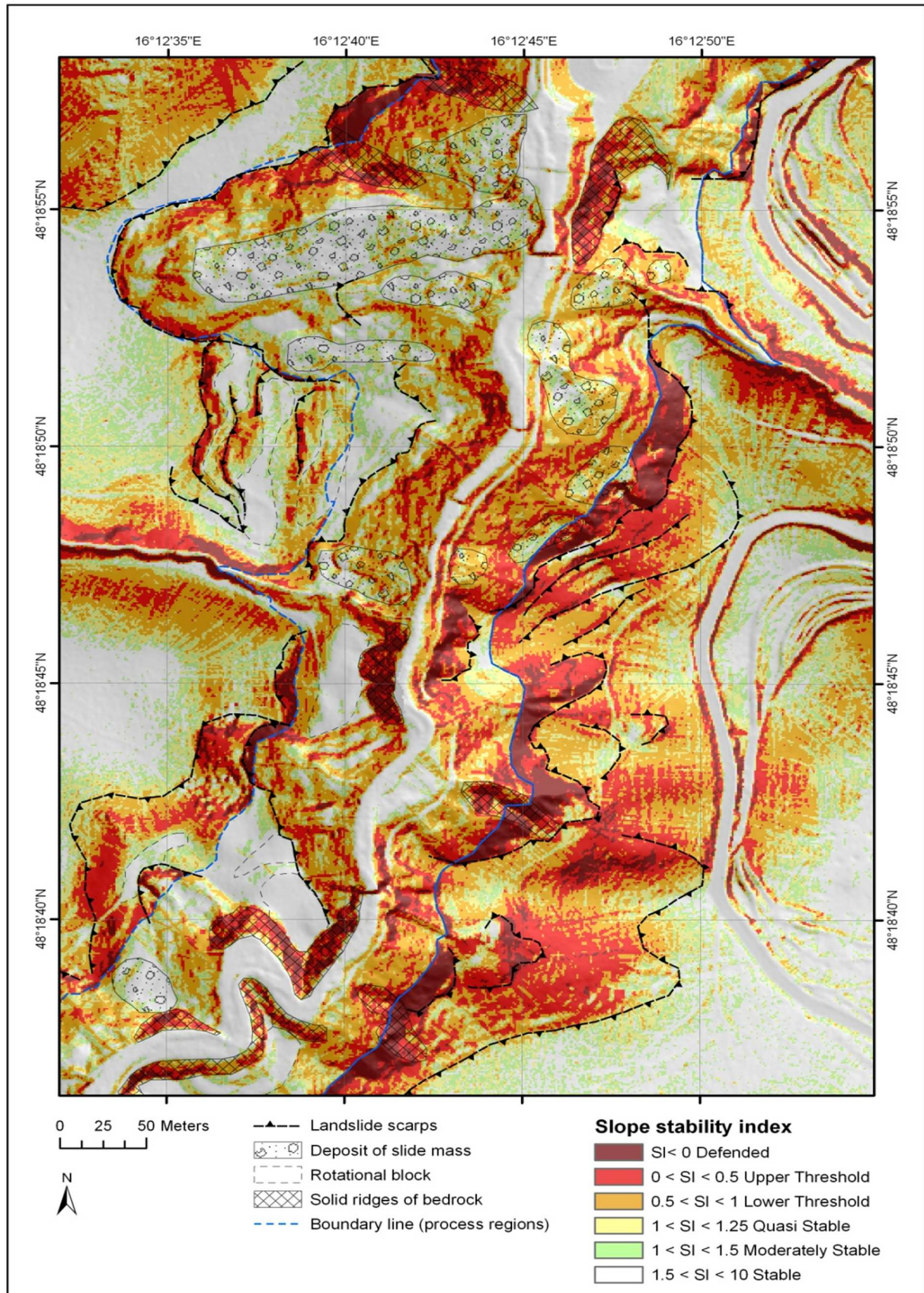


Figure 5-20. Stability index map for the “winter scenario (February)”. The scenario is based on mid-term average recharge for January and the soil-mechanical parameters for flysch bedrock (process region (1)) and quaternary sediments (process region (2)). The boundary line (blue line) divides both process regions. Quaternary sediments occur at the upper slope positions while flysch bedrock is uncovered below the decline to the valley floor.

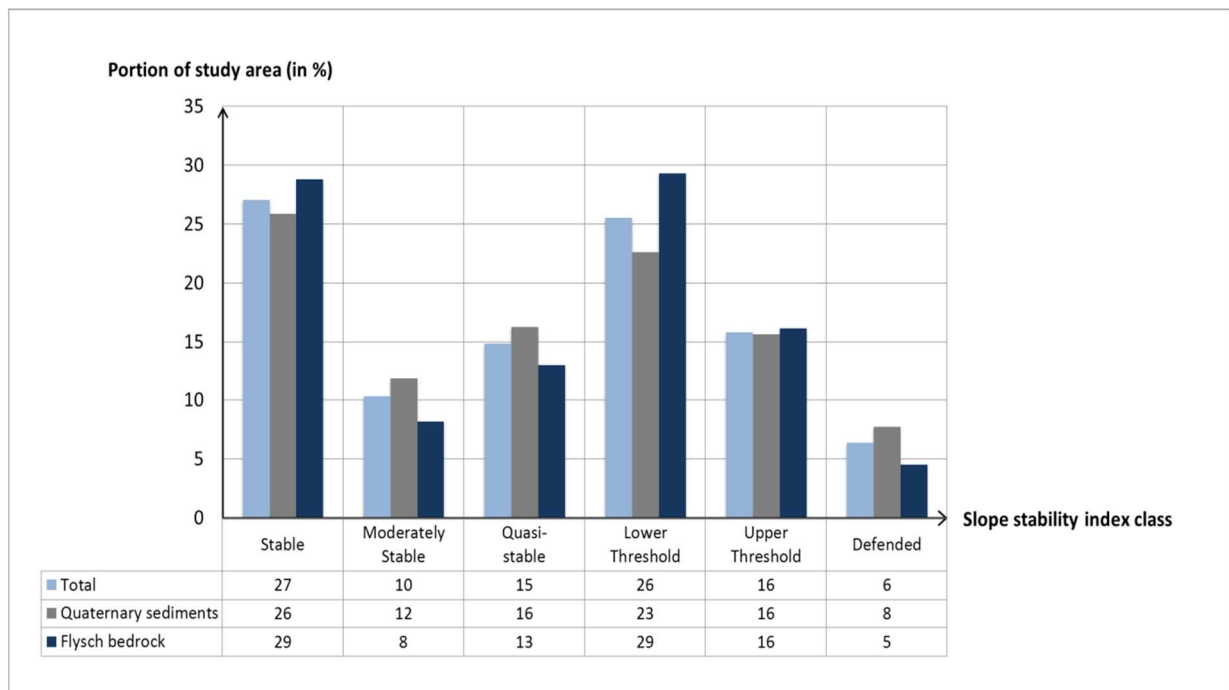


Figure 5-21. Slope stability classification for “winter scenario (February)”. The bars show the extension of the stability classes in relation to the study area and the process regions in percentage. The proportion of the classes within the study area is given in total (blue bar). The proportion of the classes within process region (1), the flysch bedrock (dark blue bar), and process region (2), the quaternary sediments (grey bar), are given, respectively.

### 5.2.3.3 Summer scenario (July)

The “summer scenario (July)” is based on the maximal dry conditions in the seasonal course, measured on an average monthly basis. A recharge of 101mm/M is applied in this scenario.

The derived topographic wetness index is displayed in Figure 5-22. The scenario is dominated by “low moisture” conditions covering 45% of the study area. These areas are predominantly found in the flysch bedrock where the quaternary sediments are eroded due to former landslide activity. In this process region (1), which represents the flysch bedrock, there is no saturation within the whole parameter range.

In the upper slope positions, in process region (2), where the quaternary sediments cover the bedrock, the steeper zones are also dry and not saturated. A proportion of 38% of the area is assessed to be “partially wet”. Areas with a saturation tendency (“threshold saturation”) cover 15% of the hillslopes and occur at the flat areas in the quaternary sediments. That means that there is a probability of saturation under the pessimistic parameters (“threshold saturation”). Saturation is only marginally developed, namely in 2% of the area. It concentrates at flow accumulation lines, mainly in the deposits of slide masses.

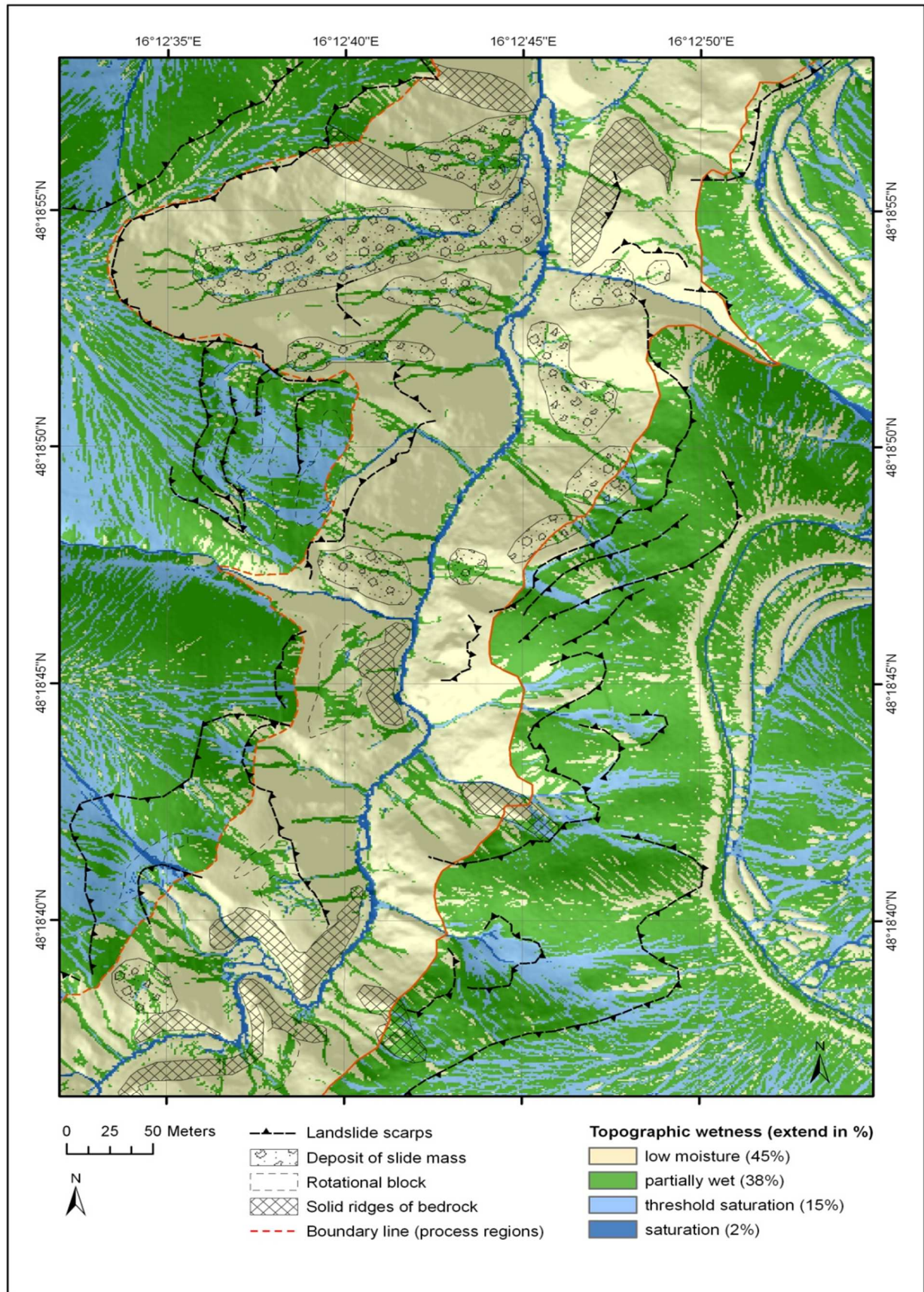


Figure 5-22. Topographic wetness map based on average monthly recharge in July. This scenario regards the transmissivity of the flysch bedrock and the impermeable quaternary sediments in relation to the estimated recharge in July.

---

The slope stability index is derived on the basis of the topographic wetness calculation. The results of slope stability index mapping are represented in Figure 5-23. In regard to slope dynamics the “summer scenario (July)” shows a similar pattern as both winter scenarios described in the previous chapters. Nevertheless, there are quantitative changes in slope stability.

The most extensive areas of highest instability are located at crowns and scarps of former landslides, as demonstrated in Figure 5-24. Quaternary sediments crop out in these areas. Therefore, previous landslides are affected by backward denudation due to shallow movements in the quaternary sediments. The deposition masses and rotational blocks of mapped landslides are classified as predominantly stable. Instable areas in process region (1), where a sliding surface in the flysch bedrock is considered, concentrate on slopes with an inclination of 36° and higher.

The proportion of the stability classes in relation to the study area is given in Figure 5-24. It indicates that 32% of the study area is classified as “stable”, 12% as “moderately stable”, and an additional 16% as “quasi-stable” (Figure 5-24). Consequently, 60% of the study area is unconditionally stable. In order to create slope failure external causes are necessary in these zones.

There is a probability for slope failure in 35% of the study area, comprising the areas classified as “lower threshold” and “upper threshold”. These conditionally instable areas are predominantly found in the upper slope positions where quaternary sediments are taken into account (Figure 5-23). This slope positions are characterised by moderate inclination as revealed in the slope gradient map shown in Figure 5-5 (page 79). However, in the quaternary sediments there are zones of “threshold saturation” which comprise a probability to develop saturation under the average summer recharge and which affect slope stability.

Similar to the “winter scenario” 6% of the area is classified as “defended”, that means that these zones are instable over the whole parameter even under the most favourable combination of parameters in regard to shear strength. Such zones are partly situated at mapped ridges of solid bedrock where landslide activity is excluded. The remaining zones classified as “defended” are regarded as permanently instable due to shallow slope movements in the cover beds.

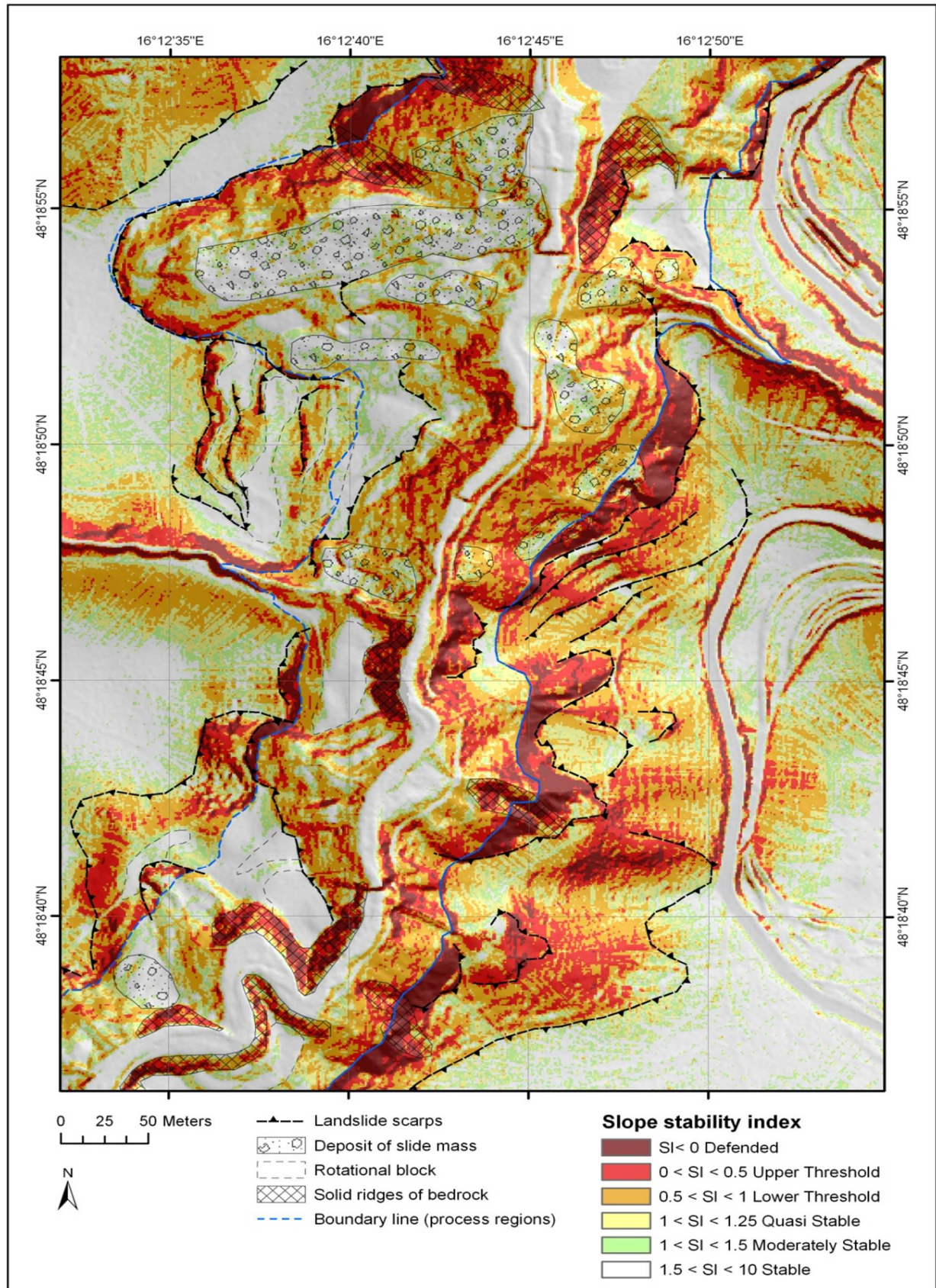


Figure 5-23. Stability index map for the "summer scenario (July)". The scenario is based on mid-term average recharge for July and the soil-mechanical parameters for flysch bedrock (process region (1)) and quaternary sediments (process region (2)). The boundary line (blue line) divides both process regions. Quaternary sediments occur at the upper slope positions while flysch bedrock is uncovered below the decline to the valley floor.

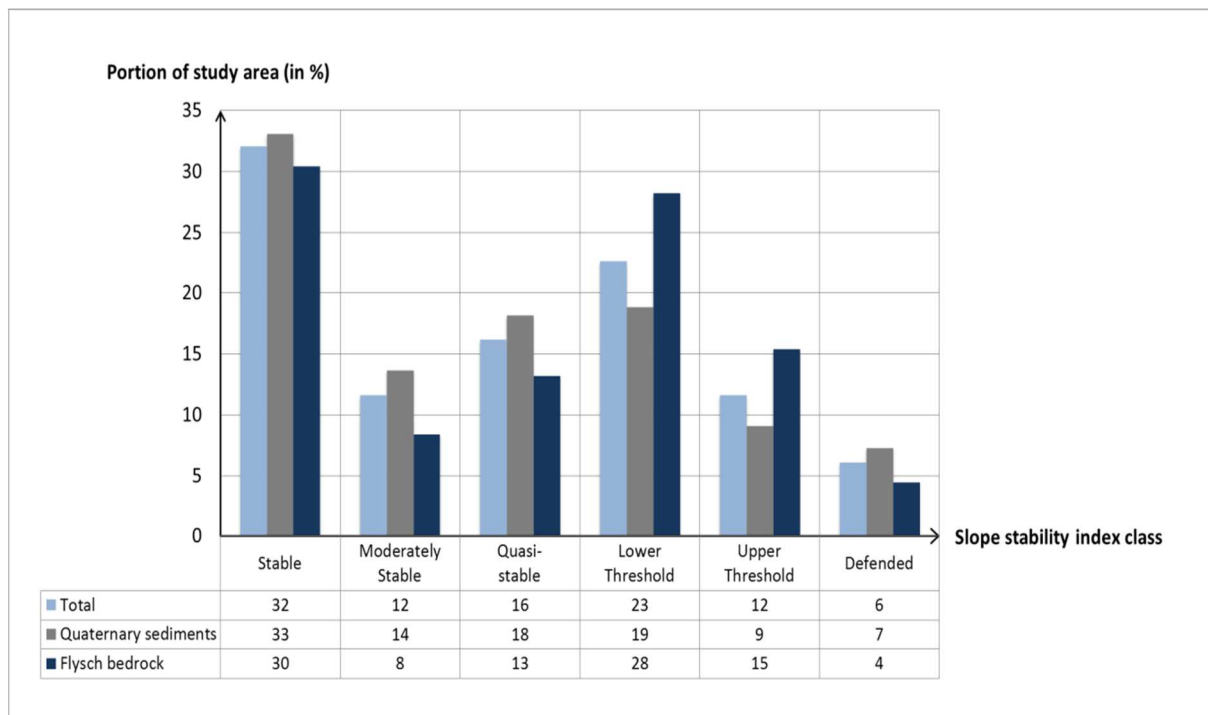


Figure 5-24. Slope stability classification for “summer scenario (July)”. The bars show the extension of the stability classes in relation to the study area and the process regions in percentage. The proportion of the classes within the study area is given in total (blue bar). The proportion of the classes within process region (1), the flysch bedrock (dark blue bar), and process region (2), the quaternary sediments (grey bar), are given, respectively.

---

## 5.2.4 Wetness scenario group “future, mid-term disposition”

The results of the modelling described in the following chapters indicate no essential change of slope dynamics in comparison with the present-day wetness scenarios. A detailed description is already given in the previous scenarios, in particular in the “winter scenario (January)” of the “present-day, mid-term disposition” group in the previous chapter 5.2.3. The distribution and pattern of stable and instable zones is similar, however, the quantities of the stability classes are shifted. Measureable change of slope stability due to modified climate conditions is revealed. Therefore, there the following description is focused on the quantities of slope stability classes and topographic wetness.

### 5.2.4.1 Future winter scenario (January)

The “future winter scenario (January)” is developed because it was affected by the most drastic change in comparison to the climate normal period (Figure 5-8). This “winter scenario (January)” takes the increase in recharge of 36% in relation to the climate normal period into account. The estimation of this change is carried out on the basis of the forecast temperature rise of 2° and a precipitation growth of 30% in the winter period according to regional climate scenarios (Reclip:more 2007).

An average monthly recharge of 238mm/M is assumed for the present scenario. In this scenario “low moisture” to “partially wet” conditions predominate with a proportion of 68% on the study area, as shown in the topographic wetness map (Figure 5-25). The maps yield “low moisture” conditions particularly calculated for the flysch bedrock. Consequently, the instability in this process region can be mainly attributed to the rock-mechanical properties and the considerable slope gradient of 36° and higher. Furthermore, the topographic wetness maps (Figure 5-25) show that flow is accumulated in the flysch bedrock, mainly in the deposits of former landslides, and that saturation is reached at linear flow lines.

It is further indicated in the topographic wetness map that a considerable proportion, i.e. 29% of the study area, develops a saturation tendency (“threshold saturation”). These areas which mainly occur in the quaternary sediments in the upper slope positions develop saturation under maximum assumed wetness. Therefore, topographic wetness is essential for slope stability in these zones. Full saturation over the whole range of assumed wetness is derived for 3% of the study area. These areas concentrate at the drainage lines in the study area (Figure 5-25).

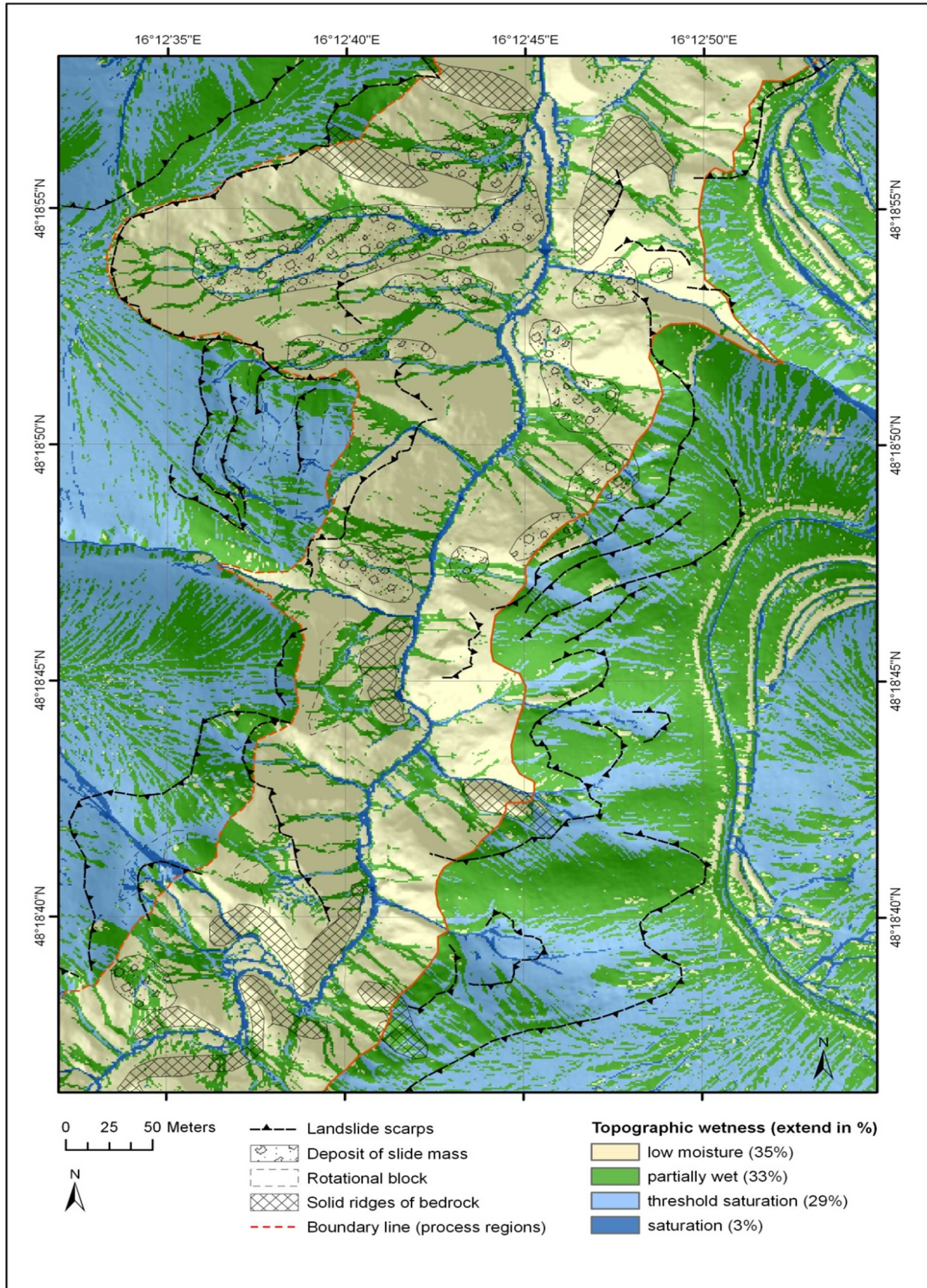


Figure 5-25. Topographic wetness map based on monthly average recharge in January in consideration of the climate change. This scenario regards the transmissivity of the flysch bedrock and the impermeable quaternary sediments in relation to the estimated recharge in January.

---

The resulting slope stability index map for the “future winter scenario (January)” is given in Figure 5-26. In general, the enhancement of recharge due to forecast climate change leads to a measurable reduction of the stable zones in this “future winter scenario (January)”.

A detailed view on the extension of the stability classes is represented in Figure 5-27. The diagram shows the proportion of the stability classes in relation to the study area and the process regions. The areas with a factor of safety greater than 1, which are considered as unconditionally stable in terms of the stability model, are shrinking to 52% of the study area. The latter percentage represents the sum of the stability classes “stable”, “moderately stable” and “quasi-stable”. The assumed substrate properties cannot cause slope failure under the considered future wetness in these areas according to the classification regime. With regard to quaternary sediments the reduction of unconditionally stable areas within the process region is even higher than in total over the whole study area. As shown in the diagram (Figure 5-27) the sum of the “stable”, “moderately stable” and “quasi-stable” classes yields 54% of process region (2), the quaternary sediments.

Simultaneously with the reduction of the unconditionally stable areas in this scenario, the instable areas (“lower threshold” and “upper threshold”) increase to 41% of the study area. These areas have a probability for slope failure due to the soil-mechanical properties, the prevailing slope gradient and the assumed wetness conditions. The slope stability index map (Figure 5-26) indicates that large-sized areas classified with “upper threshold” are found at the upper slope positions, at the scarps and crowns of former landslides. It further shows that in these topographic positions the quaternary cover beds are taken into account as critical layer. Therefore, shallow movements are probable under the pessimistic but even under the optimistic parameter range. According to the slope gradient map shown in Figure 5-5 (page 79) instabilities do not only occur at the steep slopes with an inclination greater than 35° but also in areas where a moderate slope gradient of 20° to 30° prevails. The reason for instabilities in these upper slope areas is heightened topographic wetness in the model in comparison to the steeper slopes. The topographic wetness map (Figure 5-25) shows areas of “threshold saturation” in the quaternary sediments which develop saturation under the upper bound of assumed wetness. Furthermore, instabilities are indicated by the model in the flysch bedrock, which is considered at the steep slopes near the valley bottom as process region (1) (Figure 5-26). The red line in the slope stability index maps shows the borderline between the process regions. The stability index map (Figure 5-26) reveals instable areas on slopes with an inclination of 36° and higher as shown in Figure 5-5 (page 79). Such areas are predominantly located at the crown of previous landslides and the flank of the gorge near the valley bottom. The deposition areas of sliding masses and rotational blocks of former landslides are mainly classified as unconditionally stable. Finally an area of 6% is classified as “defended”, that means that these zones are instable over the whole parameter range even under the most favourable combination of parameters in regard to shear strength. As the slopes are still intact, stabilising forces which are not taken into account by the model are present. As already described in the previous scenarios, the stabilising effect is explained by the ridges of solid bedrock outcrops (Figure 5-26). Furthermore unconditionally stable areas are calculated at the scarps of older landslides where the quaternary sediments cover the bedrock. According to the modelling results they are regarded as permanently instable due to shallow movements in the quaternary cover beds.

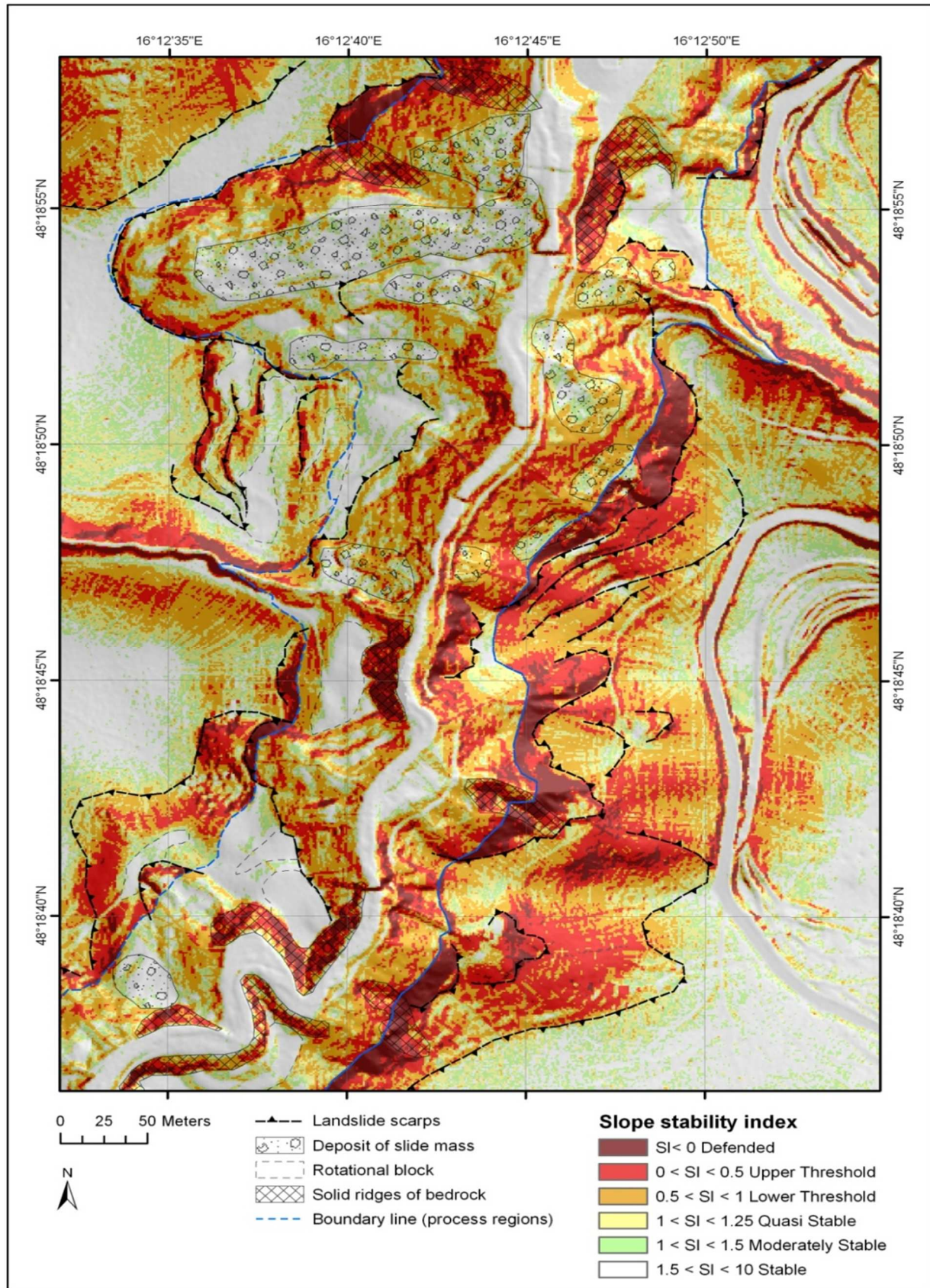


Figure 5-26. Stability index map for the future „winter scenario (January)”. The scenario is based on the average recharge for January in consideration of the climate change and the soil-mechanical parameters for flysch bedrock (process region (1)) and quaternary sediments (process region (2)). The boundary line (blue line) divides both process regions. Quaternary sediments occur at the upper slope positions while flysch bedrock is uncovered below the decline to the valley floor.

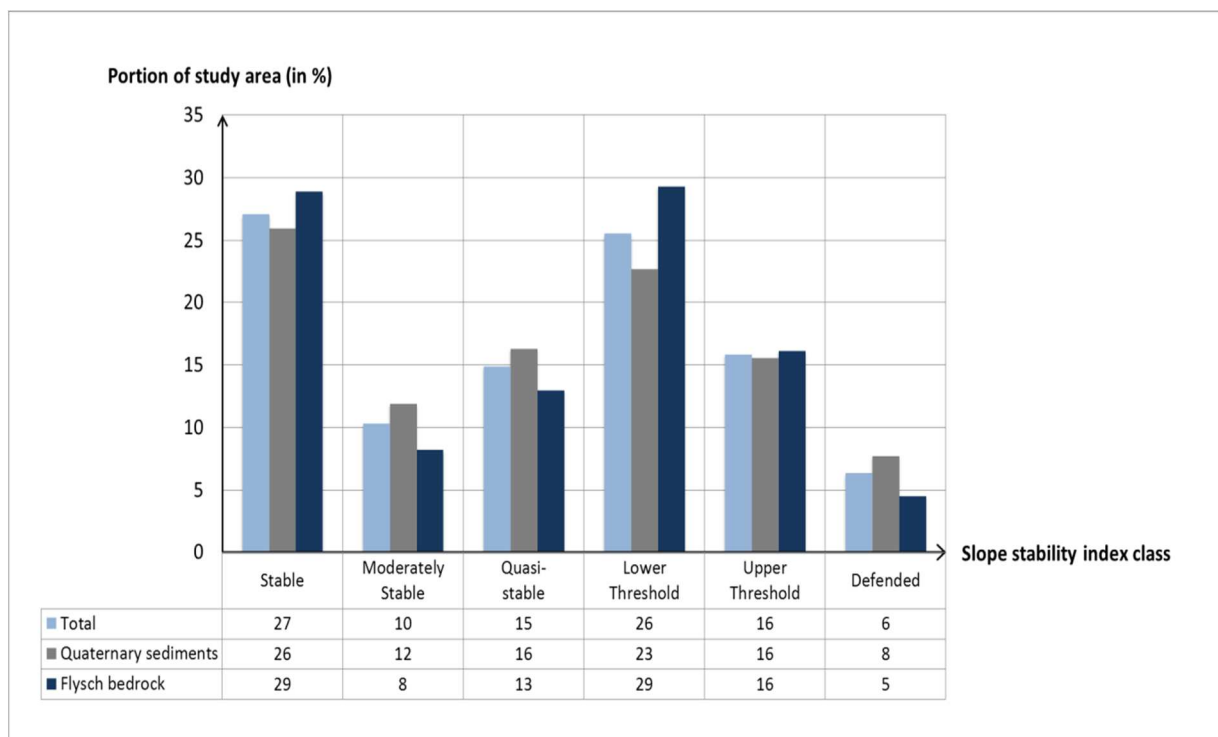


Figure 5-27. Slope stability classification for future “winter scenario (January)” in consideration of the climate change. The bars show the extension of the stability classes in relation to the study area and the process regions in percentage. The proportion of the classes within the study area is given in total (blue bar). The proportion of the classes within process region (1), the flysch bedrock (dark blue bar), and process region (2), the quaternary sediments (grey bar), are given, respectively.

#### 5.2.4.2 Future winter scenario (February)

In February recharge is raised by 7% in relation to the climate normal period. February, just like January, is the month with the highest rate of recharge. However, in comparison to the “future winter scenario (January)”, only a slight increase of 7% is evident.

An average monthly recharge of 243mm/M is assumed for the present scenario. Similar to the “future winter scenario (January)”, in this scenario “low moisture” to “partially wet” conditions predominate with a proportion of 67% of the study area, as shown in the topographic wetness map (Figure 5-28). The maps yield that “low moisture” conditions are particularly found in the flysch bedrock. Consequently, if instability is given in this area, it need not necessarily be attributed to substrate wetness but rather to slope gradient. Furthermore, the topographic wetness maps (Figure 5-28) show that flow concentrates in the flysch bedrock, mainly in the deposits of former landslides and that saturation is reached at linear flow lines.

30% of the study area develops a saturation tendency (“threshold saturation”). These areas occur in the quaternary sediments in the upper slope positions. Therefore, topographic wetness is a steering factor for slope stability only in these zones. Saturation over the whole range of assumed wetness is calculated for 3% of the study area. These areas concentrate at the drainage lines in the study area (Figure 5-28).

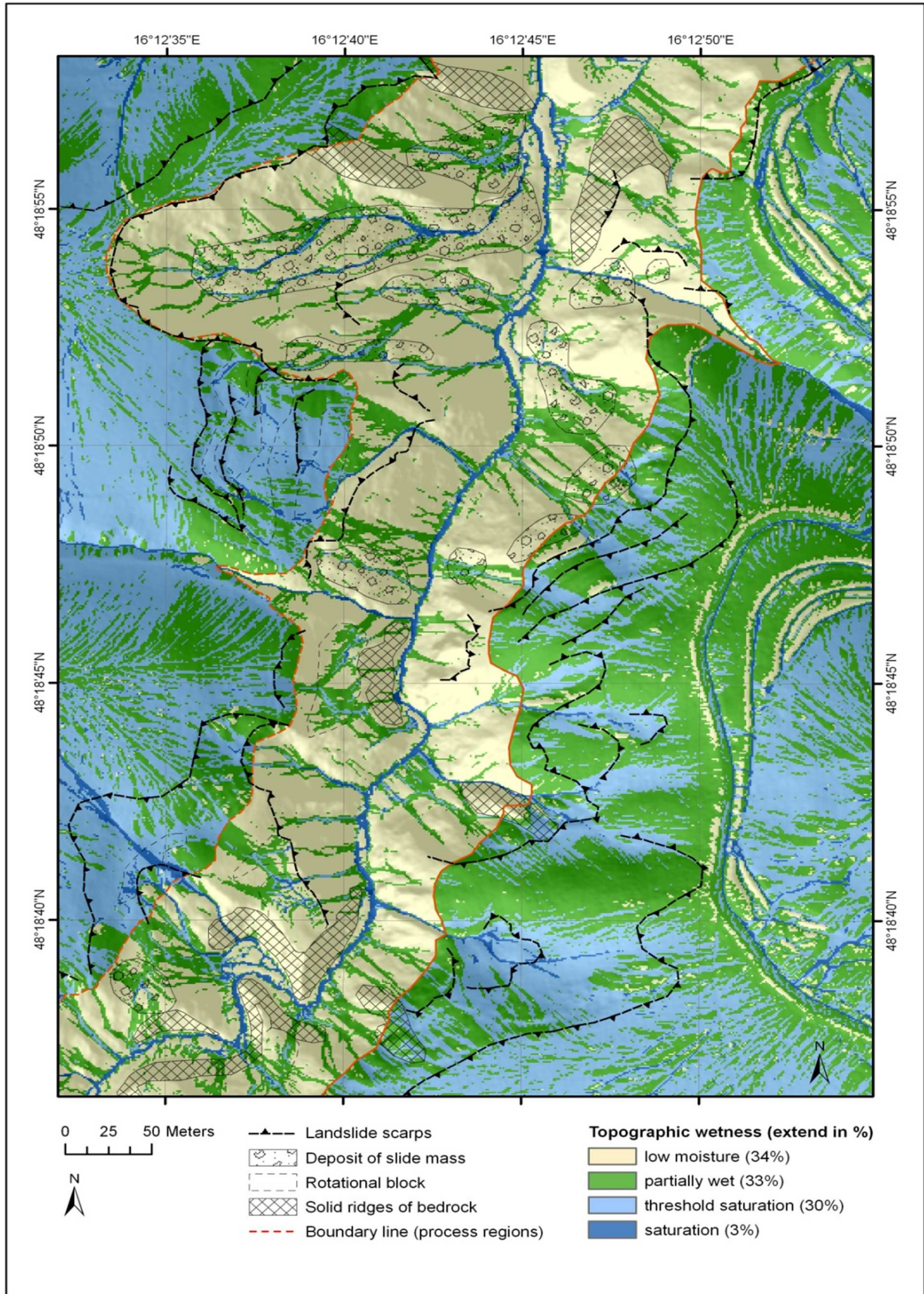


Figure 5-28. Topographic wetness map based on monthly average recharge in February in consideration of the climate change. This scenario regards the transmissivity of the flysch bedrock and the impermeable quaternary sediments in relation to the estimated recharge in February.

---

The resulting slope stability index map for the “future winter scenario (February)” is given in Figure 5-29. In general, the enhancement of recharge due to forecast climate change leads to a slight reduction of the stable zones in this “future winter scenario (February)”.

A detailed view on the extension of the stability classes is given in Figure 5-30. The diagram shows quite a similar classification to the “future winter scenario (January)” and also to the corresponding scenario “winter scenario (February)”. The areas classified as “stable”, “moderately stable” and “quasi-stable” cover 52% of the study area. The assumed substrate properties cannot cause slope failure in these areas under the considered future wetness.

The instable areas (“lower threshold” and “upper threshold”) cover up to 47% of the study area. These areas have a probability for slope failure due to the soil-mechanical properties, the prevailing slope gradient and the assumed wetness conditions. The slope stability index map (Figure 5-29) indicates that large-sized areas classified with “upper threshold” are located at the upper slope positions, at the scarps and crowns of former landslides. Quaternary cover beds occur in these topographic positions. The reason for instabilities in these upper slope areas is an increased topographic wetness in the model in comparison to the steeper slopes. The topographic wetness map (Figure 5-28) exhibits areas of “threshold saturation” in the quaternary sediments. Furthermore “defended” areas are calculated at the scarps of older landslides where the quaternary sediments cover the bedrock. According to the modelling results they are regarded as permanently instable due to movements in the quaternary cover beds.

Instabilities are indicated at the steep slopes near the valley bottom where the flysch bedrock, i.e. process region (1), is given (Figure 6-25). The stability index map (Figure 5-29) reveals instable areas on slopes with an inclination of 36° and higher. The information on slope gradient is provided in Figure 5-5 (page 79). Such areas are found at the crown of previous landslides and the flank of the gorge near the valley bottom.

The deposition areas of sliding masses and rotational blocks of former landslides are classified mainly as unconditionally “stable” and an area of 6% is classified as “defended”. As already described in the previous scenarios, the stabilising effect is explained by the ridges of solid bedrock outcrops.

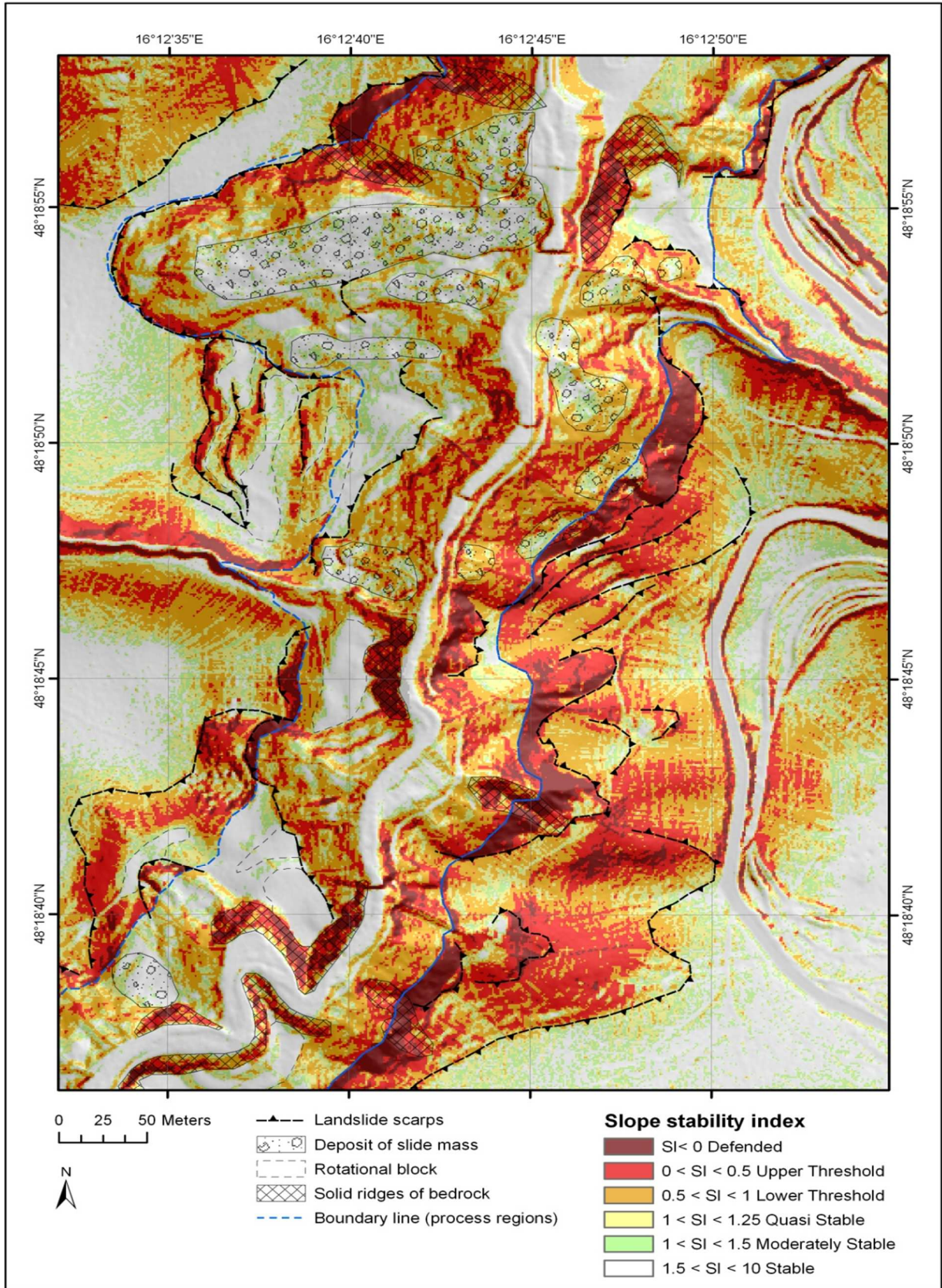


Figure 5-29. Stability index map for the future "winter scenario (February)". The scenario is based on the average recharge for February in consideration of the climate change and the soil-mechanical parameters for flysch bedrock (process region (1)) and quaternary sediments (process region (2)). The boundary line (blue line) divides both process regions. Quaternary sediments occur at the upper slope positions, while flysch bedrock is uncovered below the decline to the valley floor.

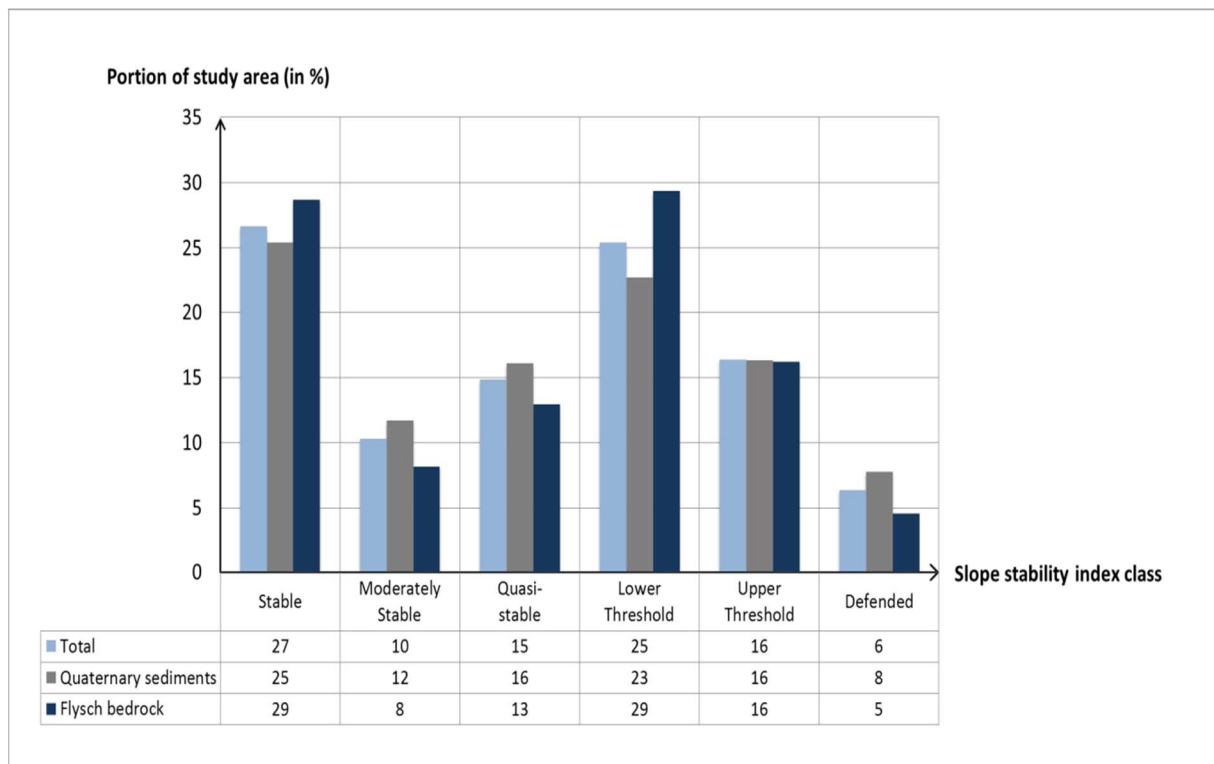


Figure 5-30. Slope stability classification for future “winter scenario (February)” in consideration of the climate change. The bars show the extension of the stability classes in relation to the study area and the process regions in percentage. The proportion of the classes within the study area is given in total (blue bar). The proportion of the classes within process region (1), the flysch bedrock (dark blue bar), and process region (2), the quaternary sediments (grey bar), are given, respectively.

#### 5.2.4.3 Future summer scenario (July)

This “future summer scenario (July)” takes a decrease in recharge of 73% in relation to the climate normal period into account. The estimation of this change is carried out on basis of the forecast temperature increase of 2.5° and a reduction of precipitation of 15% in the summer period according to the regional climate scenarios (Reclip:more 2007). The resulting slope stability index map for the “future summer scenario (July)” is given in Figure 6-31. In general, the reduction of recharge due to the forecast climate change leads to a measurable extension of the stable zones in this “future summer scenario (July)”.

The topographic wetness map (Figure 5-31) shows considerably reduced wetness due to the forecast climate change. The reduction of monthly recharge of 73% in relation to the climate normals caused a decrease of the “partially wet” areas to 28% of the study area and “threshold saturation” to 4% of the study area. The “low moisture” conditions are predominant in this scenario, covering 67% of the study area.

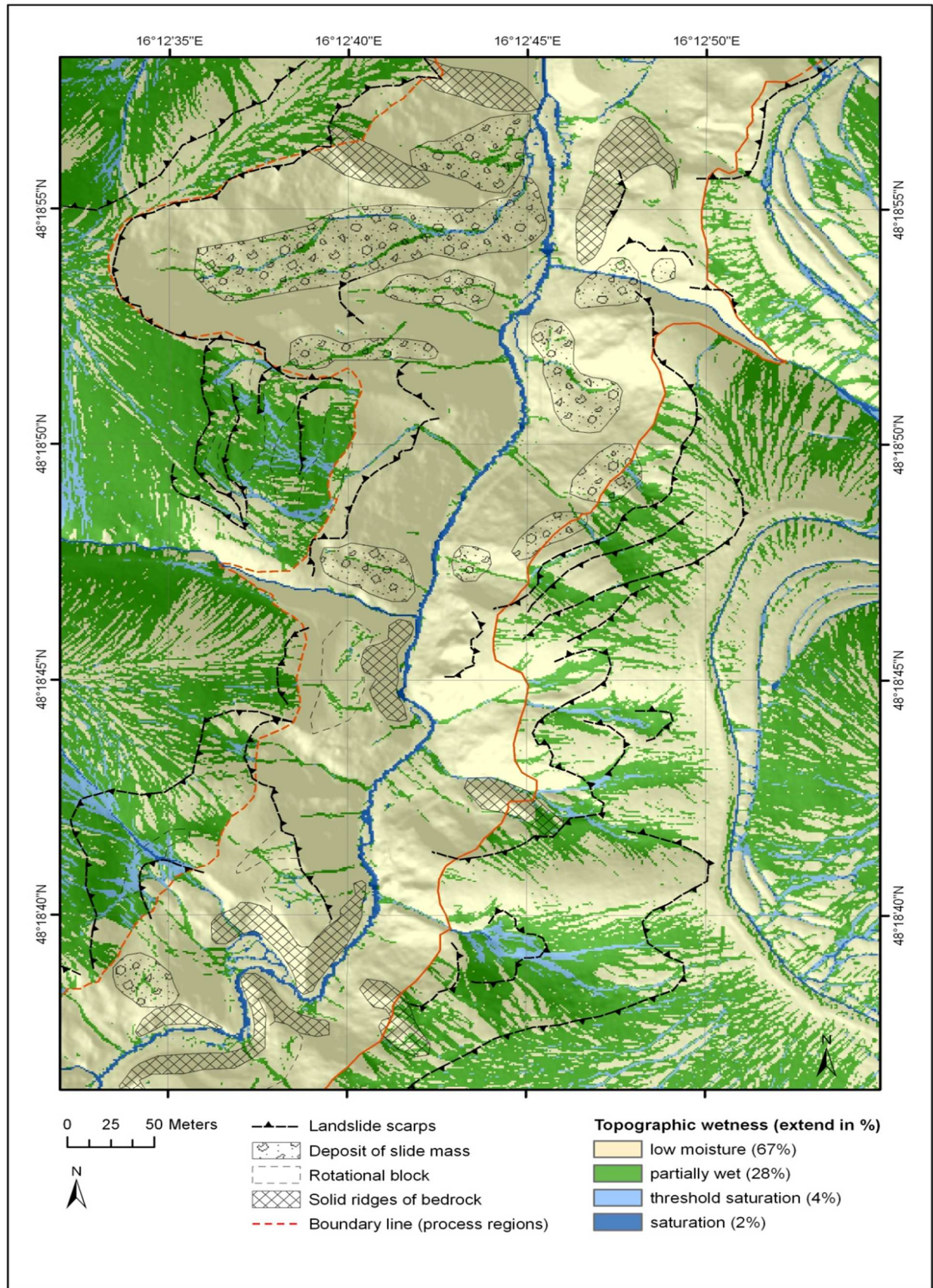


Figure 5-31. Topographic wetness map based on the monthly average recharge in July in consideration of the climate change. This scenario regards the transmissivity of the flysch bedrock and the impermeable quaternary sediments in relation to the estimated recharge in July.

---

A detailed view on the extension of the stability classes is given in Figure 5-33. The diagram shows the proportion of the stability classes in relation to the study area and the process regions. The areas classified as “stable”, “moderately stable” and “quasi-stable” grow in sum up to 67% of the study area. These areas have a factor of safety greater than 1 and are unconditionally stable in terms of the classification system. Consequently, the inherent substrate properties cannot cause slope failure under the considered future wetness.

The conditional instable areas (“lower threshold” and “upper threshold”) decrease and cover 27% of the study area. These areas have a probability for slope failure due to the soil-mechanical properties, the prevailing slope gradient and the assumed wetness conditions. Similar to the previously described scenarios, the slope stability index map (Figure 5-32) indicates that areas classified with “upper threshold” are located at the upper slope positions, at the scarps and crowns of earlier landslides.

In these slope positions the quaternary cover beds are present. Therefore, shallow movements are probable under the pessimistic but even under the optimistic parameter range. However, instabilities preferably occur at slopes with an inclination of 30° and higher (cp. Figure 5-32). In Figure 5-5 (page 79) the information on inclination is provided. The flatter zones with an inclination below this value are classified as “stable” to “lower threshold”. Consequently, these areas are unconditionally stable or show a probability for instability below 50% (“lower threshold”), which means the pessimistic parameters are required to cause instability. The reason for this reduction of the probability for slope failure compared to the other scenarios is the change of the topographic wetness, in particular in the quaternary sediments (cp. Figure 5-31).

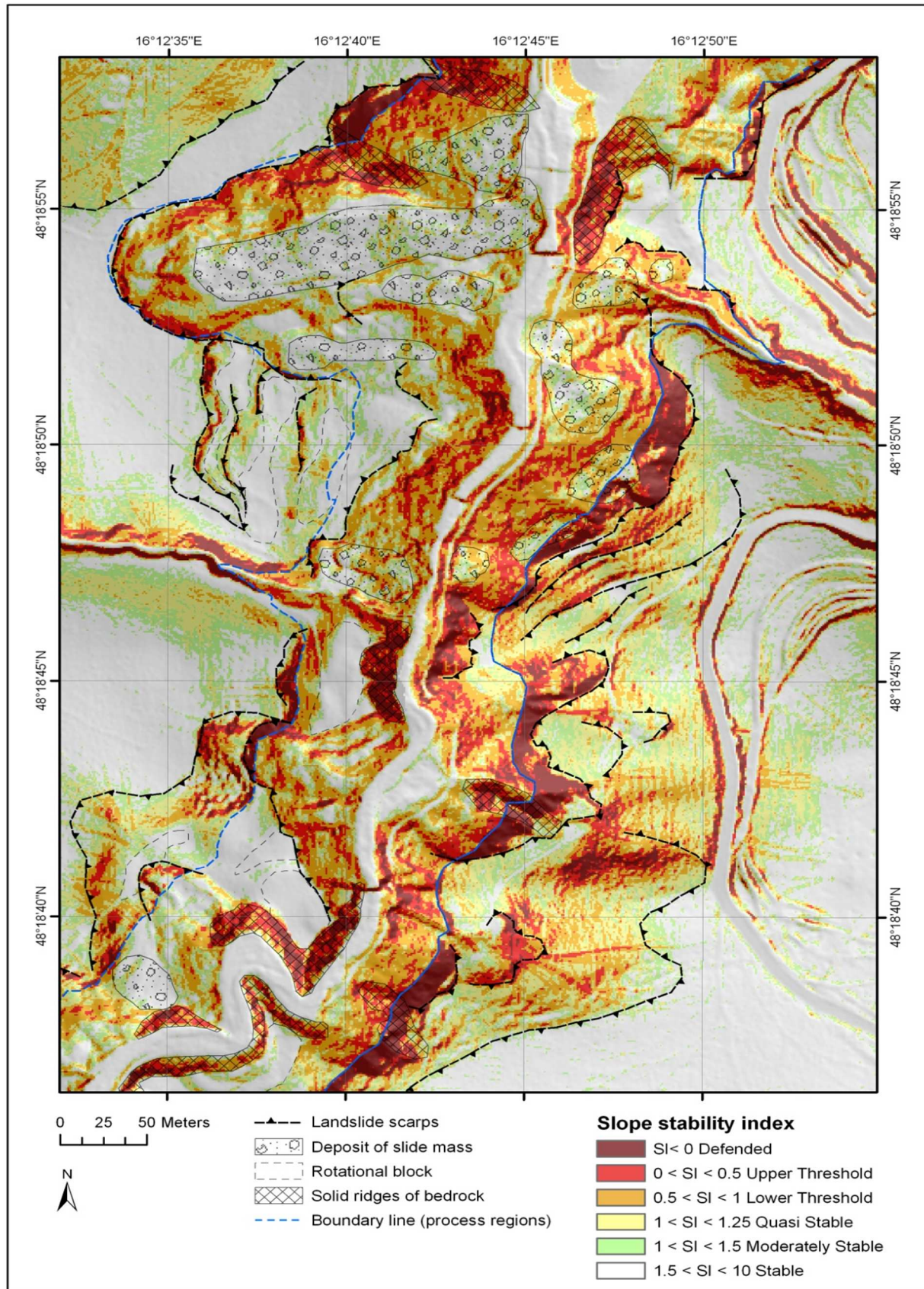


Figure 5-32. Stability index map for the “future summer scenario (July)”. The scenario is based on the average recharge for July in consideration of the climate change and the soil-mechanical parameters for flysch bedrock (process region (1)) and quaternary sediments (process region (2)). The boundary line (blue line) divides both process regions. Quaternary sediments are found at the upper slope positions, while flysch bedrock is uncovered below the decline to the valley floor.

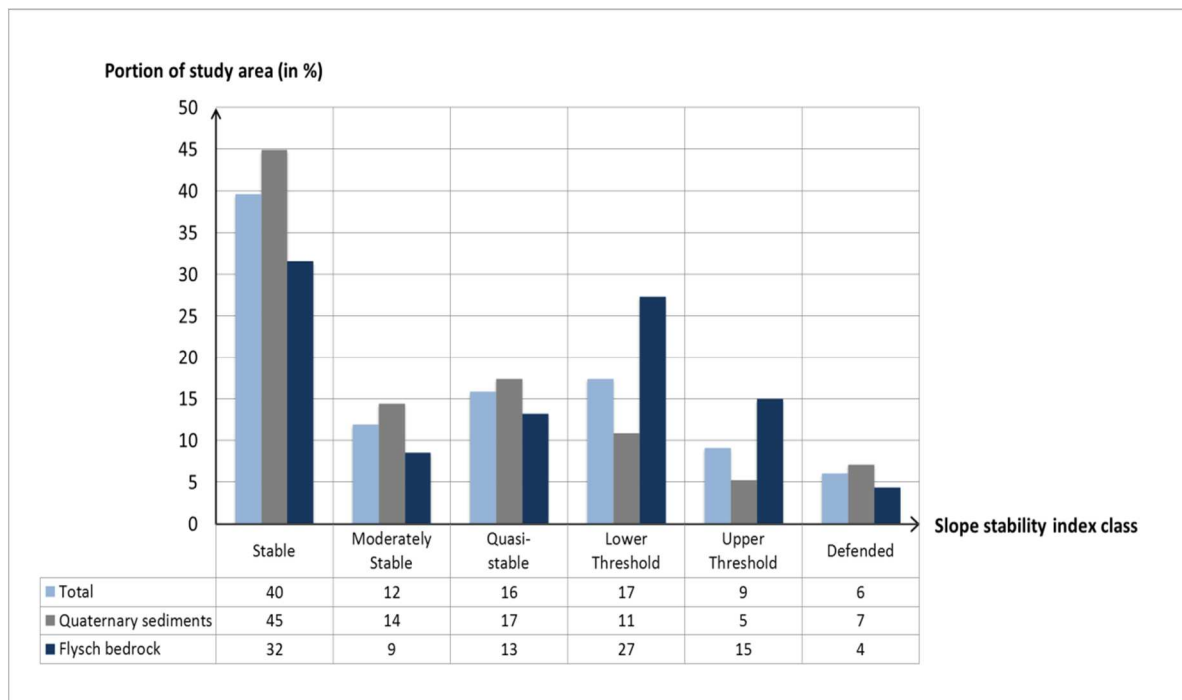


Figure 5-33. Slope stability classification for “future summer scenario (July)” in consideration of the climate change. The bars show the extension of the stability classes in relation to the study area and the process regions in percentage. The proportion of the classes within the study area is given in total (blue bar). The proportion of the classes within process region (1), the flysch bedrock (dark blue bar), and process region (2), the quaternary sediments (grey bar), are given, respectively.

## 5.2.5 Wetness scenario group “short-term disposition”

### 5.2.5.1 Critical rainfall scenario

A period of rainfall, delivering 90mm precipitation within a day, is considered (ZAMG 2010a) causing a considerable increase in instability in the scenario. The stability index map (Figure 5-35) shows the extension of the instable areas in general. According to these scenarios wide areas of the former landslide heads would slide down.

This augmentation of stability is due to the drastically raised substrate wetness as indicated by the topographic wetness map (Figure 5-34). Extensive areas, particularly in the quaternary sediments, are classified with “threshold saturation”, that means that saturation develops under the upper bounds of assumed wetness. Already 12% of the study area is computed as “saturated” under this critical rainfall event. That means that saturation is given for the whole parameter range of assumed wetness conditions. Such areas concentrate at hollows and mounds in the quaternary sediments and at linear flow lines in the flysch bedrock. These flow lines are strongly developed in the deposited slide masses. Therefore, locally a probability for slope failure in these deposits is derived in the model. In the flysch bedrock in the steep slopes saturation is not reached, however, the slopes are partially wet, which results in more distinct accumulation of flow in the former slide masses or at the landslide toes.

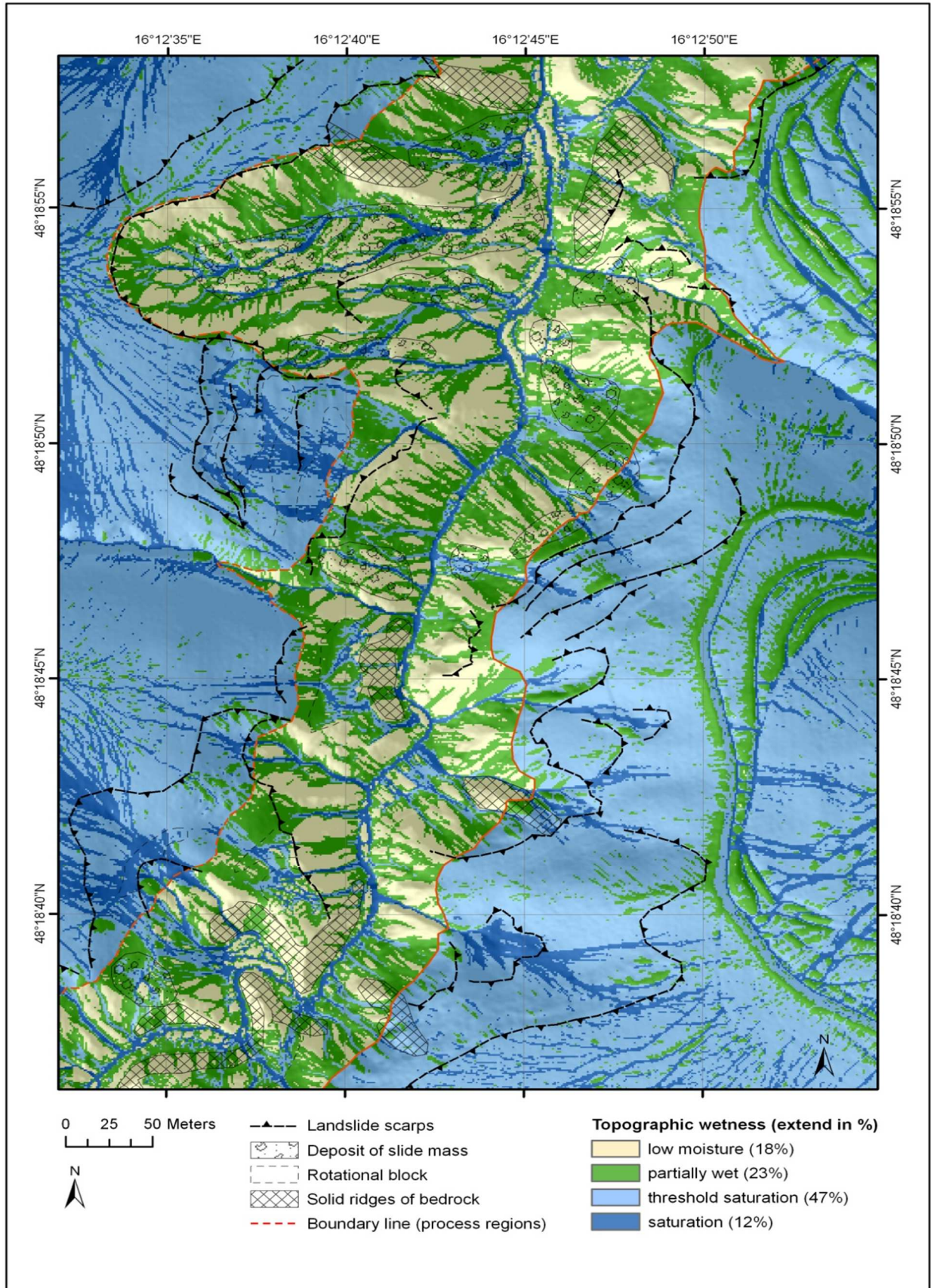


Figure 5-34. Topographic wetness map for the “critical rainfall scenario” based on a long-lasting rainfall event of 90mm/d (ZAMG 2010a). This scenario regards the transmissivity of the flysch bedrock and the impermeable quaternary sediments in relation to the estimated recharge.

---

Extensive areas in the quaternary sediments, in particular in the moderately inclined areas from 15° to 30°, are conditionally instable. The proportion of the stability classes in the study area is illustrated in Figure 5-36. The conditionally instable areas (“lower threshold” and “upper threshold”) cover 48% of the study area. In the quaternary sediments the areas with a probability for instability greater than 50% (“upper threshold”) concentrate at slopes with a moderate slope gradient of approximately 20° to 30° as shown in the slope gradient map in Figure 5-5 (page 79). At these hillslopes the optimistic parameters are required for stability; otherwise they are instable under the assumed parameters. Even the slopes with an inclination of 15° to 20° are conditionally instable with a probability for slope failure below 50% (“lower threshold”). These slopes are instable under the pessimistic parameters. A further proportion of 9% of the study area is instable (“defended”) even over the whole parameter range. These zones concentrate, in the case of the quaternary sediments, at steep slopes with a gradient of 35° and more, which are situated at existing scarps and on the flanks of the temporarily water-bearing drainage lines.

In the flysch bedrock the extension of conditionally instable areas (“lower threshold” and “upper threshold”) occur at the scarps of former landslides and near the valley bottom at the oversteepened slopes of the gorge.

Concerning the proportion of the stability classes within the process regions, in the flysch bedrock (process region (1)) the “lower threshold” class is the dominant instability class with a proportion of 32% of the region (Figure 5-36). That means that in these areas of the flysch bedrock there is a probability of instability below 50% and the slopes are instable under the pessimistic parameter range. However, in the quaternary sediments (process region (2)) the “upper threshold” class is predominant with a proportion of 28% of the area (Figure 5-36). These zones reveal a probability of instability greater than 50% and the optimistic parameters are required for stability. Furthermore, an additional 11% of the quaternary sediments are unconditionally unstable (“defended”), that means that this range cannot model stability over the whole parameter range (Figure 5-36). In comparison only a proportion of 5% of the flysch bedrock is classified as “defended”. Consequently, long-lasting rainfall events affect both, flysch bedrock and quaternary sediments, however, the destabilising effect is stronger in case of the quaternary sediments.

Stable areas (“stable”, “moderately stable” and “quasi-stable”) cover an area of 43% of the study area in total (Figure 5-36). They are classified as unconditionally stable under the whole parameter range.

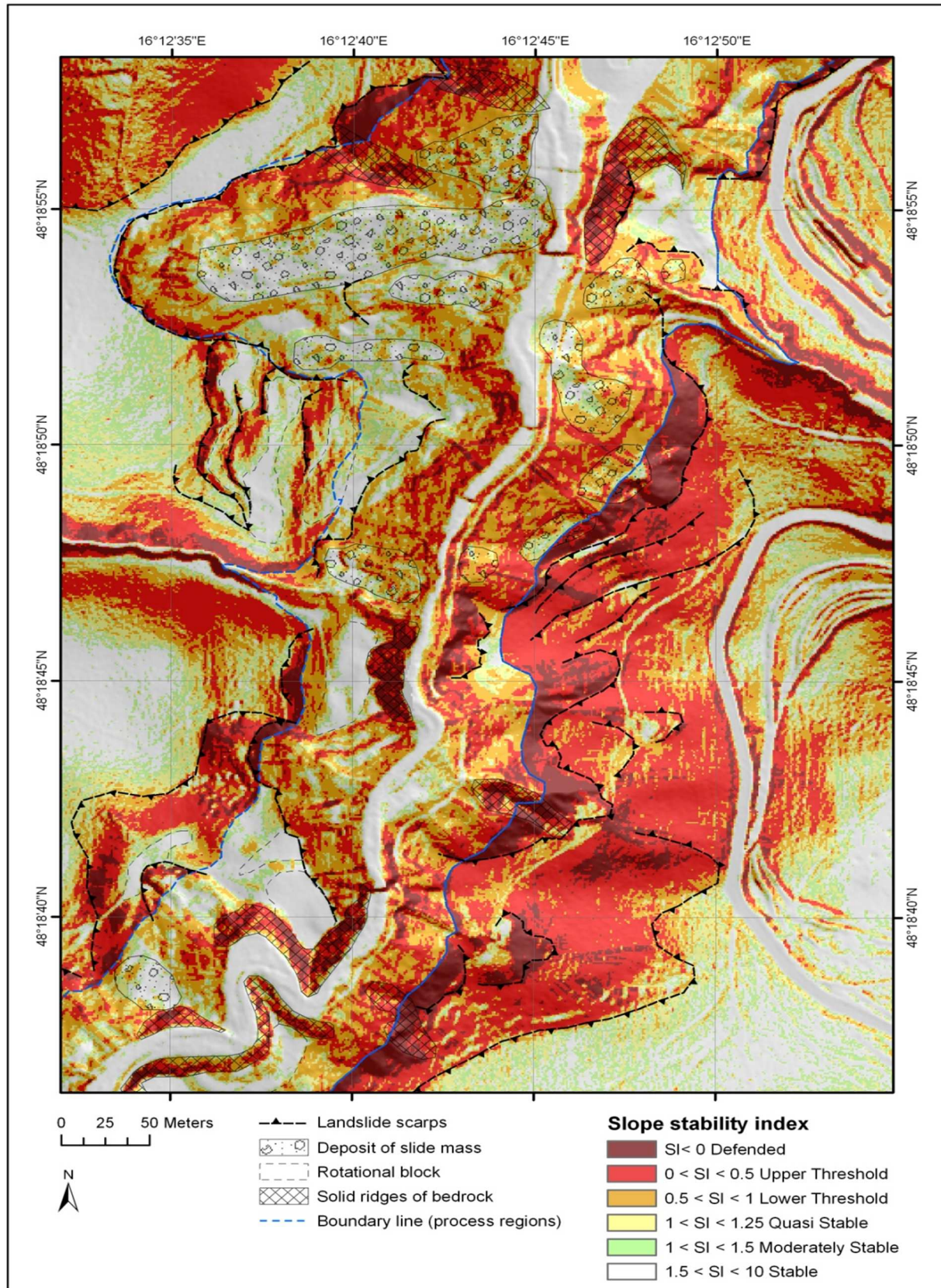


Figure 5-35. Stability index map for the critical precipitation scenario, which is based on long-lasting rainfall of 90mm/d (ZAMG 2010a). The scenario is based on short-term recharge caused by a specific weather event and the soil-mechanical parameters for flysch bedrock (process region (1)) and quaternary sediments (process region (2)). The boundary line (blue line) divides both process regions. Quaternary sediments occur at the upper slope positions, while flysch bedrock is uncovered below the decline to the valley floor.

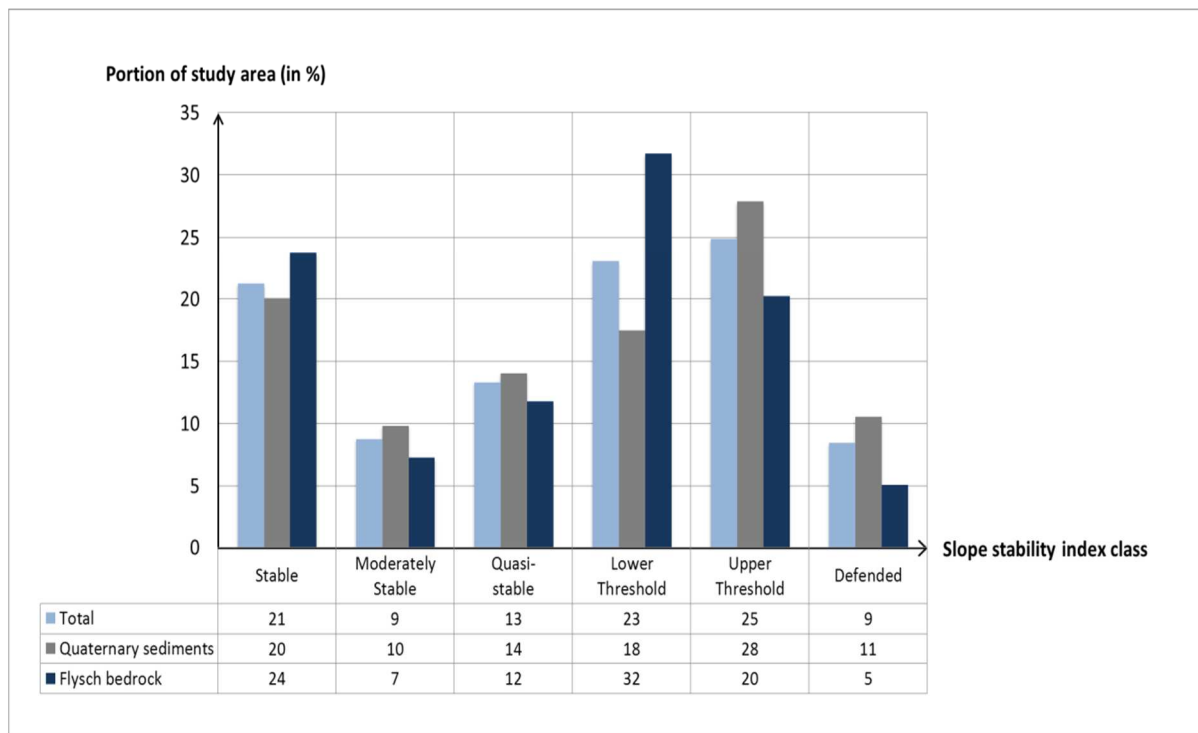


Figure 5-36. Slope stability classification for “critical rainfall scenario” based on long-lasting rainfall of 90mm/d (ZAMG 2010a). The bars show the extension of the stability classes in relation to the study area and the process regions in percentage. The proportion of the classes within the study area is given in total (blue bar). The proportion of the classes within process region (1), the flysch bedrock (dark blue bar), and process region (2), the quaternary sediments (grey bar), are given, respectively.

### 5.2.5.2 Heavy rainfall scenario

Heavy rainfall, delivering 60mm/h, is the basis for the present scenario (eHYD 2011). This event represents an extreme case as this rainfall intensity has a statistical reoccurrence period of 50 years (eHYD 2011). Respectively, it causes a drastic surge of topographic wetness (Figure 5-37) and instability in the model.

The effects of the heavy rainfall event on substrate wetness in the model are displayed in the topographic wetness map (Figure 5-37). Such a drastic increase in infiltration caused by extreme events results in an extension of the saturated zones up to 78% of the study area. That means that for this proportion of the study area saturation is computed for the whole parameter range of assumed wetness. An additional 17% of the slopes show a saturation tendency (“threshold saturation”) and therefore have a probability for saturation under maximum assumed wetness in the model (Figure 5-37).

Quaternary sediments are completely saturated at all slope positions. Flysch bedrock is partially wet, nearly over the entire area. Besides, there are extensive areas with water-saturation, in particular at the slope toe and within the decomposed slide masses (Figure 5-37).

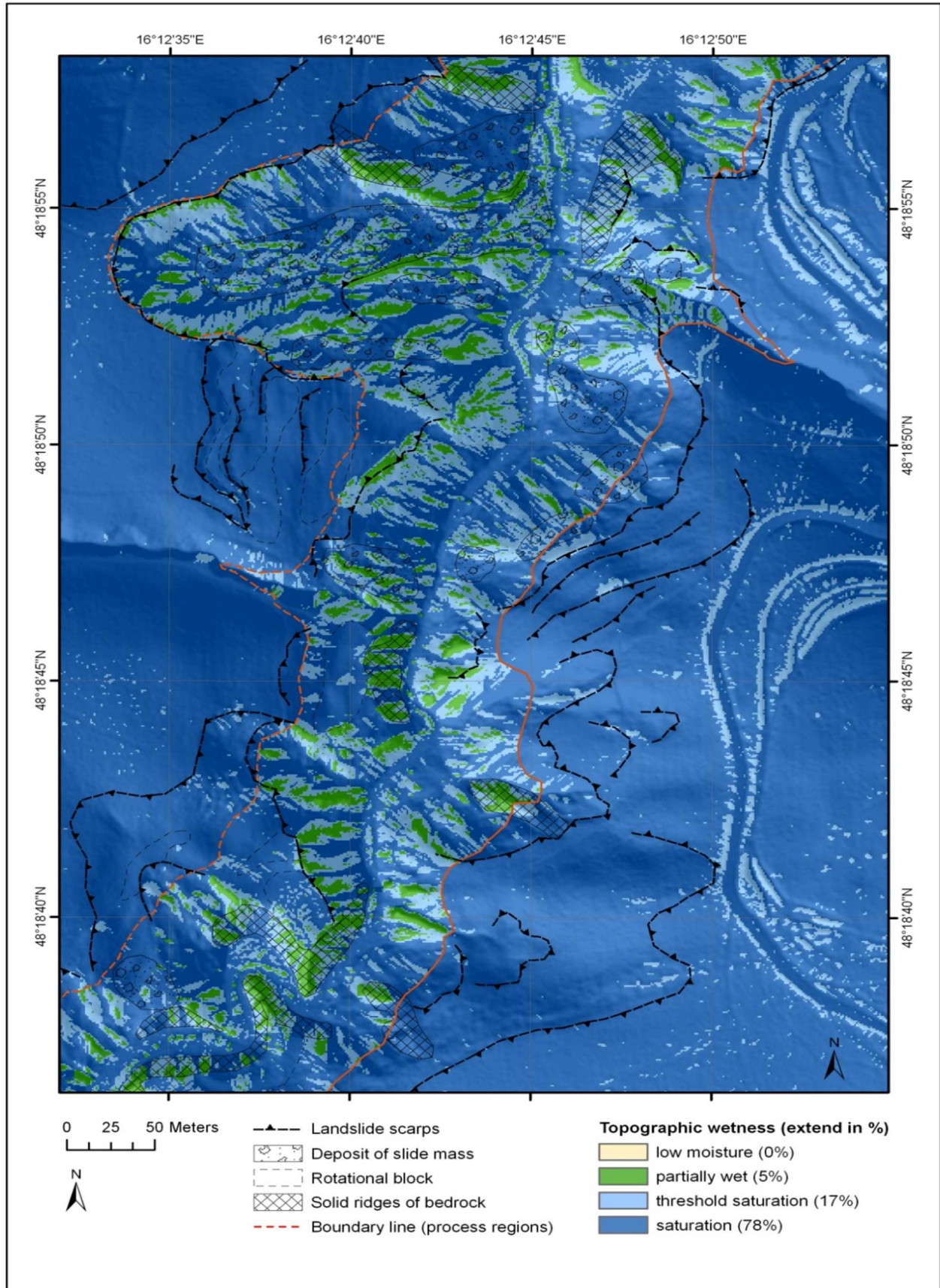


Figure 5-37. Topographic wetness map for the “heavy rainfall scenario” based on an extreme rainfall event of 60mm/h, which has a statistical reoccurrence period of 50 years in the study area (eHYD 2011). This scenario regards the transmissivity of the flysch bedrock and the impermeable quaternary sediments in relation to the estimated recharge.

---

The stability index map (Figure 5-38) shows that the areas classified as conditionally instable (“lower threshold” and “upper threshold”) or as unconditionally instable (“defended”) are widespread in the study area.

The diagram (Figure 5-39) shows the proportion of the stability classes in the study area and in the process regions.

A shifting of the stability classes to the most instable areas is given. For 38% of the area a probability for instability is computed (“lower threshold” and “upper threshold”) and for an additional 28% the model derives certainty for instability (“defended”) over the whole variety of assumed wetness in the scenario (Figure 5-39). Consequently, the prevailing soil-mechanical properties, slope gradient and substrate wetness can cause slope movements in these zones. No additional destabilising factors are required for instability. As the slope stability index map (Figure 5-38) and the slope gradient map in Figure 5-5 (page 79) illustrate, nearly all areas with an inclination above 15° are affected by instability.

The shifting of the stability classes is different within the process regions, similarly as under the previous scenario considering a critical rainfall event. In the flysch bedrock the “upper threshold” class is the dominant instability class under heavy rainfall (Figure 5-39). In the quaternary sediments, however, the “defended” class is predominant. Consequently, extreme rainfall events affect both, flysch bedrock and quaternary sediments, however, the destabilising effect is stronger in case of the quaternary sediment. In particular, the flysch bedrock has a probability of instability greater than 50% in 32% of its area (class “upper threshold”) and the optimistic parameters are required for stability. However, in case of the quaternary sediments 31% of their area (class “defended”) is unconditionally unstable, that means that this range cannot model stability over the whole parameter range (Figure 5-39).

In total the unconditionally stable areas (“stable”, “moderately stable” and “quasi-stable”) are reduced to 34% of the study area (Figure 5-39). The latter zones have a factor of safety greater than 1, therefore the internal substrate conditions in combination with the prevailing slope gradient and wetness condition cannot cause slope failure. External destabilising forces are required to cause slope failure.

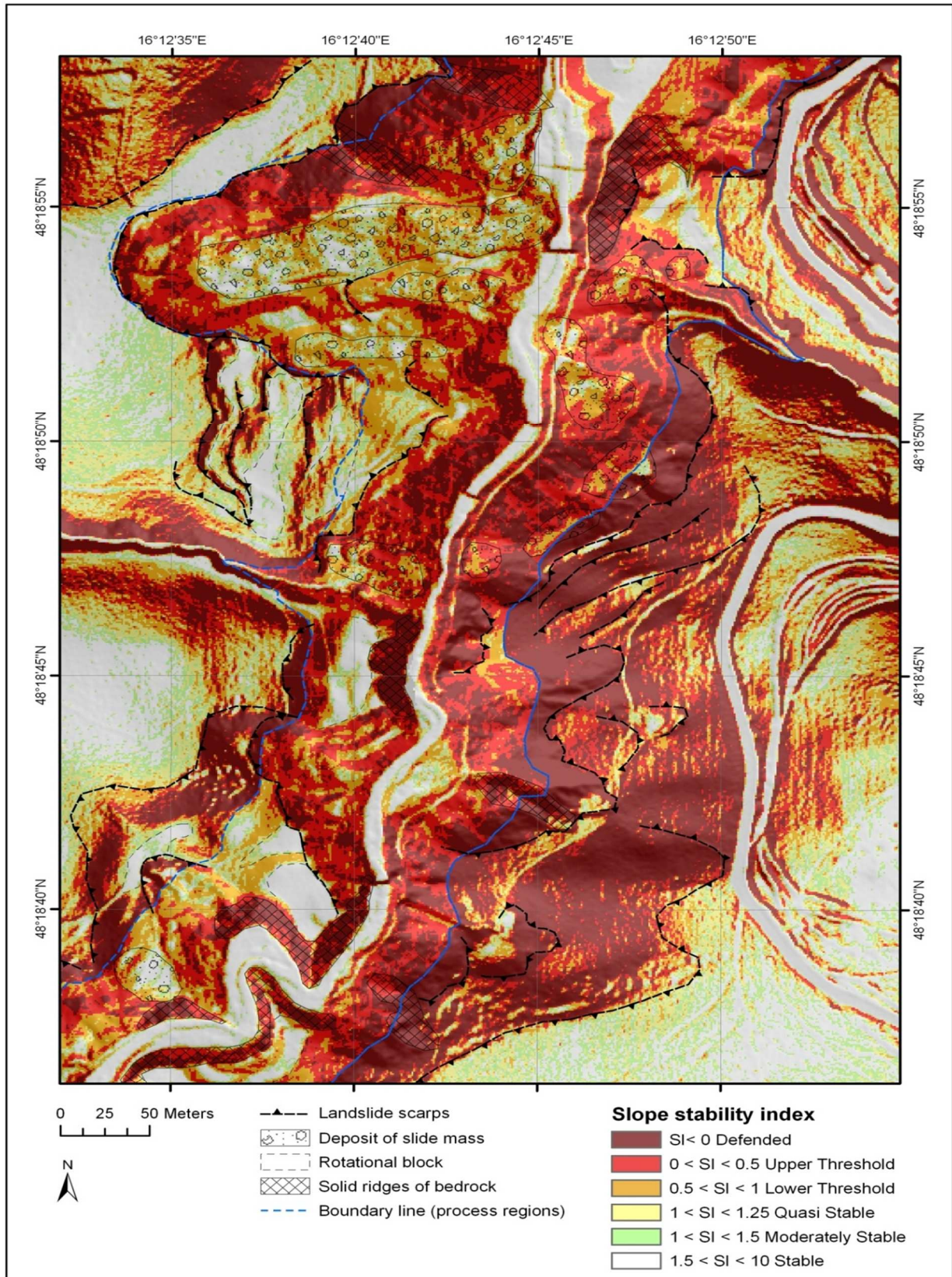


Figure 5-38. Stability index map for the critical precipitation scenario, which is based on heavy rainfall of 60mm/h with a statistical reoccurrence period of 50 years (eHYD). The scenario is based on short-term recharge caused by a specific weather event and the soil-mechanical parameters for flysch bedrock (process region (1)) and quaternary sediments (process region (2)). The boundary line (blue line) divides both process regions. Quaternary sediments occur at the upper slope positions while flysch bedrock is uncovered below the decline to the valley floor.

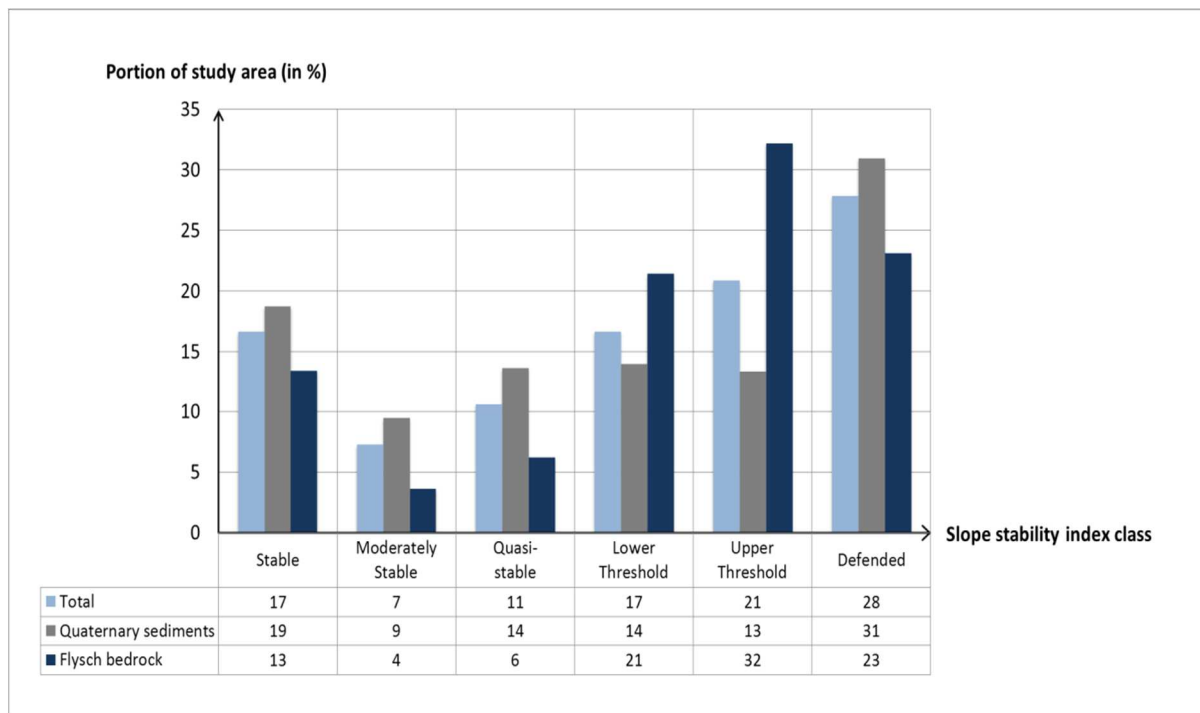


Figure 5-39. Slope stability classification for “heavy rainfall scenario” based on a 50-year rainfall event of 60mm/h (eHYD 2011). The bars show the extension of the stability classes in relation to the study area and the process regions in percentage. The proportion of the classes within the study area is given in total (blue bar). The proportion of the classes within process region (1), the flysch bedrock (dark blue bar), and process region (2), the quaternary sediments (grey bar), are given, respectively.

---

## 6 Comparison

In order to quantify the influence of the quaternary sediments and the varying wetness conditions on the slope stability calculation, it is necessary to compare the different scenarios. The results from this comparison are described in this chapter.

Possible seasonal effects on slope stability can be studied by comparing of the scenarios. Furthermore, the scenarios of this “present-day” group are compared to the corresponding scenarios focused on the future disposition. In this way, possible changes of landslide proneness due to climate change can be assessed.

### 6.1 Flysch scenario (January) and winter scenario (January)

In the first comparison the “flysch scenario (January)” and the “winter scenario (January)” are analysed. Both scenarios are based on equal wetness conditions, more specifically on average monthly recharge in January as derived from climate normals for air temperature and precipitation (ZAMG 2010c). The major difference between the scenarios is the incorporation of the quaternary sediments as additional process region in the “winter scenario (January)”. The “flysch scenario (January)” is based on the rock-mechanical parameters of the flysch bedrock only and thus considers middle to deep-seated movements in the bedrock. In contrast to this, the “winter scenario” takes into account a sliding surface in the quaternary sediments and consequently landslides in slope positions where these cover beds over the bedrock.

The objective of this comparison is to study the relevance of quaternary sediments for slope stability in the Vienna Forest. By means of the comparison of the two scenarios the changes in slope stability and slope dynamics is investigated.

The comparison of topographic wetness of the “winter scenario (January)” and the “flysch scenario (January)” is shown in Figure 6-1. The maps illustrate increased wetness when the quaternary sediments are incorporated (map A in Figure 6-1).

The “flysch scenario (January)” shows low substrate moisture and areas classified with “low moisture” are dominant with a proportion of 78% in the study area. Topographic wetness is derived on the basis of the catchment area, the transmissivity of the flysch bedrock in relation to the average January recharge. Transmissivity and recharge are combined in the relative wetness index. The hydraulic conductivity and the depth of 8-20 m of the critical layer are responsible for the extension of low moisture conditions in the flysch bedrock, in comparison to the quaternary sediments. In contrast to the “flysch scenario (January)” (map B in Figure 6-1) there is a shifting of the topographic wetness classes to more substrate moisture after integration of the quaternary sediments in the “winter scenario (January)” (map A in Figure 6-1). This effect can be explained by the lower depth of the sliding surface of 2-4 m and the low permeability of the quaternary sediments due to densely bedded periglacial cover beds rich in clay.

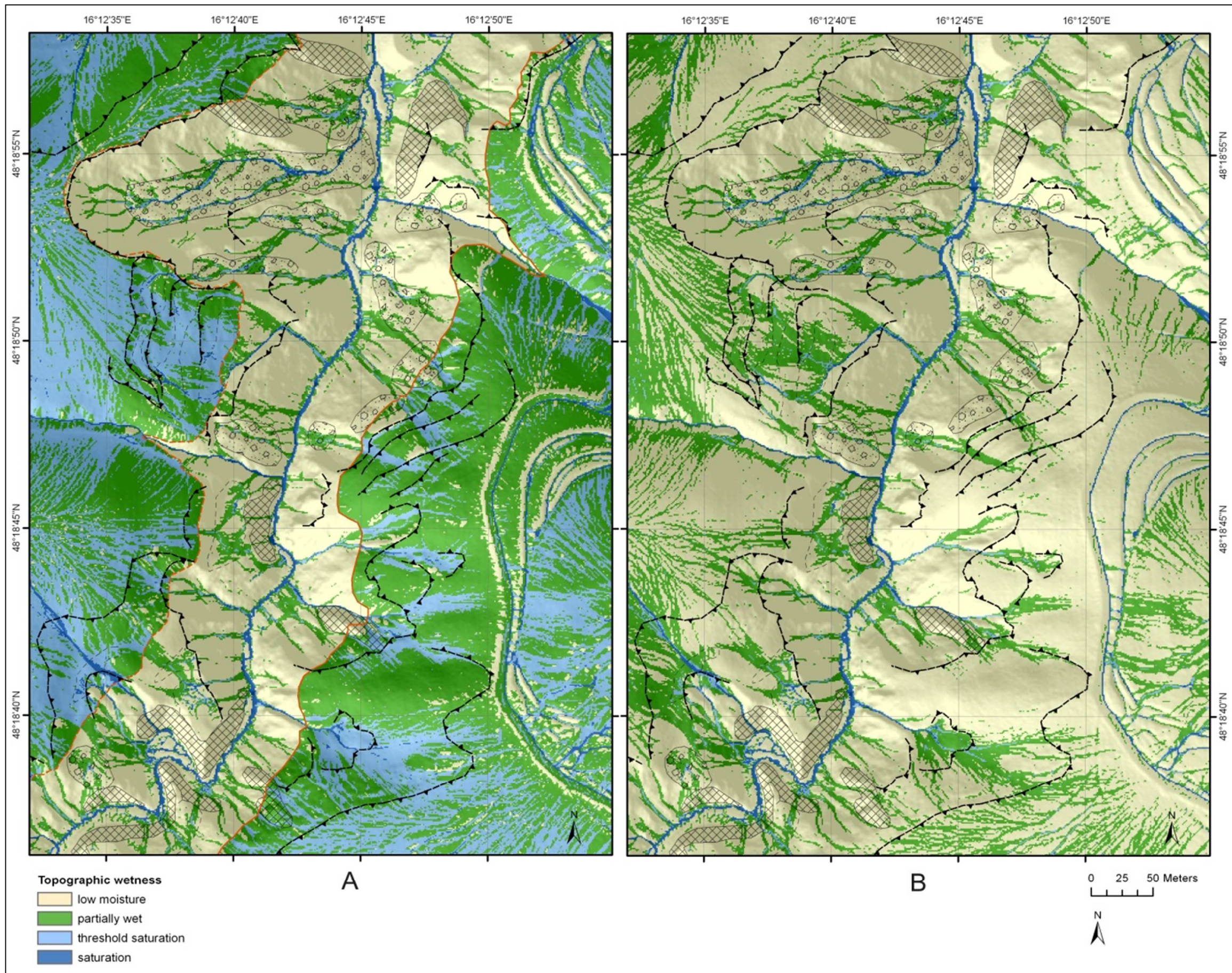


Figure 6-1. Comparison of topographic wetness maps of the "winter scenario" (A) and the "flysch scenario (January)" (B). Both scenarios are based on equal wetness conditions, i.e. on average monthly recharge in January as calculated from the climate normals for air temperature and precipitation (ZAMG 2010c). The major difference of the scenarios is the incorporation of the quaternary sediments into the "winter scenario (January)" as process region.

The difference of topographic wetness is displayed in Figure 6-2. It displays the proportion of the topographic wetness classes in the study area for the “flyscht scenario (January)” and for the “winter scenario (January)”, respectively. The comparison of the classes yields that the integration of the quaternary sediments into slope stability modelling, as conducted in the “winter scenario”, results in a distinct reduction of “low moisture” conditions by about 40% (from 78% to 38%) (Figure 6-2). This decrease takes place for the benefit of the topographic wetness classes “partially wet” with a plus of 17% and “threshold saturation” with an increase of 22% (Figure 6-2). The extension of the latter class (“threshold saturation”) implies that there is an augmented saturation tendency in the study area. According to the classification system of topographic wetness (Table 5.2) this means that saturation is reached in these areas under maximum wetness in the model. Figure 6-2 further denotes that areas classified with “saturation” rise about 1% in case of the integration of the quaternary sediments into the “winter scenario (January)”. This raised saturation and saturation tendency has a direct negative effect on slope stability. In total there is a wetness augmentation of 23% in the “winter scenario (January)”.

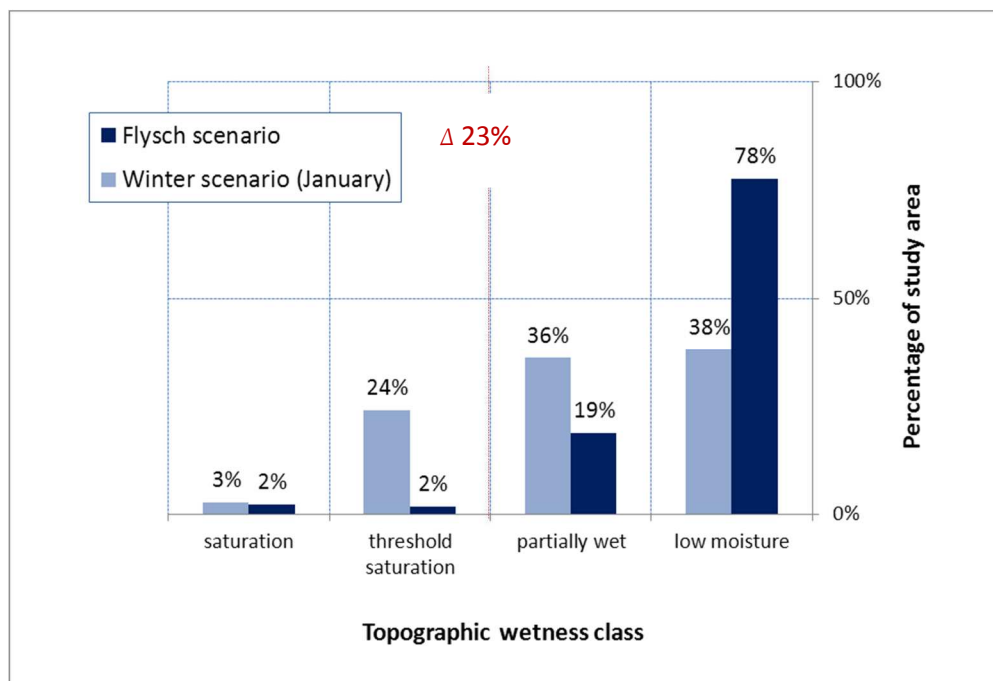


Figure 6-2. Comparison of topographic wetness classes and their proportion in the study area as given in the “flyscht scenario (January)” and the “winter scenario (January)”. Both scenarios are based on equal wetness conditions, i.e. on average monthly recharge in January as calculated from the climate normals for air temperature and precipitation (ZAMG 2010c). The major difference of the scenarios is the incorporation of the quaternary sediments into the “winter scenario (January)” as process region.

The comparison of the slope stability index maps is given in Figure 6-3. Concerning the slope dynamics, the comparison of the “winter scenario” (map A in Figure 6-3) and the “flyscht scenario (January)” (map B in Figure 6-3) revealed an extension of the instability and a changed pattern of slope stability. In the “flyscht scenario (January)”, the areas, which are most unstable, are found near the valley bottom at the oversteeped slopes close to the Hagenbach creek. Only small instable areas occur at the scarps of previous landslides. In contrast to this, most instable slopes are derived at the crown and the scarp of former landslides in the “winter scenario” where quaternary deposits crop out. Consequently the actual slope dynamics is dominated by backward denudation, which leads to an extension of the former landslides by new shallow movements.

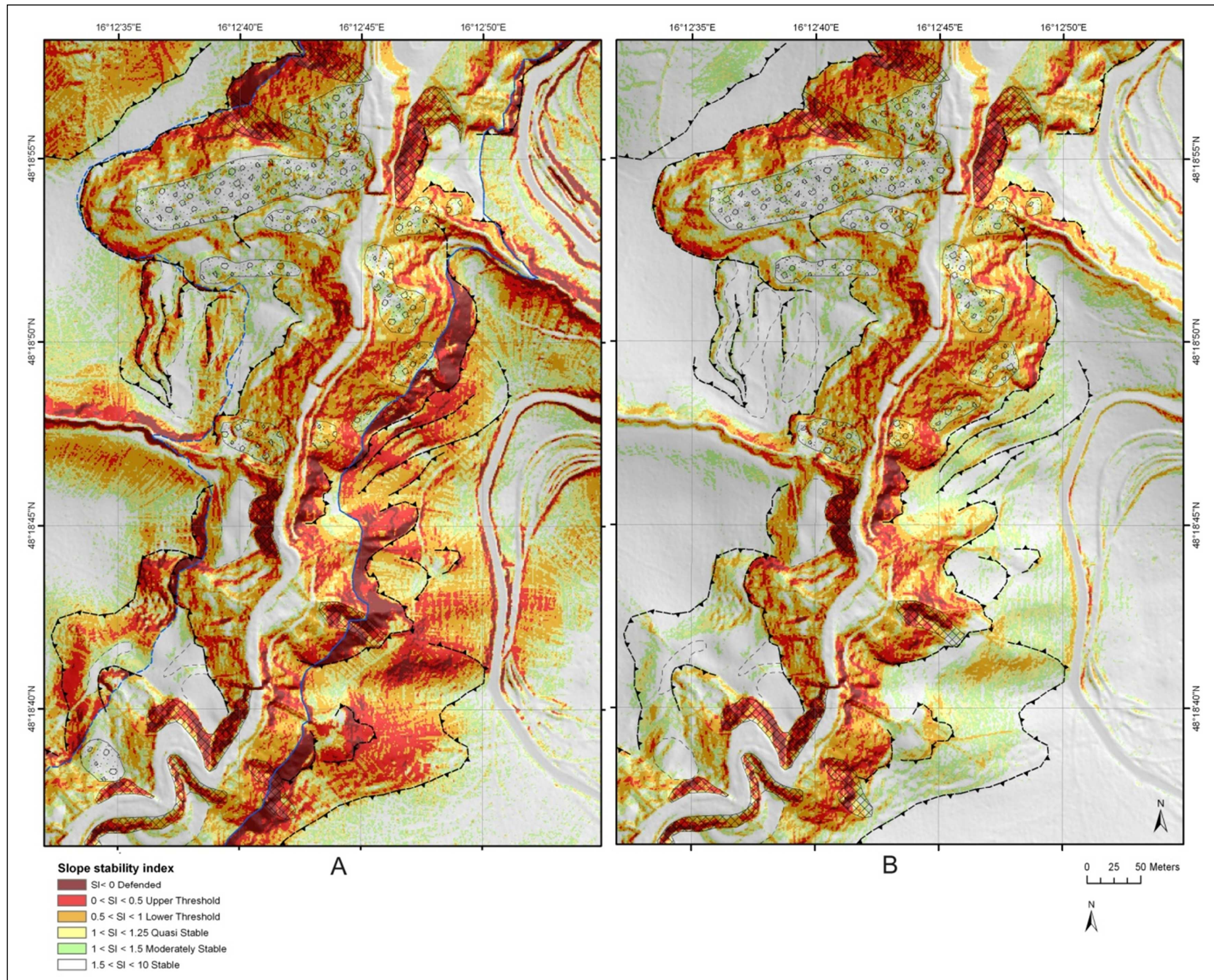


Figure 6-3. Comparison of slope stability index maps of the "winter scenario" (A) and the "flysch scenario (January)" (B). Both scenarios are based on equal wetness conditions, i.e. on average monthly recharge in January as calculated from the climate normals for air temperature and precipitation (ZAMG 2010c). The major difference of the scenarios is the incorporation of the quaternary sediments into the "winter scenario (January)" as process region.

In order to quantify the changes in slope stability the distribution and the proportion of the slope stability index classes over the study area are investigated. In this context, Figure 6-4 shows the deviation of the stability classes in the “winter scenario” in relation to the “flyscht scenario (January)”. To be more specific, the difference between the “winter scenario (January)” and the “flyscht scenario (January)” is quantified in regard to the extension of the classes, measured as percentage of the study area.

The diagram (Figure 6-4) illustrates that the integration of the quaternary sediments into the “winter scenario” leads to a decrease in the “stable” areas by 25% in comparison to the “flyscht scenario (January)”. The decline of these unconditionally stable areas where no instability can be computed over the whole parameter variety leads to a relatively homogeneous augmentation of the remaining stability index classes. More precisely, the areas in the “winter scenario” classified as “moderately stable” and “quasi-stable” increase by 1% and 5% of the study area. Corresponding to this drop in stability, the instable areas (“lower threshold”, “upper threshold” and “defended”) extend by 19% of the study area in total (cp. Figure 6-4). In total there is an extension of the instable areas by 19% in the “winter scenario (January)”.

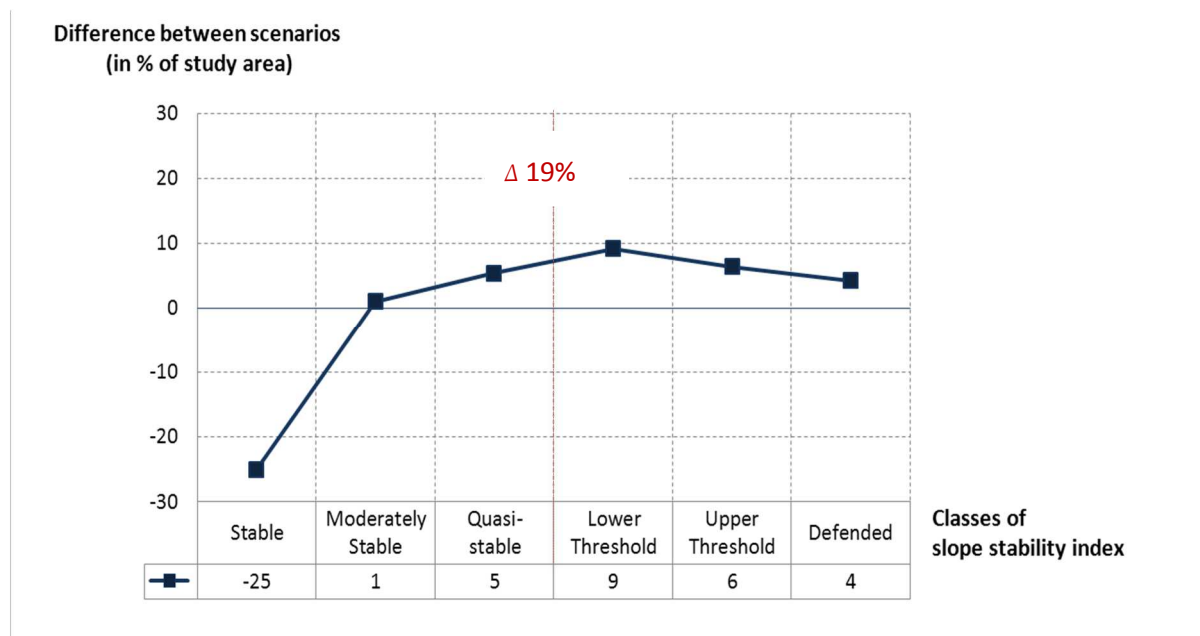


Figure 6-4. Divergence of slope stability index classification of the “flyscht scenario (January)” in relation to the “winter scenario (January)”. It is expressed as a difference (“winter scenario” minus “flyscht scenario (January)”) of the proportion of the single stability index classes in relation to the study area in percentage. The graph denotes a decrease in stability (-19%) and a corresponding extension (+19%) of instable classes in the “winter scenario”.

As the comparison of the slope stability index maps (Figure 6-3) indicates, there is a transition of the most instable zones to the upper slope positions. In the “flyscht scenario (January)” the steep flanks of the gorge are most instable. In contrast to this, the moderately inclined areas at the upper slopes are highly instable in the “winter scenario”. This aspect is investigated in detail in Figure 6-5. This graph displays the mean slope gradient within the stability classes as derived in the “winter scenario (January)” and in the “flyscht scenario (January)”. The comparison yields that the incorporation of the quaternary sediments into the slope stability modelling leads to a transition of instable areas from the steep (35° to 52°) to moderately inclined slopes (29° to 42°). Therefore, also slopes with moderate inclination show a disposition to instability under an average monthly recharge.

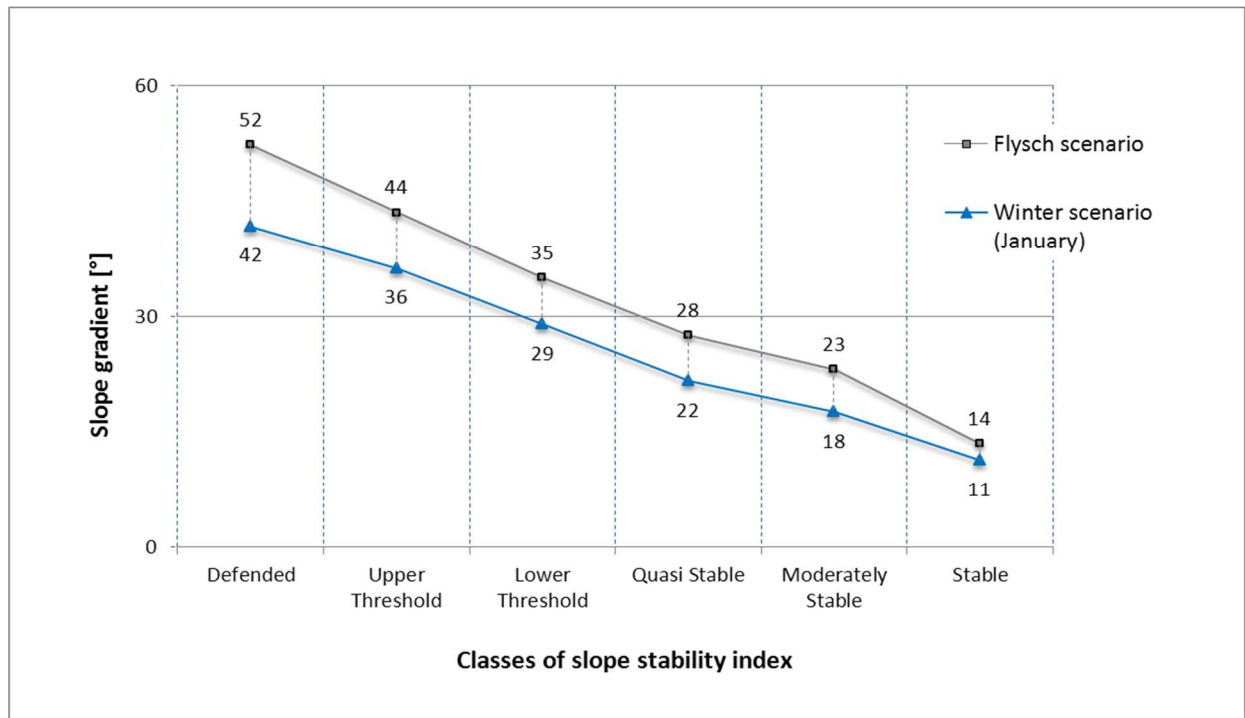


Figure 6-5. Comparison of mean slope gradient per slope stability index class for the “winter scenario” (A) and the “flysch scenario (January)” (B). The incorporation of the quaternary sediments into the slope stability modelling leads to a transition of instable areas from the steep to also moderately inclined slopes.

---

## 6.2 Summer scenario (July) and winter scenario (February)

In this comparison the scenarios of the group “present-day, mid-term disposition” are inter-compared. In particular, the differences between “winter scenario (February)” and the “summer scenario (July)” are investigated. July represents the driest month and February the wettest month in the seasonal course in regard to recharge (measured in m/s).

The objective of this inter-comparison is to investigate if seasonal changes are measurable in the models which are derived on the basis of averaged data. In case of measurable changes, possible seasonal effects on slope stability can be studied by comparing slope stability index mapping and topographic wetness maps of the “summer scenario” and the “winter scenario”. In this context the influence of mid-term substrate moisture on the landslide disposition is investigated.

The comparison of the “winter scenario (February)” and the “summer scenario (July)” demonstrates that the seasonally varying wetness conditions have a slight but measurable influence on the mid-term disposition to landslides in the study area. As the scenarios are based on equal process regions and thus similar soil-mechanical parameters, the deviation in slope stability is ascribed to the different amount of monthly recharge due to the seasonal course. While the estimated monthly recharge is 101 mm in July, it increases to 228 mm in February. These differences in recharge result from variations of monthly average air temperature and precipitation. The summer months are characterised by a mid-term average temperature of 18.9 °C and a precipitation amount of 83 mm. In the winter months a low average temperature of 0.7 °C and a lower precipitation amount of 48 mm prevails according to the climate normal period (cp. Table 5.6). The water-balance calculations reveal a distinctly elevated evapotranspiration in the summer months and consequently a reduced rate of soil-moisture storage. The different hydrological conditions in the summer and the winter months cause a reduced monthly rate of recharge in the summer months, in spite of high precipitation amounts.

The seasonal changes of monthly recharge denote a slight effect on topographic wetness in the scenarios as illustrated in Figure 6-6. There is an increase in wetness in the “winter scenario (February)” (map A in Figure 6-6) in comparison to the “summer scenario (July)” (map B in Figure 6-6).

To assess the changes in topographic wetness in more detail their proportion of the classes in the scenarios are compared in Figure 6-7. The bars in the diagram show the proportion of the topographic wetness classes expressed as percentage of the study area. In the winter months “low moisture” conditions drop by 10% (from 45% to 35%) and areas classified as “partially wet” are reduced by 5%. Corresponding to this decrease in areas which are never saturated under the assumed wetness conditions, an extension of the areas with saturation tendency (“threshold saturation”) and areas which are saturated (“saturation”) is denoted in the “winter scenario”. More precisely, the augmented recharge in February causes an extension of the saturated areas by 1% and the areas which are saturated under maximum assumed wetness by 14% (from 15% to 29%). In total there is a wetness augmentation of 15% in the “winter scenario (February)” (Figure 6-7).

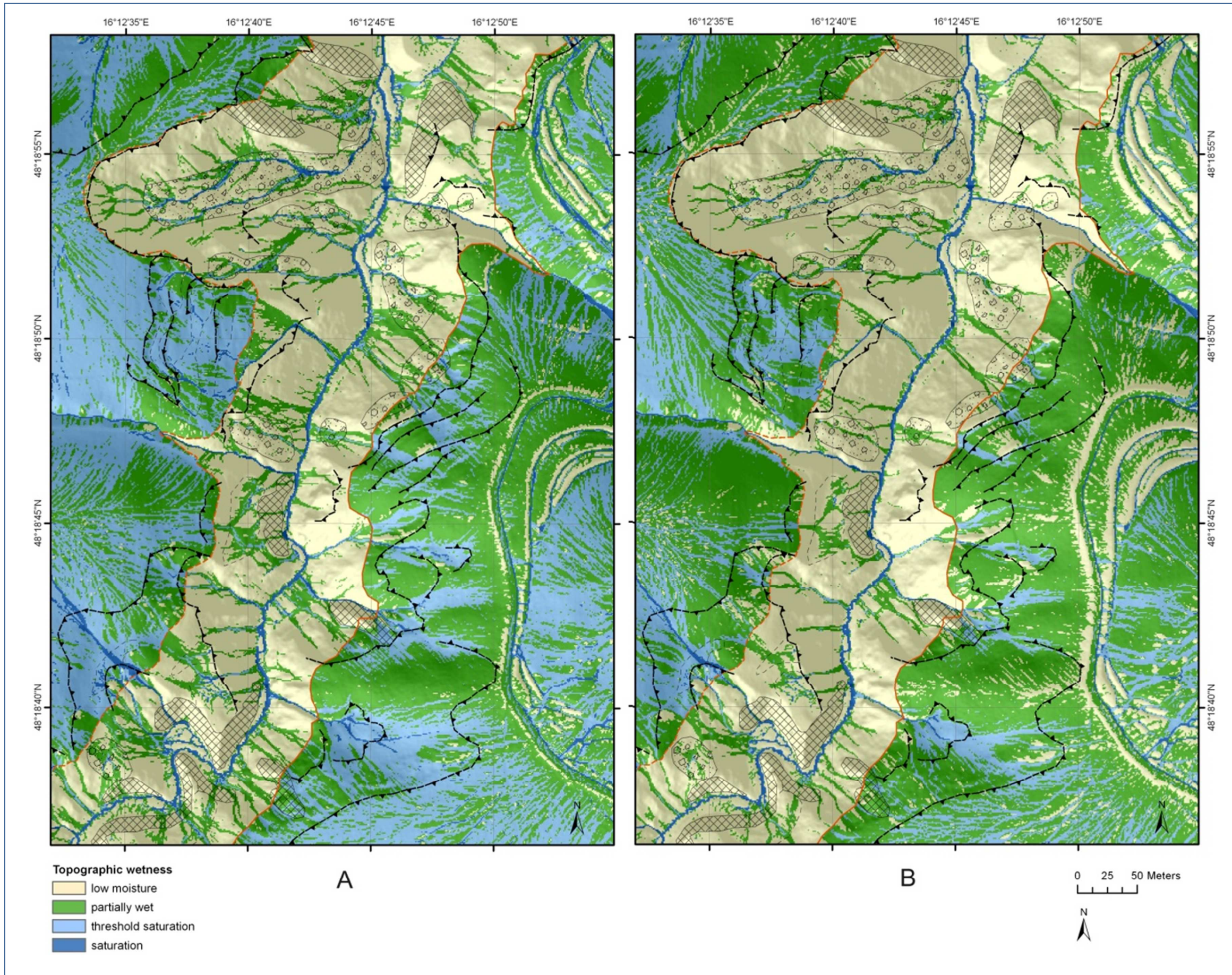


Figure 6-6. Comparison of topographic wetness maps of the “winter scenario (February)” (A) and the “summer scenario (July)” (B). The scenarios are based on climate conditions as prevailing in the climate normal period in the study area (ZAMG 2010c). The deviation in topographic wetness is ascribed to the different amount of monthly recharge as a consequence of changed climate conditions due to the seasonal course.

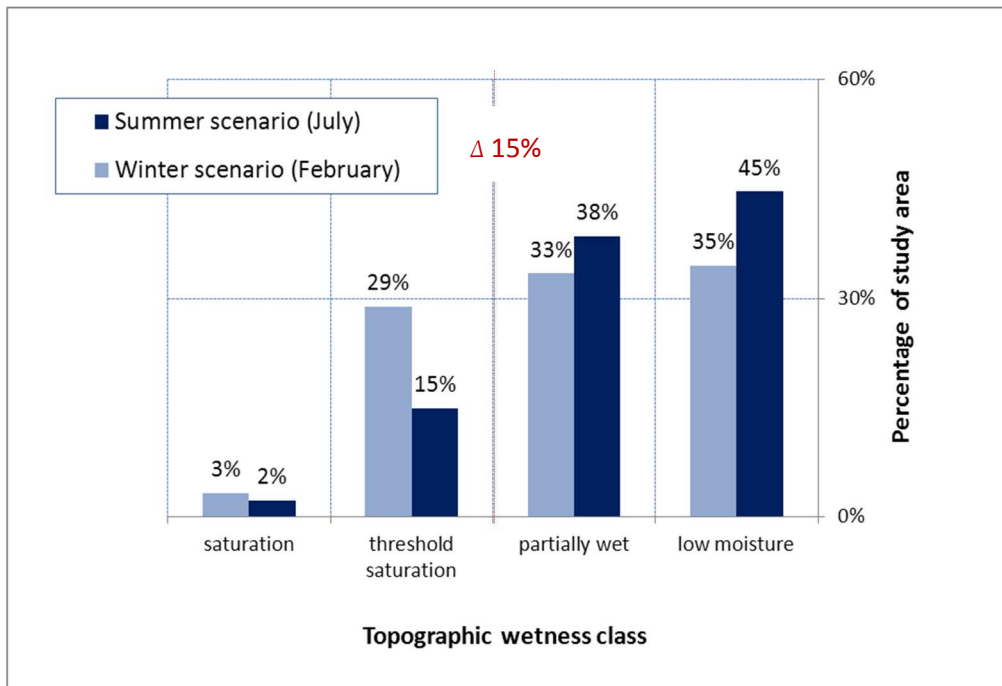


Figure 6-7. Comparison of topographic wetness classes and their proportion in the study area as given in the “summer scenario (July)” and the “winter scenario (February)”. The scenarios are based on climate conditions as prevailing in the climate normals for the period of 1961-1990 in the study area (ZAMG 2010c). The deviation in topographic wetness is ascribed to the different amount of monthly recharge as a consequence of changed climate conditions due to the seasonal course.

The elevated topographic wetness, i.e. areas with saturation tendency, in the winter months in relation to the “summer scenario (July)” has a slight negative effect on slope stability. The comparison of the slope stability index maps is illustrated in Figure 6-8. The comparison of the maps denotes that the pattern of stable and instable areas is similar in both scenarios. Consequently, no major differences can be identified between the scenarios in terms of slope dynamics. However, a slight extension of instable areas, in particular of the class “upper threshold” is visible in the upper hillslopes and at the flanks of surface drainage lines. Quaternary sediments cover the bedrock at these topographic positions.

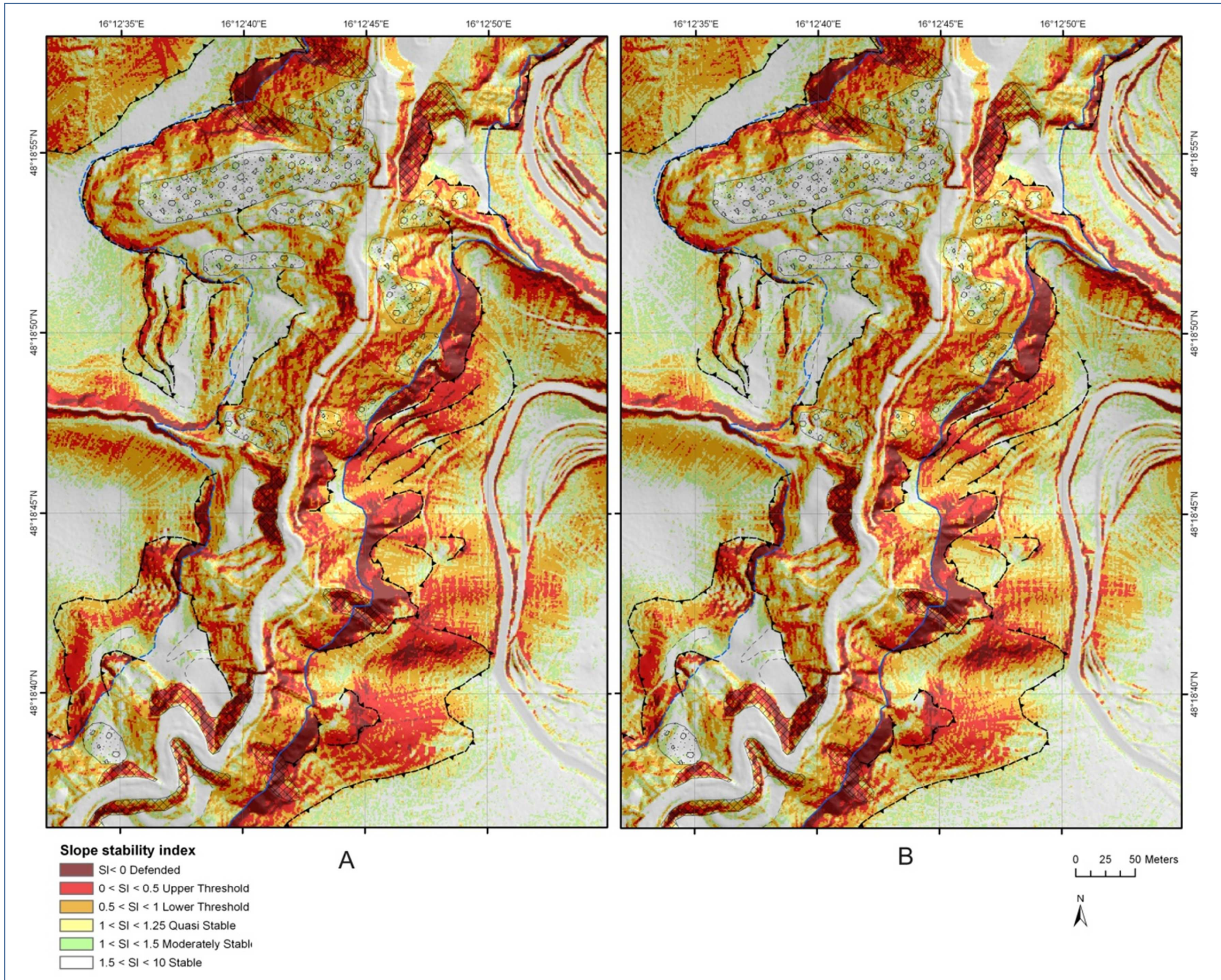


Figure 6-8. Comparison of slope stability index maps of the "winter scenario" (A) and the "summer scenario" (B). The input for soil-mechanical and hydrological soil parameters is equal in the scenarios. Different input for monthly recharge is applied. There is a slight increase in instability in the "winter scenario" (A), which is caused by augmented average monthly recharge and thus elevated topographic wetness. In relation to slope dynamics, there is no major difference between the scenarios because the pattern of stable and instable areas is similar.

To quantify the changes in slope stability more precisely, the extension of the stability classes within the study area and within the process regions are compared for the scenarios. For that purpose Figure 6-9 shows the divergence of the slope stability index classes of the “winter scenario” in relation to the “summer scenario”. The difference is measured in percentage of the study area.

The light-blue line in Figure 6-9 illustrates that there is a reduction of the stable areas (“stable”, “moderately stable” and “quasi-stable”) in the winter months by a total of 5%. Concurrently, the instable areas (“lower threshold” and “upper threshold”) extend by 5%, mainly in favour of the “upper threshold” class. Regarding the process regions separately, the negative effect on slope stability as a consequence of increased wetness in the winter months is stronger in the quaternary sediments than in the flysch bedrock (Figure 6-9). The sediments show a growth of instable areas (“lower threshold”, “upper threshold”, “defended”) by 7% and a corresponding decrease in stable zones (“stable”, “moderately stable”, “quasi-stable”). It can be concluded that the change in slope stability can be mainly attributed to the quaternary sediments, as the bedrock shows only marginal deviations of 1% in the stability classes.

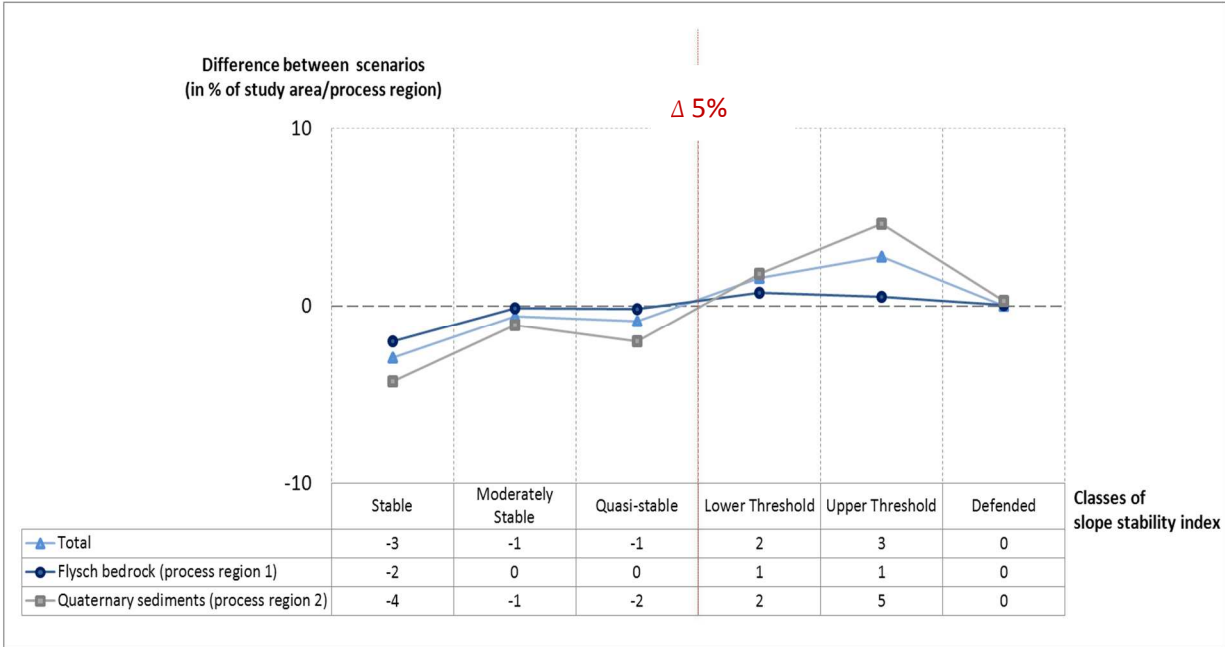


Figure 6-9. Divergence of slope stability index classification of the “winter scenario (February)” in relation to the “summer scenario (July)”. It is expressed as a difference (“winter” minus “summer scenario”) of the proportion of the single stability index classes in relation to the study area in percentage.

---

### 6.3 Future summer scenario (July) and future winter scenario (February)

The scenarios of the group “future, mid-term disposition” are compared. Similar to the comparison which is focused on the present-day disposition, the differences between the “future winter scenario (February)” and the “future summer scenario (July)” are analysed. The scenario group is based on forecasts of regional climate scenarios (Loibl et al. 2007, Reclip:more 2007, Formayer et al. 2009). Accordingly modified mid-term averages are used in the water-balance calculations in order to estimate typical recharge of aquifer as probable in 2050.

The objective of this comparison is to investigate if the seasonal changes are modified due to climate change. Future seasonal effects on slope stability can be studied by comparing slope stability index mapping and topographic wetness maps. In this context the influence of mid-term substrate moisture on the disposition to landslides is investigated under the influence of climate change.

Similar to the scenarios modelling the present-day, mid-term disposition there is a “future summer scenario (July)” and a “future winter scenario (February)” considering the future, mid-term disposition due to climate change. The comparison shows a slight, but measurable difference in slope stability due to changed seasonal wetness conditions. In summary it can be stated that the varying substrate wetness has an even stronger effect on the landslide disposition in future than under present-day conditions.

The scenarios are based on equal process regions and thus similar soil-mechanical parameters. The deviation in slope stability results from different amounts of monthly recharge as a consequence of changed climate conditions due to the seasonal course. Monthly average climate conditions as forecast by climate scenarios are regarded (Loibl et al. 2007, Reclip:more 2007, Formayer et al. 2009).

While for July the estimated future monthly average recharge is 28mm, in February it is estimated at 243mm. For recharge estimation a temperature rise of 2.5 °C for January and 2 °C in July as well as a change in the precipitation amount of -15% in July and +30% in February are taken into account (cp. Table 5-7, page 88). The water-balance calculations reveal distinctly increased evapotranspiration in the summer months and consequently a reduced rate of soil-moisture storage. Consequently, there is a reduced monthly rate of recharge in the future summer months. The variance between summer and winter recharge is even amplified due to climate change.

The seasonal changes of future monthly recharge have a visible effect on topographic wetness in the scenarios as illustrated in Figure 6-10. In contrast to the “future summer scenario (July)” (map B in Figure 6-10) where low moisture conditions are predominant there is a shifting of the topographic wetness classes to more substrate moisture in the “future winter scenario (February)” (map A in Figure 6-10).

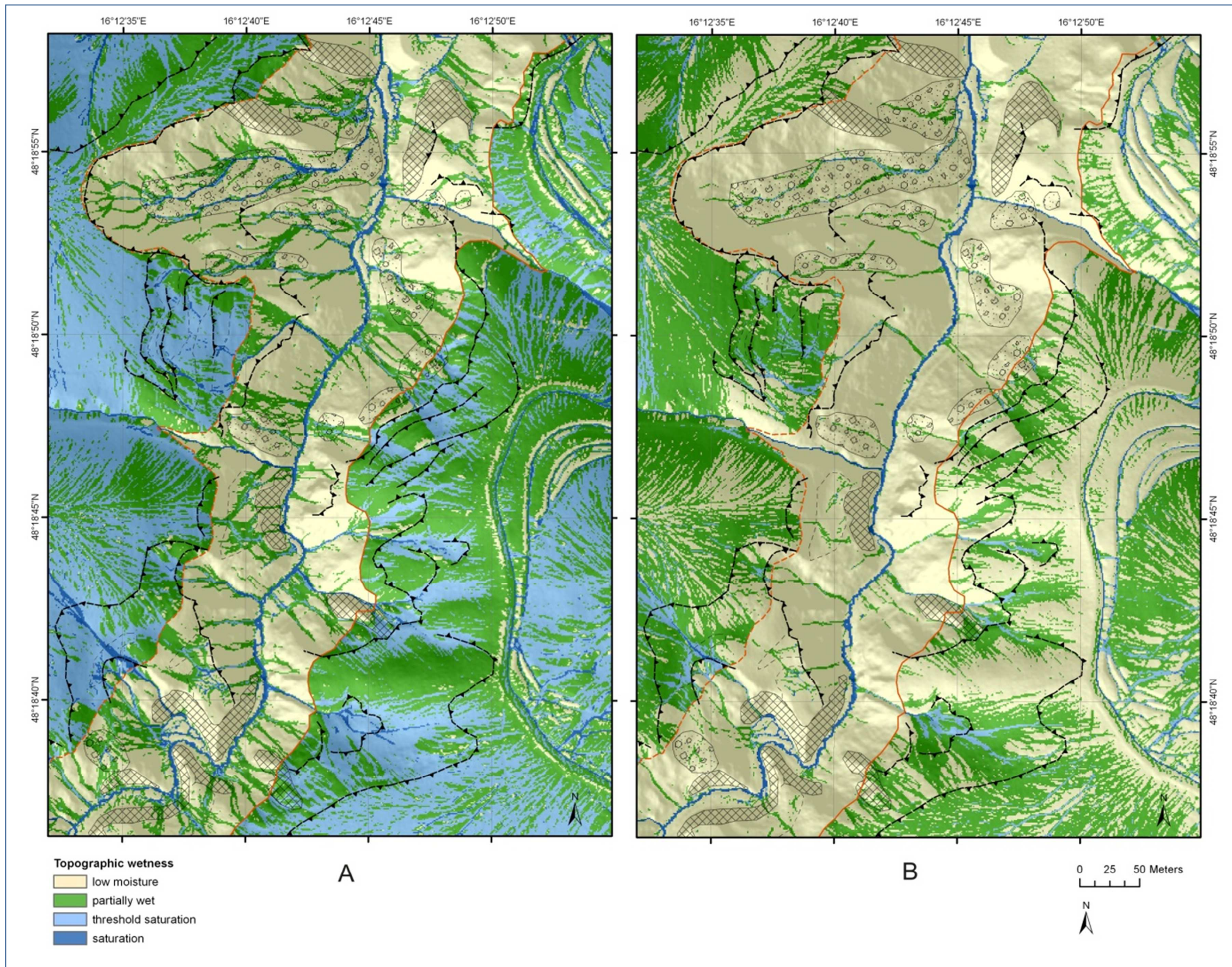


Figure 6-10. Comparison of topographic wetness maps of the "future winter scenario" (A) and the "future summer scenario (July)" (B). The scenarios take climate change as forecast by regional climate models (Reclip:more 2007) into account. The divergence in topographic wetness is ascribed to the different amount of monthly recharge as a consequence of changed climate conditions due to the seasonal course.

In order to quantify the changes in topographic wetness the extension of the wetness classes within the scenarios is compared in Figure 6-11. The diagram shows the proportion of the topographic wetness classes expressed as percentage of the study area. In the “future winter scenario (February)” “low moisture” conditions decrease by 33% (from 67% in summer to 34% in winter). Areas classified as “partially wet” increase by 5% in the future. There is a high growth of areas classified with “threshold saturation” by 4% in the “future summer scenario (July)” to 30% in the “future winter scenario (February)”. This difference of 26% implies that there is a distinct extension of areas which are saturated under maximum assumed wetness in the winter months. Besides, the augmented recharge in February causes an extension of saturated areas (“saturation”) by 1%. In total there is a wetness augmentation of 27% in the “future winter scenario (February)”.

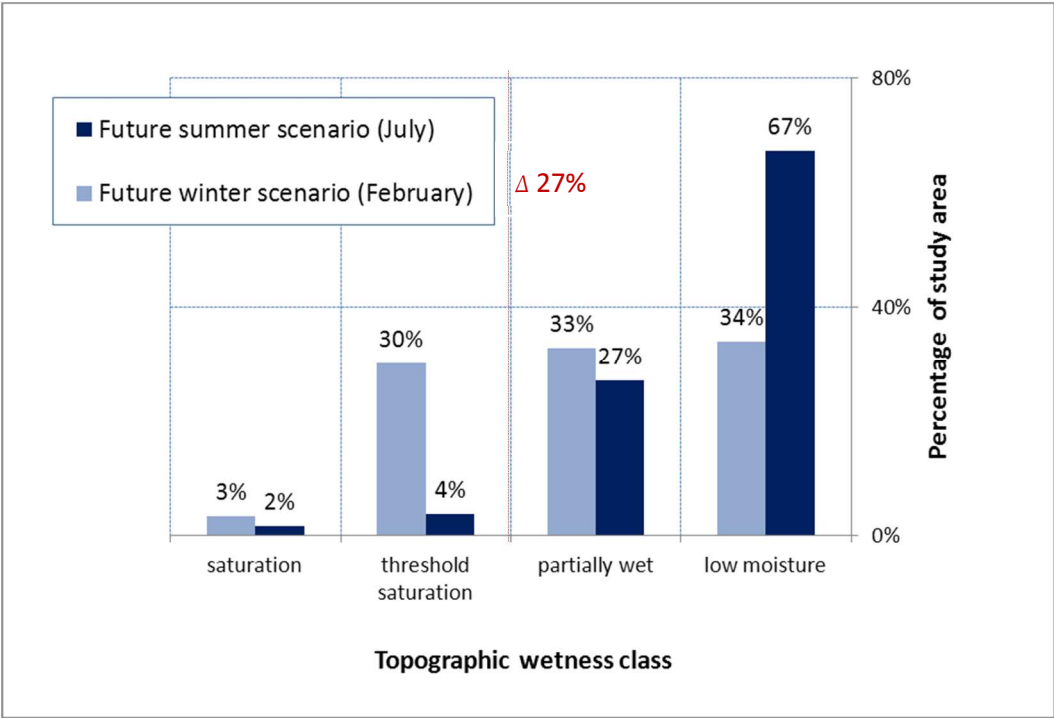


Figure 6-11. Comparison of topographic wetness classes and their proportion in the study area as given in the “future summer scenario (July)” and the future “winter scenario (February)”. The scenarios take into account climate change as forecast by regional climate models (Reclip:more 2007). The divergence in topographic wetness is ascribed to the different amount of monthly recharge as a consequence of changed climate conditions due to the seasonal course. While the estimated monthly recharge is 38 mm in July, it increases to 243 mm in February mainly due to lowered evapotranspiration and heightened soil-moisture storage in winter.

Increased topographic wetness in the winter months in relation to the “summer scenario (July)” has negative effect on slope stability. The comparison of the slope stability index maps is given in Figure 6-12. The comparison of the maps denotes an extension of instable areas in the “winter scenario (February)” (map A in Figure 6-12), in particular of the class “upper threshold” at the upper hillslopes and at the flanks of surface drainage lines. At these topographic positions quaternary sediments are evident.

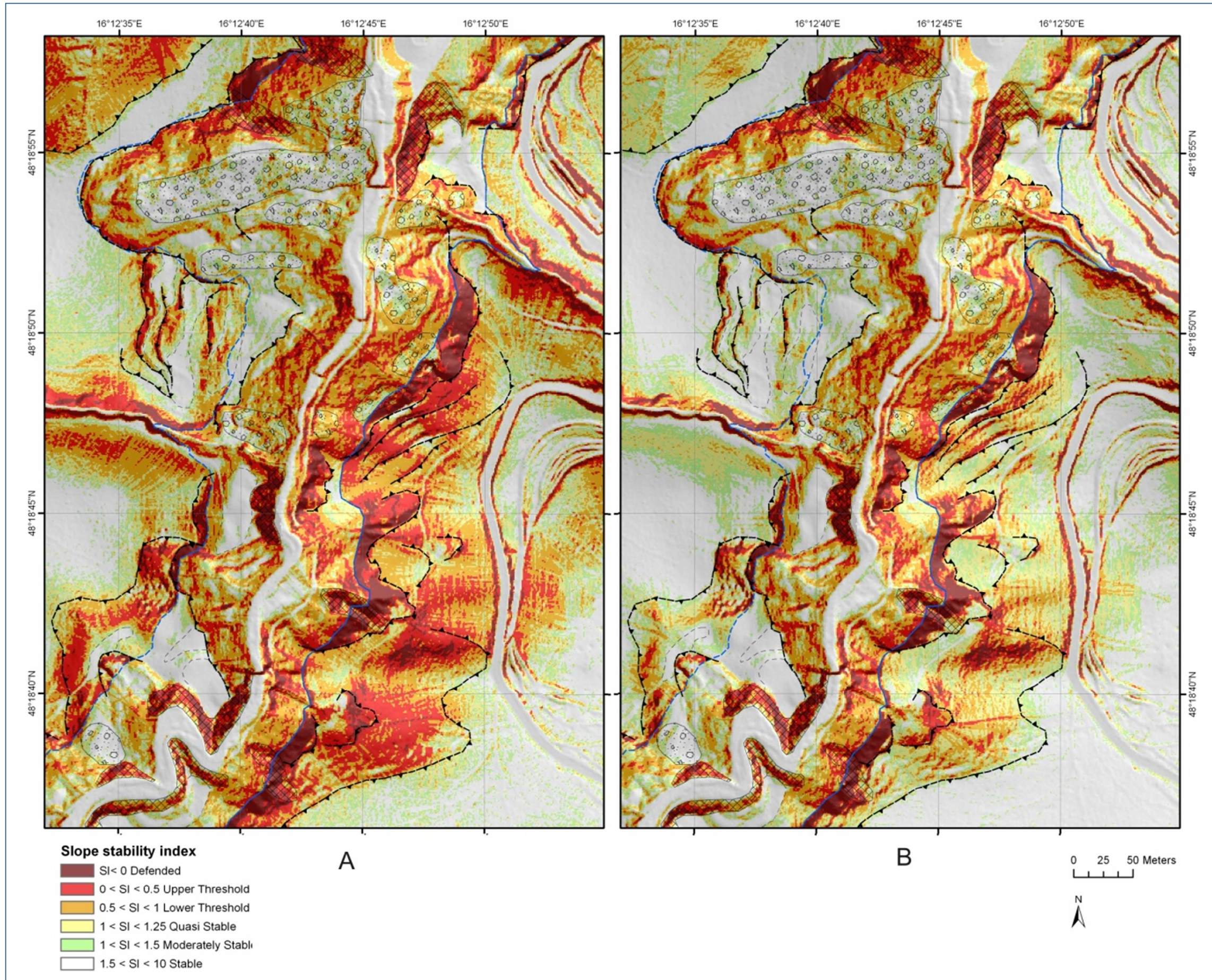


Figure 6-12. Comparison of slope stability index maps of the "future winter scenario" (A) and "future summer scenario" (B). The input for soil-mechanical and hydrological soil parameters is equal in the scenarios. Different input for monthly recharge is applied. There is an increase in instability in the "future winter scenario" (A), which is caused by augmented average monthly recharge and thus heightened topographic wetness.

To assess the changes in slope stability in a quantitative sense, the proportion of the slope stability index classes is compared in Figure 6-13. The diagram shows the divergence of the classes of the “future winter scenario” in relation to the “future summer scenario”. The difference is measured in percentage of the study area and the process region.

In total there is a decline of stable areas (“stable”, “moderately stable”, “quasi-stable”) by 16% in the “future winter scenario (February)” in comparison to the “future summer scenario (July)” (Figure 6-13). Simultaneously, instable areas (“lower threshold”, “upper threshold”, “defended”) extend by 16% in February. Furthermore, the Figure shows that the negative effect on slope stability is stronger within the quaternary sediments than in the flysch bedrock. In the quaternary sediments stability is reduced by 24% (summing up the “stable”, “moderately stable” and “quasi-stable” classes) in favour of the instable areas (“lower threshold” and “upper threshold”). In contrast, the flysch bedrock denotes only minor differences between -3% (“stable”) and 2% (“lower threshold”) in the “future winter scenario (February)” compared with the “future summer scenario (July)”.

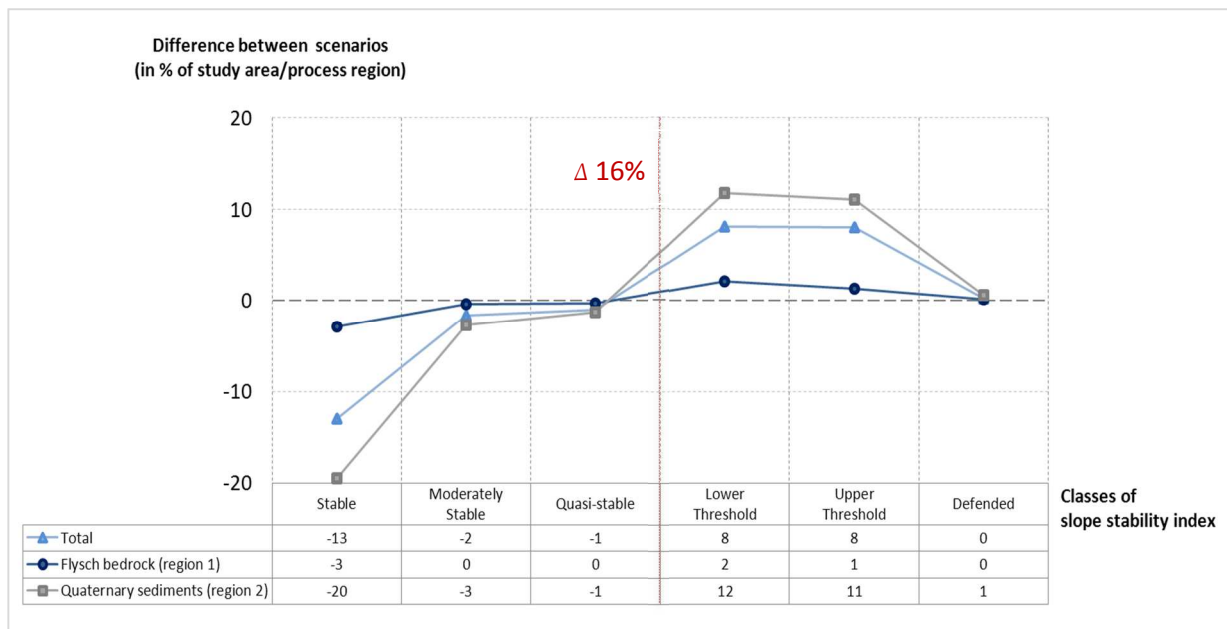


Figure 6-13. Divergence of slope stability index classification of future winter scenario (February) in relation to the “future summer scenario (July)”. It is expressed as difference (“winter scenario” minus “summer scenario”) of the proportion of the single stability index classes in relation to the study area in percentage.

---

## 6.4 Present-day summer scenario (July) and future summer scenario (July)

A major objective in the present work is the elaboration of the effect of climate change scenarios on landslide proneness. For that purpose corresponding scenarios are developed within the scenario group “present-day, mid-term disposition” and in the group “future, mid-term disposition”. All scenarios in the mentioned groups are based on equal process regions and thus equal soil-mechanical parameters. Furthermore, the same water-balance calculations are carried out in order to estimate average monthly recharge on the basis of climate data (cp. chapter 5.1.3 “Hydrological calculations for the determination of the wetness parameters”). The major difference is that in case of the scenarios which are dedicated to present-day conditions climate normals (ZAMG 2010c) are applied, and in case of the scenarios which are focused on future disposition the climate data are adapted to the forecast climate change (Reclip:more 2007).

In particular, the corresponding “summer scenarios” of both groups, “present-day” and “future, mid-term disposition”, are compared. The objective of this comparison is to evaluate if an effect of the forecast climate changes until 2050 can be quantified. In case of a measurable influence possible changes can be analysed and quantified.

Corresponding to the “summer scenario (July)” of the “present-day, mid-term disposition” group, there is a “future summer scenario (July)” in the “future, mid-term disposition” group. Because of an air temperature rise of 2.5 °C and a drop of precipitation sums by 15% in July, recharge is reduced by 73% in comparison to the average recharge in the climate normals (cp. Figure 5-8).

This drastic reduction of recharge in the future scenario has visible effects on topographic wetness. In Figure 6-14 the topographic wetness maps of the “summer scenario (July)” (map A in Figure 6-14) and the “future summer scenario (July)” (map B in Figure 6-14) are compared. The comparison shows that “low moisture” conditions are significantly extended in the future scenario. While low substrate moisture was mainly prevailing in the flysch bedrock in the “summer scenario (July)” (map A in Figure 6-14), it is extended into the areas which are covered by quaternary sediments as well in the future scenario (map B in Figure 6-14).

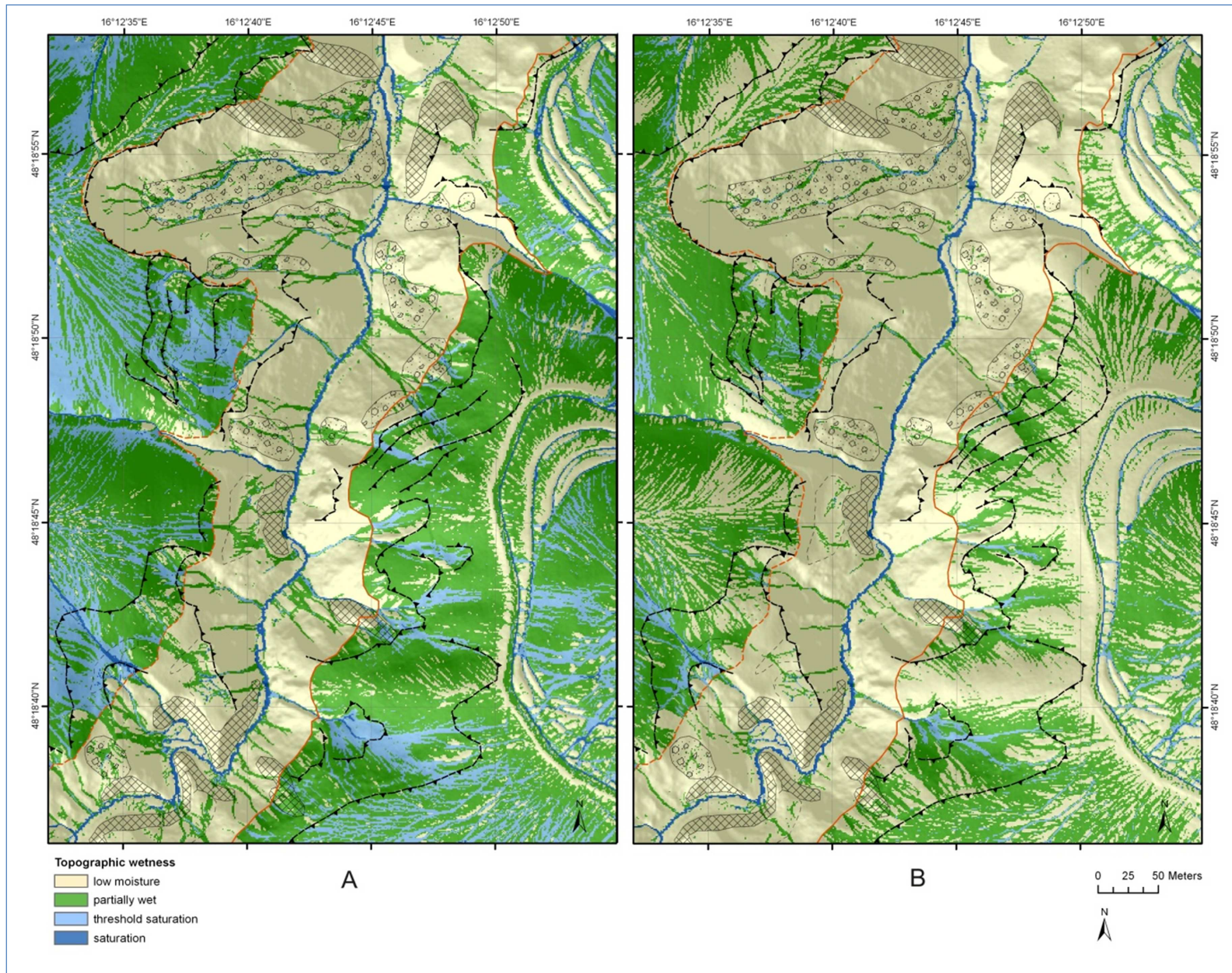


Figure 6-14. Comparison of topographic wetness maps of the “summer scenario(July)” (A) and the “future summer scenario (July)” (B). The future scenario takes climate change as forecast by regional climate models into account (Reclip:more 2007). The divergence in topographic wetness is ascribed to the different amount of recharge in July as a consequence of changed climate.

A more detailed comparison of topographic wetness is possible on the basis of Figure 6-15. This diagram shows the proportion of the topographic wetness classes in both scenarios. It indicates that there is a distinct effect of climate change (i.e. reduced precipitation and increased air temperature) on average substrate wetness. In particular, there is a reduction of wet and saturated conditions (“saturation tendency”, “saturation”) of 11% for the benefit of low substrate moisture (“low moisture” and “partially wet”) due to climate change. Low moisture conditions are extended from 45% in the “summer scenario (July)” to 67% in the “future summer scenario (July)”. This augmentation of low substrate moisture implies that an additional 22% of the study area has never been saturated over the whole range of assumed wetness in the “future summer scenario (July)”. According to this rise of low-moisture conditions, the remaining wetness classes exhibit a reduction. More precisely, “partially wet” areas decrease by 11 %, areas classified with “threshold saturation” show a reduction of 11% and saturated areas (“saturation”) drop by 1%.

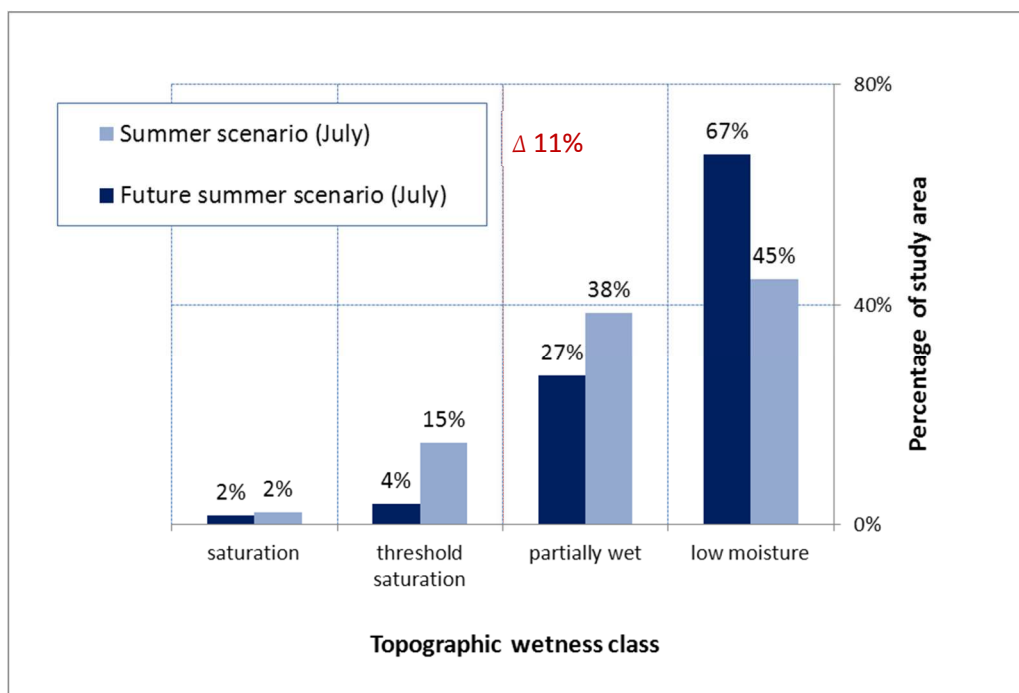


Figure 6-15. Comparison of topographic wetness classes and their proportion in the study area as given in the “summer scenario (July)” and the corresponding “future summer scenario (July)”. The future scenario takes climate change as forecast by regional climate models into account (Reclip:more 2007). The divergence in topographic wetness is ascribed to the different amount of recharge in July as a consequence of changed climate conditions.

This divergence in topographic wetness due to climate change also effects slope stability. In Figure 6-16 the slope stability index maps of the “summer scenario” (map A in Figure 6-16) and the “future summer scenario (July)” (map B in Figure 6-16) are displayed. The comparison reveals a reduction of instability in the “future summer scenario”. As the soil-mechanical parameters and the process regions are equal in the scenarios, this change can be ascribed to the reduction of recharge of 73% due to changed climate conditions.

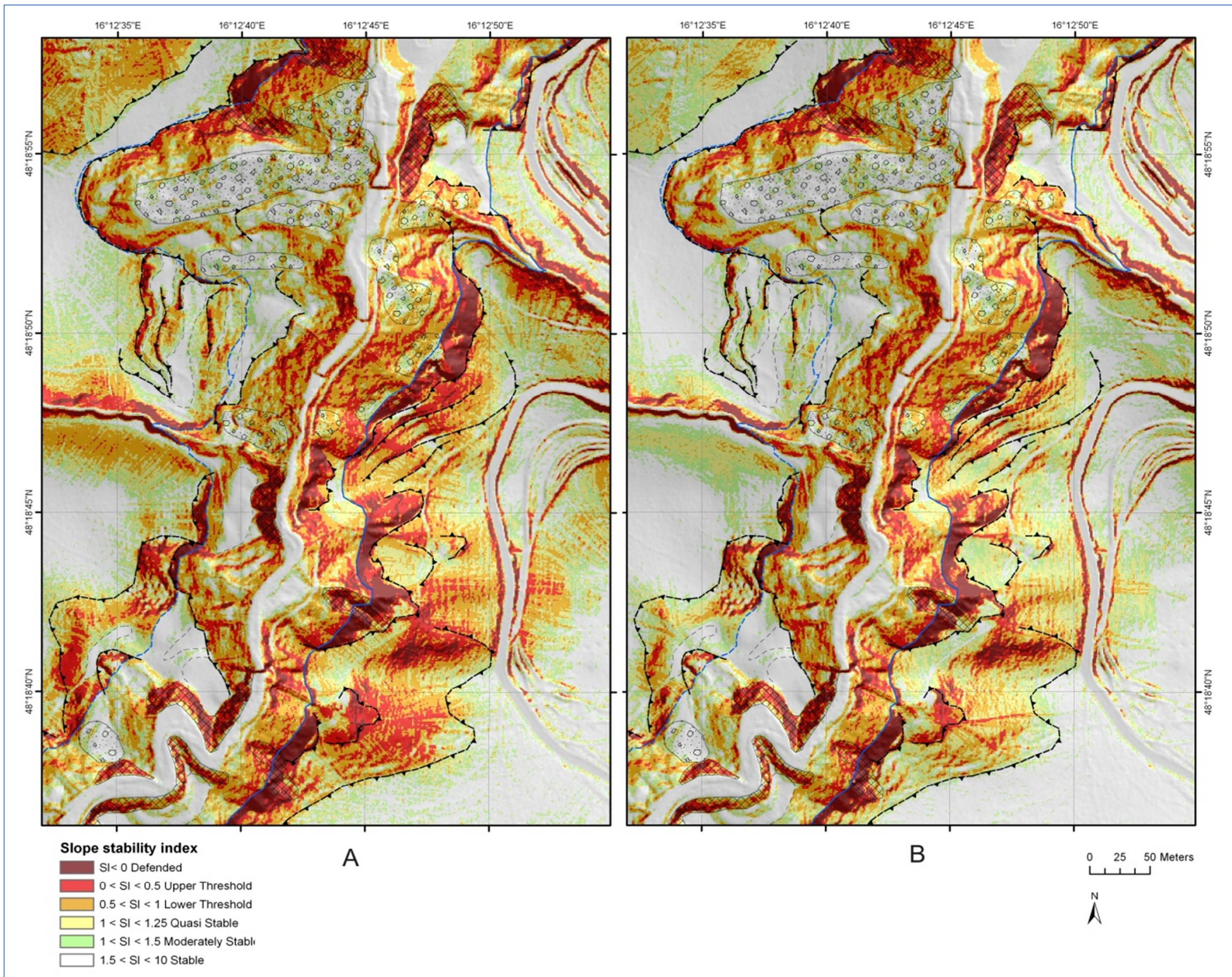


Figure 6-16. Comparison of slope stability index maps of the "summer scenario" (A) and the "future summer scenario" (B). The "summer scenario" (A) is based on the wetness conditions as prevailing in the climate normal period of 1961-1990. In the future "summer scenario" (B) the wetness conditions are adapted to the forecasts of climate change scenarios (Reclip.more 2007). There is a reduction of instability in the "future summer scenario" (B).

For a quantitative assessment of the changes in slope stability the proportions of the slope stability index classes are compared in Figure 6-17. The diagram shows the divergence of the classes of the “future summer scenario” in relation to the “summer scenario” regarding the present-day conditions. The difference is measured in percentage of the study area and the process region.

When the stability classes of the summer period scenarios are compared, a measurable difference between the climate normals and the climate change forecasts for 2050 (Figure 6-17) emerges. Due to the reduction of recharge by 73% in comparison to the average recharge estimated under normal climate conditions (Figure 5-8) a reduction of substrate wetness materialises in Figure 6-15. As a consequence of the increased dryness a future stabilising effect is indicated in Figures 6-16 and 6-17.

In the “future summer scenario” stable areas are enlarged by 11% (“stable”, “moderately stable”, “quasi-stable”). This extension of stable areas causes a corresponding reduction of instable zones (“lower threshold”, “upper threshold” and “defended”).

Figure 6-17 further illustrates that the influence of reduced recharge is stronger on the quaternary sediments where a 16% reduction of instable areas (“lower threshold” and “upper threshold”) ensues. Therefore climate change leads to a greater enhancement of stability than in the flysch bedrock, which only denotes a slight reduction of 2%.

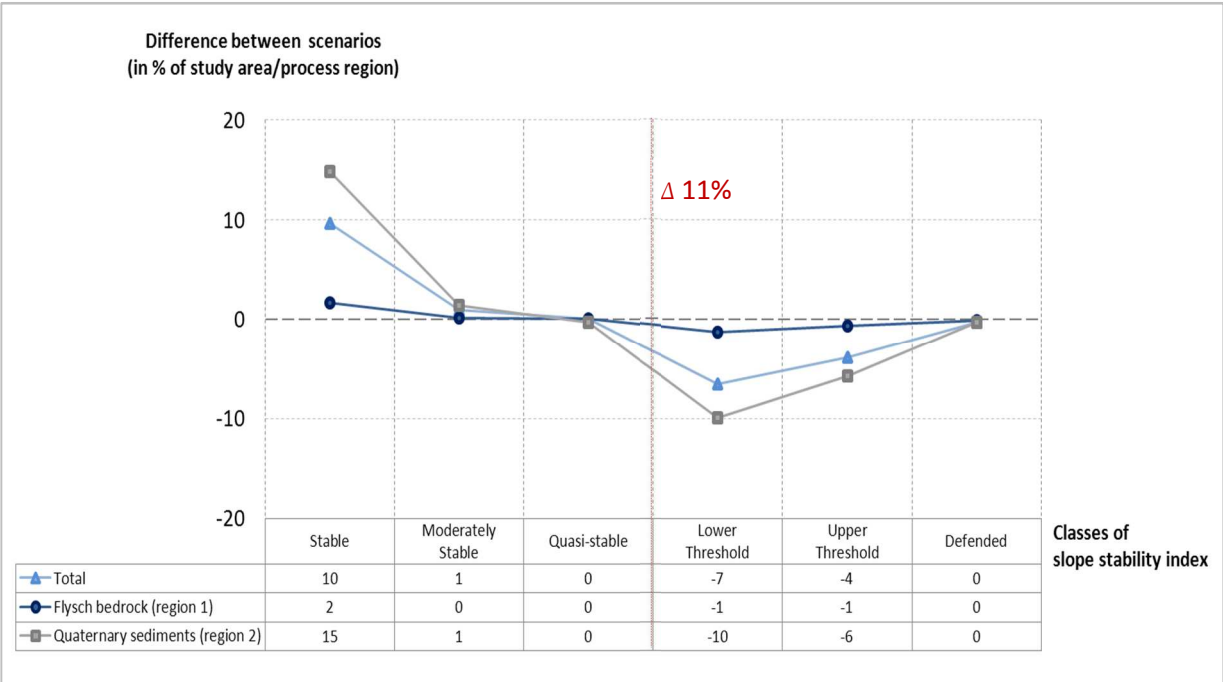


Figure 6-17. Divergence of the slope stability index classification of the “summer scenario (July)” in relation to the “future summer scenario (July)”. It is expressed as a difference (“summer scenario” minus “future summer scenario”) of the proportion of the single stability index classes in relation to the study area in percentage. The “summer scenario” is based on the wetness conditions as prevailing in the climate normal period of 1961-1990. In the “future summer scenario” the wetness conditions are adapted to the forecasts of the climate change scenarios (Reclip:more 2007).

---

## 6.5 Present-day winter scenario (January) and future winter scenario (January)

The corresponding winter scenarios of both groups, “present-day” and “future, mid-term disposition”, are compared. The scenarios are based on equal process regions and thus equal soil-mechanical parameters. The difference is that climate normals (ZAMG 2010c) are applied in the scenarios dedicated to present-day conditions, whereas climate data are adapted to the forecast climate change (Reclip:more 2007) in the scenarios analysing future disposition. The scenarios are compared in order to quantify changes in slope stability as a consequence of changed climate conditions as forecast for 2050 (Reclip:more 2007).

Although an air temperature rise of 2 °C is considered in the “future winter scenario (January)”, which brings about raised evapotranspiration and hence lowered soil-moisture storage, the water-balance calculation causes an increase in recharge for January (cp. Figure 5-8). This recharge augmentation results from the assumed monthly precipitation growth of 30% in the winter period. For the “future winter scenario (January)” an augmentation of monthly recharge of 36% is taken into account.

This augmentation of recharge in the “future winter scenario (January)” has only very slight effects on topographic wetness. In Figure 6-18 the topographic wetness maps of the “winter scenario (January)” (map A in Figure 6-18) and the “future winter scenario (January)” (map B in Figure 6-18) are displayed. The comparison of the maps indicates a minor extension of areas with a saturation tendency (“threshold saturation”), but no major difference in topographic wetness.

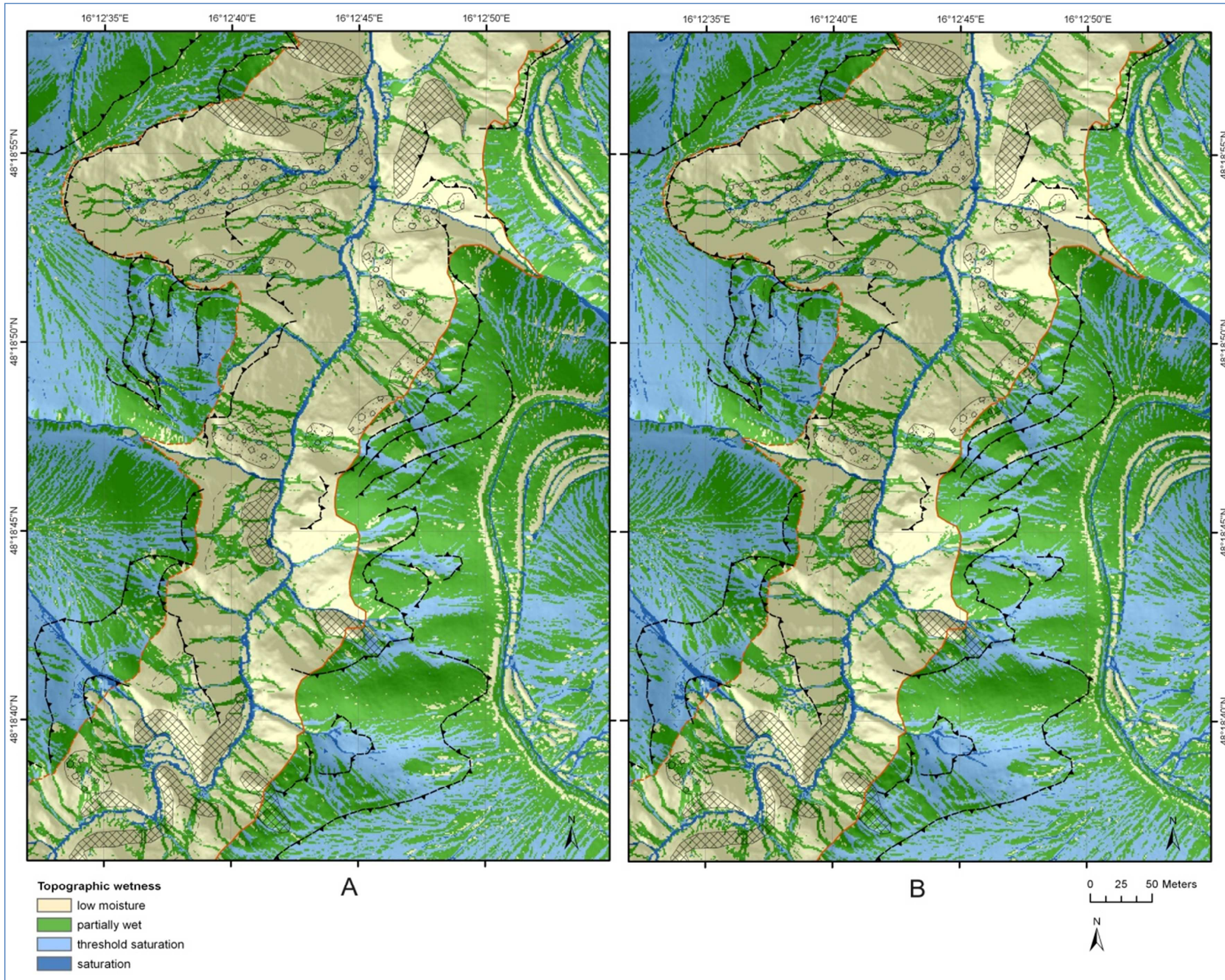


Figure 6-18. Comparison of topographic wetness maps of the "winter scenario (January)" (A) and the "future winter scenario (January)" (B). The future scenario takes climate change as forecast by regional climate models (Reclip:more 2007) into account. The divergence in topographic wetness is ascribed to the different amount of recharge in January as a consequence of changed climate.

A more detailed comparison of topographic wetness is possible on the basis of Figure 6-19. This diagram illustrates the proportion of the topographic wetness classes in both scenarios. It also shows a slight but measurable rise of topographic wetness in the “future winter scenario (January)” due to climate change. In particular, there is an increase of areas displaying a saturation tendency of 6% (“threshold saturation”). Therefore, the zones which are saturated under maximum assumed wetness in the model are enlarged. As a result of this extension of the wetness classes, the classes “partially wet” and “low moisture” are reduced by 3% each.

This augmentation of the saturation tendency implies that an additional 6% of the study area exhibits a probability for saturation because it is reached under the maximum assumed wetness conditions in the model but not under minimum wetness.

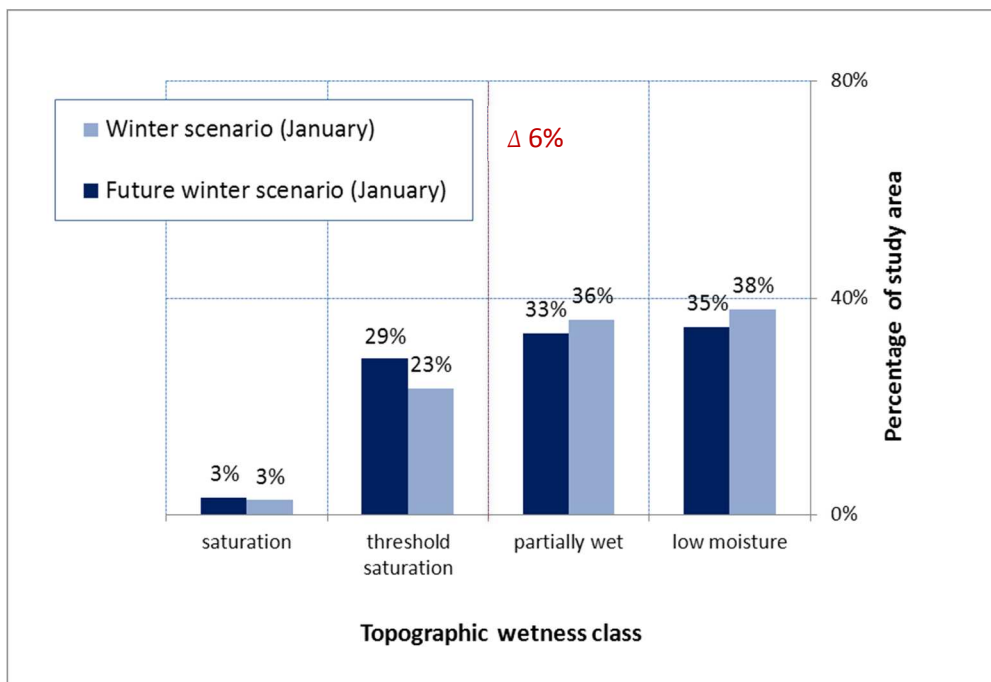


Figure 6-19. Comparison of topographic wetness classes and their proportion in the study area as given in the “winter scenario (January)” and the corresponding “future winter scenario (January)”. The future scenario takes climate change as forecast by regional climate models (Reclip:more 2007) into account. The divergence in topographic wetness is ascribed to the different amount of recharge in January as a consequence of changed climate conditions.

Therefore, also instable areas feature a slight extension in the “future winter scenario (January)”. The slope stability index maps of the “winter scenario” (map A in Figure 6-20) and the “future winter scenario (January)” (map A in Figure 6-20) are compared. The comparison of the maps shows no major difference in the distribution of stable and instable areas over the study area. Hence, no relevant change in slope dynamics can be assumed due to climate change.

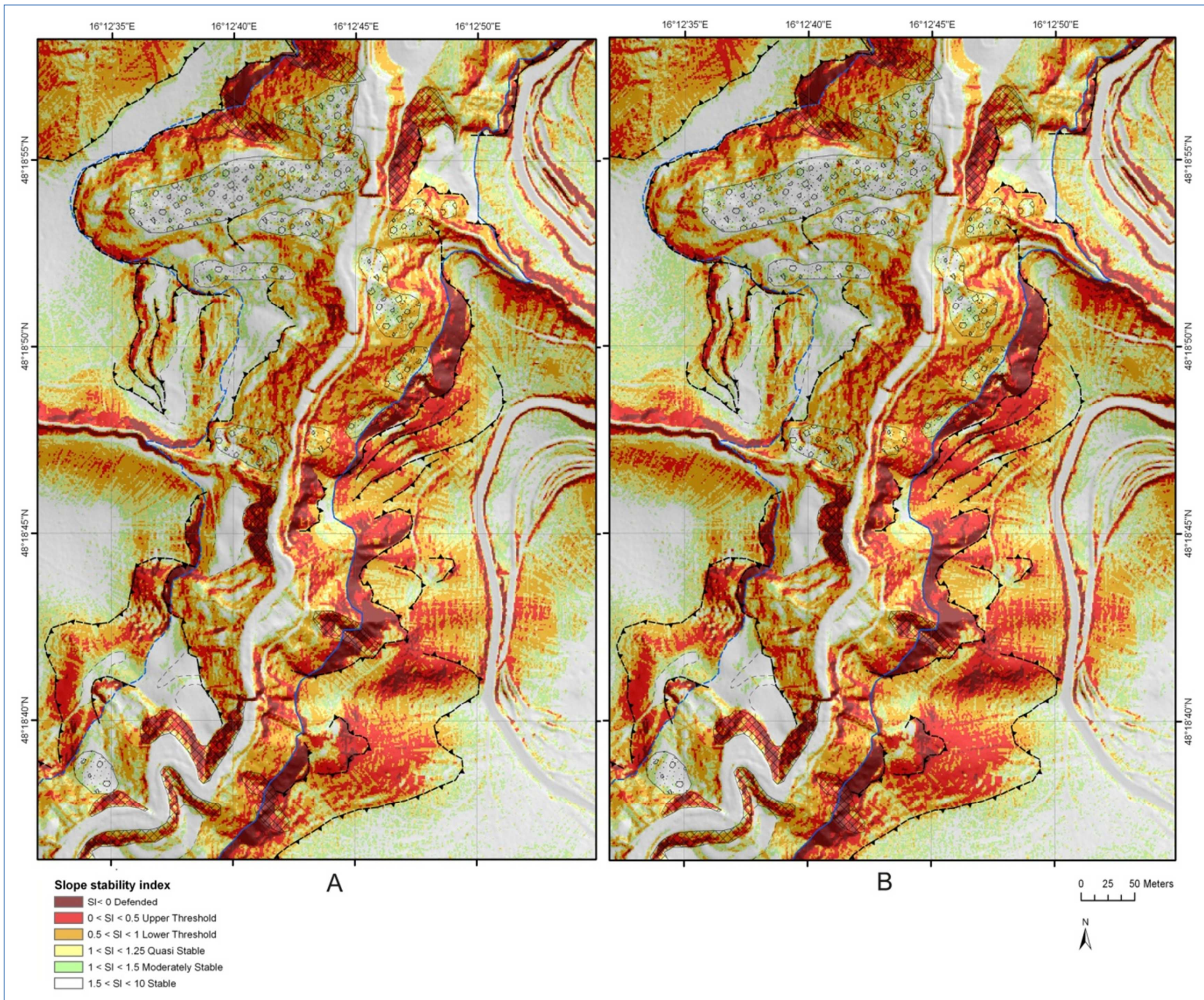


Figure 6-20. Comparison of slope stability index maps of the “winter scenario (January)” (A) and the “future winter scenario (January)” (B). The “winter scenario (January)” (A) is based on wetness conditions as prevailing in the climate normal period of 1961-1990. In the “future winter scenario (January)” (B) the wetness conditions are adapted to the forecasts of the climate change scenarios (Reclip:more 2007). There is a slight reduction of stability in the “future winter scenario (January)” (B).

Nevertheless, Figure 6-21 indicates a measurable increase of instable areas by 3% (“lower threshold”, “upper threshold”). Slopes classified as “stable” and “quasi-stable” grow by 3%, accordingly.

In the diagram reveals a surge of conditionally instable areas (“lower threshold”, “upper threshold”) in the quaternary sediments by even 4%. Hence, these sediments are more sensitive to changes in substrate moisture in regard to slope stability.

In summary, the forecast climate changes cause a reduction of slope stability in winter, which is caused by the raised monthly recharge. The forecast average rise of air temperature of 2 °C in January in combination with a 30% increased average precipitation, leads to an augmentation of recharge of 36% compared with the average monthly recharge as calculated under normal climate conditions.

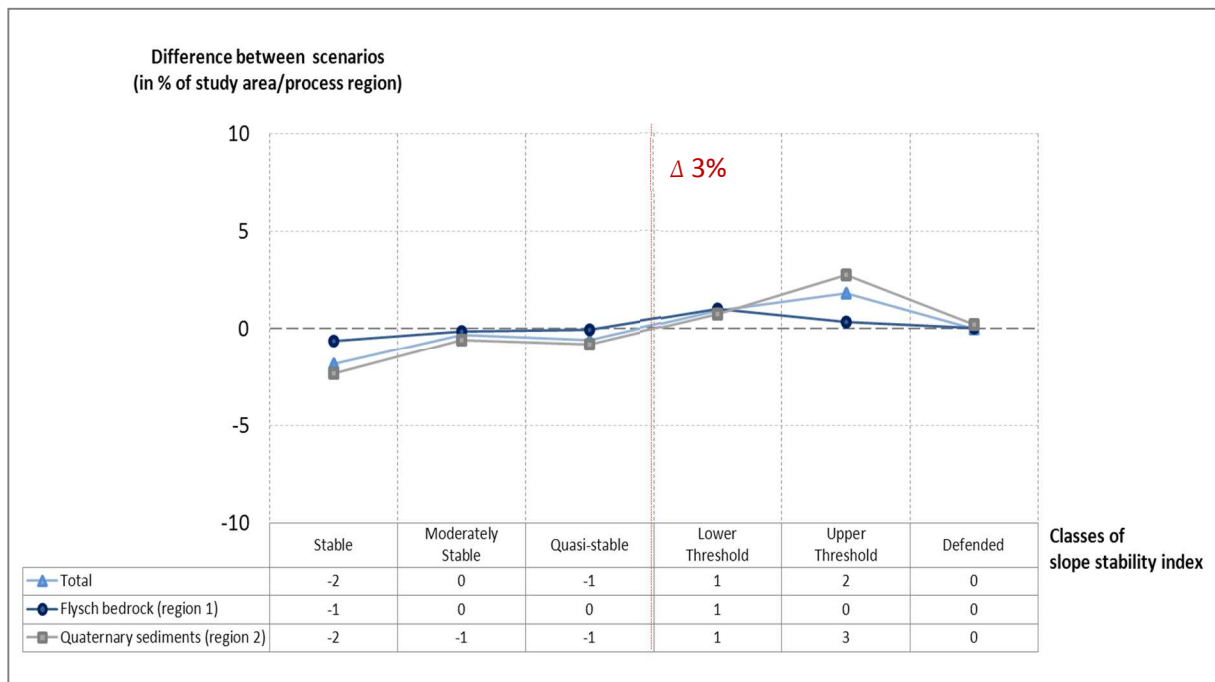


Figure 6-21. Divergence of the slope stability index classification of the “winter scenario (January)” in relation to the “future winter scenario (January)”. It is expressed as a difference (“winter scenario” minus “future winter scenario (January)”) of the proportion of the single stability index classes in relation to the study area in percentage. The “winter scenario (January)” is based on wetness conditions as prevailing in the climate normal period of 1961-1990. In the future “winter scenario (January)” the wetness conditions are adapted to the forecasts of climate change scenarios (Reclip:more 2007).

---

## 6.6 Summer scenario (July) and critical rainfall scenario

The scenarios of the group “short-term disposition” investigate the variable disposition under single meteorological situations like heavy and long-lasting rainfall. Single rainfall events are relevant for disposition assessment because they create soil water contents which can cause a critical level in relation to shear strength in the hillslope sediments (Klose et al. 2012).

A long-lasting rainfall event with an intensity of 90 mm/d (ZAMG 2010a) is applied in the “critical rainfall scenario”. It investigates slope stability in relation to short-term substrate moisture as developed under this specific 24h period of rain. In contrast to this, the scenarios of the groups “present-day, mid-term disposition” are based on mid-term average substrate moisture. By comparing the modelling results of both groups, “short-term disposition” and “present-day, mid-term disposition”, the variability of the disposition to landslides can be studied. The objective is to quantify the influence of abundant precipitation on slope stability as a function of substrate moisture. As intensive rainfall events more frequently occur in the summer period, the “summer scenario (July)” is utilised as a reference basis for the comparison. That means that changes in slope stability and topographic wetness, as a consequence of single rainfall events, are analysed in comparison to the mid-term average conditions in July. The mid-term wetness conditions are related to the climate normals from the period of 1961-1990 (ZAMG 2010c).

The “summer scenario (July)” is compared to the “critical rainfall scenario” (90 mm/d). This above-average infiltration, which is considered in the “critical rainfall scenario”, considerably affects topographic wetness. In Figure 6-22 the topographic wetness maps of the “summer scenario (July)” (map A in Figure 6-22) and the “critical rainfall scenario” (map B in Figure 6-22) are given. The comparison of the maps illustrates the increased wetness in the “critical rainfall scenario”. In the quaternary sediments the “partially wet” areas are nearly completely shifted to zones of “threshold saturation”. In the flysch bedrock an extension of “partially wet” areas is visible and “saturation” is computed for flow accumulation lines.

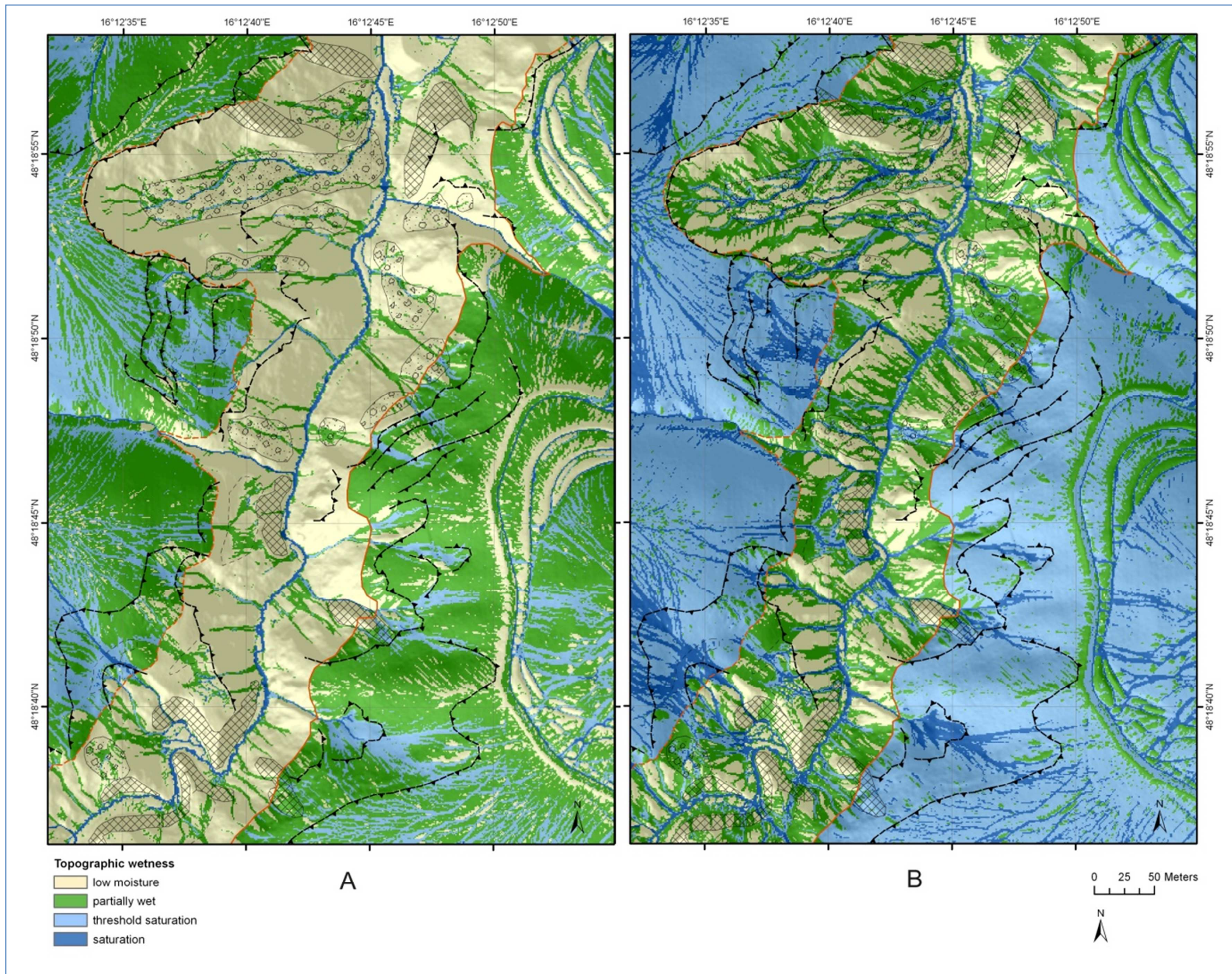


Figure 6-22. Comparison of the topographic wetness maps of the “summer scenario” (A) and the “critical rainfall scenario” (B). The “summer scenario (July)” (A) is based on mid-term topographic wetness as estimated under climate conditions as prevailing in the climate normal period in the study area (ZAMG 2010c). The “critical rainfall scenario” (B) is based on short-term topographic wetness as developed under a long-lasting rainfall event of 90 mm/d.

In Figure 6-23 the changes in topographic wetness are quantified. The Figure shows the proportion of the topographic wetness classes in comparison of both scenarios. In comparison to average monthly substrate wetness in summer, the saturated areas increase by 10% (from 2% in the “summer scenario” to 12% in the “critical rainfall scenario”). Furthermore, areas with a saturation tendency are extended by 32% under a rainfall intensity of 90mm/d in comparison to mid-term climate conditions. Therefore, there is a total wetness increase of 42%. Corresponding to this extension of saturated areas, there is a shrinking of the areas classified as “partially wet” by 15% and “low moisture” by 27%. Therefore, there is a distinct shifting (42%) of substrate moisture towards saturated conditions under a critical rainfall event. In total 59% of the study area has a probability to reach saturation under the assumed wetness (47%) or even reveals certainty for saturation (12%).

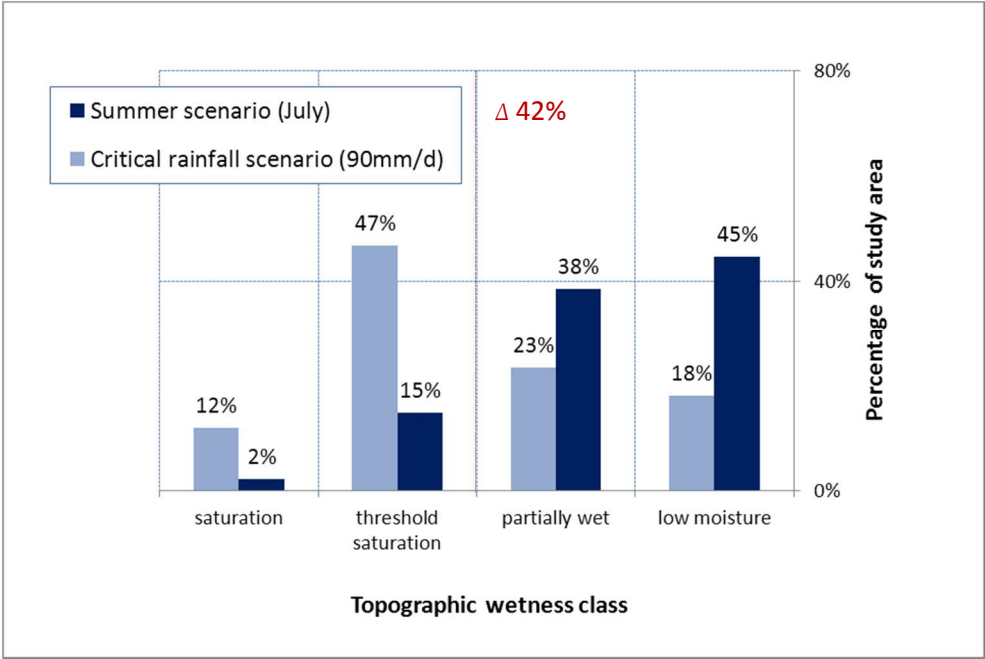


Figure 6-23. Comparison of the topographic wetness classes and their proportion in the study area as given in the “summer scenario (July)” and the “critical rainfall scenario” (90 mm/d). The “summer scenario (July)” is based on mid-term average recharge in July. The divergence in topographic wetness in the “critical rainfall scenario” is ascribed to the increase in recharge caused by a long-lasting rainfall event of 90 mm/d limited in time.

This wetness-augmentation has a negative effect on the slope stability in the study area. In Figure 6-24 the slope stability index maps of the “summer scenario (July)” (map A in Figure 6-24) and the “critical rainfall scenario” (map B in Figure 6-24) are compared. The maps show a distinct extension of instable zones under long-lasting rainfall (map B in Figure 6-24). In contrast to average mid-term substrate wetness regarded in map A in Figure 6-24, the short-term wetness causes a growth of instability in particular in the quaternary sediments, notably at the moderately inclined areas from 15° to 30° (cp. slope gradient map in Figure 5-5, page 79) on the flanks of the temporarily water-bearing drainage lines.

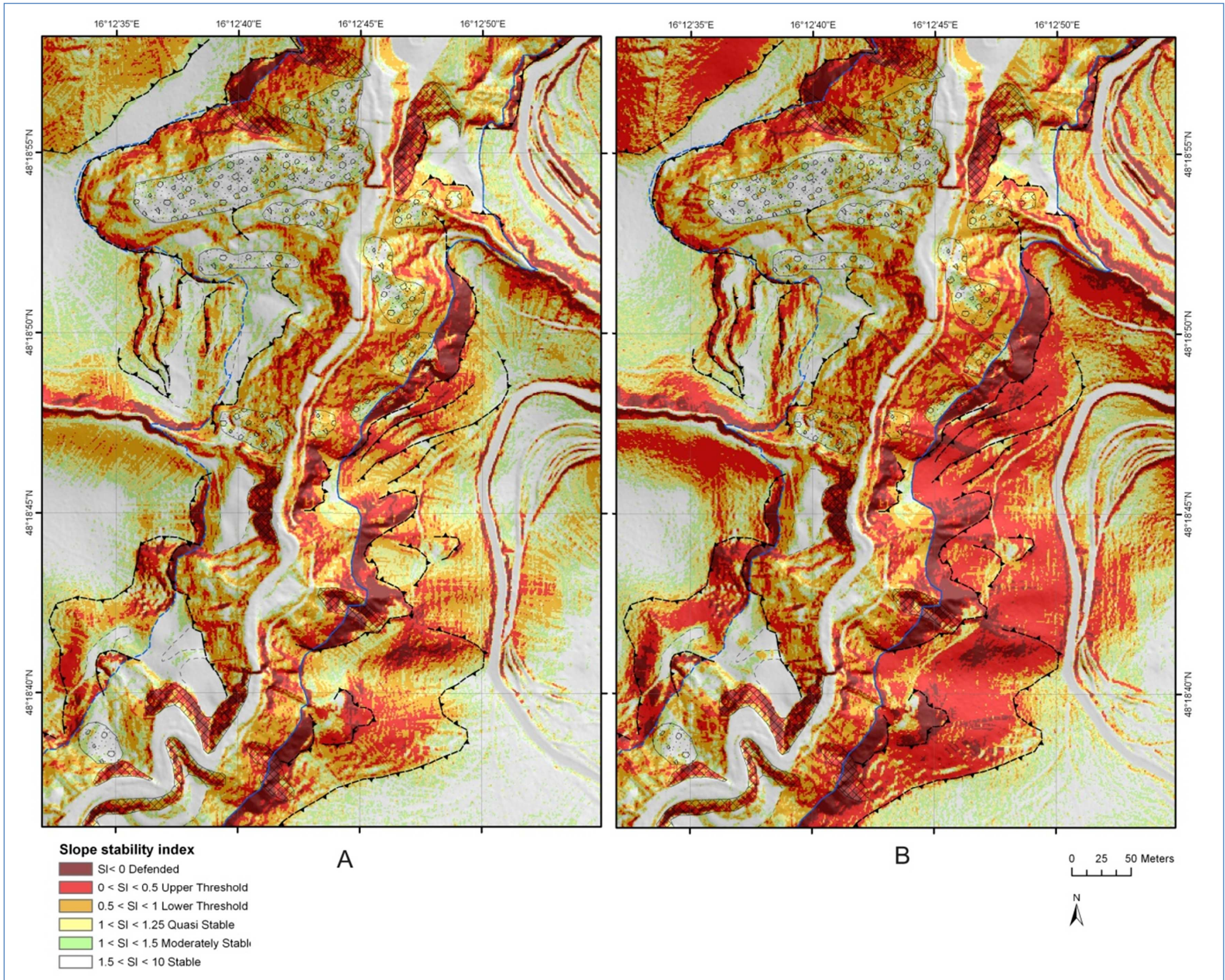


Figure 6-24. Comparison of the slope stability index maps of the “summer scenario (July)” (A) and “critical rainfall scenario” (B). The “summer scenario (July)” (A) is based on mid-term average recharge in July. The “critical rainfall scenario” (B) is based on short-term recharge as produced by a long-lasting rainfall event of 90 mm/d. There is a distinct increase in instability in the “critical rainfall scenario”.

To quantify the changes in slope stability more precisely, the extension of the stability classes within the study area and within the process regions are compared between the scenarios. For that purpose Figure 6-25 shows the divergence of the slope stability index classes of the “critical rainfall scenario” relative to the “summer scenario”. The difference is measured in percentage of the study area. The Figure indicates that the “stable” areas are reduced by 9% in the “critical rainfall scenario”, “moderately stable” and “quasi-stable” areas are shrinking by 2% each. Furthermore, instable areas classified as “lower threshold” are diminished by 1%. The reduction of these classes corresponds to a significant extension of the instable areas classified with “upper threshold” and “defended” by 14% in total. That means that the shifting from stability to instability is mainly done for the benefit of the highest instability classes. Severe weather events affect the process regions to a different degree. Figure 6-25 indicates that the instability classes “upper threshold” and “defended” rise by 20% in total.

In summary, instability is increased by a critical rainfall of 90 mm/d by 13% (“lower threshold”, “upper threshold” and “defended”) in connection with a concurrent decrease in the stable classes (“stable”, “moderately stable”, “quasi-stable”). While in the flysch bedrock an enlargement of instable areas by 9% is denoted, the quaternary sediments reveal a growth of instability of 20%. Therefore, it can be concluded that the quaternary sediments are more moisture sensitive and show a stronger response to the weather conditions related to slope stability.

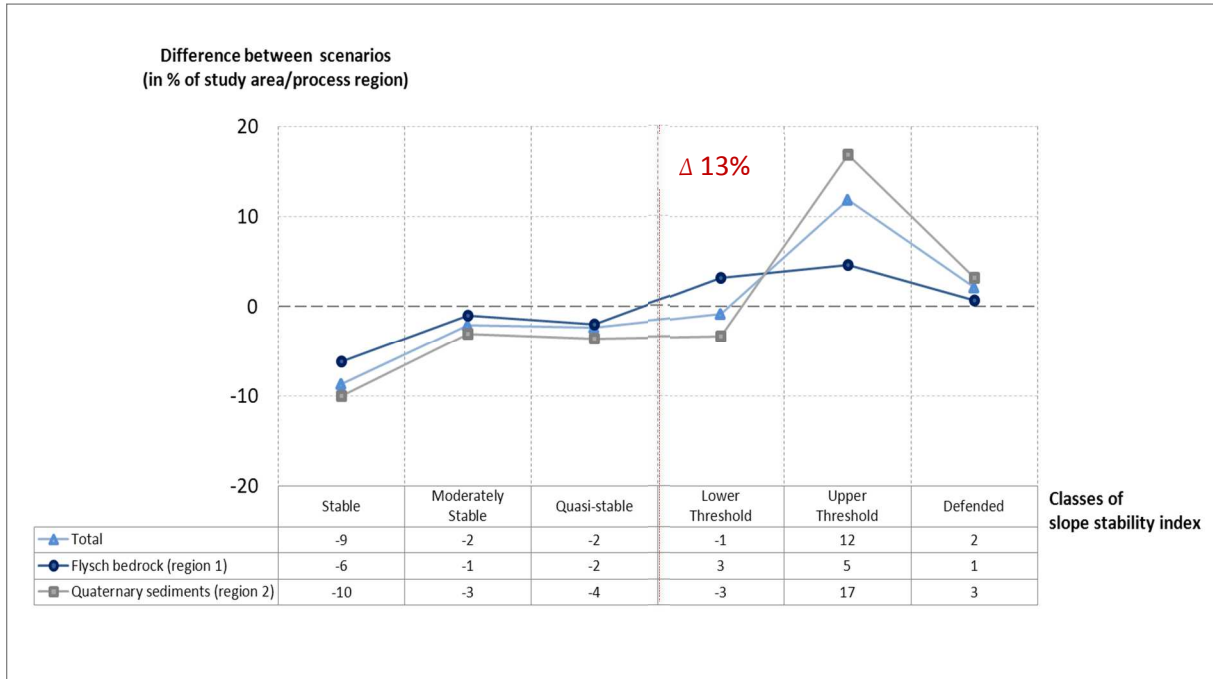


Figure 6-25. Divergence of the slope stability index classification of the “critical rainfall scenario” (90 mm/d) in relation to the “summer scenario” (July). It is expressed as a difference (“critical rainfall scenario” minus “summer scenario”) of the proportion of the single stability index classes in relation to the study area in percentage. The “summer scenario” is based on mid-term average recharge in July. The “critical rainfall scenario” is based on short-term recharge as produced by a long-lasting rainfall event of 90 mm/d. There is a distinct extension of instability in the “critical rainfall scenario”.

---

## 6.7 Summer scenario (July) and heavy rainfall scenario

The “summer scenario (July)” is compared to the “heavy rainfall scenario”. This value represents the design depth of precipitation calculated by the Hydrographical Service for the study area (eHYD 2011). Hence, it investigates slope stability in relation to short-term substrate moisture, as developed under this specific precipitation event. In contrast to this, the “summer scenario (July)” is based on mid-term average substrate moisture. The objective of this comparison is to quantify the influence of an extreme event on slope stability as a function of substrate moisture. As intensive rainfall events more frequently occur in the summer period, the “summer scenario (July)” is utilised as reference basis for the comparison.

This extreme weather event, which is considered in the “heavy rainfall scenario”, drastically affects topographic wetness. In Figure 6-26 the topographic wetness maps of the “summer scenario (July)” (map A in Figure 6-26) and the “heavy rainfall scenario” (map B in Figure 6-26) are displayed. The comparison of the maps yields saturated conditions nearly over the entire study area. “Partially wet” areas and zones with “saturation tendency” occasionally occur in the flysch bedrock. “Low moisture” conditions completely disappear under this heavy rainfall event.

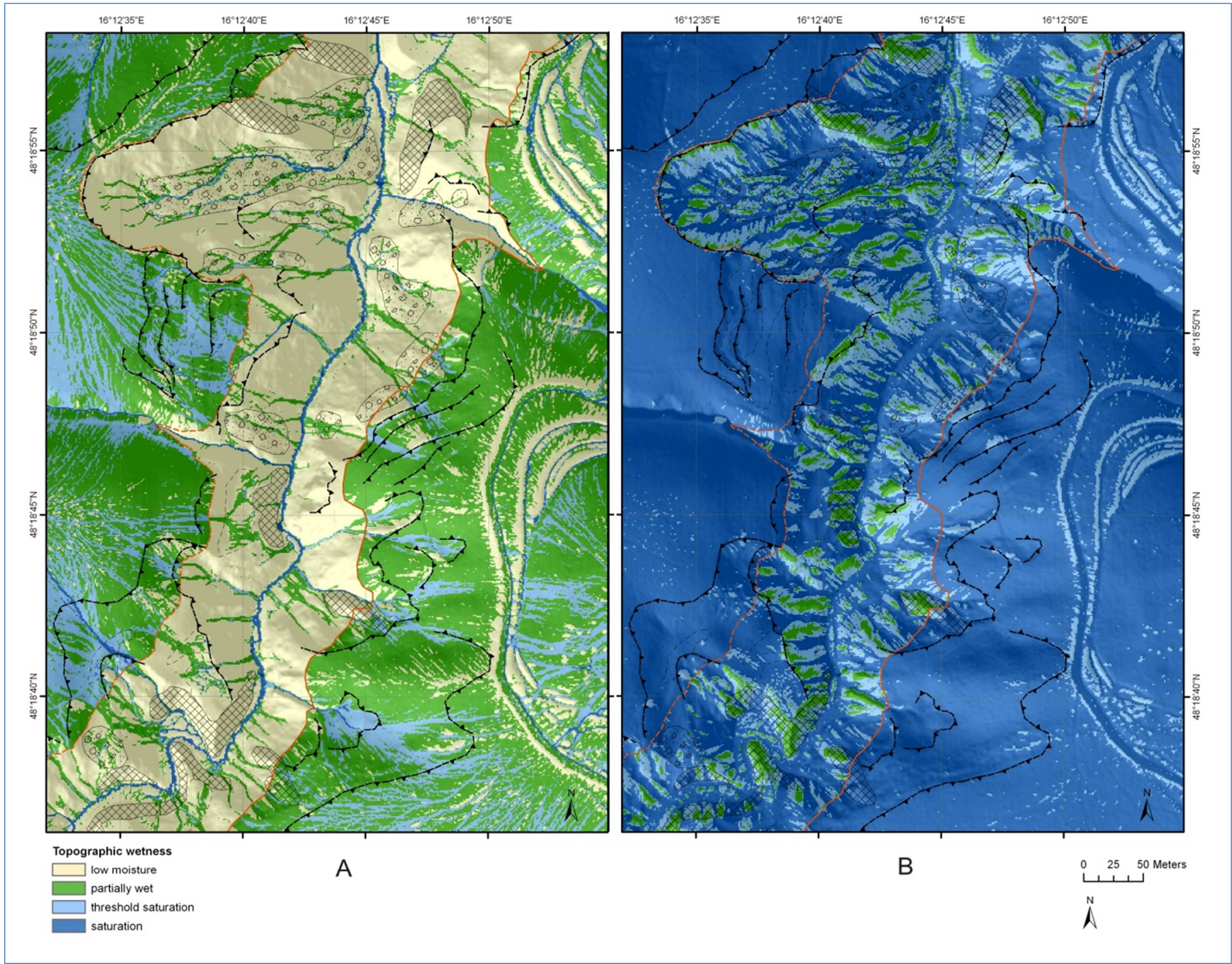


Figure 6-26. Comparison of the topographic wetness classes and their proportion in the study area as given in the “summer scenario” (A) and the “heavy rainfall scenario” (B). The “summer scenario” is based on mid-term average recharge in July. The divergence in topographic wetness in the “heavy rainfall scenario” is ascribed to the increase in recharge caused by an extreme rainfall event of 60 mm/h limited in time, which has a statistical recurrence period of 50 years in the study area. This extreme weather event drastically affects topographic wetness.

A more detailed comparison of topographic wetness is possible on the basis of Figure 6-27. This diagram demonstrates the proportion of the topographic wetness classes in both scenarios. The comparison shows that “low moisture” conditions completely disappear. In relation to the average monthly recharge, this extreme infiltration causes a reduction of “low moisture” by 45%. Furthermore, “partially wet” areas are shrinking by 33%. This reduction of partially wet and low moisture conditions corresponds to an augmentation of areas with saturation tendency (“threshold saturation”) by 2% and a drastic enlargement of saturated areas by 76%. Accordingly, 78% of the study area exhibits saturated substrate or saturation tendency under heavy rainfall.

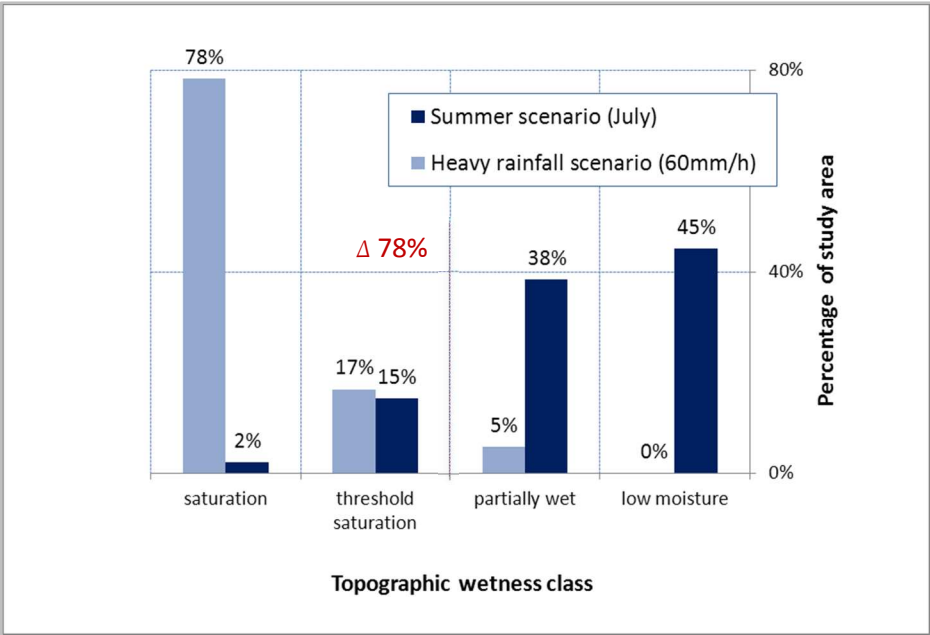


Figure 6-27. Comparison of the topographic wetness classes and their proportion in the study area in scenarios considering average wetness conditions and heavy rainfall.

This heavy rainfall event leads to a domination of instable conditions in the study area. Figure 6-28 illustrates the slope stability index maps of the “summer scenario” (map A in Figure 6-28) and the “heavy rainfall scenario” (map B in Figure 6-28). The comparison of the maps shows a huge extension of instable zones under heavy rainfall (map B in Figure 6-28). In contrast to average mid-term substrate wetness regarded in (map A in Figure 6-28), the extreme, short-term wetness causes an increase in instability in both process regions.

In the “heavy rainfall scenario” the instable areas within the quaternary sediments concentrate at slopes with a moderate slope gradient of approximately 20° to 30°, similar to the “summer scenario”. However, the extreme weather event causes instability even in slopes with an inclination of 15° to 20° (cp. slope gradient map in Figure 5-5, page 79). In the case of the quaternary sediments highly instable zones concentrate at steep slopes with a gradient of 35° and more, which occur at existing scarps and on the flanks of the temporarily water-bearing drainage lines.

Apart from the quaternary sediments also the flysch bedrock exhibits an extension of instable areas, which are found at the scarps of former landslides and near the valley bottom at the oversteepend slopes of the gorge.

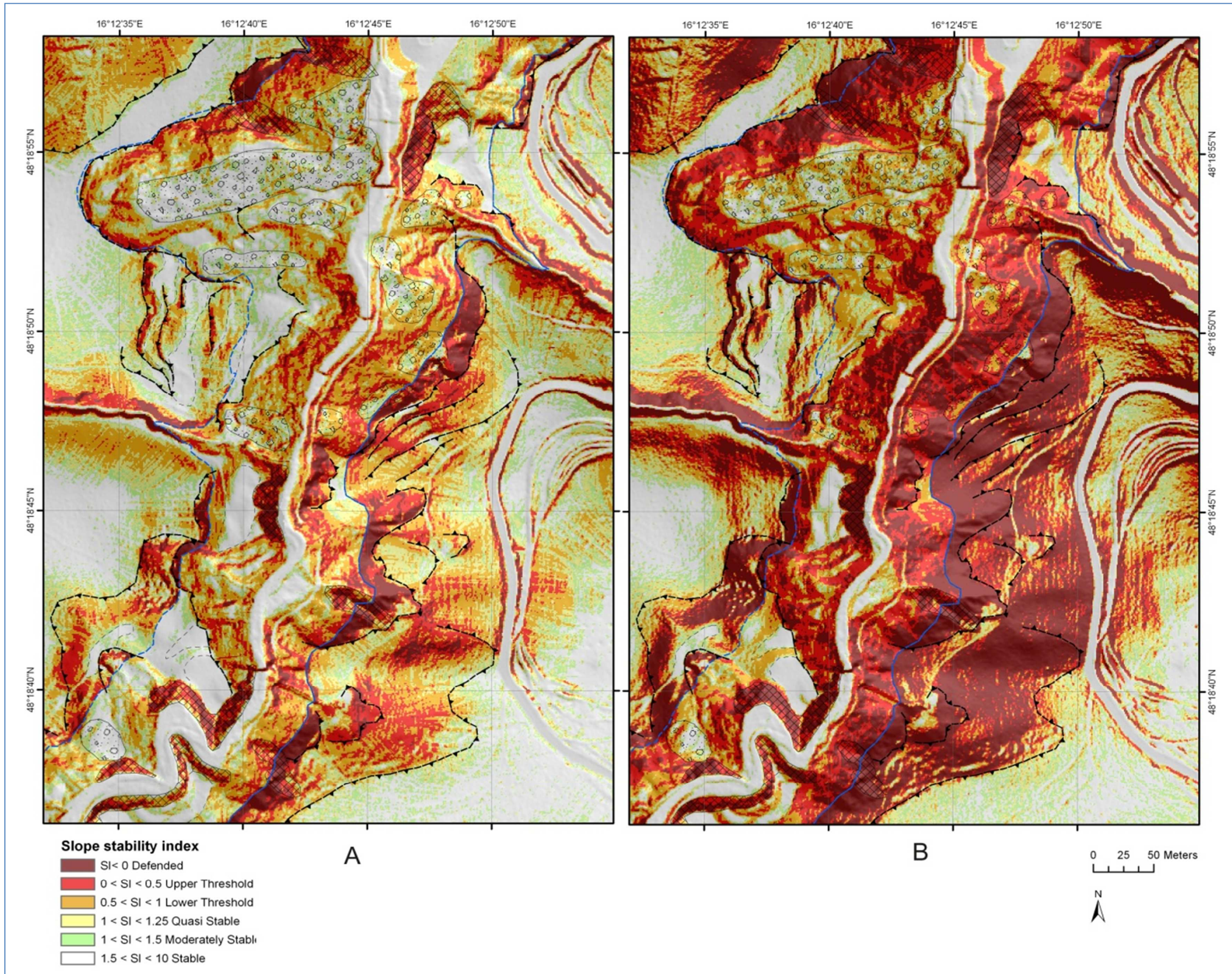


Figure 6-28. Comparison of the slope stability index maps of the “summer scenario” (A) and the “heavy rainfall scenario” (B). The “summer scenario” (A) is based on mid-term average recharge in July. The “heavy rainfall scenario” (B) is based on short-term recharge as produced by an extreme rainfall event of 60 mm/h. There is a drastic increase in instability in the “heavy rainfall scenario” for the benefit of the highest instability classes.

Figure 6-29 enables a quantitative assessment of the changes in slope stability because the proportions of the slope stability index classes of both scenarios are compared. The diagram shows the divergence of the slope stability index classes of the “heavy rainfall scenario” relative to the “summer scenario”. The difference is measured in percentage of the study area. The Figure demonstrates that instability is raised by 23% in total (“lower threshold”, “upper threshold”, “defended”). Within these instable classes there is a shifting from the low instability class “lower threshold” to the highest instability classes “upper threshold” by 8% and “defended” by 22%.

Corresponding to this increase in slope instability there is a decrease in the classes with stable conditions in the “heavy rainfall scenario”. In particular, “stable” areas are shrinking by 14%, “moderately stable” by 4% and “quasi-stable” zones by 5%. This indicates that the reduction of stability is concentrated on the class which represents unconditionally stable conditions, hence the highest stability in the model.

The diagram (Figure 6-29) indicates that the extension of instable areas is larger in the flysch bedrock than in the quaternary sediments in relation to their process region area. The flysch bedrock reveals a surge of instable areas (classified as “lower threshold”, “upper threshold” and “defended”) of 29%. In the quaternary sediments the stable areas (classified as “lower threshold”, “upper threshold” and “defended”) grow by 19%. There the flysch bedrock shows a stronger response in slope stability on heavy rainfall, in terms of the enlargement of the affected area. However, the instability in the flysch bedrock is classified with “upper threshold” and “defended” with approximately similar proportion. In contrast to this, the classification of slope stability in the quaternary sediments is strongly shifted to the highest instability class (“defended”) with 24% of the process region area. Therefore, the quaternary sediments show a stronger response in slope stability in terms of probability for slope failure than the flysch bedrock.

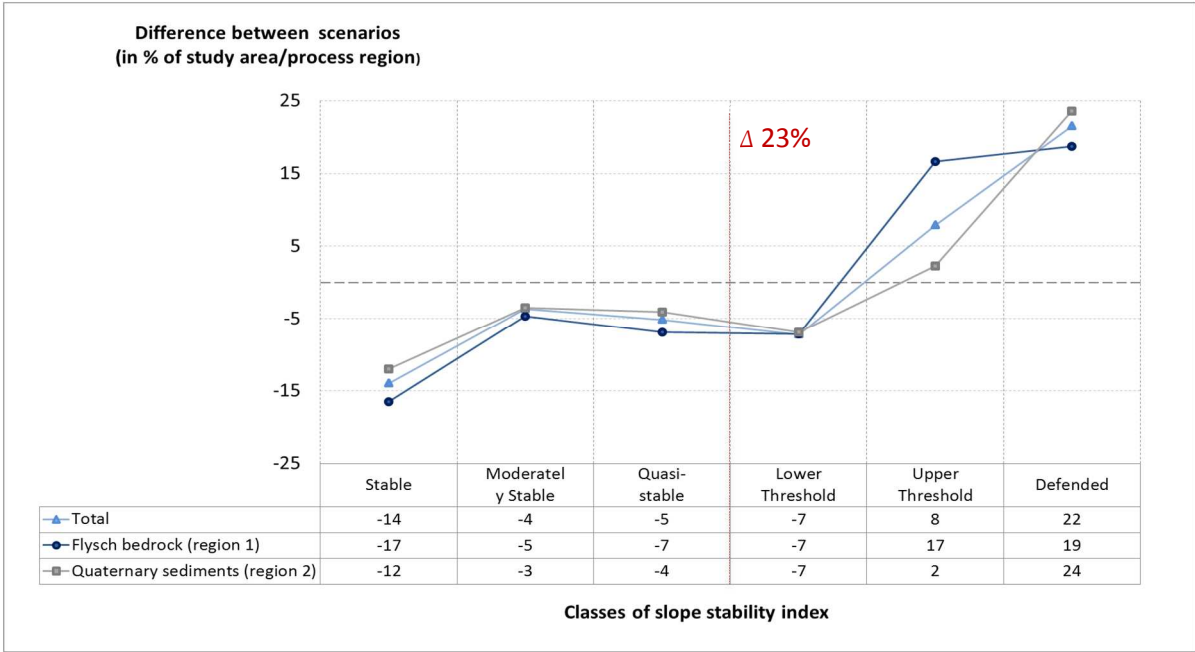


Figure 6-29. Divergence of the slope stability index classification of the “heavy rainfall scenario” (60 mm/h) in relation to the “summer scenario” (July). It is expressed as a difference (“heavy rainfall scenario” minus “summer scenario”) of the proportion of the single stability index classes in relation to the study area in percentage. The “summer scenario” is based on mid-term average recharge in July. The “heavy rainfall scenario” is based on short-term recharge as produced by an extreme rainfall event of 60 mm/h with a statistical recurrence period of 50 years. There is a distinct extension of the highest instability classes in the “heavy rainfall scenario”.

---

## 7 Discussion

An integrated assessment of landslide susceptibility was aspired, which is not limited to a single modelling approach. This objective is related to overcome incompleteness due to the specific theoretical background and inherent assumptions of one single, selected modelling approach (Bailer-Jones 2002). Therefore, two dissimilar approaches applied from a small (1:20,000) to a large scale (1:4,000) are used. Weight-of-evidence, a statistical-probabilistic method (Agterberg et al. 1990, Bonham-Carter et al. 1989, Bonham-Carter 2002, Sawatzky et al. 2009), as well as the Stability Index Mapping (SINMAP) approach according to Pack et al. (1998, 2005) were applied in an adapted manner. The basis of the regional landslide susceptibility model is a landslide inventory whose compilation was the initial step in the present paper. The methods applied in the actual work as well as the results of modelling and their syntheses are discussed in this chapter.

### 7.1 Landslide inventory for the Northern Vienna Forest

A main objective of this study is the compilation of a landslide inventory for the Northern Vienna Forest because the spatial occurrence of landslides is the fundamental basis for landslide susceptibility assessment. The first comprehensive landslide inventory covering 471 datasets on landslides taking place within a time span of approximately 90 years is produced based on archive studies, which is the first for the region of the Northern Vienna Forest.

Archive studies are applied to compile landslide data on a regional scale. The advantage of this method is that also older landslides, which are not as visible as younger events, can be incorporated. In the actual work there are landslides recorded from 1926 to 2010. Nevertheless, a certain degree of uncertainty cannot be avoided, independent of the chosen method to support landslide inventory generation (Soeters & Van Westen 1996, Van Westen et al. 2008). In general, uncertainty is given in archive studies due to the incompleteness of historical information with respect to the exact location, time of occurrence or type of movement (Soeters & Van Westen 1996, Van Westen et al. 2008). Furthermore, landslide databases, in particular from public organisations concerned with reinstatement measures, are primarily focussed on events that have affected infrastructure, such as roads (Van Westen et al. 2008). In the present work this is applicable for the databases of the authorities dealing with mitigation and reinstatement measures, like the Building Ground Register (Land NÖ 2010) and the technical reports of the Austrian Torrent and Avalanche Control (WLV 2010). Nevertheless, they offer valuable data for estimation of landslide proneness in relation to their location. However, the most valuable database is the landslide map produced by geomorphological field surveys of an expert in terms of geomorphological processes (Götzinger 1943). The landslides are registered independent of the elements at risk and are well documented in relation to their causes. These landslides cover 90% of the inventory, therefore a bias to events that caused damages can be excluded to a large extent.

A main focus of the inventory is put on the exact spatial mapping of sliding processes. A temporal assignment was not possible in all cases. However, this shortcoming is of minor relevance in the present work because the occurrence dates are not required for the subsequent susceptibility analysis. This is due to the fact that the probability of landslides is assessed in a spatial context only, and not in temporal one, which is the domain of landslide hazard estimations (Cruden & Varnes 1996, Van Westen et al. 2008, Fell et al. 2008). Nevertheless, for landslide hazard and risk

---

assessments in the future these data are required. At present no data sources which satisfy the demands of temporal landslide occurrence probability estimations are available in Austria.

Apart from the archive studies, which are applied for the generation of a landslide inventory on a regional scale, remote sensing data are used to support the mapping of mass movements in the Hagenbach gorge on a large scale. The most common approach for mapping landslides supported by remote-sensing data is the visual interpretation of aerial photographs or high-resolution satellite imagery (Soeters & Van Westen 1996, Van Westen 2004, Van Westen et al. 2008). However, this method is not applicable for the study area because it is completely covered by dense forest. Due to the age of the landslides and the density of the forest, the scarps are either already vegetated or covered by the crowns of the neighbouring trees. High-resolution topographic information from the shaded relief images of the ALS-data could be used to identify scarps, deformation features, rotational blocks and deposition areas of mass movements in a highly accurate and comprehensive way, even in cases of completely vegetated slopes. The identification of the structural components of the mass movements, like scarps, slope toes, or rotational blocks is additionally facilitated by the use of slope gradient information in conjunction with the hillshades.

It can be concluded that the LiDAR-based landslide mapping method is most suitable for the forested study area and enables highly detailed interpretation of the landslide mechanism and structure. Furthermore, the previous mapping of potential landslides on the basis of ALS-data distinctly facilitates a subsequent, geomorphological field survey. The field survey, however, enabled the identification of the landslide type, which is difficult to determine only on the basis of ALS-data.

## **7.2 Regional landslide susceptibility assessment**

The aim of providing information on the basic disposition of the Northern Vienna Forest to develop landslides on a regional scale (scale 1:20,000) could be accomplished with the present statistic-probabilistic landslide susceptibility assessment. The basic disposition describes the principal tendency of slopes to move, which is a result of the prevailing geofactors preparing mass movements. These geofactors can be regarded as static, i.e. as more or less constant over time. In particular, the study includes geological conditions, the distance to tectonic structures, like nappe boundaries and faults, the distance to drainage lines, vegetation cover, morphometric parameters (i.e. slope gradient and curvature), slope aspect, and landform category as steering geofactors for landslide susceptibility.

In relation to the selected geofactors the approach towards the incorporation of unconsolidated rock is different from the current studies (Lee & Choi 2004, Dahal et al. 2008a, 2008b). The specific model presented in this work is mainly based on various topographic parameters, geology, tectonics as well as the drainage network. Data on soils and unconsolidated rock are not directly integrated because of lacking data. In recent applications pedological information available on a medium scale are incorporated into the susceptibility assessments (cf. Lee & Choi 2004, Dahal et al. 2008a, 2008b). Area-wide, pedological information is lacking as well in the Northern Vienna Forest but the importance of soil type and material is regarded as less relevant for the assessment of landslide proneness in the study area because of the landslide depth reaching below the upper soil horizons. The geotechnical characteristics of the loose material on top of the bedrock are crucial for landslide development (Van Westen et al. 2008). Such information is typically provided in engineering maps. The availability of such maps is regarded as essential for landslide susceptibility assessments. At present there is only little information on a regional scale and even less so in Austria as a whole. Therefore, the present WofE application concentrates on relief position and landforms, which can be

---

indirectly linked to the distribution of quaternary sediments, loess deposits and their substrate properties. According to Scholten (2003) the relief is a major steering factor for the distribution system and substrate specific properties of cover beds as well as loess deposits (Scholten 2003).

In connection with the selected geofactors, a major aim was to gain new knowledge related to the landslide evolution in the Northern Vienna Forest. This was done by the assessment of spatial distribution of landslides with regard to specific preparatory geofactors which steer or prepare mass movements. Statistical weighting, which is carried out in the course of the regional landslide susceptibility assessment, provides new information on the relation of landslide processes to specific controlling geofactors, which can be summarised as follows:

**(1) Relevance of clay-shale zones for landslide proneness:** the model emphasises the link between landslides and the formations rich in clay and shale. The model demonstrates that landslides are most frequent in the area of the Altlenzbach Formation. A portion of 32% of landslides in the inventory takes place in the Altlenzbach Formation and consequently the regional landslide susceptibility model assesses this stratum as relevant for the occurrence of landslides (cp. Table 4-4, page 49 and Figure 4-7, page 51). These beds are characterised by brittle, calcareous and marly sandstones interbedded with clay shists and lime marls. The calcareous sandstones tend to profound decomposition under the conditions of waterlogging. Despite this high landslide frequency in the Altlenzbach beds, the highest landslide density and hence the largest probability values can be found in the Northern Zone (cp. Table 4-4, page 49), which is also the most extensive area classified as highly susceptible. The dominant geological formation in the Northern Zone, the Gaultflysch, is composed of clay shales, sandstones and quartzites. Such lithological conditions can be also found in a small area of the Kahlenberg Nappe where the probability values are distinctly enhanced in comparison to the remaining areas of the nappe (cp. Table 4-4, page 49).

In conclusion it can be stated that according to the susceptibility model the most landslide prone geological units are the Wolfpassing Formation, situated in the Northern Zone, and the Gaultflysch, located in the Kahlenberg Nappe. Both units are composed of coloured clay-shales alternating with sandstones. Earlier, local geomorphological studies in the Vienna Forest observed enhanced landslide activities in clay-shale zones (Götzinger 1943, Schwenk et al. 1992, Damm et al. 2008, Terhorst et al. 2009, Damm & Terhorst 2010). The results of the present modelling underline the relation between landslide occurrence and bedrock rich in clay shales. It can be concluded that clay-shale zones in the bedrock increase the landslide disposition in the Vienna Forest Flysch Zone (Neuhäuser et al. 2012b).

**(2) Influence of slope gradient and aspect on landslide proneness:** In terms of slope gradient and landslide susceptibility regional assessment shows that in general a gradient range of 7° to 31° is landslide prone. In particular, the range between 26° and 31° exhibits significantly raised numbers of landslides within the Northern Vienna Forest (cp. Table 4-8, page 58). This result is in agreement with the statistical analysis of Schwenk et al. (1992) where landslide occurrences in Lower Austria are observed in the slope range of 15°–30°. Regarding the Flysch Zone, sliding processes were particularly registered at slopes with gradients above 29° (Schwenk et al. 1992). Thus, the modelled values are in accordance with the observed values (Neuhäuser et al. 2012a).

The significance of the slope aspect as steering geofactor is discussed controversially in literature (e.g. Gupta & Joshi 1990, Baeza & Corominas 2001, Dai & Lee 2002, Kanungo et al 2009). The slope aspect plays an important role in the present regional susceptibility

assessment. With positive, statistically significant weights the slope aspect has an evident positive association with the landslide distribution (cp. Table 4-8, page 58). Therefore, the model illustrates that the slope aspect has an influence on landslide proneness. In particular, the model reveals that slopes facing north, west and north-west are conspicuously more susceptible to landslides. The direction of slopes has a significant effect on their micro-climate, for example by influencing temperature as well as evapotranspiration. Consequently, the slope aspect indirectly steers the wetness conditions on the slope (Baeza & Corominas, Dai & Lee 2002). Due to reduced evapotranspiration slopes facing north can be colder and wetter than those facing south. Moreover, rates of precipitation depend on the slope aspect and wind direction (Thein 2000, Dai & Lee 2002). In the Northern Vienna Forest rainfall has a pronounced directional component on account of the influence of the prevailing westerly and north-westerly wind. This is due to the relevance of the Northern Vienna Forest as orographic barrier for atlantic, continental and alpine weather systems. Figure 7-1 shows the prevailing wind direction in the study area for the whole year as well as for January and July.

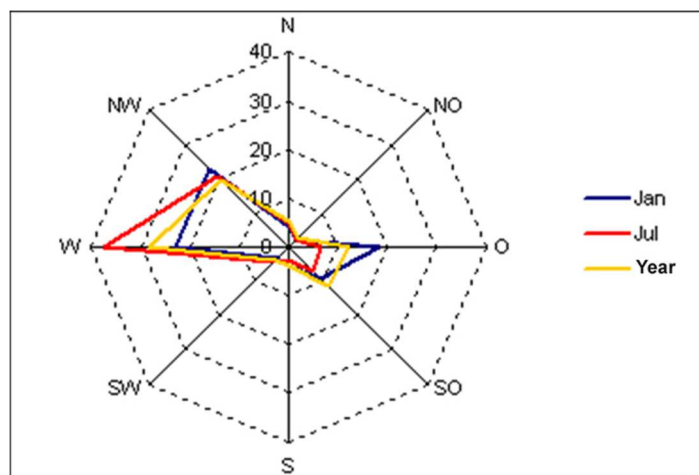


Figure 7-1. Prevailing wind direction in the Vienna Forest: distribution of wind direction in January, July and the whole year measured at the meteorological station in Mariabrunn (Zamg 2010c). The prevailing wind direction features conformity with the highest susceptible slope aspect classes (north, north-west and west) (cp. Figure 4-11, page 60).

The prevailing wind directions and slope aspects correlate with the highest susceptibility areas (cp. Figure 4-11, page 60). Therefore, it can be concluded that the windward directions west, north-west and north, which are highly susceptible to landslides, may receive higher rates of rainfall whereas slopes at the leeward slopes may be drier due to higher temperatures and rain shadow effects (Neuhäuser et al. 2012b).

- (3) Distribution of landslides related to fault systems and nappe boundaries:** The Northern Vienna Forest is tectonically highly disrupted (Schnabel 1992). Due to tectonic processes the Rhenodanubian Flysch is highly deformed and includes a lot of thrust faulting and folding as well as several thrust nappes as represented in Figure 3-6 (page 29). Regional assessment provides evidence that the occurrence of mass movements is closely connected to the fault system and nappe boundaries (cp. Figure 4-8, page 53). Landslide frequency increases with decreasing distance to the tectonic structures (cp. Table 4-5, page 52). The highest density of landslides (20%) is close (0 to 75m) to the thrust faults or nappe boundaries (Neuhäuser et al.

---

2012a, 2012b). It has been demonstrated in other studies that slope stability can be influenced by faults and other tectonic structures in different ways (Poisel & Eppensteiner 1986, Margielevski 2006, Damm et al. 2010, Pánek et al. 2010). In particular, nappe boundaries and thrust faults represent tectonically weak areas causing structural destabilisation (Margielevski 2006), intensified interflow, raised water permeability, and consequently intensified weathering. The mentioned factors have direct or indirect impact on slope stability (Pánek et al. 2010).

**(4) Landslide occurrence close to drainage lines:** The Northern Vienna Forest is characterised by a high density of streams creeks and temporarily water-bearing gullies. The regional model indicates a conspicuous spatial relationship between drainage lines and the occurrence of landslides (Neuhäuser et al. 2012a, 2012b). 38% of the registered landslides are located at a distance between 0 and 70m where the highest landslide density is present (cp. Table 4-7, page 56). Studies on the hydrological causes of landslides show that the presence of streams influences stability by toe erosion and/or by saturating the toe material and that increased landslide susceptibility is given in the proximity to drainage lines (Schmanke 1999, Thein 2000, Ercanoglu & Gokceoglu 2004, Sujatha et al. 2012). Hence, the distance to drainage lines is a commonly used geofactor in landslide susceptibility studies (Soeters & Van Westen 1996, Kanungo et al. 2009). However, an augmented landslide occurrence near drainage lines is not revealed in all study areas where comparable methods are applied to investigate landslide susceptibility (cf. Dai & Lee 2002). This indicates that the specific hydrological and hydro-geological conditions of a region are decisive for landslide proneness.

In the Northern Vienna Forest the raised density of landslides near streams and creeks can be explained by the fact that after heavy or long-lasting rainfall the region is affected by rapid surface runoff leading to floods and considerable erosive power in the drainage lines. Slope stability is reduced in the adjacent slopes by slope toe erosion or by water saturation of slope sediments. A further effect that has to be mentioned is the steepness and shape of the adjacent slopes. The streams and creeks are in many cases deeply incised and characterised by steep slopes, gullies or gorge-like structures like the Hagenbach valley.

**(5) Relevance of treeless areas for landslide evolution:** In this study an increased landslide density is observed in agriculturally used areas scattered between the forest areas (Neuhäuser et al. 2012a, 2012b). Although the majority of landslides affect areas with broad-leaved forest, treeless areas cause higher landslide dispositions in the Northern Vienna Forest (cp. Figure 4-9, page 55).

In general, a stabilising effect according to the root matrix system of forests can be assumed (Endo & Tsuruta 1969, Wu 1984, Greenway 1987). Stabilisation by vegetation is possible by hydrological and mechanical effects, which both elevate soil cohesion. However, field investigations and soil-mechanical investigations in the study area point out that a stabilising effect due to trees is not given (cf. Damm et al. 2008, Terhorst et al. 2009, Damm & Terhorst 2010). There is no evidence of considerable root development in the critical layers with a depth of 4 to 20m in general. Therefore, the low landslide density in forested areas may be attributed to the interception of rainfall by the crowns of the trees, leading to a reduced volume of rain infiltrating into the stratum (Götzinger 1943, Schwenk et al. 1992). This result is in agreement with former geomorphological studies in the Vienna Forest having also demonstrated that sliding processes are particularly found in treeless areas in the Flysch Zone (Götzinger 1943).

---

Subsequent to the analysis of the geofactors, described above, a regional landslide susceptibility map is produced on the basis of the landslide inventory and the weighted geofactors. The aim was to delineate landslide prone areas and to provide a regional landslide susceptibility map, which is not available up to now. In summary, the resulting regional susceptibility map (cp. Figure 4-12, page 63) reveals that the Northern Zone, a tectonic unit in the north of the study area, has extensive areas with the highest degree of landslide susceptibility. In this overthrust area to the Molasse Zone there are geological units which are highly susceptible to landslides. The modelling shows that the Wolfpassing Formation and the calcareous Klippen of the Northern Zone feature significantly high landslide densities (cp. Figure 4-7, page 51). These geological zones start in the north near St. Andrä-Wördern and continue in south-western direction along the ridges of the Tulbinger Kogel, Klosterberg, Frauenberg, and Eichberg as illustrated in the landslide susceptibility map (cp. Figure 4-12, page 63). The Greifenstein Nappe, which is located in the south of the Northern Zone, and the Kahlenberg Nappe are classified by moderate to locally high susceptibility. However, the series of the Gaultfölysch rich in clay situated in the Kahlenberg Nappe, drastically enhance landslide susceptibility. This stratum occurs at the north-east edge of Vienna and in Purkersdorf in Lower Austria. As no regional landslide susceptibility map exists, this information is new to the region. Although a small-scale hazard map for Lower Austria is being developed (Pomaroli et al. 2011), a study on regional scale is not available with the present level of detail until now.

Concerning the used method, the statistical/probabilistic method referred to as Weights-of-Evidence (WofE) (Agterberg et al. 1990, Bonham-Carter et al. 1989, Bonham-Carter 2002, Sawatzky et al. 2009) could provide quantitative spatial information on the predisposition to landslides. In this context, it must be stated that in WofE the susceptibility index provided in the final map must be regarded as relative degrees of susceptibility due to conditional dependence in the model. This potential overestimation of probabilities in WofE is a consequence of the inherent model assumption of conditional independence. A violation of this assumption, which can be hardly avoided because of the natural relations of geofactors, leads to an inflation of the probability values in absolute terms. On the other hand, underestimation cannot be precluded either due to possible undiscovered landslides in the study area (Agterberg & Cheng 2002). Therefore, the resulting probabilities represent relative degrees of susceptibility, which are appropriate and valid measures for landslide proneness. Thus, an appropriate quantification of landslide susceptibility can be reached with WofE.

Other methods may not feature difficulties associated with the violation of conditional independence. In logistic regression, for example, the assumption is immanent and need not be verified (Agterberg & Cheng 2002). Nevertheless, WofE is not constrained by the classical assumptions of the other parametric methods such as regression analysis or discriminant analysis including distributional assumptions, which cannot be fulfilled by spatial data.

The handling of uncertainty in the susceptibility index calculation and simplifications in the model were major claims of modelling. Apart from validation, the treatment of uncertainty is regarded as a crucial quality criterion in landslide susceptibility modelling (Chung & Fabbri 2003, Remondo et al. 2003, Van Westen et al. 2003, Fell et al. 2008). The demand for uncertainty measures for a reliable susceptibility assessment (Carrara et al. 1999, Chung & Fabbri 2003, Remondo et al. 2003, Van Westen et al. 2003, Fell et al. 2008) can be satisfied with WofE. It provides a measure for uncertainty of the weights and confidence of the final susceptibility index. A measure of confidence of the statistical parameters is calculated by the studentised contrast, which is the contrast divided by its standard deviation. This enables the estimation and mapping of relative uncertainty in posterior probability. The confidence of the calculation can be assessed by providing a normalised posterior probability, which is the posterior probability rescaled by the total standard deviation (Kemp et al.

---

1999). These measures, offered together with the results, improve the quality of susceptibility models (Fell et al. 2008).

A major effort was made to provide a high level of detail in the present work in spite of the huge size of the study area (573 km<sup>2</sup>) with a target scale of 1:20,000. This aspect is crucial because simplification is one of the major drawbacks in landslide susceptibility assessments (Carrara et al. 1991, Chung & Fabbri 2003, Remondo et al. 2003, Van Westen et al. 2003). Simplification is often done in regard to resolution but mainly by a reduction of the variety of geofactor classes, i.e. generalisation of data (Carrara et al. 1991, Chung & Fabbri 2003, Remondo et al. 2003, Van Westen et al. 2003). The multitude of geofactor classes depends on the level of detail of the input maps and on the size of the study area. The larger the study area and the level of detail, the higher the number of investigated geofactor classes. The number of classes, in turn, affects the statistical robustness of the calculated variables. Consequently, a sufficient number of landslide events are required in order to produce reliable statistical measures for each of the geofactor classes. Therefore, many WofE applications which contain a high level of detail are carried out at larger scales between 1:5,000 and 1:10,000 (e.g. Lee & Choi 2004, Dahal et al. 2008a, 2008b).

In this context the present work was able to show that a high level of detail could be kept related to the number of classes and a resolution of 30m despite the huge study area. It has been proven that a comprehensive landslide inventory as produced in the present work is the precondition for a detailed susceptibility assessment on a regional scale. The high number of mapped landslide events (471) warranted statistical robustness in spite of the high number of geofactor classes.

A further common simplification in WofE is achieved by the conversion of geofactor maps into a simple binary type (cf. Bonham-Carter 1994, Wang et al. 2002). Such a conversion of continuous datasets causes loss of information of the original geospatial character, which is recognised as a major drawback in landslide susceptibility studies (Carrara et al. 1991, Chung & Fabbri 2003, Remondo et al. 2003, Van Westen et al. 2003). With regard to this drawback as much variety as possible is kept in the data. This was accomplished by a multi-class generalisation of the geofactors (cf. Kemp et al. 1999, Porwal et al. 2001, Van Westen et al. 2003, Neuhäuser & Terhorst 2007). This is an extended approach of the original binary reclassification of the geofactors in WofE modelling (Bonham-Carter 1994, Wang et al. 2002).

In this context, the capability of WofE to process continuous data is an advantage in contrast to other statistical methods like logistic regression. Although a subsequent generalisation of the continuous data like slope gradient or distance layers is advisable in order to enhance the significance of the weights, the original character of the datasets can be preserved. This is reached by previous weighting of the continuous datasets without generalisation by applying a cumulative ascending or descending method for the calculation of the weights (Kemp et al. 1999, Porwal et al. 2001, Van Westen et al. 2003, Neuhäuser & Terhorst 2007). By means of this method the spatial relation of the geofactor to the landside distribution can be studied and proper class borders can be identified. Thus, the final classification reflects the original spatial association of geofactors and landslides as illustrated in the cumulative weighting (Kemp et al. 1999, Porwal et al. 2001, Van Westen et al. 2003, Neuhäuser & Terhorst 2007).

---

### 7.3 Local slope stability scenarios

The landslide phenomenon is further investigated by physically based slope stability scenarios in the Hagenbach valley in the Northern Vienna Forest. The development of various wetness scenarios for a comprehensive assessment of slope stability was a main aspect. Variable disposition which depends on conditions changing in the short and medium term is investigated, like substrate moisture depending on meteorological conditions (Zimmermann et al. 1997, Heckmann & Becht 2006).

Single precipitation events as well as monthly averages of precipitation are integrated for the assessment of substrate wetness. Thus, both short-term conditions due to singular weather events like abundant or heavy rainfall and medium-term conditions due to average monthly wetness conditions are considered in the scenarios.

Originally, the SINMAP approach (Pack et al. 2005) was designed to incorporate a single precipitation event or a period of wet weather for the estimation of recharge and consequently of topographic wetness (Pack et al. 2005). Most commonly recharge is equated with precipitation or effective precipitation (e.g. Mesina & Scarabelli 2007, Deb & El-Kadi 2009). In doing so, the quantity of recharge represents the flow created by a single rainfall event or critical period of wet weather, which is able to trigger landslides (Pack et al. 2005). Therefore, the development of a methodology to incorporate monthly averages of precipitation and air temperature into slope stability scenarios was necessary. The integration of water-balance calculations into the assessment of recharge represented an adequate method to adequately assess recharge volumes and consequently topographic wetness. In particular, average monthly recharge is deduced from water-balance calculations, which take soil water storage, surface runoff, evapotranspiration, and snow melting or storage into account (Steenhuis & Van der Molen 1986, McCabe & Markstrom 2007). This enabled the estimation of medium-term substrate moisture and the quantification of its change due to seasonal variability and forecast climate change. Therefore, a contribution to research on the hydrological causes of mass movements is provided with the actual work.

In total, the results of modelling demonstrate the high variability of landslide disposition due to varying wetness conditions. A detailed discussion of this variable disposition is specified in the following points:

- (1) Slope stability under average monthly wetness conditions:** Slope stability was analysed under average monthly climate conditions. The objective was to investigate if long-term substrate wetness has an influence on slope stability during the seasonal course. Long-term substrate moisture is still insufficiently integrated into slope stability and susceptibility assessment in current practice applications (cf. Brocca et al. 2008, Klose et al. 2012).

The scenarios display that under average monthly climate conditions the slope dynamics is characterised by an extension of old landslides. The slope stability maps show that the highest instability is found at the crown of old landslides where quaternary sediments crop out, leading to a backward denudation as illustrated in slope stability maps for January (cp. Figure 5-16, page 109), February (cp. Figure 5-20, page 114) as well as for July (cp. Figure 5-23, page 118). Movements in the quaternary sediments are responsible for slope instability at these moderately inclined slope positions (with slope gradients between 29° and 36°). Apart from the quaternary sediments the flysch bedrock is classified as instable over wide areas. In particular, hillslopes with an inclination of 36° and higher are considered instable. Such strongly inclined areas are present at the steep declivity to the valley bottom, i.e. the

---

flanks of the gorge as well as near the scarps of earlier landslides. Under average monthly wetness the deposited slide masses of former landslides are mainly classified as stable.

In summary, the comparison of the scenarios in the seasonal course gives evidence of the influence of medium-term development of the wetness conditions in the substrate on slope stability. In particular, the comparison of the scenarios based on the recharge volumes produced in the summer month of July and the winter month of February respectively yields a slight but measurable influence (5%) of average monthly wetness conditions on slope stability. As a consequence of increased topographic wetness in the winter month, there is an extension of instable areas by 5% in winter. The modelling results indicate that quaternary sediments are more moisture sensitive and exhibit a stronger response to the weather conditions related to slope stability. Therefore, the actual work strengthens the importance to integrate antecedent soil moisture conditions into slope stability calculations and disposition modelling. The changes in the wetness conditions could be quantified in spite of the application of medium-term monthly averaged data (ZAMG 2010c) and the connected smoothing and low temporal resolution.

Up to now research on the hydrological causes of landslides has mainly focused on the determination of rainfall-related thresholds (cf. Guzzetti et al. 2006a). Most commonly the intensity and duration of triggering rainfall events (cf. Cain 1980, Guzzetti et al. 2008) or the cumulative precipitation prior to landslide occurrence is taken into account (cf. Ibsen & Casagli 2004, Cardinali et al. 2006). However, the question is if soil moisture conditions, which are indeed partly regulated by precipitation, can be properly explained by any kind of rainfall data (cf. Brocca et al. 2008). The present work rather denotes that rainfall data can inadequately assess substrate wetness because there is a measurable influence of medium-term meteorological conditions and other components of the hydrological cycle, like evapotranspiration, soil moisture storage, surface runoff as well as snow storage and melting. It could be demonstrated by integration of water-balance calculations into the present work that substrate wetness is enhanced in the winter months although there is less precipitation than in the summer period. If only the precipitation amount was regarded for the determination of soil wetness, this would lead to an inverse interpretation of landslide instability during the seasonal course because there is typically less precipitation in winter. This finding strengthens the importance of hydrological analysis for the estimation of wetness conditions in the soils. The major challenge for future research efforts is the quantification and integration of antecedent soil moisture conditions into the assessment of slope stability and disposition modelling.

**(2) Slope stability under single precipitation events:** The models indicate that single rainfall events, have drastic influence on the short-term landslide disposition. The short-term effects of severe weather events on substrate wetness and slope stability are investigated in scenarios. In case of a precipitation event of 90 mm/day (ZAMG 2010a) there is a distinct shifting of substrate moisture towards saturated conditions in comparison to average monthly wetness in the summer month of July. This increased wetness causes a growth of instable areas of 13% of the study area (cp. Figure 6-24, page 170).

In case of the heavy rainfall event of 60 mm/h, which statistically reoccurs every 50 years (eHYD 2011), instability is even raised by 23% in comparison to average monthly wetness conditions in summer (cp. Figure 6-29, page 176). This extreme weather event drastically affects topographic wetness. The comparison of the maps yields saturated conditions nearly over the entire study area (cp. Figure 6-26, page 173).

---

Long-lasting rainfall does not solely enlarge instable areas. Such intensive precipitation affects overall slope dynamics because former landslide deposits are likely to be instable, too (cp. Figure 6-28, page 175). A reactivation of the former landslides is most probable. Those scenarios investigating the basic disposition to slope stability under average wetness conditions identified flow accumulation lines in relatively dry disposal masses. It can be concluded that the deposited slide masses are stable under average wetness conditions but have a disposition to instability due to accumulation of lateral discharge. It is shown that such flow convergence can grow to considerable zones of soil-saturation under above-average recharge.

**(3) Integration of quaternary sediments into slope stability calculation:** A further objective was the integration of shallow slope movements taking place in the quaternary sediments of the Vienna Forest into disposition modelling. The aim was to assess the relevance of quaternary sediments for slope dynamics in the Vienna Forest. In this context the target was to develop a site-specific process model which is able to incorporate movements into the quaternary deposits and the flysch bedrock, as well.

In summary, the integration of quaternary sediments into slope stability modelling results in a more realistic assessment of topographic wetness. In particular, low moisture conditions are drastically reduced (about 23%) in comparison to the model based on flysch bedrock only (cp. Figure 6-2, page 143). This decrease takes place for the benefit of partially wet conditions and saturation tendency in the stratum under average monthly recharge. In conclusion, it can be stated that the consideration of quaternary sediments in disposition modelling leads to increased substrate wetness in the models, which is more realistic in relation to field surveys, i.e. Damm et al. (2008), Terhorst et al. (2009), and Damm & Terhorst (2010). These studies point out that the sediments in the study area are characterised by hydromorphism due to moisture excess. Such hydromorphic characteristics are soils featuring stagnic features (pseudogleyification) and hematite coatings, which develop under water logging. Furthermore, the occurrence of seepage springs (so-called "Nassgallen"), which represent permanently wet areas, gives evidence of episodic or periodic water-oversaturation in the Northern Vienna Forest. These phenomena cannot be adequately explained by the scenario which takes the flysch bedrock into account only as a critical layer for the development of landslides.

The integration of quaternary sediments into disposition modelling leads not only to an extension of endangered areas by 19% but also to modified slope dynamics in the models (cp. Figure 6-3, page 144). In the model taking flysch bedrock into account only as a critical layer, the most instable areas are located near the valley bottom at the oversteepened slopes close to the Hagenbach creek. Only small instable areas occur at the scarps of previous landslides. In contrast to this, in the scenario which additionally takes quaternary sediments into account, the most instable slopes are situated at the crown and the scarp of former landslides where these deposits crop out. Consequently, the actual slope dynamics is dominated by backward denudation, which leads to an extension of the former landslides, by new shallow movements. Besides, areas in the upper slope positions with moderate inclination are highly landslide prone according to the modelling. The scenarios indicate that at such moderately inclined hillslopes shallow landslides in the quaternary sediments are responsible for slope instability.

The integration of quaternary sediments into the modelling is facilitated by specific process regions based on a geomorphological model of slope formation in the Hagenbach valley. The

---

process regions represent areas where different sliding planes are relevant. In general, landslide susceptibility and slope stability assessments can be applied only to a single landslide type (e.g. Van Westen et al. 2003, Neuhäuser & Terhorst 2007, Neuhäuser et al. 2012a). However, slope dynamics in the Hagenbach Valley is complex because different types of movements take place on the same slopes depending on the slope position and the state of development in relation to slope formation (Damm & Terhorst 2010). The processes can hardly be considered separately if the stability of the slopes is to be assessed. Taking into account the complexity of movements, the process regions are integrated into slope stability calculations as new kinds of mapping units.

In general, mapping or terrain units are defined as the proportion of land surface containing a set of ground conditions that differ from the adjacent units across definable boundaries (Fell et al. 2008, Kanungo et al. 2009). Common mapping units are geomorphological units, like landform units (cf. Carrara et al. 1991) or units automatically derived from overlays of parameters maps, like unique condition units (cf. Bonham-Carter et al. 1989, Aleotti & Chowdhury 1999) as well as simple regular grids (cf. Carrara et al. 1999). In SINMAP terminology the mapping units are referred to as calibration regions. By applying several calibration regions the physical input parameters can vary over the study area. Usually slope stability assessments using SINMAP are based on pedological (cf. Wawer & Nowocien 2003, Meisina & Scarabelli 2007) or geological mapping units, assuming that the geotechnical properties are related to these units (cf. Lan et al. 2004, Terhorst & Kreja 2009, Bai et al. 2010, Klimes & Blahut 2012). In the actual work these calibration regions are used to implement the concept of process regions as a new mapping unit. This enabled the consideration of complexity of the slope dynamics in the Vienna Forest. In particular different critical layers and consequently different types of movements could be integrated.

In spite of the applicability of the SINMAP method for slope stability scenarios in the actual case, there are some limitations of the approach in relation to investigated processes in the study area. The method of SINMAP is designed for shallow translational landsliding phenomena controlled by shallow groundwater flow convergence (Pack et al. 1998, 2005). Consequently, it is suited for shallow movements in the quaternary cover beds, whose stability is mainly controlled by the influence of water (Damm & Terhorst 2010). The actual work demonstrates that the application of the deep-seated movements in the flysch bedrock was possible but the modelling results showed reduced substrate wetness for the flysch bedrock in comparison with the quaternary sediments. Low moisture conditions are dominant throughout the seasonal course. This is due to the high transmissivity of the flysch bedrock, which in turn depends on the depth of the sliding layer. Therefore, the substrate wetness of the flysch bedrock might not be ideally represented by the SINMAP approach. Therefore, slope stability in the flysch bedrock is mainly steered by slope gradient in the modelling, whereas substrate wetness has minor influence on slope stability. The incorporation of deep-seated movements is subject to some restrictions.

- (4) Effects of climate change on slope stability:** Most of the susceptibility studies are based on the assumption that future landslides will develop under similar conditions as in the past and present. This accepted principle of “the past is the key to the future” becomes obsolete when climate change is taken into account. The conditions that prevailed in the past may be significantly altered by climate change (Crozier & Glade 2006). There are investigations on the effect of changed precipitation and temperature on the frequency and magnitude of landslides (Collison et al. 2000, Trauth et al. 2000, Soldati et al. 2004, Jakob & Lambert 2009).

---

However, climate change is hardly integrated into disposition modelling and landslide susceptibility studies (Klose et al. 2012). Therefore, an adaptation of landslide disposition modelling to climate change was carried out, which is regarded as a major challenge in the research field.

The results of the modelling based on the forecast climate change (Loibl et al. 2007, Reclip:more 2007, Formayer et al. 2009) demonstrate that a moderate change of slope stability in relation to average monthly substrate wetness is possible. Hence, the effect of changed air temperature and precipitation amount on slope stability could be quantified.

A slight but measurable impact of changing climate conditions on slope stability as forecast by climate scenarios (Loibl et al. 2007, Reclip:more 2007, Formayer et al. 2009) was determined in the modelling. The winter scenario based on the prognosticated climate change for 2050 (Loibl et al. 2007, Reclip:more 2007, Formayer et al. 2009) exhibits a negative effect on slope stability in comparison to the winter scenario based on average conditions as prevailing in the climate normals of the period of 1961 to 1990 (ZAMG 2010c). The average monthly temperature rise of 2° in combination with a precipitation increase of 30% in the winter months lead to a maximum augmentation of recharge of 36% in January in comparison to the climate normals. There is a slight augmentation of topographic wetness in the model, resulting in an extension of the instable areas by 3% (cp. Figure 6-21, page 166). This slightly raised instability under average monthly wetness reduces critical triggering thresholds for single rainfall events. This means that already lower precipitation thresholds can cause landslides in the study area compared to the present-day conditions. In general, the winter and spring periods exhibit the highest landslide activity during the seasonal course (Becht & Damm 2004, Schweigl & Hervas 2009). According to the modelling results climate change can additionally aggravate this landslide proneness by an increase of wetness.

In contrast to the winter months, the incorporation of forecast climate change until 2050 (Loibl et al. 2007, Reclip:more 2007, Formayer et al. 2009) into the modelling has a positive effect on slope stability in the summer months. The forecast average air temperature rise of 2.5° in combination with a reduction of the average monthly precipitation amount of 15% drastically decreases substrate moisture in summer. This raised dryness in the substrate causes a reduction of the instable areas by 11% in favour of the stable zones, according to the modelling results. This positive effect on slope stability in the model mainly results from the reduced monthly rainfall amounts and the increased evapotranspiration as a consequence of the raised air temperature. Despite this positive effect on slope stability in the scenario based on average recharge in the summer month of July, a drastic, short-term growth of instability is revealed under heavy and long-lasting rainfall events in the modelling. In case of a heavy rainfall event of 60mm/h, which has a statistical re-occurrence period of 50 years (eHYD 2011), instability is augmented by 23% in comparison to average monthly wetness conditions in July (cp. 6-29, page 176). Climate scenarios indicate that precipitation intensities will rise in the summer period (Frei et al. 2006, Formayer & Kromp-Kolb 2006, Hofstätter et al. 2010). Therefore, the summer months can reveal increased landslide proneness due to raised precipitation intensities in the future.

Furthermore it becomes apparent that the seasonal variance between summer and “winter scenario” in regard to slope stability is amplified due to climate change. According to the modelling results the instable areas are extended by 16% in the “future winter scenario” in comparison to the “future summer scenario” (cp. Figure 6-13, page 156). This greater difference is mainly due to the enhanced deviation of average monthly recharge in the summer and the winter scenarios.

---

Concluding it must be stated, that in order to consider soil-moisture more precisely in disposition modelling, new slope stability models should focus on an adaptation of the hydrological parameter. In this context the hydrological parameter (T/R) of the SINMAP method is a practicable variable but it has some major limitations due to its steady-state assumption. It represents a ratio of subsurface flow to the ability of the soil to drain water. Therefore, it is not able to take the time span of a rainfall event and the accumulation of recharge into account due to long-lasting periods of rainfall. The development of a hydrological model which is able to treat the latter issues and which can be properly integrated into slope stability calculations is the major challenge of forthcoming research efforts in disposition modelling.

## 7.4 Synthesis

By the application of two dissimilar modelling approaches the synthesis of the results shall provide a more complete assessment of the landside phenomenon in the study area. The results from the different disposition models complement each other and provide an integrated assessment of landslide susceptibility. It enables a comprehensive investigation of the disposition to landslides in the Vienna Forest.

On the one hand, the statistic-probabilistic landslide susceptibility zonation, as carried out in this paper, provides information on the basic disposition of the Northern Vienna Forest to develop landslides on a regional scale (scale 1:20,000). On the other hand, the large-scale, physically-based assessment allows the elaboration of the variable disposition, which depends on conditions changing in the short or medium term, like substrate wetness. Quaternary sediments are incorporated into the physically-based approach as a potential sliding layer. The synthesis of the results provides a more comprehensive assessment of landslide susceptibility than a single modelling approach.

Due to the hydrological conditions in the Vienna Forest heavy or long-lasting rainfall causes torrential conditions in streams and creeks, which fosters landslide proneness in adjacent hillslopes. The regional landslide susceptibility model underpins that fact by identifying an increased frequency of landslides in the proximity of drainage lines. Furthermore the regional model indicates that landslide susceptibility is enhanced on slopes facing north-west, which are exposed to the prevailing direction of advective rainfall in the study area. The latter geofactors display the significance of meteorological and hydrological conditions for the occurrence of landslides. These results of the regional susceptibility model are strengthened by the findings of the large-scale, physically-based models. They underpin the relevance of precipitation and hydrological conditions for landslide proneness. It has been shown in various wetness scenarios that slope instability is highly dependent on wetness conditions in the stratum. Beside short-term soil moisture conditions produced by a single weather event, the medium-term development of substrate moisture has a measurable effect on landslide activity in the Vienna Forest. A heavy rainfall event causes drastic reduction (23%) of instable areas but also persistent wetness conditions changing in the seasonal course influence the disposition to slope movements (by 5%), as well. It has been proven that quaternary sediments are more moisture sensitive and the influence of changing wetness conditions is stronger in these layers than in the bedrock.

Furthermore regional landslide susceptibility modelling depicts the relevance of zones rich in clay within the flysch formations as controlling geofactor. Until now the opinion that landslides primarily take place in the weathered flysch sandstones rich in clay-shales and marl (Götzinger 1943, Plöschinger & Prey 1993, Faupl 1996, Wessely 2006, Ivkovits 2005) has prevailed in the scientific

---

community. Also the present regional study emphasises the relevance of deep-seated mass movements in the zones rich in clay-shales.

However, the modellings demonstrate that landslide evolution and development cannot fully be explained on the basis of this process comprehension. Regional landslide susceptibility assessment gives evidence of increased landslide occurrence at slopes with moderate inclination. It confirms that hillslopes with a moderate inclination (26° to 31°) are highly landslide prone. The physically based models point out that shallow landslides in the quaternary sediments are responsible for slope instability at these moderately inclined hillslopes. When quaternary sediments are integrated into slope stability calculations also the upper slope positions with moderate inclination are highly landslide prone.

This finding is in accordance with geomorphological studies (Terhorst & Damm 2009, Damm & Terhorst 2010) in the Vienna Forest which give evidence that apart from the petrography of the flysch bedrock the soil-mechanical properties of the quaternary sediments can control the actual slope dynamics. It has been demonstrated that loess layers, periglacial cover beds and sandstones, partly decomposed, form the slope surface (Terhorst & Damm 2009, Damm & Terhorst 2010). Together with densely bedded basal periglacial layers, quaternary sediments are responsible for the development of landslides. It is assumed that the discrepancy between the permeability of the loess-influenced layers and the underlying basal periglacial cover bed, mainly consisting of marly and clayey material, is a fundamental controlling factor for the initiation and spatial distribution of mass movements (Damm et al. 2008, Terhorst et al. 2009).

Therefore, it can be concluded that beside of the Flysch bedrock, quaternary sediments are crucial for slope dynamics in the Vienna Forest according to modelling results. Consequently, it is most probable that a considerable portion of known landslides mapped in flysch actually occurred in quaternary sediments.

---

## References

- Agterberg, F.P. & Cheng, Q. (2002): Conditional independence test for Weights-of-Evidence modelling. *Natural Resource Research* 11(4): 249-255.
- Agterberg, F.P., Bonham-Carter, G.F. & Wright, D.F. (1990): Statistical pattern integration for mineral exploration. In: Gaal, G. & Merriam, D.F. (Eds.): *Computer application in resource estimation: prediction and assessment for metals and petroleum*. Pergamon, Oxford, 1-21.
- Akgun, A. (2012): A comparison of landslide susceptibility maps produced by logistic regression, multi-criteria decision, and likelihood ratio methods: a case study at Izmir, Turkey. *Landslides*, 9(1): 93-106.
- Aleotti, P. & Chowdhury, R. (1999): Landslide hazard assessment: Summary, review and new perspectives. *Bulletin of Engineering Geology & Environment* 58: 21-44.
- Anbalagan, R. (1992): Landslide hazard evaluation and zonation mapping in mountainous terrain. *Engineering Geology* 32: 269-277.
- Aspinall, R. (1992): An inductive modelling procedure based on Bayes' theorem for analysis of pattern in spatial data. *International Journal of Geographical Information Systems* 6(2): 105-121.
- Atkinson, P.M. & Massari, R. (1998): Generalized linear modeling of susceptibility to landsliding in the central Apennines, Italy. *Computers and Geosciences* 24: 373-385.
- Auer, I., Böhm, R., Mohnl, H., Potzmann, R., Schöner, W. & Skomorowski, P. (2001): ÖKLIM . Digitaler Klimaatlas Österreichs. Eine interaktive Reise durch die Vergangenheit, Gegenwart und Zukunft des Klimas. In: Hammerl, C., Lenhardt, W., Steinacker, R. & Steinhauser, P. (Eds.): *Die Zentralanstalt für Meteorologie und Geodynamik 1851-2001 - 150 Jahre Meteorologie und Geophysik in Österreich*. Leycam, Vienna. (CD ROM)
- Ayalew, L. & Yamagishi, H. (2005): The application of GIS-based logistic regression for landslide susceptibility mapping in the Kakuda-Yahiko Mountains, Central Japan. *Geomorphology* 65: 15-31.
- Bäk, R., Raetzo, H. & Mayer, K., von Poschinger, A. & Posch-Trözmüller, G. (2011): Mapping of geological hazards; Methods, Standards and Procedures (State of Development) – Overview. In: Skolaut, C. (Ed.) *Gefahrendarstellungen für Massenbewegungen (Hazard Mapping for Mass Movements)*, *Journal für Wildbach-, Lawinen-, Erosions- und Steinschlagschutz*, Society of Engineers in the Austrian Torrent and Avalanche Control, Austria, 166: 54-69.
- Baeza, C. & Corominas, J. (2001): Assessment of shallow landslide susceptibility by means of multivariate statistical techniques. *Earth Surface Processes and Landforms* 26(12): 1251-1263.
- Bai, S., Thiebes, B., Bell, R., Glade, T., & Wang, J. (2010): A comparison of susceptibility maps created with logistic regression and SINMAP for spatial planning in the Lanzhou City, China. *EGU General Assembly Conference Abstracts* 12: 6130 pp.
- Bailer-Jones, D. (2002): Naturwissenschaftliche Modelle. Von Epiostemologie zu Ontologie: In: Beckermann, A. & Nimitz, C. (Eds.): *Argument und Analyse – Sektionsvorträge*, Paderborn.
- Barredo, J., Benavides, A., Hervás, J., & van Westen, C. J. (2000): Comparing heuristic landslide hazard assessment techniques using GIS in the Tirajana basin, Gran Canaria Island, Spain. *International Journal of Applied Earth Observation and Geoinformation* 2(1): 9-23.
- Bathrellos, G.D., Kalivas, D.P. & Skilodimou, H., D. (2009): GIS-based landslide susceptibility mapping models applied to natural and urban planning in Trikala, Central Greece. *Estudios Geológicos* 65:49-65.
- Becht, M. & Damm, B. (2004): Geomorphologische und hydrologische Naturgefahren in Mitteleuropa. *Annals for Geomorphology Suppl.* 135: 180 pp.

- 
- Beguería, S. & Lorente, A. (1999): Landslide hazard mapping by multivariate statistics: Comparison of methods and case study in the Spanish Pyrenees. Project report of Damocles (Debris Fall Assessment in Mountain Catchments for Local End-Users), EVG1-Ct-1999-00007:5-16.
- Beven, K. J. & Kirkby, M. J. (1979): A physically based variable contributing area model of basin hydrology. *Hydrological Sciences Bulletin* 24(1): 43-69.
- Blaszczynski, J.S. (1997): Landform characterization with geographic information systems. *Photogrammetric Engineering and Remote Sensing* 63:183-191.
- Bonham-Carter, G.F. (2002) *Geographic information systems for geoscientist: Modelling with GIS*. Pergamon, New York, 302-334.
- Bonham-Carter, G.F., Agterberg, F.P. & Wright, D.F. (1989): Weights of evidence modelling: A new approach to mapping mineral potential. *Statistical Applications in Earth Science* 89(9): 171-183.
- Brabb, E.E. (1984): Innovative approaches to landslide hazard and risk mapping. In: *Proceedings of the 4th International Symposium on Landslides*, Canadian Geotechnical Society, Toronto: 307-323.
- Brunsdon, D. (1993): Mass movements; the research frontier and beyond: a geomorphological approach. *Geomorphology* 7: 85–128.
- Brix, F. (1969): On the stratigraphy and lithology of the flysch zone in the surroundings of the Hagenbach Valley (Northern Vienna Woods, Austria). *Rocznik Polskiego Towarzystwa Geologicznego, Annales de la Société Géologique de Pologne* 39 (1-3): 455-469.
- Brix, F. (1972): Hydrologie, Geologie und Bodenkunde. In: Ehrendorfer, F., Kaltenbacher, A., Niklfeld, H. & F. Starmühlner (Eds.): *Naturgeschichte Wiens. Jugend und Volk, Band II*, 51-73.
- Brocca, L., Melone, F. & Moramarco, T. (2008): On the estimation of antecedent wetness conditions in rainfall-runoff modeling. *Hydrological Processes* 22: 629-642.
- Cain, N. (1980): The rainfall intensity-duration control of shallow landslides and debris flows. *Geografiska Annaler* 62(A): 23-27.
- Calcaterra, D., De Riso, R., & Di Martire, D. (2004): Assessing shallow debris slide hazard in the Agnano Plain (Naples, Italy) using SINMAP, a physically based slope-stability model. In: Lacerda, W.A., Ehrlich, M., Fontoura, S.A.B. & Sayao, A.S.F. (Eds.): *Landslides: evaluation and stabilization*. Balkema, Taylor & Francis Group, London, 177-186.
- Cardinali, M., Galli, M., Guzzetti, F., Reichenbach, P. & Borri, C. (1994): Relationships between mass-movements and tectonic setting in the Carpina Basin, northern Umbria. *Geografia Fisica e Dinamica Quaternaria* 17: 3-17.
- Cardinali, M., Antonini, G., Reichenbach, P. & Guzzetti, F. (2001): Photo-geological and landslide inventory map for the Upper Tiber River Basin. *CNR Gruppo Nazionale per la Difesa dalle Catastrofi Idrogeologiche* 2154.
- Cardinali, M., Reichenbach, P., Guzzetti, F., Ardizzone, F., Antonini, G., Galli, M., Cacciano, M., Castellani, M. & Salvati, P. (2002a): A geomorphological approach to estimate landslide hazard and risk in urban and rural areas in Umbria, central Italy. *Natural Hazards and Earth System Sciences* 2(1–2): 57–72.
- Cardinali, M., Carrara, A., Guzzetti, F., & Reichenbach, P. (2002b): Landslide hazard map for the Upper Tiber River basin, *CNR Gruppo Nazionale per la Difesa dalle Catastrofi Idrogeologiche* 2116.
- Cardinali, M., Galli, M., Guzzetti, F., Ardizzone, F., Reichenbach, P. & Bartoccini, P. (2006): Rainfall induced landslides in December 2004 in south-western Umbria, central Italy: Types, extent, damage and risk assessment. *Natural Hazards and Earth System Sciences* 6: 237–260.
- Castellanos Abella, E.A. & Van Western, C.J. (2007): Generation of a landslide risk index map for Cuba using spatial multi-criteria evaluation. *Landslides* 4(4): 311-325.

- 
- Castellanos Abella, E.A. & van Westen, C.J. (2008): Qualitative landslide susceptibility assessment by multicriteria analysis: A case study from San Antonio del Sur, Guantánamo, Cuba. *Geomorphology* 94(3-4): 453-466.
- Carrara, A., Sorriso-Valvo, M. & Reali, C. (1982): Analysis of landslide form and incidence by statistical technique, Southern Italy. *Catena* 9: 35–62.
- Carrara, A. (1983): Multivariate models for landslide hazard evaluation. *Mathematical Geology* 15(3): 403–426.
- Carrara, A., Cardinali, M., Detti, R., Guzzetti, F., Pasqui, V. & Reichenbach, P. (1991): GIS techniques and statistical models in evaluating landslide hazard. *Earth Surface Processes and Landforms* 16(5): 427–445.
- Carrara, A., Cardinali, M., Guzzetti, F. & Reichenbach, P. (1995): GIS technology in mapping landslide hazard. In: Carrara, A., Guzzetti, F. (Eds.): *Geographical information systems in assessing natural hazards*, Kluwer, Dordrecht, 135-175.
- Carrara, A., Guzzetti, F., Cardinali, M. & Reichenbach, P. (1999): Use of GIS technology in the prediction and monitoring of landslide hazard. *Natural Hazards* 20: 117-135.
- Carrara, A., Giovanni, C. & Frattini, P. (2003): Geomorphological and historical data in assessing landslide hazard. *Earth Surface Processes and Landforms* 28: 1125-1142.
- Chen, C.L. (1982): Infiltration formulas by curve number procedure. *Journal of Hydraulics Division of the American Society of Civil Engineers* 108(HY7): 823-829.
- Chen, C.L. & Lee, C.F. (2003): A dynamic model for rainfall-induced landslides on natural slopes. *Geomorphology* 51(4): 269-288.
- Chleborad, A. F. (2003): Preliminary Evaluation of a Precipitation Threshold for Anticipating the Occurrence of Landslides in the Seattle, Washington, Area. U.S. Geological Survey Open-File Report 03-463.
- Chung, C.F & Fabbri, A. (2003): Validation of spatial prediction models for landslide hazard mapping. *Natural Hazards* 30(3): 451-472.
- Chung, C.F. (2006): Using likelihood ratio functions for modeling the conditional probability of occurrence of future landslides for risk assessment. *Computers & Geosciences* 32(8): 1052–1068.
- Collison, A., Wade, S., Griffiths, J., & Dehn, M. (2000): Modelling the impact of predicted climate change on landslide frequency and magnitude in SE England. *Engineering Geology*, 55(3): 205-218.
- Crozier, M. J., & Glade, T. (2006): *Landslide hazard and risk: Issues, concepts and approach*. Landslide hazard and risk. Wiley, West Sussex, 1-40.
- Dahal, R.K, Hasegawa, S., Nonomura, A, Yamanaka, M., Masuda, T. & Nishino, K. (2008a): GIS-based weights-of-evidence modelling of rainfall-induced landslides in small catchments for landslide susceptibility mapping. *Environmental Geology* 54(2): 311-324.
- Dahal, R.K, Hasegawa, S., Nonomura, A, Yamanaka, M., Dhakal, S. & Paudyal, p. (2008b): Predictive modelling of rainfall-induced hazard in the Lesser Himalaya of Nepal based on weights-of-evidence. *Geomorphology* 102(3): 496-510.
- Dai, F.C., Lee, C.F., Li, J. & Xu, Z.W. (2001): Assessment of landslide susceptibility on the natural terrain of Lantau Island, Hong Kong. *Environmental Geology* 40: 381– 391.
- Dai, F.C. & Lee, C.F. (2002): Landslide characteristics and slope instability modelling using GIS, Lantau Island, Hong Kong. *Geomorphology* 42(3): 213-228.
- Dai, F.C., Lee, C.F. & Ngai, Y.Y. (2002): Landslide risk assessment and management: An overview. *Engineering Geology* 64: 65-87.

- 
- Damm, B., Pflum, S. (2004): Geomorphologische Naturgefahren und Raumplanung – Bewertungsprobleme am Beispiel von Rutschgefahren in Südniedersachsen. *Annals of Geomorphology Suppl.* 135: 127-146.
- Damm, B., Becht, M., Varga, K. & Heckmann, T. (2010): Relevance of tectonic and structural parameters in Triassic bedrock formations to landslide susceptibility in quaternary hillslope sediments. *quaternary International* 222: 143-153.
- Damm, B. & Terhorst, B. (2010): A model of slope formation related to landslide activity in the Eastern Prealps, Austria. *Geomorphology* 122: 338-350.
- Damm, B., Terhorst, B., Kötritsch, E., Ottner, F. & Mayrhofer, M. (2008): Zum Einfluss bodenphysikalischer und bodenmechanischer Parameter in quartären Deckschichten auf Massenbewegungen im Wienerwald. *Abhandlungen der Geologischen Bundesanstalt* 62: 33-37.
- Deb, S.K. & El-Kadi, A.I. (2009): Susceptibility assessment of shallow landslides on Oahu, Hawaii, under extreme-rainfall events. *Geomorphology* 108: 219-213.
- Dietrich, W.E, Wilson, C.J., Montgomery, D.R., McKean, J. & Bauer, R. (1992): Erosion thresholds and land surface morphology, *Geology* (20): 675-679.
- Dikau, R., Brundsdon, D., Schrott, L. & Ibsen, M. (1996): *Landslide Recognition: Identification, Movement and Causes*. John Wiley & Sons: 251.
- DIN 1055-2 (1976): Lastannahmen für Bauten. Bodenkenngrößen, Wichte, Reibungswinkel, Kohäsion, Wandreibungswinkel. Deutscher Normenausschuss, Berlin.
- Endo, T. & Tsurata, T. (1969): Effects of tree's roots upon the shearing strengths of soils. 18th Annual Report of the Hokkaido Branch, Government Forest Experimental Station, Tokyo, 176-182.
- Ercanoglu, M. & Gokceoglu, C. (2004): Use of fuzzy relations to produce landslide susceptibility map of a landslide prone area (West Black Sea Region, Turkey). *Engineering Geology* 75(3-4): 229-250.
- Faupl, P. (1996): Tiefwassersedimente und tektonischer Bau der flyschzone des Wienerwaldes. In: Wagenreich, M. [Ed.]: *Exkursionsführer 11 - Sediment '96*, Geologische Bundesanstalt, Wien, 1-32.
- Fell, R., Corominas, J., Bonnard, C., Cascini, L., Leroi, E. & Savage, W.Z. (2008): Guidelines for landslide susceptibility, hazard and risk zoning for land-use planning. *Engineering Geology* 102(3-4): 85-98.
- Fels, J.E. & Zobel, R. (1995): Landscape position and classified landtype mapping for statewide DRASTIC mapping project. North Carolina State University Technical Report VEL.95.1. North Carolina Department of Environment, Health and Natural Resources, Division of Environmental Management, Raleigh, North Carolina.
- Fels, J.E. (1994): Modeling and mapping potential vegetation using digital terrain data: Applications in the Ellicott rock wilderness of North Carolina, South Carolina, and Georgia. Dissertation, North Carolina State University.
- Fiorucci, F., Cardinali, M., Carlà, R., Rossi, M., Mondini, A.C., Santurri, L., Ardizzone, F. & Guzzetti, F. (2011): Seasonal landslides mapping and estimation of landslide mobilization rates using aerial and satellite images. *Geomorphology* 129 (1–2): 59–70.
- Formayer, H., Clementschitsch, L., Hofstätter, M. & Kromp-Kolb, H. (2009): Vor Sicht Klima! Klimawandel in Österreich, regional betrachtet (Endbericht Global 2000). BOKU-Met Report 16, Institute for Meteorology, University of Natural Resources and Life Sciences, Vienna. [http://www.boku.ac.at/met/report/BOKU-Met\\_Report\\_16\\_online.pdf](http://www.boku.ac.at/met/report/BOKU-Met_Report_16_online.pdf).
- Formayer H., & Kromp-Kolb, H. (2006). Hochwasser & Klimawandel. Auswirkungen des Klimawandels auf Hochwasserereignisse in Österreich (Final Report WWF 2006). BOKU-Met Report 7, Institute for Meteorology, University of Natural Resources and Life Sciences, Vienna. [http://www.boku.ac.at/met/report/BOKU-Met\\_Report\\_07\\_online.pdf](http://www.boku.ac.at/met/report/BOKU-Met_Report_07_online.pdf).
-

- 
- Frei, C., Schöll, R., Fukutome, S., Schmidli, J. & Vidale, P.L. (2006): Future change of precipitation extremes in Europe: Intercomparison of scenarios from regional climate models. *Geophysical Research - Atmospheres* (1984-2012) 111: D06105.
- Gao, J. & Maroa, J. (2010): Topographic controls on evolution of shallow landslides in pastoral Wairarapa, New Zealand, 1979–2003. *Geomorphology* 114(3): 373–381.
- Ghini, A. (2003): A new contribution to the assessment of snow avalanche susceptibility: Application in Tyrol (Austria) and Alta Val Badia (Dolomites, Italy). Dissertation, Università Degli Studi de Modena e Reggio Emilia, 52-63.
- Gomez, H.T. & Kavzoglu, T. (2005): Assessment of shallow landslide susceptibility using artificial neural networks in Jabonosa River Basin, Venezuela. *Engineering Geology* 78(1-2): 11–27.
- Gorsevski, P.V., Gessler, P. & Foltz, R. B. (2000): Spatial prediction of landslide hazard using logistic regression and GIS. In: *Proceedings of the 4th International Conference on Integrating GIS and Environmental Modeling* 305(9): 234-241.
- Gorsevski, P.V., Jankowski, P., & Gessler, P.E. (2005): Spatial prediction of landslide hazard using fuzzy k-means and Dempster-Shafer theory. *Transactions in GIS* 9(4): 455-474.
- Götzinger, G. (1943): Neue Beobachtungen über Bodenbewegungen in der flysch Zone. *Mitteilungen der Österreichischen Geographischen Gesellschaft* 86: 87-104.
- Götzinger, G., Grill, R., Küpper, H. & Vettors, H. (1952): Geologische Karte der Umgebung von Wien 1:75,000. Geological Survey of Austria, Vienna.
- Götzinger, G. (1954): flyschzone. In: *Erläuterungen zur geologischen Karte der Umgebung von Wien 1:75,000*. Geological Survey of Austria, Vienna, 43-93.
- Govi, M., Mortara, G. & Sorzana, P.F. (1985): Hydrological events and landslides. *Geologia Applicata e Idrogeologia* 20: 359-375.
- Greenway, D.R. (1987): Vegetation and slope stability. In: Anderson, M.G., Richards, K.S. (Eds.): *Slope stability*. Wiley, New York, 187-230.
- Grill, R. (1968): Erläuterungen zur geologischen Karte des nordöstlichsten Weinviertels und zu Blatt Gänserndorf. Geological Survey of Austria, Vienna.
- Gritzner, M.L., Marcus, W.A., Aspinall, R. & Custer, S.G. (2001): Assessing landslide potential using GIS, soil wetness modelling and topographic attributes, Payette River, Idaho. *Geomorphology* 37: 149-165.
- Gupta, R.P. & Joshi, B.C. (1990): Landslide hazard zonation using the GIS approach - A case study from the Ramganga Catchment, Himalayas. *Engineering Geology* 28: 119-131.
- Guzzetti, F., Carrara, A., Cardinali, M. & Reichenbach, P. (1999): Landslide hazard evaluation: a review of current techniques and their application in a multi-scale study, Central Italy. *Geomorphology* 31: 181-216.
- Guzzetti, F., Reichenbach, P., Cardinali, M., Galli, M. & Ardizzone, F. (2005): Probabilistic landslide hazard assessment at the basin scale. *Geomorphology* 72: 272–299.
- Guzzetti, F., Galli, M., Reichenbach, P., Ardizzone, F. & Cardinali, M. (2006a): Landslide hazard assessment in the Collazzone area, Umbria, Central Italy. *Natural Hazards and Earth System Sciences* 6: 115–131.
- Guzzetti, F., Reichenbach, P., Ardizzone, F., Cardinali, M. & Galli, M. (2006b). Estimating the quality of landslide susceptibility models. *Geomorphology* 81: 166–184.
- Guzzetti, F., Peruccacci, S., Rossi, M. & Stark, C.P. (2008): The rainfall intensity-duration control of shallow landslides and debris flows: an update. *Landslides* 5: 3-17.
- Guzzetti F., Mondini A.C., Cardinali M., Fiorucci F., Santangelo M. & Chang K.T. (2012): Landslide inventory maps: new tools for and old problem. *Earth-Science Reviews* 112: 42-66.

- 
- Hammond, C., Hall, D., Miller S. & Swetik, P. (1992): Level I stability analysis (LISA) documentation for Version 2.0. General Technical Report INT-285, USDA Forest Service Intermountain Research Station.
- Hamon, W.R. (1961): Estimating potential evapotranspiration: Journal of the Hydraulics Division of the American Society of Civil Engineers 87: 107–120.
- Haneberg, W.C. (2004): The ins and outs of airborne LiDAR: An introduction for practicing engineering geologists. AEG News. 48(1): 16-10.
- Haneberg, W.C., Cole, W.F. & Kasali, G. (2009): High-resolution Lidar-based landslide hazard mapping and modeling, UCSF Parnassus Campus, San Francisco, USA. Bulletin of Engineering Geology and the Environment 68: 263–276.
- Hassing, H. (1905): Geomorphologische Studien. Aus dem inneralpinen Wiener Becken und seinem Randgebiet. In: Penk, A. (Ed.): Geographische Abhandlungen, Band VIII, 3.
- Haugerud, R.A., Harding, D.J., Johnson, S.Y., Harless, J.L, Weaver, C.S. & Sherrod, B.L. (2003): High-resolution LiDAR topography of the Puget Lowland, Washington. GSA Today 13(6): 4-10.
- Heckerman, D. (1986): Probabilistic interpretation of MYCIN's certainty factors. In: Kanal, L.N. & Lemmer, J.F.(Eds.): Uncertainty in Artificial Intelligence, North-Holland, New York, 167–196.
- Heckmann, T. & Becht, M. (2006): Statistical position modelling of mass movements. SAGA-analysis and modelling applications. Göttinger Geographische Abhandlungen 115: 61-73.
- Hjelmfelt, A.T. (1980): Curve number procedure as infiltration method. Journal of the Hydraulics Division of the American Society of Civil Engineers 106(6): 1107-1110.
- Hofstätter, M., Matulla C., Wang, J. & Wagner, S. (2010): PRISK-CHANGE. Veränderung des Risikos extremer Niederschlagsereignisse in Folge des Klimawandels. Project Report, Federal Meteorological Service of the Federal Ministry for Science and Research (Zentralanstalt für Meteorologie und Geodynamik des Bundesministeriums für Wissenschaft und Forschung), Austria. [http://www.zamg.at/cms/de/dokumente/klima/dok\\_projekte/prisk-change/endbericht-prisk-change](http://www.zamg.at/cms/de/dokumente/klima/dok_projekte/prisk-change/endbericht-prisk-change) (Jan 2012).
- Horton, R.E. (1945): Erosional development of streams and their drainage basins: hydro physical approach to quantitative morphology. Geological Society of America Bulletin 56: 275–370.
- Hutchinson, J.N. (1988): General report: morphological and geotechnical parameters of landslides in relation to geology and hydrology. In: Bonnard, C. (Ed.): Proceedings of the 5th International Symposium on Landslides, Balkema, Rotterdam, Netherlands, 1: 3–35.
- Hydrographischer Dienst (2009): Hydrographisches Jahrbuch von Österreich 2009, Band 117. Department VII/3 – Hydrologic Balance of the Ministry of Agriculture, Forestry, Environment and Water Management (Abteilung VII/3 des Bundesministeriums für Land- und Forstwirtschaft, Umwelt und Wasserwirtschaft).
- Ivkovits, T. (2005): Hangbewegungen im Einzugsgebiet des Hagenbaches im nordöstlichen Wienerwald. Diploma thesis, University of Vienna.
- Jakob, M., Holm, K., Lange, O. & Schwab, J. W. (2006): Hydrometeorological thresholds for landslide initiation and forest operation shutdowns on the north coast of British Columbia. Landslides 3: 228-238.
- Jakob, M., & Lambert, S. (2009): Climate change effects on landslides along the southwest coast of British Columbia. Geomorphology 107(3): 275-284.
- Jakob, M. & Weatherly, H. (2003): A hydroclimatic threshold for landslide initiation on the North Shore Mountains of Vancouver, British Columbia. Geomorphology 54: 137-156.
- Jemec, M. & Komac, M. (2011): An overview of approaches for hazard assessment of slope mass movements. In: Skolaut, C. (Ed.) Gefahrendarstellungen für Massenbewegungen (Hazard Mapping for Mass Movements), Journal für Wildbach-, Lawinen-, Erosions- und

- 
- Steinschlagschutz, Society of Engineers in the Austrian Torrent and Avalanche Control, Austria, 166: 55-69.
- Jenness, J. (2006): Topographic position index (tpi\_jen.avx) extension for ArcView 3.x, v. 1.3a. Jenness Enterprises Web. <http://www.jennessent.com/arcview/tpi.htm> (June 2010).
- Jibson, R. W., Harp, E. L., & Michael, J. A. (2000): A method for producing digital probabilistic seismic landslide hazard maps. *Engineering Geology* 58(3): 271-289.
- Kanungo, D.P., Arora, M.K., Sarkar, S. & Gupta, R.P. (2009): Landslide susceptibility zonation (LSZ) mapping – A review. *Journal of South Asia Disaster Studies* 2(1): 81-105.
- Kemp, L.D., Bonham-Carter, G.F. and Raines, G.L. (1999): Arc-WofE: Arcview extension for weights of evidence mapping. United States Geological Survey, Canada. <http://ntserv.gis.nrcan.gc.ca/sdm/> (March 2010)
- Khazai, B. & Sitar, N. (2000): Assessment of seismic slope stability using GIS modeling. *Geographic Information Sciences* 6(2): 121-128.
- Kienholz, H. (1977): Kombinierte geomorphologische Gefahrenkarte 1: 10.000 von Grindelwald. *Catena* 3(3-4): 265-294.
- Klimes, J. & Blahut, J. (2012): Landslide risk analysis and its application in regional planning: an example from the highlands of the Outer Western Carpathians, Czech Republic. *Natural Hazards* 64(2): 1779-1803.
- Klose, M., Damm, B. & Gerold, G. (2012): Analysis of Landslide Activity and Soil Moisture in Hillslope Sediments Using Landslide Database and Soil Water Balance Model. *Geoöko* 33(3-4): 204-231.
- Kociu A., Kautz H., Tilch N., Grösel K., Heger H. & Reischer J. (2007): Massenbewegungen in Niederösterreich. *Yearbook of the Geological Survey of Austria* 147: 215-220.
- Köttritsch, E.E. (2008): Quartäre Landschaftsentwicklung und aktuelle Morphodynamik am Beispiel von Rutschungshängen in der Hagenbachklamm (Wienerwald). Diploma thesis, University of Vienna.
- Kraut, C. (1999): Der Einfluss verschiedener Geofaktoren auf die Rutschempfindlichkeit an der Schichtstufe der Schwäbischen Alb. *Tübinger Geoscientific Works* D5: 1-148.
- Lan, H.X, Zhoua, C.H, Wangb, L.J, Zhangc, H.Y & Li, R.H. (2004): Landslide hazard spatial analysis and prediction using GIS in the Xiaojiang watershed, Yunnan, China. *Engineering Geology* 76: 109–128.
- Lee, S. & Min, K.D. (2001): Statistical analysis of landslide susceptibility at Yongin, Korea. *Environmental Geology* 40(9): 1095-1113.
- Lee, S. (2004): Application of likelihood ratio and logistic regression models to landslide susceptibility mapping using GIS. *Environmental Management* 34(2): 223-232.
- Lee, S. & Choi, J. (2004): Landslide susceptibility mapping using GIS and the weights-of-evidence model. *International Journal of Geographical Information Science* 18(8): 789-814.
- Lee, S., Ryu, J.H., & Kim, I.S. (2007): Landslide susceptibility analysis and its verification using likelihood ratio, logistic regression, and artificial neural network models: Case study of Youngin, Korea. *Landslides* 4(4): 327-338.
- Lin, M-L. & Tung, C-C. (2003): A GIS-based potential analysis of the landslides induced by the Chi-Chi Earthquake. *Engineering Geology* 71: 63-77.
- Liu, J.G., Mason, P.J, Clerici N., Chen, S.A., Davis, A., Miao, F., Deng, H. & Liang, L. (2004): Landslide hazard hazard assessment in the Three Gorges area of the Yangtze River using ASTER imagery: Zigui–Badong. *Geomorphology* 61: 171-187.
- Loibl W., Beck, A., Dorninger, M., Formayer, H., Gobiet, A. & Schöner, W. (2007): reclip:more - research for climate protection: model run elevation. Final Report, ARC-sys-0123, Austrian Research Centres GmbH, Vienna, Austria.

- 
- Magliulo, P., Di Lisio, A., Ruso, F. & Zelano, A. (2008): Geomorphology and landslide susceptibility assessment using GIS and bivariate statistics: a case study in southern Italy. *Natural Hazard* 47: 411-435.
- Marcelino, E.V., Formaggio, A.R. & Maeda, E.E. (2009): Landslide inventory using image fusion techniques in Brazil. *Applied Earth Observation and Geoinformation* 11: 181–191.
- Margielewski, W. (2006): Structural control and types of movements of rock mass in anisotropic rocks: Case studies in the Polish flysch Carpathians. *Geomorphology* 77: 7–68.
- Martha, T.R., Kerle, N., Jetten, V., van Westen, C. & Vinod Kumar, K. (2010): Characterising spectral, spatial and morphometric properties of landslides for semi-automatic detection using object-oriented methods. *Geomorphology* 116: 24–36.
- Mather, J.R. (1979): Use of the climatic water budget to estimate streamflow. In Mather, J.R. (Ed.): *Use of the climatic water budget in selected environmental water problems*. Laboratory of Climatology, *Publications in Climatology* 32(1): p. 1–52.
- Matulla, C., Penlap, E. K & von Storch, H. (2002). Empirisches Downscaling - Überblick und zwei Beispiele. In: *Deutscher Wetterdienst (Eds.): Klimastatusbericht 2002*, Offenbach, 20-31.
- Mayrhofer, M., Ottner, F., Terhorst, B., Köttritsch, E., Damm, B. (2008): Clay minerals and slope stability of quaternary sediments in landslide areas of the Wienerwald flysch Zone (Vienna Forest/Lower Austria). In: *Proceedings of the 4th Mid-European Clay Conference, Mineralogia, Zakopane*, 111-117.
- McCabe, G.J., & Wolock, D.M. (1999): Future snowpack conditions in the western United States derived from general circulation model climate simulations. *Journal of the American Water Resources Association* 35: 1473–1484.
- McCabe, G.J & Markstrom, S.L (2007): A monthly water-balance model driven by a graphical user interface. *U.S. Geological Survey Open-File Report 2007-1088*: 1- 6.
- Mehrotra, G.S., Sarkar, S., Kanungo, D.P., & Mahadevaiah, K. (1996): Terrain analysis and spatial assessment of landslide hazards in parts of Sikkim Himalaya. *Geological Society of India* 47:491–498.
- Meisina, C. & Scarabelli, S. (2007): A comparative analysis of terrain stability models for predicting shallow landslides in colluvial soils. *Geomorphology* 87: 207-223.
- Miles, S. B., & Ho, C. L. (1999): Rigorous landslide hazard zonation using Newmark's method and stochastic ground motion simulation. *Soil Dynamics and Earthquake Engineering* 18(4): 305-323.
- Mondini, A.C., Guzzetti, F., Reichenbach, P., Rossi, M., Cardinali, M. & Ardizzone, F. (2011): Semi-automatic recognition and mapping of rainfall induced shallow landslides using satellite optical images. *Remote Sensing of Environment* 115: 1743–1757.
- Montgomery, D.R. & Dietrich, W.E. (1994): A physically based model for the topographic control on shallow landsliding. *Water Resources Research* 30(4): 1153-1171.
- Morrissey, M.M., Wieczorek, G.F., & Morgan, B.A. (2004): Transient hazard model using radar data for predicting debris flows in Madison County, Virginia. *Environmental & Engineering Geoscience* 10(4): 285-296.
- Nagarajan, R., Roy, A., Vinod Kumar, R., Mukhetjess, A., & Khire, M. V. (2000): Landslide hazard susceptibility mapping based on terrain and climatic factors for tropical monsoon regions. *Bulletin of Engineering Geology and the Environment* 58(4): 275–287.
- Neubauer, f. & Höck, V. (2000): Aspects of geology in Austria and adjoining areas: Introduction. *Mitteilungen der Österreichischen Geologischen Gesellschaft* 92: 7-14.
- Neuhäuser, B. & Terhorst, B. (2007): Landslide susceptibility assessment using weights-of-evidence applied on a study site at the Jurassic escarpment of the Swabian Alb (SW-Germany). *Geomorphology* 86:12-24.

- 
- Neuhäuser, B. & Terhorst, B. (2009): GIS-gestützte, probabilistische Beurteilung der Hangrutschungsgefährdung an der Juraschichtstufe der Schwäbischen Alb. *Zeitschrift für Photogrammetrie – Fernerkundung – Geoinformation (PFG)* 2009(2): 143-160.
- Neuhäuser, B., Damm, B. & Terhorst, B. (2012a): GIS-based assessment of landslide susceptibility on the base of the weights-of-evidence model. *Landslides* 9(4): 511-528.
- Neuhäuser, B., Terhorst, B., Damm, B. (2012b): Identification and modelling in flysch areas of the European Alpine Foreland. In: Damm, B., Terhorst, B. & Thiemeyer, H. (Eds.): *Hillslope processes in geomorphic systems on varying temporal and spatial scales. Annals for Geomorphology* 56(4): 115–146.
- Neuhäuser, B., Schweigl, J., Damm, B. & Terhorst, B., (2012c): Rutschprozesse im Wienerwald in NÖ und Wien. In: Rudolf-Miklau, F. (Ed.) *Modellierung von Naturgefahren-Prozessen, Journal für Wildbach-, Lawinen-, Erosions- und Steinschlagschutz, Society of Engineers in the Austrian Torrent and Avalanche Control, Austria*, 169: 294-303.
- Norer R. (2011): Legal framework for hazard assessment and mapping of geological hazards on the international European and national level. In: Skolaut, C. (Ed.) *Gefahrendarstellungen für Massenbewegungen (Hazard Mapping for Mass Movements), Journal für Wildbach-, Lawinen-, Erosions- und Steinschlagschutz, Society of Engineers in the Austrian Torrent and Avalanche Control, Austria*, 166: 70-75.
- Oberhauser, R. (1980): *Der Geologische Aufbau Österreichs*. Springer, Vienna.
- Ohlmacher, C.G. & Davis, C.J. (2003): Using multiple regression and GIS technology to predict landslide hazard in northeast Kansas, USA. *Engineering Geology* 69: 331–343.
- Önorm L1061-1,-2 (2002): *Physikalische Bodenuntersuchungen - Bestimmung der Korngrößenverteilung des Mineralbodens*. Österreichisches Normungsinstitut, Wien.
- Önorm B4412 (1974): *Erd- und Grundbau - Untersuchung von Bodenproben - Korngrößenverteilung*. Österreichisches Normungsinstitut, Wien.
- Öwav (2013): *Arbeitsbehelf Niederschlag-Abfluss Modellierung*, Österreichischen Wasser- und Abfallwirtschaftsverbandes, Wien.
- Pachauri, A.K., & Pant, M. (1992): Landslide hazard mapping based on geological attributes. *Engineering Geology* 32: 81–100.
- Pack, R.T., Tarboton, D.G. & Goodwin, C.N. (1998): The SINMAP approach to terrain stability mapping. 8th congress of the international association of engineering geology, Vancouver, British Columbia, Canada.
- Pack, R.T., Tarboton, D.G., Goodwin, C.N. & Prasad, A. (2005): *A stability index approach to terrain stability hazard mapping, technical description and user guide for version 2.0.*, Utah State University.
- Pánek, T., Hradecký, J., Minár, J. & Silhán, K. (2010): Recurrent landslides predisposed by fault-induced weathering of flysch in the Western Carpathians. *Engineering Geology Special Publications* 23:183-199.
- Park, N. W. (2011): Application of Dempster-Shafer theory of evidence to GIS-based landslide susceptibility analysis. *Environmental Earth Sciences* 62(2): 367-376.
- Passalacqua, P., Tarolli, P. & Fofoula-Georgiou, E. (2010): Testing space-scale methodologies for automatic geomorphic feature extraction from LiDAR in a complex mountainous landscape. *Water Resources Research* 46: W11535.
- Perotto-Baldviezoa, H.L., Thurowb, T.L., Smithc, C.T., Fisherd, R.F. & Wu, X.B. (2004): GIS-based spatial analysis and modeling for landslide hazard assessment in steeplands, southern Honduras. *Agriculture, Ecosystems & Environment* 103(1): 165–176.
- Plöschinger, B. & Prey, S. (1993): *Der Wienerwald*. In: Schnabel W. (Ed.) *Sammlung Geologischer Führer* 59, Gebrüder Borntraeger, Berlin, Stuttgart.

- 
- Poisel, R. & Eppensteiner, W. (1986): Control of a large natural slope in a suburb of Vienna. In: Engineers Proceedings of the Conference on Rock Engineering and Excavation in an Urban Environment, Hong Kong, Institution of Mining and Metallurgy, London, 335-340.
- Pomaroli, G., Bell, R., Glade, T., Heiss, G., Leopold, P., Petschko, H., Proske, H. & J. Schweigl (2011): Darstellung der Gefährdung durch gravitative Massenbewegungen im Bundesland Niederösterreich als Grundlage der Raumplanung. In: Skolaut, C. (Ed.) *Gefahrendarstellungen für Massenbewegungen (Hazard Mapping for Mass Movements)*, Journal für Wildbach-, Lawinen-, Erosions- und Steinschlagschutz, Society of Engineers in the Austrian Torrent and Avalanche Control, Austria, 166: 198-212.
- Porwal, A., Carranza, E.J.M & Hale, M. (2001): Extended weights-of-evidence modelling for predictive mapping of base metal deposit potential in Aravalli province, western India. *Exploration and Mining Geology* 10(4): 273-287.
- Pradhan, B. & Lee, S. (2010): Regional landslide susceptibility analysis using back-propagation neural network model at Cameron Highland, Malaysia. *Landslides* 7(1): 13-30.
- Prey, S. (1965): Neue Gesichtspunkte zur Gliederung des Wienerwaldflysches, *Verhandlungen der Geologische Bundesanstalt* 68, Geological Survey of Austria, Vienna, 107-118.
- Ramos, V.M., Guimarães, R.F., Carvalho Júnior, O. A., Redivo, A. L., Gomes, R.A.T., Cardoso, F.B.F., & Fernandes, N.F. (2007): Algorithm development for incorporating soil physical properties of each different soil class in a landslide prediction model (SHALSTAB). *Solos e Rochas* 30: 139-148.
- Refice, A. & Capolongo, D. (2002): Probabilistic modelling of uncertainties in earthquake-induced landslide hazard assessment. *Computers & Geosciences* 28(6): 735-749.
- Reger, J.P. (1979): Discriminant analysis as a possible tool in landslide investigations. *Earth Surface Processes and Landforms* 4: 267-273.
- Rieder, A. (2002): *Der Wienerwald. Natur, Geschichte und Kultur einer einzigartigen Landschaft.* Verlag Christian Brandstätter, Vienna.
- Rietz, P.D. & Hawkins, R.H. (2000): Effects of land use on runoff curve numbers. In: *Proceedings Watershed Management Symposium 2000*, American Society of Civil Engineers, Fort Collins Co. (CD Rom)
- Rudolf-Miklau, F. (2009): *Naturgefahren-Management in Österreich. Vorsorge – Bewältigung – Information.* LexisNexis, Vienna, 1-252.
- Rudolf-Miklau, F., Bäk, R., Schmid, F. & Skolaut, C. (2011): Hazard mapping for mass movements: Strategic importance and transnational development of standards in the ASP-project AdaptAlp. In: Skolaut, C. (Ed.) *Gefahrendarstellungen für Massenbewegungen (Hazard Mapping for Mass Movements)*, Journal für Wildbach-, Lawinen-, Erosions- und Steinschlagschutz, Society of Engineers in the Austrian Torrent and Avalanche Control, Austria, 166: 12-19.
- Saha, A.K., Gupta, R.P., Sarkar, I., Arora, M.K. & Csaplovics, E. (2005): An approach for GIS-based statistical landslide susceptibility zonation - with a case study in the Himalayas. *Landslides* 2: 61-69.
- Sawatzky, D.L., Raines, G.L., Bonham-Carter, G.F. & Looney, C.G. (2009): Arc-SDM: Spatial data modeller (SDM): ArcMap 9.3 geoprocessing tools for spatial modelling using weights of evidence, logistic regression, fuzzy logic and neural networks. <http://www.ige.unicamp.br/sdm/> (June 2010).
- Schmidt, J.A. & Dikau, R. (2004): Modelling historical climate variability and slope stability. *Geomorphology* 60(3-4): 433-447.
- Schnabel, W. (1992): New data on the flysch Zone of the Eastern Alps in the Austrian sector and new aspects concerning the transition to the flysch Zone of the Carpathians. *Cretaceous Research* 13: 405-419.

- 
- Schnabel, W. (2002): Niederösterreich, Geologische Karte 1:200,000 mit Kurzerläuterung. Geological Survey of Austria, Vienna.
- Scholten, T. (2003): Beitrag zur flächendeckenden Ableitung der Verbreitungssystematik und Eigenschaften periglazialer Lagen in deutschen Mittelgebirgen. In: Bremer, H., Brunnacker, K., Heine, K., Lauer, W. (Eds.): Relief, Boden, Paläoklima (19), Gebrueder Borntraeger, Berlin, Stuttgart: 16-46.
- Schweigl, J. & Hervas, J. (2009): Landslide Mapping in Austria. JRC Scientific and Technical Report EUR 23785 EN, Institute for Environment and Sustainability of the Joint Research Centre, European Commission, Luxembourg, 1-61.
- Schwenk, H., Spendlingwimmer, R. & Salzer, F. (1992): Massenbewegungen in Niederösterreich. Yearbook of the Geological Survey of Austria 135 (2): 597-660.
- Semmel, A. & Terhorst, B. (2010): The concept of the Pleistocene periglacial cover beds in Central Europe – A review. *quaternary International* 222(1-2): 120-128.
- Shafer, G. (1976): A mathematical theory of evidence. Princeton University Press, 6-18.
- Shortliffe, E.H. & Buchanan, G.G. (1975): A model of inexact reasoning in medicine. *Mathematical Bioscience* 23: 351–379.
- Soeters R. & Van Westen, C.J. (1996): Slope stability recognition, analysis, and zonation: Application of geographical information system to landslide hazard zonation. In: Turner, A.K., Schuster, R.L. (Eds.): Landslides investigation and mitigation. Special Report 247, Transportation Research Board of the National Research Council, National Academy Press, Washington D.C.
- Soldati, M., Corsini, A., & Pasuto, A. (2004): Landslides and climate change in the Italian Dolomites since the Late glacial. *Catena* 55(2): 141-161.
- Steenhuis, T.S. & Van der Molen, W.H. (1986): The Thornthwaite-Mather procedure as a simple engineering method to predict recharge. *Journal of Hydrology* 84: 221-229.
- Stevenson, P.C. (1977): An empirical method for the evaluation of relative landslide risk. *Bulletin of the International Association of Engineering Geology* 16(1): 69-72.
- Stumpf, A. & Kerle, N. (2011): Object-oriented mapping of landslides using Random Forest. *Remote Sensing of Environment* 115(10): 2564–2577.
- Sujatha, E.R, Rajamanickam, , E.R. & Kumaravel, G,V. (2012): Landslide susceptibility analysis using probabilistic certainty factor approach: A case study on Tevankarai stream watershed, India. *Journal of Earth System Science* 121: 1337-1350.
- Suzen, M.L. & Doyuran, V. (2004): A comparison of the GIS based landslide susceptibility assessment methods: multivariate versus bivariate. *Environmental Geology* 45: 665-679.
- Tangestani, M.H. (2004): Landslide susceptibility mapping using the fuzzy gamma approach in a GIS, Kakan catchment area, southwest Iran. *Australian Journal of Earth Sciences* 51(3): 439-450.
- Tangestani, M.H. (2009): A comparative study of Dempster–Shafer and fuzzy models for landslide susceptibility mapping using a GIS: An experience from Zagros Mountains, SW Iran. *Journal of Asian Earth Sciences* 35(1): 66-73.
- Tarolli, P., Sofia, G. & Dalla Fontana, G. (2010): Geomorphic features extraction from high resolution topography: landslide crowns and bank erosion. *Natural Hazards* 61(1): 65-83.
- Terlien, M.T.J., van Westen, C.J. & Asch T.W.J. (1995): Deterministic modelling in GIS based landslide hazard assessment. In: Carrara, A. & Guzzetti, F. (Eds.): Geographical information systems in assessing natural hazards. Kluwer Academic Publishers, Netherlands, 57-77.
- Terhorst, B. (2001): Mass movements of various ages on the Swabian Jurassic escarpment: Geomorphological processes and their causes. *Annals of Geomorphology Supp.* 125: 105-127.
- Terhorst, B. (2007): Soil distribution and periglacial cover beds in the Jurassic Cuesta scarp in SW-Germany. *Catena* 71: 467–476.

- 
- Terhorst, B., & Kreja, R. (2009): Slope stability modelling with SINMAP in a settlement area of the Swabian Alb. *Landslides* 6(4): 309-319.
- Terhorst, B., Damm, B., Peticzka, R. & Kötttritsch, E. (2009): Reconstruction of quaternary landscape formation as a tool to understand present geomorphological processes in the Eastern Prealps (Austria). *quaternary International* 209: 66-78.
- Terhorst, B. & Damm, B. (2009): Slope stability and slope formation in the flysch Zone of the Vienna Forest (Austria). *Journal of Geological Research* 2009: 1-10.
- Thein, S. (2000): Massenverlagerungen an der Schwäbischen Alb; Statistische Vorhersagemodelle und regionale Gefährdungskarten unter Anwendung eines Geographischen Informationssystems. In: Bibus, E., Terhorst, B. (Eds.): *Tübinger Geowissenschaftliche Arbeiten, Reihe D: Geoökologie und Quartärforschung*, Tübingen, 1-38.
- Thenius, E. (1974): *Niederösterreich. Geologie der österreichischen Bundesländer in kurzgefassten Einzeldarstellungen*, 2. Auflage, Geologische Bundesanstalt, Wien.
- Thiebes, B. (2006): Räumliche Gefährdungsmodellierung flachgründiger Hangrutschungen – GIS gestützte Analyse an der Schwäbischen Alb. Master Thesis, University of Bonn, Germany.
- Thorntwaite, C.W. (1948): An approach toward a rational classification of climate. *Geographical Review* 38: 55–94.
- Thorntwaite, C.W. & Mather, J.R. (1957): Instructions and tables for computing potential evapotranspiration and the water balance. *Publications in Climatology*, Centerton, New Jersey, Laboratory of Climatology 10(3): 185-311.
- Thiebes, B. (2007): Deterministic landslide susceptibility analysis using SINMAP- a case study in the Swabian Alb. *Geophysical Research Abstracts* 9(11199).
- Trauth, M.H., Alonso, R.A., Haselton, K.R., Hermanns, R.L., & Strecker, M.R. (2000): Climate change and mass movements in the NW Argentine Andes. *Earth and Planetary Science Letters* 179(2): 243-256.
- Trigila, A., Iadanza, C. & Spizzichino, D., (2010): Quality assessment of the Italian landslide inventory using GIS processing. *Landslides* 7: 455–470.
- Tufescu, V. (1970): Mudflows in the flysch Carpathians and Bend Sub-Carpathians of Romania. *Annals of Geomorphology N.F.* (9): 146-156.
- Van Asch, T.W.J., Buma, J. & Van Beek, L.P.H (1999): A view on some hydrological triggering systems in landslides. *Geomorphology* 30(1): 25-32.
- Van Beek, L.P.H. & Van Asch, T.W.J. (2003): Regional assessment of the effects of land-use change on landslide hazard by means of physically based modelling. *Natural Hazards* 31: 289-304.
- Van Den Eeckhaut, M., Poesen, J., Verstraeten, G., Vanacker, V., Moeyersons, J., Nyssen, J., Van Beek, L.P.H. & Vandekerckhove, L. (2007): Use of LIDAR-derived images for mapping old landslides under forest. *Earth Surface Processes and Landforms* 32: 754–769.
- Van Den Eeckhaut, M., Reichenbach, P., Guzzetti, F., Rossi, M., & Poesen, J. (2009): Combined landslide inventory and susceptibility assessment based on different mapping units: an example from the Flemish Ardennes, Belgium. *Natural Hazards and Earth Systems Science* 9: 507–521.
- Van Westen, C.J., Saldaña López, A., Uria Cornejo, S.P. & Chavez Ardanza (1997): Statistical landslide hazard analysis. In: *ILWIS 2.1 for Windows Application Guide*. International Institute for Aerospace Survey & Earth Sciences (ITC), Enschede: 73–84.
- Van Westen, C.J., Seijmonsbergen, A.C. & Mantovani, F. (1999): Comparing landslide hazard maps. *Natural Hazards* 20: 137-158.
- Van Westen, C.J., Rengers, N. & Soeters, R. (2003): Use of geomorphological information in indirect landslide susceptibility assessment. *Natural Hazards* 30: 399–419.

- 
- Van Westen, C.J. (2004): Geo-information tools for landslide risk assessment: An overview of recent developments. In: *Landslides: Evaluation and Stabilization, Proceedings of the 9th International Symposium on Landslides*, Rio de Janeiro, Brazil, 39-56.
- Van Westen, C.J., Van Asch, T.W. & Soeters, R. (2006): Landslide hazard and risk zonation-why is it still so difficult?. *Bulletin of Engineering Geology and the Environment* 65(2): 167-184.
- Van Westen, C.J., Castellanos Abella, E.A. & Sekhar, L.K. (2008): Spatial data for landslide susceptibility, hazards and vulnerability assessment : An overview. *Engineering Geology* 102(3-4): 112-131.
- Varnes, D.J. (1987): Slope movement types and processes. In: Schuster, R.L. & Krizek R.J. (Eds.): *Landslides, Analysis, and Control, Special Report 176*, Transportation Research Board, Washington, 12-33.
- Wang, H., Chai, G. & Cheng, Q. (2002): Data integration using weights of evidence model: application in mapping mineral resource potentials. *International Archives of Photogrammetry, Remote Sensing and Spatial Information Science* 34(4): 48-53.
- Wang, H.B., Xu, W.Y. & Xu, R.C. (2005): Slope stability evaluation using back propagation neural networks. *Engineering Geology* 80 (3-4): 302-315.
- Wawer, R. & Nowocien, E. (2003): Application of SINMAP terrain stability model to Grodarz stream watershed. *Electronic Journal of Polish Agricultural Universities, Environment Development* 6(1): 1-17.
- Weilguni, V. (2009): Bemessungsniederschläge in Österreich. *Wiener Mitteilungen Wasser-Abwasser-Gewässer* 216: 71-84.
- Weiss, A. (2001): Topographic position and landforms analysis. *ESRI User Conference*, San Diego, CA.
- Weppner, E., Hoyt, J. & Haneberg, W.C. (2008): Lidar-based landslide hazard modeling using PISA-m, SHALSTAB, and SMORPH. In: *AGU Fall Meeting Abstracts 1, Freshwater Creek and Ryan Slough watershed, Humboldt County, California*.
- Wessely, G. (2006): *Niederösterreich. Geologie der Österreichischen Bundesländer*. Geologische Bundesanstalt, Vienna.
- Wiche, K. (1952): Die Oberflächenformen des Wienerwaldes. In: Arnberger, E. & R. Wismeyer (Eds): *Ein Buch vom Wienerwald – Vom Wesen und der Gestaltung seiner Landschaft*. Jugend und Volk, 15-18.
- Wieczorek, G.F. (1984): Preparing a detailed landslide-inventory map for hazard evaluation and reduction. *Bulletin of the Association of Engineering Geologists* 21(3): 337-342.
- Wolock, D.M. & McCabe, G.J. (1999): Effects of potential climatic change on annual runoff in the conterminous United States: *Journal of the American Water Resources Association* 35: 1341–1350.
- World Meteorological Organization (1989): Calculation of monthly and annual 30-year standard normals. WCDP-No. 10, WMO-TD/No. 341, World Meteorological Organization.
- World Meteorological Organization (2007): The role of climatological normals in a changing climate. WCDP-No. 61, WMO-TD/No. 1377, World Meteorological Organization.
- Wu, T.H. (1984): Effect of vegetation on slope stability. – Soil reinforcement and moisture effects on slope stability, Transportation Research Board, Washington.
- Yin, K.L. & Yan, T.Z. (1988): Statistical prediction model for slope instability of metamorphosed rocks. In: Bonnard, C. (Ed.): *Proceeding Fifth International Symposium on Landslides*, Lausanne, Balkema, Rotterdam 2: 1269-1272.
- Zadeh, L.A. (1965): Fuzzy Sets. *Information and Control* 8: 338-353.
- ZAMG (2010a): Monatsrückblick (Juni 2009). *Klima aktuell*. Federal Meteorological Service of the Federal Ministry for Science and Research (Zentralanstalt für Meteorologie und Geodynamik des

- 
- Bundesministeriums für Wissenschaft und Forschung), Austria. <http://www.zamg.ac.at> (May 2010)
- ZAMG (2010b): Jahresrückblick (2009). Klima aktuell. Federal Meteorological Service of the Federal Ministry for Science and Research (Zentralanstalt für Meteorologie und Geodynamik des Bundesministeriums für Wissenschaft und Forschung), Austria. <http://www.zamg.ac.at> (May 2010)
- Zêzere, J. L., Trigo, R. M. & Trigo, I. F. (2005): Shallow and deep landslides induced by rainfall in the Lisbon region (Portugal): assessment of relationships with the North Atlantic Oscillation. *Natural Hazards and Earth System Sciences* 5: 331-344.
- Zimmermann, M., Mani, P. Gamma, P., Gsteiger, P., Heiniger, O. & Hunziger, G. (1997): Murgefahren und Klimaänderung – ein GIS-basierter Ansatz. Final Report of the Swiss National Research Programme „Climate Change and Natural Disasters (NFP 31)“, vdf Publisher of the Swiss Federal Institute of Technology Zurich: 1-162.

## Data & Maps

- Aster (2010): ASTER Global Digital Elevation Model. Earth Remote Sensing Data Analysis Center (ERSDAC)
- Auer, I., Böhm, R., Mohnl, H., Potzmann, R., Schöner, W. & Skomorowski, P. (2001): ÖKLIM . Digitaler Klimaatlas Österreichs. Eine interaktive Reise durch die Vergangenheit, Gegenwart und Zukunft des Klimas. In: Hammerl, C., Lenhardt, W., Steinacker, R. & Steinhauser, P. (Eds.): Die Zentralanstalt für Meteorologie und Geodynamik 1851-2001 - 150 Jahre Meteorologie und Geophysik in Österreich. Leycam, Vienna. (CD ROM)
- BEV (2010): Digitales Landschaftsmodell (DLM): Gewässer, Geographische Namen, Siedlung, Verkehr. Landscape information - Survey Group (Landschaftsinformation - Gruppe Vermessungswesen), Federal Office of Metrology and Surveying (Bundesamt für Eich- und Vermessungswesen), Austria.
- CLC (1990): CORINE Land cover 1990 dataset. Produced in the Coordination of Information on the Environment (CORINE) Programme of the European Commission. European Environment Agency (EEA), Denmark. <http://eea.europa.eu/data-and-maps/data/corine-land-cover-1990-raster-2> (December 2009).
- eHYD (2011): Das Portal für hydrographische Daten Österreichs im Internet. Department VII/3 – Hydrologic Balance of the Ministry of Agriculture, Forestry, Environment and Water Management (Abteilung VII/3 des Bundesministeriums für Land- und Forstwirtschaft, Umwelt und Wasserwirtschaft. <http://ehyd.gv.at> (Jan 2011).
- GBA (2010): GBA-Online: Web-Applikation Massenbewegungen (Mass movements). Online database on mass movements. Geological Survey of Austria (Geologische Bundesanstalt), Austria. <http://geomap.geolba.ac.at/MASS/index.cfm> (May 2010).
- Götzinger, G. (1943): Neue Beobachtungen über Bodenbewegungen in der flysch Zone. *Mitteilungen der Österreichischen Geographischen Gesellschaft* 86: 87-104.
- Götzinger, G., Grill, R., Küpper, H. & Vettors, H. (1952): Geologische Karte der Umgebung von Wien 1:75,000. Geological Survey of Austria, Vienna.
- Provincial Government of Lower Austria (2006): Laserscan, ASCII-Grid format. Construction Group – Division of Survey and Geoinformation (Gruppe Baudirektion – Abteilung Vermessung und Geoinformation), Provincial Government of Lower Austria (Niederösterreichische Landesregierung), Austria.

- 
- Provincial Government of Lower Austria (2010): Building Ground Register (Baugrundkataster). Construction Group, Provincial Government of Lower Austria (Niederösterreichische Landesregierung), Austria.
- Reclip:More (2007): Klimazukunft Österreich. Kleinräumige Klimaszenarien 1981-1990 und 2041-2050. Signale des Klimawandels. Final reports, Research Project of the Kwiss-Programme: Research for Climate Protection: Model Run Evaluation.
- Schnabel, W. (2002): Niederösterreich, Geologische Karte 1:200,000 mit Kurzerläuterung. Geological Survey of Austria, Vienna.
- WLV (2010): Technical reports for reinstatement measures (Technische Berichte für Instandsetzungsarbeiten). Forest Technical Service (Forsttechnischer Dienst), Austrian Service of Torrent and Avalanche Control – Department IV/5 of the Ministry of Agriculture, Forestry, Environment and Water Management (Wildbach und Lawinenverbauung - Abteilung IV/5 des Bundesministeriums für Land- und Forstwirtschaft, Umwelt und Wasserwirtschaft).
- ZAMG (2010a): Monatsrückblick (Juni 2009). Klima aktuell. Federal Meteorological Service of the Federal Ministry for Science and Research (Zentralanstalt für Meteorologie und Geodynamik des Bundesministeriums für Wissenschaft und Forschung), Austria.  
<http://www.zamg.ac.at/cms/de/klima/monatsrueckblick> (May 2010)
- ZAMG (2010b): Jahresrückblick (2009). Klima aktuell. Federal Meteorological Service of the Federal Ministry for Science and Research (Zentralanstalt für Meteorologie und Geodynamik des Bundesministeriums für Wissenschaft und Forschung), Austria.  
<http://www.zamg.ac.at/cms/de/klima/jahresrueckblick> (May 2010)
- ZAMG (2010c): Klimanormalwerte Österreich 1961-1990. Klimaübersichten. Federal Meteorological Service of the Federal Ministry for Science and Research (Zentralanstalt für Meteorologie und Geodynamik des Bundesministeriums für Wissenschaft und Forschung), Austria.  
<http://www.zamg.ac.at/cms/de/klima/klimauebersichten> (May 2010)

---

## Table of figures

Figure 1-1. Damage caused by mass movements in the Northern Vienna Forest. ....	4
Figure 3-1 . Study areas.....	23
Figure 3-2. Hagenbach Valley.....	25
Figure 3-3. Proportion of landslides related to the main geological units in Lower Austria.....	25
Figure 3-4. Deep-seated landslide in the municipality of Purkersdorf. ....	27
Figure 3-5. Landslide in the municipality of St. Andrä-Wördern.....	27
Figure 3-6. Geological and tectonic setting of the Northern Vienna Forest.....	29
Figure 3-7. Location of the Hagenbach Valley.....	30
Figure 4-1. Landform classification by the two Topographic Position Indexes (Weiss 2001).....	37
Figure 4-2. Landslide inventory of the Vienna Forest Flysch Zone.....	43
Figure 4-3. Landslide frequency versus slope gradient.....	45
Figure 4-4. Cumulative descending weighting of the slope gradient.....	47
Figure 4-5. Cumulative ascending weighting of the tectonic lines.....	47
Figure 4-6. Cumulative ascending weighting of drainage lines.....	48
Figure 4-7. Results of the weighting of the geology geofactor.....	51
Figure 4-8. Results of the weighting of the proximity to tectonic lines.....	53
Figure 4-9. Results of the weighting of land cover on the basis of CORINE land cover data.....	55
Figure 4-10. Results of the weighting of the proximity of drainage lines.....	57
Figure 4-11. Results of the weighting of the slope aspect.....	60
Figure 4-12. Susceptibility map for the Vienna Forest Flysch Zone.....	63
Figure 4-13. Prediction rate and success rate curve.....	65
Figure 5-1. Conventional workflow in SINMAP application.....	67
Figure 5-2. Adapted slope stability assessment.....	68
Figure 5-3. Landslides between solid bedrock outcrops.....	70
Figure 5-4. Stability Index defined in area-slope space (Pack et al. (2005)).....	75
Figure 5-5. Borderline of process regions.....	79
Figure 5-6. Difference (in %) to precipitation normals in June 2009.....	83
Figure 5-7. Scheme of the hydrological cycle.....	84
Figure 5-8. Change of recharge, soil moisture storage and potential evapotranspiration.....	94
Figure 5-9. Shaded relief images for the study area.....	99
Figure 5-10. Large-scale landslide inventory.....	101
Figure 5-11. Topographic wetness map for “flysch scenario (January)”.....	103
Figure 5-12. Slope stability index map for the “flysch scenario (January)”.....	104
Figure 5-13. Slope stability index classification for “flysch scenario (January)”.....	106
Figure 5-14. Slope gradient analysis within slope stability classes for “flysch scenario (January)”.....	106
Figure 5-15. Topographic wetness map based on average monthly recharge in January.....	108
Figure 5-16. Stability index map for the “winter scenario (January)”.....	109
Figure 5-17. Slope stability classification for “winter scenario (January)”.....	111
Figure 5-18. Slope gradient analysis within slope stability classes for “winter scenario (January)”.....	111
Figure 5-19. Topographic wetness map based on average monthly recharge in February.....	113
Figure 5-20. Stability index map for the “winter scenario (February)”.....	114
Figure 5-21. Slope stability classification for “winter scenario (February)”.....	115
Figure 5-22. Topographic wetness map based on average monthly recharge in July.....	116
Figure 5-23. Stability index map for the “summer scenario (July)”.....	118

---

Figure 5-24. Slope stability classification for “summer scenario (July)” .....	119
Figure 5-25. Topographic wetness map based on monthly average recharge in January in consideration of the climate change .....	121
Figure 5-26. Stability index map for the future “winter scenario (January)” .....	123
Figure 5-27. Slope stability classification for future “winter scenario (January)” .....	124
Figure 5-28. Topographic wetness map based on monthly average recharge in February in consideration of the climate change .....	125
Figure 5-29. Stability index map for the future “winter scenario (February)” .....	127
Figure 5-30. Slope stability classification for future “winter scenario (February)” .....	128
Figure 5-31. Topographic wetness map based on the monthly average recharge in July in consideration of the climate change.....	129
Figure 5-32. Stability index map for the “future summer scenario (July)” .....	131
Figure 5-33. Slope stability classification for “future summer scenario (July)” in consideration of the climate change.....	132
Figure 5-34. Topographic wetness map for the “critical rainfall scenario” .....	133
Figure 5-35. Stability index map for the critical precipitation scenario.....	135
Figure 5-36. Slope stability classification for “critical rainfall scenario” .....	136
Figure 5-37. Topographic wetness map for the “heavy rainfall scenario” .....	137
Figure 5-38. Stability index map for the critical precipitation scenario.....	139
Figure 5-39. Slope stability classification for “heavy rainfall scenario” .....	140
Figure 6-1. Comparison of topographic wetness maps of the “winter scenario” (A) and the “flysch scenario (January)” (B) .....	142
Figure 6-2. Comparison of topographic wetness classes and their proportion in the study area as given in the “flysch scenario (January)” and the “winter scenario (January)” .....	143
Figure 6-3. Comparison of slope stability index maps of the “winter scenario” (A) and the “flysch scenario (January)” (B) .....	144
Figure 6-4. Divergence of slope stability index classification of the “flysch scenario (January)” in relation to the “winter scenario (January)” .....	145
Figure 6-5. Comparison of mean slope gradient per slope stability index class for the “winter scenario” (A) and the “flysch scenario (January)” (B) .....	146
Figure 6-6. Comparison of topographic wetness maps of the “winter scenario (February)” (A) and the “summer scenario (July)” (B).....	148
Figure 6-7. Comparison of topographic wetness classes and their proportion in the study area as given in the “summer scenario (July)” and the “winter scenario (February)” .....	149
Figure 6-8. Comparison of slope stability index maps of the “winter scenario” (A) and the “summer scenario” (B) .....	150
Figure 6-9. Divergence of slope stability index classification of the “winter scenario (February)” in relation to the “summer scenario (July)” .....	151
Figure 6-10. Comparison of topographic wetness maps of the “future winter scenario” (A) and the “future summer scenario (July)” (B) .....	153
Figure 6-11. Comparison of topographic wetness classes and their proportion in the study area as given in the “future summer scenario (July)” and the future “winter scenario (February)” ....	154
Figure 6-12. Comparison of slope stability index maps of the “future winter scenario” (A) and “future summer scenario” (B) .....	155
Figure 6-13. Divergence of slope stability index classification of future winter scenario (February)” in relation to the “future summer scenario (July)” .....	156

---

Figure 6-14. Comparison of topographic wetness maps of the “summer scenario(July)” (A) and the “future summer scenario (July)” (B). .....	158
Figure 6-15. Comparison of topographic wetness classes and their proportion in the study area as given in the “summer scenario (July)” and the corresponding “future summer scenario (July)”. .....	159
Figure 6-16. Comparison of slope stability index maps of the “summer scenario” (A) and the “future summer scenario” (B).....	160
Figure 6-17. Divergence of the slope stability index classification of the “summer scenario (July)” in relation to the “future summer scenario (July)”. .....	161
Figure 6-18. Comparison of topographic wetness maps of the “winter scenario (January)” (A) and the “future winter scenario (January)” (B). .....	163
Figure 6-19. Comparison of topographic wetness classes and their proportion in the study area as given in the “winter scenario (January)” and the “future winter scenario (January)”. .....	164
Figure 6-20. Comparison of slope stability index maps of the “winter scenario (January)” (A) and the “future winter scenario (January)” (B).....	165
Figure 6-21. Divergence of the slope stability index classification of the “winter scenario (January)” in relation to the “future winter scenario (January)”. .....	166
Figure 6-22. Comparison of the topographic wetness maps of the “summer scenario” (A) and the “critical rainfall scenario” (B).....	168
Figure 6-23. Comparison of the topographic wetness classes and their proportion in the study area as given in the “summer scenario (July)” and the “critical rainfall scenario” (90 mm/d).....	169
Figure 6-24. Comparison of the slope stability index maps of the “summer scenario (July)” (A) and “critical rainfall scenario” (B).....	170
Figure 6-25. Divergence of the slope stability index classification of the “critical rainfall scenario” (90 mm/d) in relation to the “summer scenario” (July).....	171
Figure 6-26. Comparison of the topographic wetness classes and their proportion in the study area as given in the “summer scenario” (A) and the “heavy rainfall scenario” (B).....	173
Figure 6-27. Comparison of the topographic wetness classes and their proportion in the study area in scenarios considering average wetness conditions and heavy rainfall. ....	174
Figure 6-28. Comparison of the slope stability index maps of the “summer scenario” (A) and the “heavy rainfall scenario” (B).....	175
Figure 6-29. Divergence of the slope stability index classification of the “heavy rainfall scenario” (60 mm/h) in relation to the “summer scenario” (July).....	176
Figure 7-1. Prevailing wind direction in the Vienna Forest.....	181